

生体・口腔環境の過酷腐食性と
適合耐食合金の溶出・環境劣化の評価
に関する研究

課題番号 15560632

平成15年度～平成17年度科学研究費補助金
(基盤研究 (C)) 研究成果報告書

平成18年8月

研究代表者 酒井 潤一
早稲田大学理工学術院 教授

Study of the evaluations of the severe
corrosivity of body and oral cavity
environments and environmental
degradation and dissolution of
adequately high corrosion resistant
alloys

Grant No. 1 5 5 6 0 6 3 2

2 0 0 3 ~ 2 0 0 5

Grand-in-Aid for Scientific Research (C)

Final Report

August 2 0 0 6

SAKAI, Jun'ichi

Faculty of Science and Engineering,

Waseda University

はしがき

本研究成果報告書は、平成 15 年度～17 年度科学研究費補助金(基盤研究(C))によって行われた「生体・口腔環境の過酷腐食性と適合耐食合金の溶出・環境劣化の評価に関する研究」の成果を取りまとめたものである。

高齢化の進行に伴い、さらには整形技術の進歩に伴い、これまでも増して、各種生体器官などの金属材料などによる代替が進んでくるのは必須である。生体用材料としての金属材料などは生体内で長期間に亘って使用されるので、その信頼性、安全性の確保が最重要課題である。腐食性の見地からの生体液・使用条件などの特性は十分には解明されていない。およそ自然生活環境で遭遇する腐食形態のいずれも生体内において生起する可能性がある。以上の観点から、生体、口腔の腐食環境のキャラクタリゼーション、用いられる金属材料の溶出傾向やその程度、機構に基づいた損傷の再現、耐食性・環境劣化の評価、およびその改善は今日的な重要課題といえる。近年はその優れた耐食性、生体適合性、超弾性などの観点から、Ti 合金の重要度が高まりつつある。

本研究はステンレス鋼などと比較しながら、Ti 合金の特性評価を例にとり、生体環境下での材料劣化挙動を環境のキャラクタリゼーション、腐食機構のモデル化、評価法の確立などの観点から解明せんとするものである。

研究組織

研究代表者：酒井 潤一 (早稲田大学 理工学術院・教授)
研究分担者：中江 秀雄 (早稲田大学 理工学術院・教授)
研究分担者：石川 雄一 (横浜国立大学 留学生センター・教授)
研究分担者：横山 賢一 (徳島大学 歯学部・助手)
研究分担者：斉藤 良行 (早稲田大学 理工学術院・教授)

交付決定額 (配分額)

(金額単位：円)

	直接経費	間接経費	合計
平成 15 年度	1,900,000-	0-	1,900,000-
平成 16 年度	800,000-	0-	800,000-
平成 17 年度	1,000,000-	0-	1,000,000-
総 計	3,700,000-	0-	3,700,000-

研究発表

1) 学会誌など

【原著論文】

Ken'ichi Yokoyama, Toshio Ogawa, Kenzo Asaoka and Jun'ichi Sakai, "Evaluation of Hydrogen Absorption Properties of Ti-0.2% Pd Alloy in Fluoride Solutions", *Journal of Alloys and Compounds*, 2005, vol. 400, pp. 227-233.

Toshio Ogawa, Ken'ichi Yokoyama, Kenzo Asaoka and Jun'ichi Sakai, "Distribution and Thermal Desorption Behavior of Hydrogen in Titanium Alloys Immersed in Acidic Fluoride Solutions", *Journal of Alloys and Compounds*, 2005, vol. 396, pp. 269-274.

Ken'ichi Yokoyama, Toshio Ogawa, Kenzo Asaoka and Jun'ichi Sakai, "Susceptibility to Delayed Fracture of Alpha-Beta Titanium Alloy in Fluoride Solutions", *Corrosion Science*, 2005, vol. 47, pp. 1778-1793.

Toshio Ogawa, Ken'ichi Yokoyama, Kenzo Asaoka and Jun'ichi Sakai, "Hydrogen Embrittlement of Ni-Ti Superelastic Alloy in Ethanol Solution Containing Hydrochloric Acid", *Materials Science and Engineering A*, 2005, vol. 393, pp. 239-246.

Ken'ichi Yokoyama, Kazuyuki Kaneko, Toshio Ogawa, Keiji Moriyama, Kenzo Asaoka and Jun'ichi Sakai, "Hydrogen Embrittlement of Work-Hardened Ni-Ti Alloy in Fluoride Solutions", *Biomaterials*, 2005, vol. 26, pp. 101-108.

Ken'ichi Yokoyama, Toshio Ogawa, Kenzo Asaoka and Jun'ichi Sakai, "Hydrogen Absorption of Titanium in Acidic Fluoride Solutions", *Materials Science and Engineering A*, 2004, vol. 384, pp. 19-25.

Toshio Ogawa, Ken'ichi Yokoyama, Kenzo Asaoka and Jun'ichi Sakai, "Hydrogen Absorption Behavior of Beta Titanium Alloy in Acid Fluoride Solutions", *Biomaterials*, 2004, vol. 25, pp. 2419-2425.

Ken'ichi Yokoyama, Kazuyuki Kaneko, Keiji Moriyama, Kenzo Asaoka, Jun'ichi Sakai and Michihiko Nagumo, "Delayed Fracture of Ni-Ti Superelastic Alloys in Acidic and Neutral Fluoride Solutions", *Journal of Biomedical Materials Research Part A*, 2004, vol. 69A, pp. 105-113.

Kazuyuki Kaneko, Ken'ichi Yokoyama, Keiji Moriyama, Kenzo Asaoka, and Jun'ichi Sakai, "Degradation in Performance of Orthodontic Wires Caused by Hydrogen Absorption During Short-Term Immersion in 2.0% Acidulated Phosphate Fluoride Solution", *The Angle Orthodontist*, 2004, vol. 74, pp. 487-495.

Ken'ichi Yokoyama, Kazuyuki Kaneko, Eiji Yabuta, Kenzo Asaoka and Jun'ichi Sakai, "Fracture of Nickel-Titanium Superelastic Alloy in Sodium Hypochlorite Solution", *Materials Science and Engineering A*, 2004, vol. 369, pp. 43-48.

Ken'ichi Yokoyama, Kazuyuki Kaneko, Youji Miyamoto, Kenzo Asaoka, Jun'ichi Sakai and Michihiko Nagumo, "Fracture Associated with Hydrogen Absorption of Sustained Tensile-Loaded Titanium in Acid and Neutral Fluoride Solutions", *Journal of Biomedical Materials Research Part A*, 2004, vol. 68A, pp. 150-158.

Ken'ichi Yokoyama, Toshio Ogawa, Kenzo Asaoka, Jun'ichi Sakai and Michihiko Nagumo, "Degradation of Tensile Strength of Ni-Ti Superelastic Alloy Due to Hydrogen Absorption in Methanol Solution Containing Hydrochloric Acid", *Materials Science and Engineering A*, 2003, vol. 360, pp. 153-159.

Kazuyuki Kaneko, Ken'ichi Yokoyama, Keiji Moriyama, Kenzo Asaoka, Jun'ichi Sakai and Michihiko Nagumo, "Delayed Fracture of Beta Titanium Orthodontic Wire in Fluoride Aqueous Solutions", *Biomaterials*, 2003, vol. 24, pp. 2113-2120.

Ken'ichi Yokoyama, Kazuyuki Kaneko, Keiji Moriyama, Kenzo Asaoka, Jun'ichi Sakai and Michihiko Nagumo, "Hydrogen Embrittlement of Ni-Ti Superelastic Alloy in Fluoride Solution", *Journal of Biomedical Materials Research Part A*, 2003, vol. 65A, pp. 182-187.

Ken'ichi Yokoyama, Shiyozo Watabe, Kenichi Hamada, Jun'ichi Sakai, Kenzo Asaoka and Michihiko Nagumo, "Susceptibility to Delayed Fracture of Ni-Ti Superelastic Alloy", *Materials Science and Engineering A*, 2003, vol. 341, pp. 91-97.

2) 口頭発表

【プロシーディングス】

Jun'ichi Sakai, Eiji Yabuta and Ken'ichi Yokoyama "Effects of Martensite Phase of Ni-Ti Shape Memory Alloy on Corrosion Behavior in Sodium Hypochlorite Solutions", 13th Asian Pacific Corrosion Control Conference, November 16-21, 2003, Osaka, Japan, Paper No. L-04, pp. 1-8.

Jun'ichi Sakai, Eiji Yabuta and Ken'ichi Yokoyama, "Effects of Hypochlorite and Fluoride on Corrosion Behavior of Ti-Ni Alloy", V LATINCORR CONGRESS, 5th NACE Latin-American Region Corrosion Congress, 8th Ibero-American Congress of Congress of Corrosion and Protection, October 20-24, 2003, Santiago, Chile, pp. 186-191.

【国際会議アブストラクト】

Ken'ichi Yokoyama, Toshio Ogawa, Kenzo Asaoka and Jun'ichi Sakai, "Fractography of Biomedical Titanium Alloys Fractured in Fluoride Solution", First International Conference on Mechanics of Biomaterials and Tissues, December 11-15, 2005, Hawai'i, USA, P071.

Ken'ichi Yokoyama, Toshio Ogawa, Kenzo Asaoka and Jun'ichi Sakai, "Hydrogen Embrittlement of Ti and Ti-6Al-4V Alloy in Fluoride Solution", Seventh World Biomaterials Congress, May 17-21, 2004, Sydney, Australia, p. 951.

Ken'ichi Yokoyama, Kazuyuki Kaneko, Eiji Yabuta, Kenzo Asaoka and Jun'ichi Sakai, "Fracture of Sustain-Loaded Nickel-Titanium Superelastic Alloy in Sodium Hypochlorite Solutions", Journal of Dental Research vol. 83 (IADR Abstracts) March 10-14, 2004, Hawai'i, USA, # 0622.

Ken'ichi Yokoyama, Kazuyuki Kaneko, Keiji Moriyama, Kenzo Asaoka, Jun'ichi Sakai and Michihiko Nagumo, "Degradation of Tensile Strength Due to Hydrogen Absorption of Nickel-Titanium Superelastic Alloys in Fluoride Solution", Journal of Dental Research vol. 82 (IADR Abstracts) June 25-28, 2003, Göteborg, Sweden, p. 341.

Kazuyuki Kaneko, Ken'ichi Yokoyama, Keiji Moriyama, Kenzo Asaoka, Jun'ichi Sakai and Michihiko Nagumo, "Delayed Fracture of Beta Titanium Alloy in Fluoride Solutions", Journal of Dental Research vol. 82 (IADR Abstracts) June 25-28, 2003, Göteborg, Sweden, p. 341.

【国内シンポジウム】

横山賢一, 金子和之, 藪田英二, 浅岡憲三, 酒井潤一, "次亜塩素酸ナトリウム水溶液中におけるNi-Ti超弾性合金の腐食破壊", 日本金属学会講演概要, 2003年秋期(第133回)大会, シンポジウム講演, バイオインテリジェント基盤材料, 北海道大学, p. 161.

横山賢一, 金子和之, 宮本洋二, 浅岡憲三, 酒井潤一, 南雲道彦, "口腔内環境におけるチタンの破壊—フッ化ナトリウム水溶液の影響—", 日本金属学会講演概要, 2002年秋期(第131回)大会, シンポジウム講演, 歯科材料—開発の現状と次世代への展望, 大阪大学, p. 108.

【一般講演】

横山賢一, 小川登志男, 高島克利, 浅岡憲三, 酒井潤一, "Ni-Ti超弾性合金の水素脆化—大気中放置による水素濃度分布の変化—", 日本金属学会学術講演会, 2006年春期(第138回)大会, 早稲田大学, #171, p230

高島克利, 横山賢一, 浅岡憲三, 酒井潤一, "中性NaF水溶液中におけるCP-Tiの水素吸収に及ぼす電位卑化の影響", 日本金属学会学術講演会, 2006年春期(第138回)大会, 早稲田大学, #14, p178

横山賢一, 佐藤良介, 高島克利, 浅岡憲三, 酒井潤一, "純チタンのフレッティング疲労に及ぼすハイドロキシアパタイトの影響", 日本金属学会学術講演会, 2005年秋期(第137回)大会, 広島大学, #957, p. 443.

藤田篤, 横山賢一, 浅岡憲三, 酒井潤一, "過酸化水素を含有した生理食塩水中におけるNi-Ti超弾性合金の腐食挙動" 日本金属学会学術講演会, 2005年秋期(第137回)大会, 広島大学, #963, p. 445.

横山賢一, 小川登志男, 浅岡憲三, 酒井潤一, "過酸化水素を含有した生理食塩水中におけるNi-Ti超弾性合金の破壊", 日本金属学会学術講演会, 2005年春期(第136回)大会, 横浜国立大学, #318, p. 236.

是永圭太, 小川登志男, 横山賢一, 浅岡憲三, 酒井潤一, “フッ化ナトリウム水溶液中における Ni-Ti 超弾性合金の水素吸収抑制-硝酸浸漬による表面処理-”, 日本金属学会学術講演会, 2005 年春期(第 136 回)大会, 横浜国立大学, #338, p. 243.

小川登志男, 横山賢一, 浅岡憲三, 酒井潤一, “フッ化ナトリウム水溶液中で Ti 合金が吸収した水素の昇温放出分析による特徴付け”, 日本金属学会学術講演会, 2004 年秋期(第 135 回)大会, 秋田大学, #1003, p. 574.

藤田篤, 小川登志男, 横山賢一, 浅岡憲三, 酒井潤一, “酸性フッ化ナトリウム水溶液中における Ti-6Al-4V 合金の水素吸収と腐食挙動”, 日本金属学会学術講演会, 2004 年秋期(第 135 回)大会, 秋田大学, #772, p. 497.

小川登志男, 横山賢一, 酒井潤一, “フッ化ナトリウム水溶液中で遅れ破壊した Ti 合金の表面及び破面観察”, 第 51 回材料と環境討論会講演集(2004)、#B101, p.101

横山賢一, 金子和之, 小川登志男, 浅岡憲三, 酒井潤一, “フッ化ナトリウム水溶液中におけるチタンおよびチタン合金の遅れ破壊特性”, 日本金属学会講演概要, 2004 年春期(第 134 回)大会, 東京工業大学, #32, p. 126.

小川登志男, 横山賢一, 浅岡憲三, 酒井潤一, “塩酸を含むエタノール溶液中における Ni-Ti 超弾性合金の水素脆化”, 日本金属学会講演概要, 2004 年春期(第 134 回)大会, 東京工業大学, #173, p. 173.

大鶴俊司, 酒井潤一, 横山賢一, “生体適合性に優れた Ti の陽極酸化皮膜の生成・制御とその耐食性評価” 第 50 回材料と環境討論会講演集(2003)、#B205, p.177

藪田英二, 酒井潤一, 横山賢一 “次亜塩素酸ナトリウム水溶液中における Ni-Ti 超弾性合金の腐食挙動” 第 50 回材料と環境討論会講演集(2003)、#B206, p.179

小川登志男, 横山賢一, 浅岡憲三, 酒井潤一, “フッ化ナトリウム水溶液中におけるベータチタン合金の水素吸収特性”, 日本金属学会講演概要, 2003 年秋期(第 133 回)大会, 北海道大学, #181, p. 324.

Evaluation of hydrogen absorption properties of Ti–0.2 mass% Pd alloy in fluoride solutions

Ken'ichi Yokoyama^{a,*}, Toshio Ogawa^b, Kenzo Asaoka^a, Jun'ichi Sakai^b

^a Department of Biomaterials and Bioengineering, Institute of Health Biosciences, The University of Tokushima Graduate School, 3-18-15 Kuramoto-cho, Tokushima 770-8504, Japan

^b Department of Materials Science and Engineering, Waseda University, 3-4-1 Okubo, Shinjuku-ku, Tokyo 169-8555, Japan

Received 24 February 2005; received in revised form 21 March 2005; accepted 21 March 2005

Available online 27 April 2005

Abstract

The hydrogen absorption properties of Ti–0.2 mass% Pd (Ti–0.2Pd) alloy in 2.0% and 0.2% acidulated phosphate fluoride (APF) and neutral 2.0% NaF solutions (25 °C) has been evaluated by hydrogen thermal desorption analysis. During the early stage of immersion (120 h) in the 2.0% APF solution, the amount of absorbed hydrogen was lower than 500 mass ppm. A thermal desorption of hydrogen primary appearing with a peak at 500–600 °C and a broad desorption ranging from 100 to 400 °C were observed. In the 0.2% APF solution, the amount of absorbed hydrogen saturated at 100–200 mass ppm; the thermal desorption of hydrogen appeared with a single peak at 550 °C. In the 2.0% NaF solution, hydrogen absorption was negligible even after 1000 h of immersion, although corrosion pits were observed. The results of the present study suggest that the hydrogen absorption of Ti–0.2Pd alloy, as compared with commercial pure titanium, is suppressed in fluoride solutions.

© 2005 Elsevier B.V. All rights reserved.

Keywords: Ti–Pd alloy; Hydrogen embrittlement; Corrosion; Fluoride

1. Introduction

Titanium and its alloys are widely used as materials in dental devices such as dental implants, because of its superior corrosion resistance and biocompatibility. However, titanium is considerably subjected to corrosion in the presence of fluoride in oral environments [1–9]. Fluoride such as NaF protects against dental caries. NaF ranging from 2.0% to 0.2% is generally added to prophylactic agents and toothpastes from pH 3.5 to neutral.

We have recently reported that hydrogen absorption through corrosion in fluoride solutions results in a pronounced degradation of the mechanical properties and fracture of titanium and its alloys, that is, hydrogen embrittlement [10–14]. The mechanisms of hydrogen embrittlement and the amount of hydrogen absorbed during immersion in

fluoride solutions appear to depend strongly on the crystalline structure of titanium alloys. In general, for alpha titanium and alpha titanium alloys, hydrogen absorption leads to the formation of titanium hydride, which plays important roles in mechanical properties [15–17]. Upon immersion in 0.2% acidulated phosphate fluoride (APF) solution, the amount of absorbed hydrogen in alpha titanium (commercial pure titanium) [18] is approximately 300 mass ppm, whereas those in alpha–beta titanium (Ti–6Al–4V) [19] and beta titanium (Ti–11.3Mo–6.6Zr–4.3Sn) alloys [20] are 30–50 and 2000–3500 mass ppm, respectively. It is desirable to suppress hydrogen absorption as much as possible, although the amount of absorbed hydrogen is not necessarily the sole criterion for hydrogen embrittlement.

Adding a small quantity of palladium to titanium has been considered to be one of the methods of suppressing hydrogen absorption of titanium [21]. Ti–Pd alloy is an alpha titanium alloy and has a high corrosion resistance in various solutions [22–28]. Nakagawa et al. [29–31] demonstrated by electro-

* Corresponding author. Tel.: +81 88 633 7334; fax: +81 88 633 9125.

E-mail address: yokken@dent.tokushima-u.ac.jp (K. Yokoyama).

chemical methods that the corrosion resistance of Ti–Pd alloy is higher than that of pure titanium in fluoride solutions. Ti–Pd alloy is anticipated to be useful as a new alpha titanium alloy in dental implants. However, few studies have been carried out on hydrogen absorption. Therefore, the hydrogen absorption properties of Ti–Pd alloy in fluoride solutions must be investigated.

The objective of the present study is to evaluate the hydrogen absorption properties of Ti–Pd alloy in acidic and neutral fluoride solutions by hydrogen thermal desorption analysis (TDA). In this article, we focus on comparing the hydrogen absorption properties of this alloy with those of commercial pure titanium reported previously [18].

2. Experimental procedures

A Ti–0.2 mass% Pd alloy (Ti–0.2Pd alloy; Daido Steel Co. Ltd., Nagoya, Japan) wire of 0.50 mm diameter was cut into specimens of 50 mm length. The chemical composition of the wire is given in Table 1. Percent in this paper means mass percent, unless otherwise stated. For the comparison, the experimental conditions of the present study were the same as those of our previous study [18]. The specimens were carefully polished with 600-grit SiC paper and ultrasonically washed in acetone for 5 min. The specimens were immersed separately in 50 ml aqueous solutions of 2.0% and 0.2% APF (0.48 mol/l NaF + 0.18 mol/l H₃PO₄ and 0.048 mol/l NaF + 0.018 mol/l H₃PO₄) without applied stress at pH 5.0 at room temperature (25 ± 2 °C). For the evaluation of the effects of pH on corrosion and hydrogen absorption, a neutral 2.0% NaF solution (pH 6.5) was prepared. The NaF contents in the 2.0% and 0.2% APF solutions correspond to those in commercial prophylactic agents and toothpastes, respectively.

The corrosion potentials of the specimens in test solutions were measured at room temperature under aerated conditions. The counter and reference electrodes used were a platinum electrode and a saturated calomel electrode (SCE), respectively. Measurements were started 10 s after immersion in the test solutions.

The side surface of the immersed specimens was observed by scanning electron microscopy (SEM). The corrosion products on the surface of the immersed specimens were examined using an X-ray diffractometer with Cu K α radiation at a wavelength $\lambda = 1.54056 \text{ \AA}$ in 2θ angles ranging from 10° to 90° operated at 40 kV and 30 mA. The mass and diameter changes

Table 1

Chemical composition of Ti–0.2Pd alloy tested (mass%)

C	0.01
H	0.0010
O	0.06
N	0.005
Fe	0.03
Pd	0.21
Ti	Balance

of the specimens were measured using a microbalance and a micrometer caliper, respectively. Standard deviations were calculated from the results obtained from five specimens.

The amount of desorbed hydrogen was measured by TDA for the immersed specimens. The immersed specimens were cut at both ends and subjected to ultrasonic cleaning with acetone for 2 min. Subsequently, the specimens were dried in ambient air and then subjected to TDA, which was started 30 min after the removal of specimens from the test solutions. A quadrupole mass spectrometer (ULVAC, Kanagawa, Japan) was used for hydrogen detection. Sampling was conducted at 30 s intervals at a heating rate of 100 °C/h.

3. Results and discussion

The shifts of the corrosion potentials of Ti–0.2Pd alloy specimens in test solutions under aerated conditions are shown in Fig. 1. The corrosion potentials of the specimens in 2.0%, 0.2% APF and 2.0% NaF solutions reached –0.75, –0.65 and –0.30 V (versus SCE), respectively. The corrosion potentials of the Ti–0.2Pd alloy, compared with those of commercial pure titanium [18], located in the noble direction under the same conditions. These results agree with those obtained by Nakagawa et al. [29–31]. Stern and Wissenberg [22] demonstrated that Ti–Pd alloys markedly improve corrosion resistance to H₂SO₄, HCl and other reducing-type solutions, since the mixed potentials of Ti–Pd alloys are more noble than the critical potential for passivity of pure titanium. Armstrong et al. [25] proved that when Ti–Pd alloys undergo corrosion in H₂SO₄ solution, palladium enrichment at the surface occurs, thereby improving corrosion resistance. Similarly, in fluoride solutions, palladium enrichment at the surface has been

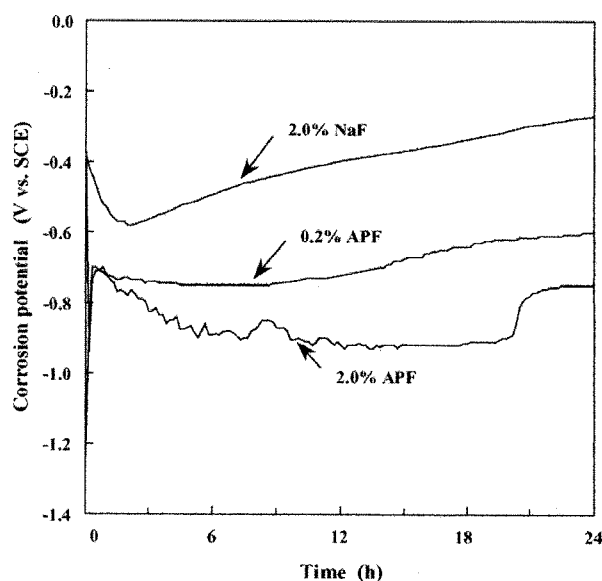


Fig. 1. Changes in corrosion potentials of Ti–0.2Pd alloy specimens in 2.0%, 0.2% APF and 2.0% NaF solutions.

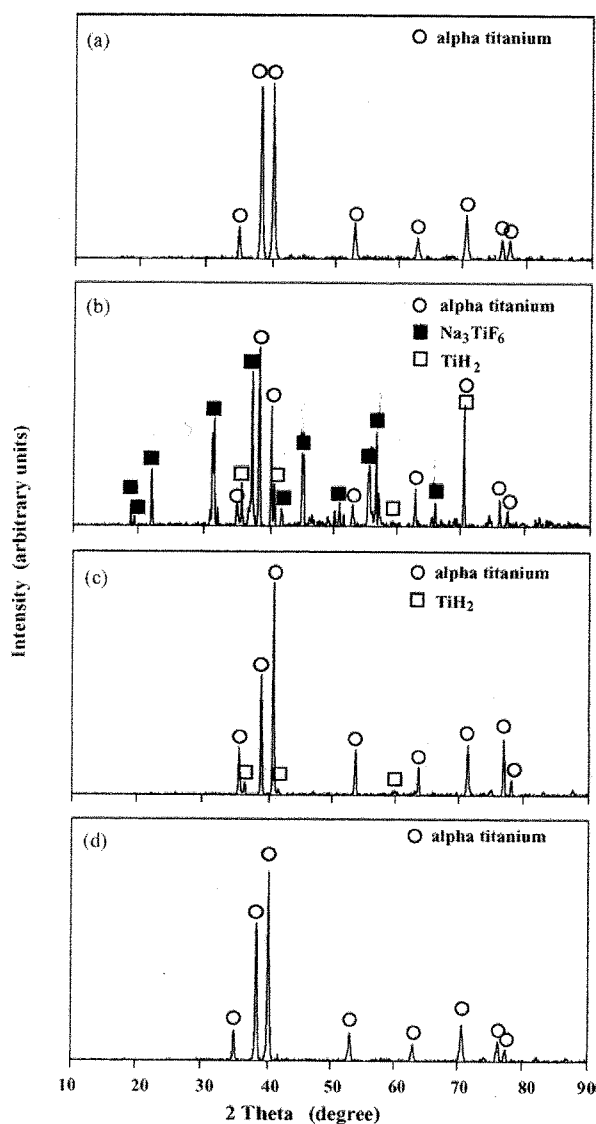


Fig. 2. XRD patterns for the surface of Ti-0.2Pd alloy specimens; (a) nonimmersed, (b) immersed in 2.0% APF solution for 24 h, (c) immersed in 0.2% APF solution for 24 h and (d) immersed in 2.0% NaF solution for 1000 h.

observed [29]. The improvement in the corrosion resistance of Ti-Pd alloys in fluoride solutions has been discussed previously [29–31]; hence, further discussion is omitted in the present report.

Fig. 2(a) shows the results of X-ray diffraction (XRD) measurements of the side surface of the nonimmersed Ti-0.2Pd alloy specimen; alpha titanium peaks were observed. The XRD pattern of the surface of the specimen immersed in the 2.0% APF solution for 24 h is shown in Fig. 2(b); sodium titanium fluoride (Na_3TiF_6) and titanium hydride (TiH_2) were identified. This result is consistent with that of commercial pure titanium immersed in the 2.0% APF solution [18]. For the surface of the Ti-0.2Pd alloy specimens immersed in the 0.2% APF solution for 24 h (Fig. 2(c)), TiH_2 was identified, but corrosion products were not detected even

after 240 h of immersion. In the case of commercial pure titanium immersed in the 0.2% APF solution for 24 h, not only TiH_2 but also titanium fluoride (TiF_2) was identified in our previous study [18]. For the surface of the Ti-0.2Pd alloy specimen immersed in the 2.0% NaF solution even for 1000 h, neither corrosion products nor titanium hydrides were detected, as shown in Fig. 2(d).

On the side surface of the nonimmersed Ti-0.2Pd alloy specimen, scratches due to SiC paper polishing during specimen preparation were observed, as shown in Fig. 3(a) and (b). After the 24 h immersion in the 2.0% APF solution, crystalline corrosion products deposited on the surface of the specimen, as shown in Fig. 3(c). The corrosion products were 5–10 μm in diameter, as shown in Fig. 3(d); they very readily peeled off from the surface. The topography of the surface of the Ti-0.2Pd alloy specimen subjected to corrosion was different from that of commercial pure titanium reported previously [18], although the type of corrosion product was the same. As shown in Fig. 3(e), general corrosion was observed on the surface of the Ti-0.2Pd alloy specimen immersed in the 0.2% APF solution for 24 h. The surface showed corrosion, the scratches due to SiC paper polishing disappeared and the surface became smooth. Corrosion pits were observed at a high magnification (Fig. 3(f)). On the basis of surface observation, the Ti-0.2Pd alloy in the 0.2% APF solution is presumably less susceptible to corrosion than commercial pure titanium [18]. Fig. 3(g) and (h) shows the surface of the Ti-0.2Pd alloy specimen immersed in the 2.0% NaF solution for 1000 h. Innumerable corrosion pits were revealed on the entire surface, although scratches due to SiC paper polishing remained. For the 24 h immersion in the 2.0% NaF solution, corrosion pits were rarely observed.

The mass and diameter changes of Ti-0.2Pd alloy specimens immersed in the test solutions as functions of immersion time are shown in Figs. 4 and 5, respectively. The mass of the specimen immersed in the 2.0% APF solution decreased linearly with immersion time, although the data points were scattered widely. One reason for the scatter was the peeling of corrosion products. For more than 120 h, the mass loss of the Ti-0.2Pd alloy specimen was larger than that of commercial pure titanium specimen (approximately 0.10 mg/mm^2) [18]. The diameter of the Ti-0.2Pd alloy specimen immersed in the 2.0% APF solution decreased with immersion time, although it sometimes increased during the early stage of the immersion. The diameter increase due to corrosion products deposited on the surface of the specimen appears to be larger than the diameter loss arising from dissolution and/or peeling. It is noteworthy that the diameter loss of the Ti-0.2Pd alloy specimen was larger than that of commercial pure titanium specimen [18] for all immersion times, because the corrosion products of the Ti-0.2Pd alloy specimen easily peeled off the surface. This peeling may be related to TiH_2 formation. The diameter loss will result in fracture due to the reduction in the cross-section of the specimen, if immersion tests under applied stress are conducted.

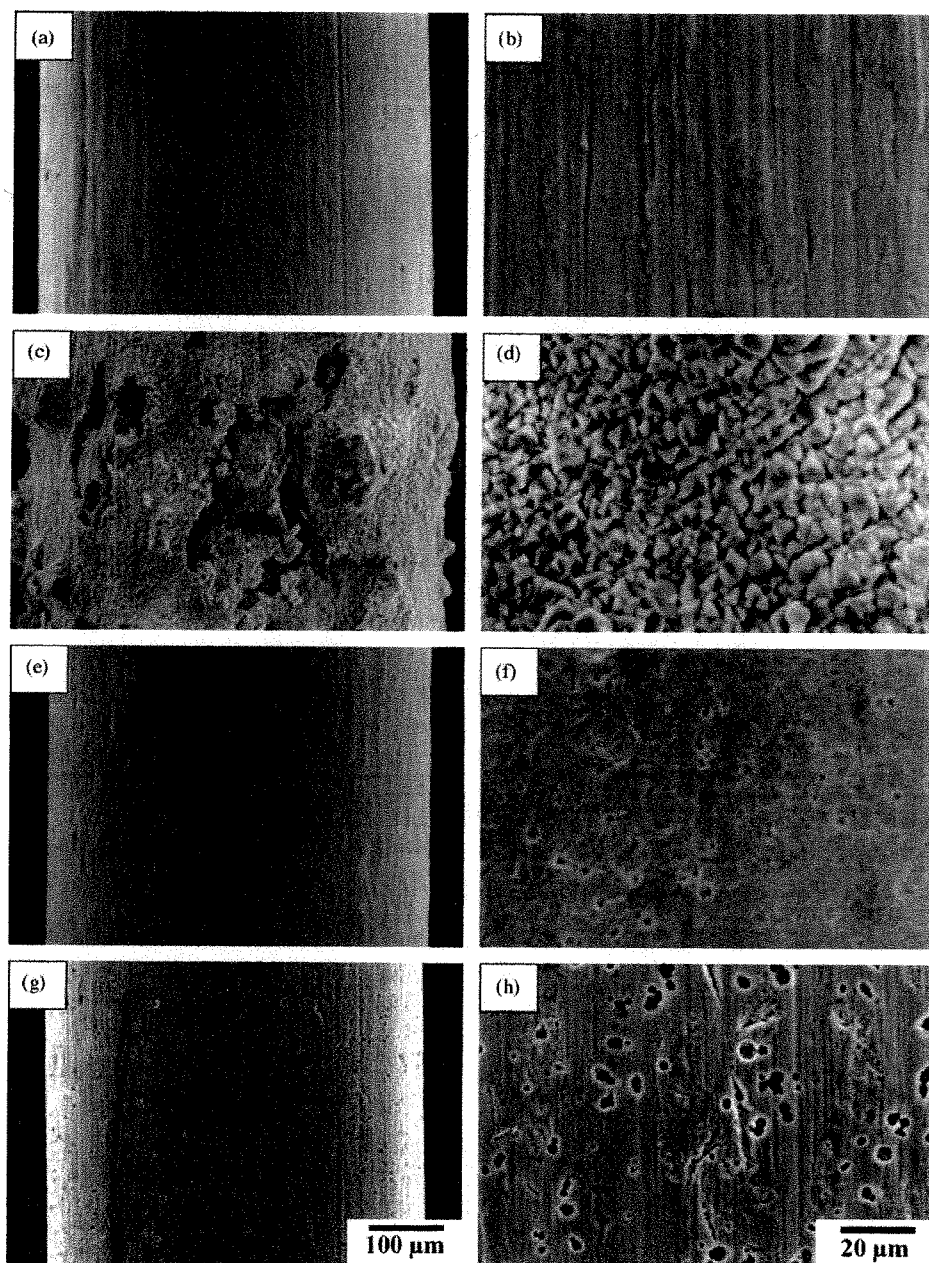


Fig. 3. SEM images of a typical side surface: (a) low-magnification and (b) high-magnification views of a nonimmersed specimen; (c) low-magnification and (d) high-magnification views of a specimen immersed in 2.0% APF solution for 24 h; (e) low-magnification and (f) high-magnification views of a specimen immersed in 0.2% APF solution for 24 h; and (g) low-magnification and (h) high-magnification views of a specimen immersed in 2.0% NaF solution for 1000 h.

After the immersion in the 0.2% APF solution, the mass and diameter decreased gradually, and then mass and diameter losses saturated. The mass loss of the Ti–0.2Pd alloy specimen was one-half that of commercial pure titanium specimen [18], whereas the diameter loss of the Ti–0.2Pd alloy specimen was slightly large. The reason for this is likely that corrosion products rarely deposited on the surface of the Ti–0.2Pd alloy in the 0.2% APF solution. In the 2.0% NaF solution, the mass and diameter changes of the Ti–0.2Pd alloy speci-

mens were negligible even after 1000 h immersion, although corrosion pits were observed.

The representative hydrogen-thermal-desorption curves of the Ti–0.2Pd alloy specimens immersed in the 2.0% and 0.2% APF solutions for various periods are shown in Fig. 6(a) and (b), respectively. In the figures, the desorption curve of the nonimmersed specimen is also included. For the specimens immersed in the 2.0% APF solution, a primary desorption appeared at 400–700 °C, and a broad desorption was observed

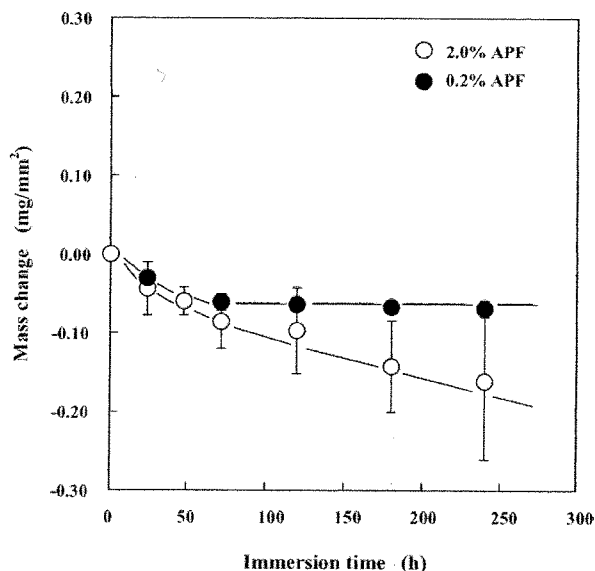


Fig. 4. Mass changes of Ti-0.2Pd alloy specimens immersed in 2.0% and 0.2% APF solutions. Standard deviation was calculated from the results of five specimens.

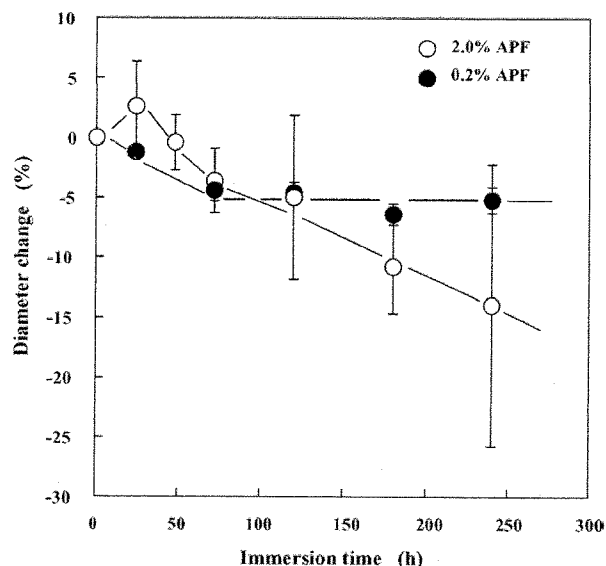


Fig. 5. Diameter changes of Ti-0.2Pd alloy specimens immersed in 2.0% and 0.2% APF solutions. Standard deviation was calculated from the results of five specimens.

ranging from 100 to 400 °C. The desorption at the high-temperature region increased with immersion time, while that at the low-temperature region hardly changed. When the desorption behavior of commercial pure titanium reported previously [18,32] is compared, the desorption at the low-temperature region is clearly noticed for that of the Ti-0.2Pd alloy. In particular, the desorption-start temperature of the Ti-0.2Pd alloy was 100 °C lower than that of commercial pure titanium. For commercial pure titanium with a large amount of titanium hydride in the surface layer, the desorp-

tion at the low-temperature region (200–300 °C) often results from the dissociation of the hydride [32]. The temperature of the dissociation of the hydride of the Ti-0.2Pd alloy might be lower than that of commercial pure titanium. The primary desorption of immersed Ti-0.2Pd alloy specimens shifted to the high-temperature region, compared with that of the non-immersed Ti-0.2Pd alloy specimen. The origin of this shift is probably analogous to that of commercial pure titanium immersed in the 2.0% APF solution. Details have been reported in our previous article [32].

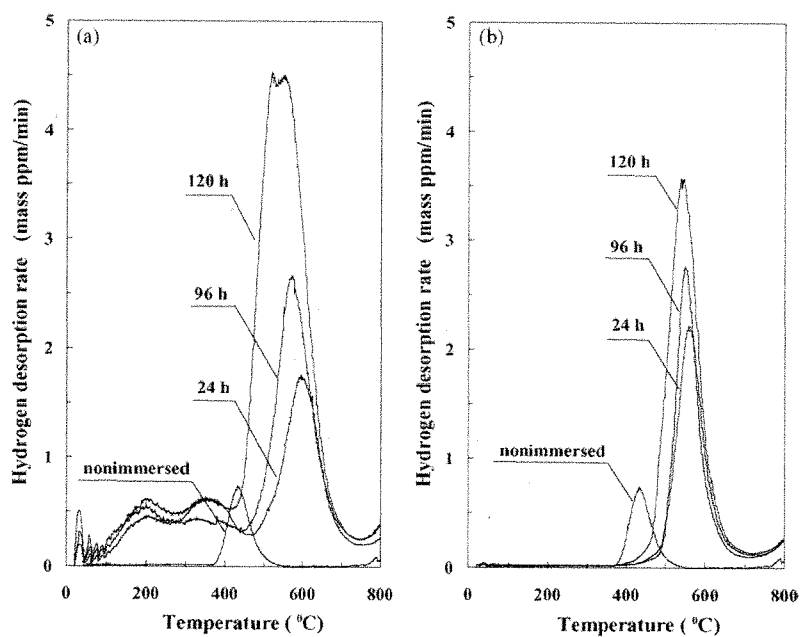


Fig. 6. Hydrogen thermal desorption curves for Ti-0.2Pd alloy specimens immersed for various periods in (a) 2.0% and (b) 0.2% APF solutions.

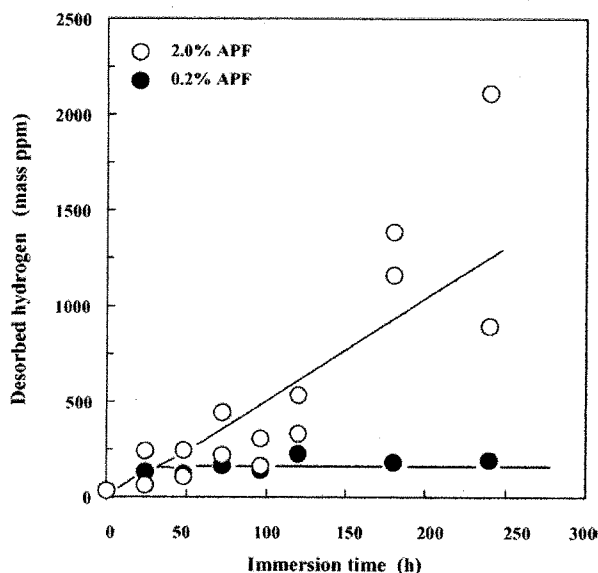


Fig. 7. Amounts of desorbed hydrogen obtained from thermal desorption analysis of Ti–0.2Pd alloy specimens immersed in 2.0% and 0.2% APF solutions as functions of immersion time.

In the case of the Ti–0.2Pd alloy specimens immersed in the 0.2% APF solution, a single desorption peak was observed at 600 °C. Similarly to commercial pure titanium [18,32], it appears that the amount of the hydride was small, thereby the desorption did not occur at the low-temperature region.

The amount of desorbed hydrogen was calculated by integrating desorption peak intensity up to 800 °C. The amount of desorbed hydrogen is shown in Fig. 7 for the Ti–0.2Pd alloy specimens immersed in 2.0% and 0.2% APF solutions. The amount of desorbed hydrogen for the nonimmersed specimen obtained from TDA, that is, predissolved hydrogen content, was 34 mass ppm. Thus, the amount of hydrogen absorbed during the immersion test can be calculated by subtracting predissolved hydrogen content from the amount of desorbed hydrogen. The behavior of hydrogen absorption was consistent with that of mass (Fig. 4) and diameter (Fig. 5) changes. In the 2.0% APF solution, the amount of absorbed hydrogen increased with immersion time, although the data points were scattered. For commercial pure titanium reported previously [18], the amount of hydrogen absorbed during immersion in the 2.0% APF solution saturated to 800–900 mass ppm after 72 h. Up to 120 h, the amount of absorbed hydrogen of the Ti–0.2Pd alloy specimens was lower than 500 mass ppm, suggesting the suppression of hydrogen absorption. However, it should be noticed that the amount of absorbed hydrogen of the Ti–0.2Pd alloy was larger than that of commercial pure titanium after more than 120 h of immersion.

Upon the immersion in the 0.2% APF solution, the amount of absorbed hydrogen of the Ti–0.2Pd alloy specimens saturated to approximately 100–200 mass ppm. For commercial pure titanium under the same conditions, hydrogen absorption saturated up to approximately 300 mass ppm for 48 h of immersion [18]. In the 0.2% APF solution, hydrogen ab-

sorption of the Ti–0.2Pd alloy was certainly suppressed in comparison with commercial pure titanium. The hydrogen absorption of commercial pure titanium generally saturates in association with the hydride formation at the surface layer [33]. For the Ti–0.2Pd alloy, the saturation of hydrogen absorption is perhaps attributable to a high corrosion resistance as well as the hydride formation.

When the amount of absorbed hydrogen exceeds a few hundred mass ppm, the mechanical properties of alpha titanium degrades [34]. In the present study, the amounts of absorbed hydrogen of Ti–0.2Pd alloy specimens immersed in 2.0% and 0.2% APF solutions exceed 100 mass ppm even for 24 h immersion. The hydrogen concentration near the surface of the immersed Ti–0.2Pd alloy specimens appears to be considerably high due to the hydride formation, similar to the case of commercial pure titanium reported previously [32]. Moreover, in the early stage of the immersion, the amounts of absorbed hydrogen of Ti–0.2Pd alloy specimens immersed in 2.0% and 0.2% APF solutions were almost the same. These findings suggest that the time to fracture is not significantly different between a specimen in 2.0% APF solution and that in 0.2% APF solution under a sustained tensile-loading test.

After the immersion in the 2.0% NaF solution, the increment in hydrogen desorption was scarcely confirmed irrespective of immersion time within 1000 h. However, since the amount of absorbed hydrogen generally increases with immersion temperature [35], the Ti–0.2Pd alloy may absorb hydrogen at 37 °C. For commercial pure titanium, the amount of absorbed hydrogen was 10–30 mass ppm in the 2.0% NaF solution at 37 °C for 1000 h [36]. Furthermore, the applied stress occasionally enhances the hydrogen absorption and/or corrosion [20]. Under the sustained tensile-loading test in the 2.0% NaF solution, commercial pure titanium fractures within 1000 h even at 25 °C [12], whereas the alpha–beta titanium [19] and beta titanium alloys [11] do not fracture. It is therefore necessary to confirm in future studies whether the mechanical properties of Ti–Pd alloys degrades under applied stress in neutral fluoride solutions.

4. Conclusions

In this study, we have evaluated the hydrogen absorption properties of Ti–0.2Pd alloy immersed in fluoride solutions using TDA. During the early stage of the immersion in the 2.0% APF solution, the amount of absorbed hydrogen is lower than 500 mass ppm, which is lower than that of commercial pure titanium. In the 0.2% APF solution, the amount of absorbed hydrogen of the Ti–0.2Pd alloy is 100–200 mass ppm and one-half or two-thirds of that of commercial pure titanium. In neutral 2.0% NaF solution, hydrogen absorption is negligible. Immersion tests under an applied stress, for example, a sustained tensile-loading test, are necessary to conclude whether the degradation of mechanical properties is caused by a marked diameter loss associated with hydrogen absorption and/or corrosion.

Acknowledgements

This study was supported in part by a Grant-in-Aid for Young Scientists (B) (14771090) and a Grant-in-Aid for Scientific Research (C) (15560632) from the Ministry of Education, Culture, Sports, Science and Technology, Japan.

References

- [1] J. Lausmaa, B. Kasemo, S. Hansson, *Biomaterials* 6 (1985) 23.
- [2] H.S. Siirilä, M. Könönen, *Int. J. Oral Max. Implants* 6 (1991) 50.
- [3] M.H.O. Könönen, E.T. Lavonius, J.K. Kivilahti, *Dent. Mater.* 11 (1995) 269.
- [4] H. Mimura, Y. Miyagawa, *Jpn. J. Dent. Mater. Dev.* 15 (1996) 283.
- [5] Y. Oda, E. Kawada, M. Yoshinari, K. Hasegawa, T. Okabe, *Jpn. J. Dent. Mater. Dev.* 15 (1996) 317.
- [6] L. Reclaru, J.-M. Meyer, *Biomaterials* 19 (1998) 85.
- [7] M. Nakagawa, S. Matsuya, T. Shiraiishi, M. Ohta, *J. Dent. Res.* 78 (1999) 1568.
- [8] H.H. Huang, *Biomaterials* 23 (2002) 59.
- [9] N. Schiff, B. Grosogeat, M. Lissac, F. Dalard, *Biomaterials* 23 (2002) 1995.
- [10] K. Yokoyama, K. Kaneko, K. Moriyama, K. Asaoka, J. Sakai, M. Nagumo, *J. Biomed. Mater. Res.* 65A (2003) 182.
- [11] K. Kaneko, K. Yokoyama, K. Moriyama, K. Asaoka, J. Sakai, M. Nagumo, *Biomaterials* 24 (2003) 2113.
- [12] K. Yokoyama, K. Kaneko, Y. Miyamoto, K. Asaoka, J. Sakai, M. Nagumo, *J. Biomed. Mater. Res.* 68A (2004) 150.
- [13] K. Yokoyama, K. Kaneko, K. Moriyama, K. Asaoka, J. Sakai, M. Nagumo, *J. Biomed. Mater. Res.* 69A (2004) 105.
- [14] K. Yokoyama, K. Kaneko, T. Ogawa, K. Moriyama, K. Asaoka, J. Sakai, *Biomaterials* 26 (2005) 101.
- [15] C.R. McKinsey, M. Stern, R.A. Perkins, *Trans. ASM* 50 (1958) 438.
- [16] D.S. Shih, I.M. Robertson, H.K. Birnbaum, *Acta Metall.* 36 (1988) 111.
- [17] C.Q. Chen, S.X. Li, H. Zheng, L.B. Wang, K. Lu, *Acta Mater.* 52 (2004) 3697.
- [18] K. Yokoyama, T. Ogawa, K. Asaoka, J. Sakai, *Mater. Sci. Eng. A* 384 (2004) 19.
- [19] K. Yokoyama, T. Ogawa, K. Asaoka, J. Sakai, *Corros. Sci.* 47 (2005) 1778.
- [20] T. Ogawa, K. Yokoyama, K. Asaoka, J. Sakai, *Biomaterials* 25 (2004) 2419.
- [21] A. Takamura, T. Yamagata, *Titanium Zirconium* 15 (1967) 192.
- [22] M. Stern, H. Wissenberg, *J. Electrochem. Soc.* 106 (1959) 759.
- [23] N.D. Tomashov, R.M. Altovsky, G.P. Chernova, *J. Electrochem. Soc.* 108 (1961) 113.
- [24] A. Takamura, *Corrosion* 23 (1967) 306.
- [25] R.D. Armstrong, R.E. Firman, H.R. Thirsk, *Corros. Sci.* 13 (1973) 409.
- [26] T. Watanabe, H. Naito, *J. Jpn. Inst. Met.* 52 (1988) 780.
- [27] C.S. Brossia, G.A. Cragnolino, *Corrosion* 57 (2001) 768.
- [28] C.S. Brossia, G.A. Cragnolino, *Corros. Sci.* 46 (2004) 1693.
- [29] M. Nakagawa, S. Matsuya, K. Udoh, *Dent. Mater. J.* 20 (2001) 305.
- [30] M. Nakagawa, S. Matsuya, K. Udoh, *Dent. Mater. J.* 21 (2002) 83.
- [31] M. Nakagawa, Y. Matono, S. Matsuya, K. Udoh, K. Ishikawa, *Biomaterials* 26 (2005) 2239.
- [32] T. Ogawa, K. Yokoyama, K. Asaoka, J. Sakai, *J. Alloy. Compd* 396 (1–2) (2005) 269–274.
- [33] I.I. Phillips, P. Poole, L.L. Shreir, *Corros. Sci.* 12 (1972) 855.
- [34] D.N. Williams, *J. Inst. Met.* 91 (1962) 147.
- [35] I.I. Phillips, P. Poole, L.L. Shreir, *Corros. Sci.* 14 (1974) 533.
- [36] K. Yokoyama, T. Ogawa, K. Asaoka, J. Sakai, submitted for publication.

Distribution and thermal desorption behavior of hydrogen in titanium alloys immersed in acidic fluoride solutions

Toshio Ogawa^a, Ken'ichi Yokoyama^{b,*}, Kenzo Asaoka^b, Jun'ichi Sakai^a

^a Department of Materials Science and Engineering, Waseda University, 3-4-1 Okubo, Shinjuku-ku, Tokyo 169-8555, Japan

^b Department of Biomaterials and Bioengineering, Institute of Health Biosciences, The University of Tokushima Graduate School, 3-18-15 Kuramoto-cho, Tokushima 770-8504, Japan

Received 9 December 2004; accepted 20 December 2004

Available online 9 February 2005

Abstract

The distribution and thermal desorption behavior of hydrogen in alpha titanium (commercial pure titanium) and beta titanium alloy (Ti–11.3Mo–6.6Zr–4.3Sn) immersed in acidic fluoride solutions (pH 5.0, 25 ± 2 °C) have been investigated. For alpha titanium, most of the hydrogen absorbed in the fluoride solution existed as titanium hydride within approximately 50 μm from the surface of the specimen. The local hydrogen concentration in the vicinity of the surface was evaluated above 5000 mass ppm. Hydrogen thermal desorption was observed in the temperature range from 200 to 700 °C. It is likely that the desorption at a low temperature resulted from the dissociation of the hydride, whereas that at a high temperature was caused by hydrogen strongly trapped in matrix defects induced by hydride formation. For the beta titanium alloy, the absorbed hydrogen diffused toward the center of the specimen without hydride forming. Hydrogen was almost uniformly distributed over the whole cross-section of the specimen, although hydrogen content was high at the surface layer of the specimen. Hydrogen desorption appeared in the range from 400 to 600 °C, implying that the absorbed hydrogen was mostly hydrogen in solution. The corrosion product (TiF₃) on the surface of the specimen caused the desorption temperature to rise more than 100 °C, suggesting the origin of the scatter of desorption behavior.

© 2005 Elsevier B.V. All rights reserved.

Keywords: Titanium; Corrosion; Hydrogen embrittlement; Thermal desorption analysis; Fluoride

1. Introduction

Hydrogen thermal desorption analysis (TDA) is one of the few means of characterizing hydrogen in various materials [1–8]. The desorption behavior such as desorption temperature and the amount of desorption provide information on the state of hydrogen in materials. The state of hydrogen, e.g., hydride, weakly or strongly trapped at defects and in solution, as well as the hydrogen content greatly affect mechanical properties. Hydrogen desorbed at around room temperature is associated with diffusive hydrogen resulting in the pronounced degradation of mechanical properties of high-strength steel [7,9]. Hydride formation often leads to ductility loss of titanium and its alloys [10,11]. The

thermal dissociation behavior of titanium hydride formed in commercial pure titanium by cathodic hydrogen charging was investigated by Takasaki et al. [3] using TDA, high-temperature X-ray diffractometry and differential thermal analysis (DTA). On the other hand, no hydride forms in many beta titanium alloys, since quite a large amount of hydrogen can be achieved in solid solution prior to hydride formation. In this case, hydrogen embrittlement is considered to be due to hydrogen-induced decohesion [12]. Correlations between hydrogen states and the hydrogen desorption behavior of beta titanium alloys have not been well known, and are important in understanding the influence of hydrogen on mechanical behavior.

Alpha titanium (pure titanium) and beta titanium alloys are widely used as dental applications such as implants and orthodontic wires, but they are subjected considerably to corrosion in the presence of fluoride contained in prophylactic

* Corresponding author. Tel.: +81 88 633 7334; fax: +81 88 633 9125.
E-mail address: yokken@dent.tokushima-u.ac.jp (K. Yokoyama).

agents and toothpastes [13–18]. We have recently demonstrated using TDA that hydrogen absorption of alpha titanium [19,20] and beta titanium alloy [21,22] occurs in acidulated phosphate fluoride (APF) solutions, thereby causing the pronounced degradation of mechanical properties. For alpha titanium [20], the thermal desorption behavior of hydrogen absorbed in APF solutions was not always in agreement with that of cathodic-charged hydrogen. In the case of Ni–Ti superelastic alloy, the desorption behavior strongly depends on hydrogen absorbing conditions such as the type of immersing solution [23–25]. Furthermore, the desorption behavior of alpha titanium changes with fluoride concentration and immersion time [20], even though the amount of absorbed hydrogen was the same. The cause of the desorption behavior changes of not only alpha titanium but also that of the beta titanium alloy are not understood. The desorption behavior of titanium and its alloys immersed in APF solutions must be characterized. Moreover, since the amount of hydrogen obtained from TDA is the average value over the entire specimen, it is necessary to evaluate local hydrogen concentration in the specimen.

The purpose of the present study is to evaluate hydrogen distribution and to analyze the hydrogen thermal desorption behavior of alpha titanium and beta titanium alloy immersed in APF solutions.

2. Experimental

Alpha titanium, i.e., commercial pure titanium, wire (Nippon Mining & Metals Co., Ltd., Japan) with a diameter of 0.50 mm and the beta titanium wire (TMA; Ormco Corporation, Glendora, CA) with a diameter of 0.45 mm were cut into specimens of 50 mm length, the chemical compositions of which are given in Table 1. After polishing the surface of the specimens with 600-grit SiC paper, they were ultrasonically washed in acetone for 5 min. The specimens were immersed separately in 50 ml of aqueous solutions of 2.0% or 0.2% APF (0.48 M NaF + 0.18 M H₃PO₄ or 0.048 M NaF + 0.018 M H₃PO₄) with pH 5.0 at room temperature (25 ± 2 °C). To evaluate hydrogen distribution in immersed specimens, the surfaces of the immersed specimens were ground every 25 μm. The surface grinding was carefully conducted with 180-grit SiC paper by measuring a micrometer caliper.

The surfaces of nonground and ground specimens immersed in test solutions were examined using X-ray diffraction (XRD) analysis with Co K α radiation of wavelength

$\lambda = 1.78897 \text{ \AA}$ in the 2θ angle range from 10° to 90° operated at 40 kV and 20 mA.

TDA was performed in a vacuum at 10⁻⁶ Pa with a quadrupole mass spectrometer (ULVAC, Kanagawa, Japan). Sampling time was at 30-s intervals at a heating rate of 100 °C/h. Immersed specimens were subjected to ultrasonic cleaning with acetone for 2 min immediately before measurement. TDA was started 60 min after the removal of the specimens from test solutions.

3. Results and discussion

3.1. Alpha titanium

Fig. 1(a) shows the results of the XRD measurement for the side surface of the nonground alpha titanium specimen immersed in the 2.0% APF solution for 120 h. Sodium titanium fluoride (Na₃TiF₆) and titanium hydride (TiH₂) were identified. The diameter of the nonground specimen increased from 0.50 to 0.52 mm, since corrosion products (Na₃TiF₆) deposited on the surface of the specimen [20]. The XRD patterns of the specimen ground up to 0.50, 0.45 and 0.40 mm diameters are shown in Fig. 1(b)–(d), respectively. The hydride was identified in the 0.50- and 0.45-mm diameter specimens, whereas it was not detected in the 0.40-mm diameter specimen. Thus, the thickness of the hydride layer was approximately 50 μm for the specimen immersed in the 2.0% APF solution for 120 h. It was reported that the electrochemically formed hydride at several tens of micrometers from the surface of alpha titanium prevents hydrogen diffusion to the center of the specimen at room temperature [26,27]. This hydride also serves as a barrier to further enhance hydrogen absorption.

In our previous result obtained by TDA [20], the amounts of absorbed hydrogen in nonground specimens immersed in 2.0 and 0.2% APF solutions for 120 h were approximately 900 and 300 mass ppm, respectively. However, these amounts of hydrogen obtained from TDA were average value over the entire specimen. In the present study, hence, the hydrogen concentration corresponding to the distance from the surface was evaluated from the immersed specimens ground surface. Fig. 2 shows the hydrogen distribution of the specimen immersed in 2.0 and 0.2% APF solutions for 120 h. The major portion of absorbed hydrogen existed within approximately 50 μm from the surface. Hydrogen hardly diffused toward the center of the specimen. The hydrogen contents within 20 μm from the surface of specimens immersed in 2.0

Table 1
Chemical compositions of tested alpha titanium and beta titanium alloy (mass%)

	Ti	C	H	O	N	Fe	Mo	Zr	Sn
Alpha titanium	Balance	0.003	0.0010	0.107	0.003	0.026	–	–	–
Beta titanium alloy	77.8	–	–	–	–	–	11.3	6.6	4.3

and 0.2% APF solutions were evaluated at approximately 5000 and 2000 mass ppm, respectively. The hydrogen distribution obtained by TDA is in accord with that obtained by the above-mentioned XRD measurement. It is likely that ab-

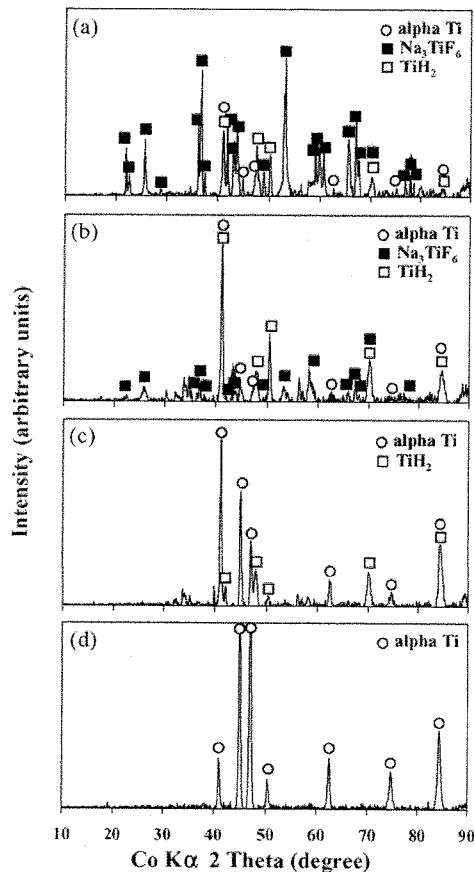


Fig. 1. XRD patterns of (a) nonground surface and surfaces ground to (b) 0.50 mm, (c) 0.45 mm and (d) 0.40 mm for alpha titanium specimens immersed in 2.0% APF solution for 120 h.

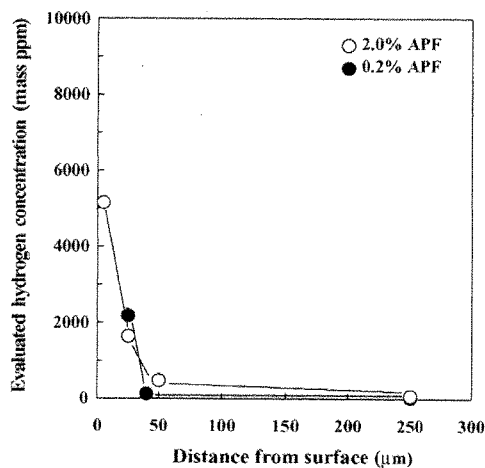


Fig. 2. Hydrogen concentration evaluated from TDA as function of distance from surface of alpha titanium specimens immersed in 2.0 and 0.2% APF solutions for 120 h.

sorbed hydrogen mostly existed in alpha titanium as titanium hydride.

Hydrogen thermal desorption curves from nonground and ground specimens immersed in 2.0% APF solution for 120 h is shown in Fig. 3(a). For nonground specimen, a primary desorption was observed ranging from 400 to 700 °C, and a secondary desorption also appeared at around 300 °C. The amount of primary desorption decreased with decreasing specimen diameter. Note that the peak temperature of the primary desorption shifted from 500 to 600 °C in the specimen diameter range 0.52 (nonground) to 0.45 mm and the secondary desorption disappeared for the diameter of less than 0.45 mm.

Although a wide temperature range of hydrogen thermal desorption suggests that there are different states of hydrogen in alpha titanium, we wish to focus on the effects of the hydride on the desorption behavior in the present study. On the basis of the titanium–hydrogen phase diagram [28], titanium hydride in alpha titanium dissociates at 300 °C. The hydride dissociation ranging from 100 to 300 °C was microscopically observed by McKinsey et al. [29], who reported that although the hydride dissociated partially after 1 h at 300 °C, the hydride dissociation occurred completely after 24 h at 300 °C or after 1 h at 400 °C. Takasaki et al. [3] also showed that from the results of high-temperature XRD analysis and DTA, the electrochemically formed titanium hydride dissociated up to 300 °C; however, hydrogen thermal desorption appeared ranging from 380 to 650 °C at a heating rate 300 °C/h. The reason for no hydrogen desorption during the dissociation process is considered to be that hydrogen atom diffused and/or dissolved into the specimen after hydride dissociation. In the present study, the thermal desorption behavior of 0.45 mm diameter specimen immersed in the 2.0% APF solution for 120 h almost agreed with that reported by Takasaki et al. [3]. Nevertheless, it should be noted that hydrogen desorption of nonground and 0.50-mm diameter specimens appeared at around 300 °C. Because hydrogen or hydride content of the surface layer of these specimens was very high as shown in Fig. 2, it appears that hydride dissociation did not finish completely at 300 °C at a heating rate of 100 °C/h. The remaining hydride probably inhibited hydrogen to diffuse toward the center of the specimen. Therefore, some hydrogen in the vicinity of the surface of the specimen desorbed from the specimen at around 300 °C. On the other hand, since the hydride layer of 0.45 mm diameter specimen was thin, it is likely that the hydride easily dissociated and hydrogen diffused to the center of the specimen after hydride dissociation; the desorption at around 300 °C was not observed.

Upon hydride formation, the matrix around the hydride is subjected to a large stress because of the large specific volume of the hydride; the stress appears to be accommodated either elastically or plastically [30]. That is, the hydride formation leads to defect nucleation in the matrix. For specimens containing hydride, i.e., nonground, 0.50- and 0.45-mm diameter specimens, hydrogen desorption at 600–700 °C is perhaps interpreted as hydrogen trapped strongly in

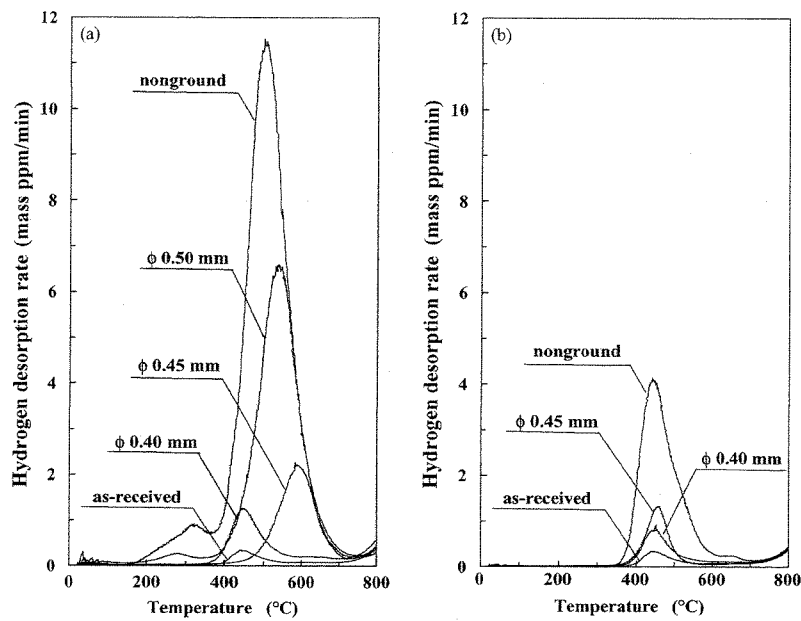


Fig. 3. Hydrogen thermal desorption curves from nonground or ground alpha titanium specimens immersed in (a) 2.0% and (b) 0.2% APF solutions for 120 h.

matrix defects. When hydrogen traps strongly in defects, hydrogen desorption often shifts to higher temperature [6]. In contrast, for specimens without hydride, i.e., as-received (nonimmersed) and 0.40-mm diameter specimens, the reason for no hydrogen desorption at 600–700 °C is probably due to the absence of such defects. The analysis of hydrogen desorption behavior at a high-temperature region may be essential for detecting defects in alpha titanium.

For the immersion in the 0.2% APF solution for 120 h (Fig. 3(b)), hydrogen desorption appeared with a single peak at approximately 450 °C irrespective of the specimen diameter. The diameter of the nonground specimen was 0.48 mm as a result of dissolution by corrosion or peeling of the surface layer [20]. For specimen containing hydride, i.e., nonground specimen, the desorption at a high temperature was observed, whereas for specimens without hydride, i.e., 0.45- and 0.40-mm diameter specimens, desorption at above 500 °C was hardly observed. These results are analogous to the case of that of specimens immersed in the 2.0% APF solution.

3.2. Beta titanium alloy

The diffusion constant of hydrogen in beta titanium at room temperature is of the order of 10^{-11} m²/s [31], which is sufficient that hydrogen diffuses from the surface to the center of the specimen, without taking into account the effects of hydrogen trapping. Our previous results [21] of Vickers microhardness measurements from the surface to the center of the specimen and fractography indicate that hydrogen diffuses toward the center of the beta titanium alloy immersed in APF solutions at room temperature. No hydride formation was detected on the surface of the beta titanium alloy immersed in APF solutions by XRD measurements.

Table 2

Diameter of beta titanium alloy specimens immersed in 2.0 and 0.2% APF solutions for various periods

Immersion time (h)	Diameter of specimen immersed in 2.0% APF solution (mm)	Diameter of specimen immersed in 0.2% APF solution (mm)
0	0.450 ± 0.0022	0.450 ± 0.0022
6	0.433 ± 0.0027	—
12	0.414 ± 0.0055	—
24	0.348 ± 0.0084	0.452 ± 0.0027
60	—	0.455 ± 0.0061
120	—	0.415 ± 0.0050
240	—	0.407 ± 0.0067

Standard deviation was calculated from five specimens.

Table 2 gives the diameters of specimens immersed in 2.0 and 0.2% APF solutions as functions of immersion time. The decrease in diameter is due to the peeling of the surface and dissolution by corrosion. The diameter of specimens immersed in the 0.2% APF solution up to 60 h slightly increased with the deposition of corrosion products on the surface of the specimen. The corrosion products on the surface of the specimen immersed in the 2.0% APF solution were Na₅Ti₃F₁₄ and Na₃TiF₆, while that in the 0.2% APF solution was TiF₃ [22].

Fig. 4 shows the evaluated distribution of hydrogen obtained by TDA of ground specimens immersed in the 2.0% APF solution for 24 h and the 0.2% APF solution for 60 h. The average contents of hydrogen in both specimens were approximately 4000 and 2500 mass ppm, respectively. In the immersion in the 2.0% APF solution for 24 h, hydrogen content at the surface of the specimen was much higher than that at the center of the specimen. The original surface in the range of 0–50 μm peeled and dissolved by corrosion in the 2.0%

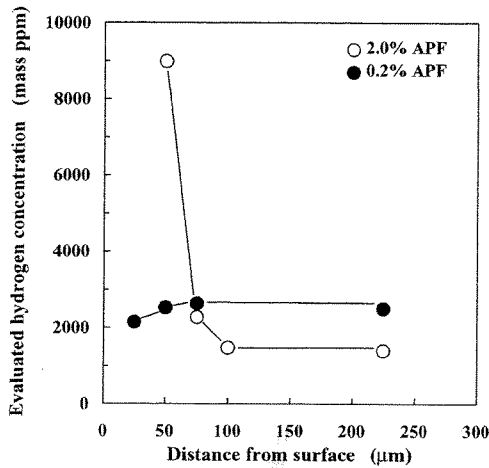


Fig. 4. Hydrogen concentration evaluated from TDA as function of distance from surface of beta titanium alloy specimens immersed in 2.0% APF solution for 24 h and 0.2% APF solution for 60 h.

APF solution. In the 0.2% APF solution for 60 h, hydrogen distributed uniformly in the center of the specimen. Because hydrogen absorption saturated due to the formation of corrosion products in the 0.2% APF solution after 48 h [22], it appears that hydrogen at the surface adequately diffused to the center of the specimen.

The hydrogen thermal desorption curves of nonground and ground specimens immersed in the 2.0% APF solution for 24 h are shown in Fig. 5(a). The desorption peak temperature slightly shifted to the lower side with decreasing specimen diameter. Fig. 5(b) shows the desorption curves from nonground and ground specimens immersed in the 0.2% APF solution for 60 h. The desorption behavior of ground

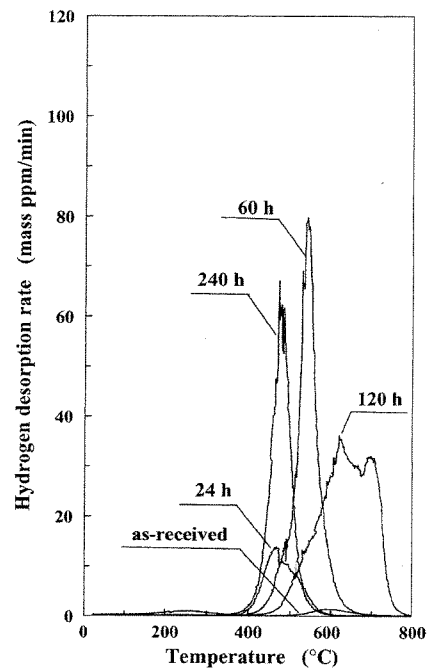


Fig. 6. Hydrogen thermal desorption curves for nonground beta titanium alloy specimens immersed in 0.2% APF solution for up to 240 h.

specimens hardly differed from the diameter. The desorption temperature range of the nonground specimen was higher than that of ground specimens. On carefully removing the corrosion product (TiF_3) from the surface of the nonground specimen, the desorption behavior became almost the same as that of the ground specimens. For Mg–Ni–H alloys [32], the oxide film on the surface of the specimen results in a peak

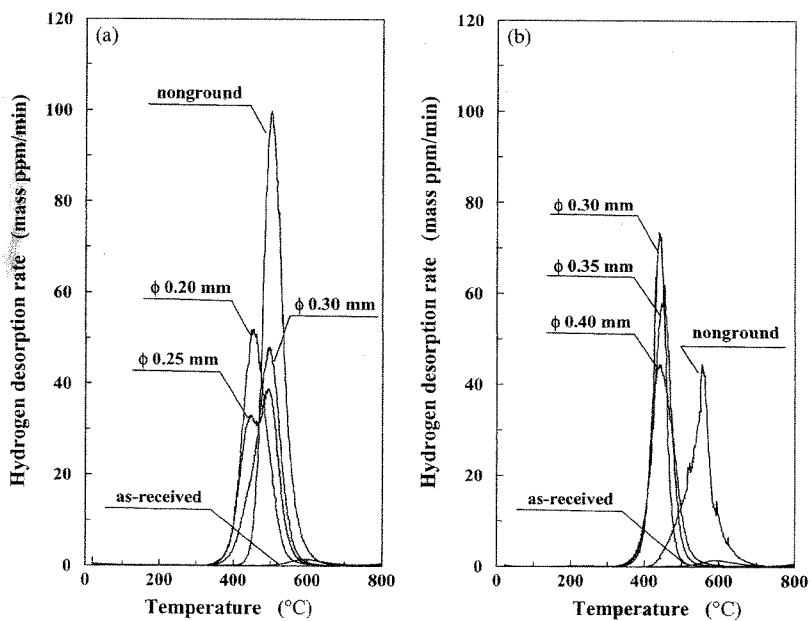


Fig. 5. Hydrogen thermal desorption curves for nonground or ground beta titanium alloy specimens immersed in 2.0% APF solution for 24 h and 0.2% APF solution for 60 h.

shift of hydrogen desorption to a higher temperature of more than 100 °C. Thus, it seems that this corrosion product on the surface of the specimen obstructed hydrogen desorption.

Changes in the desorption behavior of the nonground specimen immersed in the 0.2% APF solution for various periods (Fig. 6) are perhaps due to this corrosion product, since the product partially peeled off during not only the immersion test but also ultrasonic cleaning before TDA. In the case of the specimen immersed in the 2.0% APF solution, such effects of the corrosion products on the desorption behavior were small as shown in our previous article [22]. These results suggest that corrosion product conditions including type and distribution sometimes influence thermal desorption behavior. Consequently, it is likely that absorbed hydrogen in the beta titanium alloy distributed uniformly as in solution irrespective of hydrogen content.

In a separate experiment, we observed that the desorption behavior of alpha titanium and beta titanium alloy did not change when immersed specimens were maintained at room temperature for 1 month, suggesting that the absorbed hydrogen was mostly nondiffusive in nature. The effects of other states of hydrogen on the desorption behavior should be investigated in future studies.

4. Conclusions

Distribution and thermal desorption behavior of hydrogen in alpha titanium and beta titanium alloy immersed in 2.0 and 0.2% APF solutions have been examined. For alpha titanium, local hydrogen content in the vicinity of the surface of specimen is evaluated above 5000 mass ppm. Most of the absorbed hydrogen exists as titanium hydride within approximately 50 μm from the surface of the specimen. Hydrogen desorption at the lower temperature (200–300 °C) is attributable to the dissociation of the hydride. For the beta titanium alloy, hydrogen distribution is almost uniform over the whole of the specimen without hydride forming, although hydrogen content is high at the surface layer of the specimen. Hydrogen concentration and distribution influence the desorption behavior of alpha titanium, while it hardly influence that of beta titanium alloy. Corrosion products on the surface of the specimen sometimes strongly affect the desorption behavior.

Acknowledgements

This study was supported in part by a Grant-in-Aid for Young Scientists (B) (14771090) and a Grant-in-Aid for

Scientific Research (C) (15560632) from the Ministry of Education, Culture, Sports, Science and Technology, Japan.

References

- [1] W.Y. Choo, J.Y. Lee, *Metall. Trans. A* 13 (1982) 135.
- [2] K. Ono, M. Meshii, *Acta Metall. Mater.* 40 (1992) 1357.
- [3] A. Takasaki, Y. Furuya, K. Ojima, Y. Taneda, *J. Alloys Compd.* 224 (1995) 269.
- [4] A. Turnbull, R.B. Hutchings, D.H. Ferriss, *Mater. Sci. Eng. A* 238 (1997) 317.
- [5] S.W. Smith, J.R. Scully, *Metall. Mater. Trans. A* 31 (2000) 179.
- [6] M. Nagumo, M. Nakamura, K. Takai, *Metall. Mater. Trans. A* 32 (2001) 339.
- [7] K. Takai, R. Watanuki, *ISIJ Int.* 43 (2003) 520.
- [8] T. Nishiue, Y. Kaneno, H. Inoue, T. Takasugi, *J. Alloys Compd.* 364 (2004) 214.
- [9] M. Nagumo, *ISIJ Int.* 41 (2001) 590.
- [10] G.A. Lenning, C.M. Craighead, R.I. Jaffee, *Trans. AIME* 200 (1954) 367.
- [11] D.N. Williams, *J. Inst. Met.* 91 (1962) 147.
- [12] D.F. Teter, I.M. Robertson, H.K. Birnbaum, *Acta Mater.* 49 (2001) 4313.
- [13] J. Lausmaa, B. Kasemo, S. Hansson, *Biomaterials* 6 (1985) 23.
- [14] H.S. Siirilä, M. Könönen, *Int. J. Oral. Maxillofac. Implants* 6 (1991) 50.
- [15] M.H.O. Könönen, E.T. Lavonius, J.K. Kivilahti, *Dent. Mater.* 11 (1995) 269.
- [16] L. Reclaru, J.-M. Meyer, *Biomaterials* 19 (1998) 85.
- [17] M. Nakagawa, S. Matsuya, T. Shiraiishi, M. Ohta, *J. Dent. Res.* 78 (1999) 1568.
- [18] H.H. Huang, *Electrochim. Acta* 47 (2002) 2311.
- [19] K. Yokoyama, K. Kaneko, Y. Miyamoto, K. Asaoka, J. Sakai, M. Nagumo, *J. Biomed. Mater. Res. A* 68 (2004) 150.
- [20] K. Yokoyama, T. Ogawa, K. Asaoka, J. Sakai, *Mater. Sci. Eng. A* 384 (2004) 19.
- [21] K. Kaneko, K. Yokoyama, K. Moriyama, K. Asaoka, J. Sakai, M. Nagumo, *Biomaterials* 24 (2003) 2113.
- [22] T. Ogawa, K. Yokoyama, K. Asaoka, J. Sakai, *Biomaterials* 25 (2004) 2419.
- [23] K. Yokoyama, K. Kaneko, K. Moriyama, K. Asaoka, J. Sakai, M. Nagumo, *J. Biomed. Mater. Res. A* 65 (2003) 182.
- [24] K. Yokoyama, T. Ogawa, K. Asaoka, J. Sakai, M. Nagumo, *Mater. Sci. Eng. A* 360 (2003) 153.
- [25] T. Ogawa, K. Yokoyama, K. Asaoka, J. Sakai, *Mater. Sci. Eng. A* 393 (2005) 239.
- [26] I.I. Phillips, P. Poole, L.L. Shreir, *Corros. Sci.* 14 (1974) 533.
- [27] Z.F. Wang, C.L. Briant, K.S. Kumar, *Corrosion* 54 (1998) 553.
- [28] A.D. McQuillan, *Proc. R. Soc. A* 204 (1950) 309.
- [29] C.R. Mckinsey, M. Stern, R.A. Perkins, *Trans. ASM* 50 (1958) 438.
- [30] H. Numakura, M. Koiwa, *Acta Metall.* 32 (1984) 1799.
- [31] W.R. Holman, R.W. Crawford, F. Paredes Jr., *Trans. Met. Soc. AIME* 233 (1965) 1836.
- [32] M. Komaki, M. Amano, H. Numata, C. Nishimura, *J. Jpn. Inst. Met.* 62 (1998) 111.



Susceptibility to delayed fracture of alpha–beta titanium alloy in fluoride solutions

Ken'ichi Yokoyama^{a,*}, Toshio Ogawa^b,
Kenzo Asaoka^a, Jun'ichi Sakai^b

^a *Department of Dental Engineering, School of Dentistry, The University of Tokushima, 3-18-15
Kuramoto-cho, Tokushima 770-8504, Japan*

^b *Department of Materials Science and Engineering, Waseda University, 3-4-1 Okubo, Shinjuku-ku,
Tokyo 169-8555, Japan*

Received 31 March 2004; accepted 19 August 2004

Available online 22 October 2004

Abstract

The susceptibility to delayed fracture of the alpha–beta titanium alloy Ti–6Al–4V has been investigated in acidic and neutral fluoride solutions at room temperature. The time to fracture decreased with increasing applied stress in 2.0% and 0.2% acidulated phosphate fluoride (APF) solutions at pH 5.0. The time to fracture in the 2.0% APF solution was shorter than that in the 0.2% APF solution, although at an applied stress higher than 1000 MPa, the times to fracture were almost the same in both the solutions. For immersion in the 0.2% APF solution, when the applied stress was lower than 700 MPa, delayed fracture did not occur within 1000 h. The fracture surface of specimens immersed in the 2.0% APF solution exhibited brittleness associated with hydrogen absorption, while that in the 0.2% APF solution was ductile and characterized macroscopically as having a cup–cone morphology. The amounts of hydrogen absorbed in 2.0% and 0.2% APF solutions for 24 h were approximately 200 and 30 mass ppm, respectively. As the immersion time increased, the amount of hydrogen absorbed in the 2.0% APF solution increased, whereas that in the 0.2% APF solution hardly increased. In neutral 2.0% and 0.2% NaF solutions, the delayed fracture did not occur within 1000 h, although general corrosion was observed. These results indicate that the susceptibility to

* Corresponding author. Tel.: +81 88 633 7334; fax: +81 88 633 9125.

E-mail address: yokken@dent.tokushima-u.ac.jp (K. Yokoyama).

delayed fracture of alpha–beta titanium alloy, compared with those of the alpha titanium and beta titanium alloy reported previously, is low in acidic and neutral fluoride solutions.

© 2004 Elsevier Ltd. All rights reserved.

Keywords: Ti–6Al–4V alloy; Delayed fracture; Hydrogen embrittlement; Corrosion; Fluorides

1. Introduction

Alpha–beta titanium alloys such as Ti–6Al–4V and Ti–6Al–7Nb are used increasingly in biomedical applications because their mechanical properties are much better than those of pure titanium. Moreover, the alloys have a high corrosion resistance equivalent to pure titanium and good biocompatibility [1–6]. In the oral environment, however, the corrosion resistance of titanium and its alloys is not satisfactory [7]. In the presence of fluoride such as NaF, the corrosion resistances of titanium and its alloys are markedly reduced [8–25]. A concentration of 0.2–2.0% NaF is present in commercial toothpastes and prophylactic agents for caries prevention. It has been reported that discoloration of titanium occurs even when a small amount of fluoride is released from glass ionomer cements [26].

In addition, titanium devices sometimes fracture in the oral cavity after a long period of use [27–31]. The mechanism of the fracture of titanium devices has several complicated causes. The authors of this paper have recently insisted that one of the causes of fracture is the degradation of the mechanical properties associated with hydrogen absorbed in a biological environment [32–41]. Hydrogen absorption may result from the breakdown of a passive film on the surface of titanium and its alloys. Commercial pure titanium, i.e., alpha titanium [38,39], and beta titanium alloy [40,41] absorb substantial amounts of hydrogen from acidic fluoride solutions, thereby causing pronounced degradation of their mechanical properties. Because hydrogen embrittlement of alpha–beta titanium alloys is an important issue from the industrial point of view, it has been extensively investigated by cathodic hydrogen charging or exposure to gaseous hydrogen [42–49]. When the hydrogen content exceeds a few hundreds mass ppm, the mechanical properties of the alloys degrade. However, no data exist for the hydrogen embrittlement of alpha–beta titanium alloys in fluoride solutions. Furthermore, the hydrogen embrittlement characteristic of alpha–beta titanium alloys does not always agree with those of alpha titanium and beta titanium alloys. It is therefore necessary to confirm experimentally whether hydrogen embrittlement of the alloys occurs in fluoride solutions. The understanding of hydrogen absorption behavior is necessary for the prevention and control of fracture in titanium devices.

The objective of this study is to examine the hydrogen embrittlement of alpha–beta titanium alloy in fluoride solutions by hydrogen thermal desorption analysis (TDA). For the evaluation of the susceptibility to hydrogen embrittlement, a delayed-fracture test was conducted. This article focuses on comparing the delayed fracture properties in the fluoride solutions of the alpha–beta titanium alloy with those of the alpha titanium [38,39] and beta titanium alloy [40,41] reported previously.

2. Experimental procedures

2.1. Materials

Commercial Ti–6Al–4V alloy wire with a diameter of 0.50 mm was cut into specimens 150 mm in length. The nominal chemical composition is given in Table 1. The specimens were polished with 600-grit SiC paper and ultrasonically cleaned in acetone for 5 min. To measure mechanical properties, tensile tests were performed at room temperature (25 ± 2 °C) using an Instron-type machine (Autograph AG-100A, Shimadzu) at a strain rate of $8.33 \times 10^{-4} \text{ s}^{-1}$. The yield strength, i.e., 0.2% proof strength, and tensile strength were 993 and 1356 MPa, respectively. Hardness tests were carried out on the transverse cross-section using a Vickers microhardness tester under an applied load of 0.98 N for 15 s. The mechanical properties of the specimens are summarized in Table 2. The standard deviation was calculated from the results for more than five specimens.

2.2. Delayed fracture test

The delayed fracture test, i.e., a sustained tensile-loading test in solution, was carried out at room temperature. The applied stress was calculated as the ratio of the applied load to the initial cross-sectional area and was varied to determine the fracture life characteristics. The immersion length of each specimen in a solution was 50 mm and the time to fracture of the specimens was determined. The test was terminated when no delayed fracture occurred after more than 1000 h. The test solutions used were 50 ml each of aqueous solutions of 2.0% or 0.2% acidulated phosphate fluoride (APF; 2.0% NaF + 1.7% H_3PO_4 or 0.2% NaF + 0.17% H_3PO_4) at pH 5.0, and 2.0% or 0.2% NaF at pH 6.5. Percent in this paper means mass percent unless otherwise stated. Immediately after fracture, the specimens were taken from the solution, cleaned with acetone and dried in ambient air. The fracture surface and side surface of the delayed-fracture-tested specimens were examined by scanning electron microscopy (SEM). The corrosion products on the surface of the immersed specimens and the surfaces after removal of the corrosion products were examined using an X-ray diffractometer with Cu K_α radiation of wavelength $\lambda = 1.54056 \text{ \AA}$ in the 2θ

Table 1
Chemical composition of the Ti–6Al–4V alloy (mass %)

Ti	Al	V	Fe	C	N	O	H
Balance	6.22	4.1	0.22	0.01	0.01	0.18	0.0011

Table 2
Mechanical properties of the Ti–6Al–4V alloy

Yield strength (MPa)	Tensile strength (MPa)	Reduction in area (%)	Vickers microhardness (Hv)
993 ± 38	1356 ± 10	21.9 ± 4.7	337 ± 16

angle range from 10 to 90° with a 2°/min sweep rate operated at 40 kV and 30 mA. The corrosion products were carefully removed from the surface of the immersed specimens using 600-grit SiC paper.

2.3. Thermal desorption analysis

The amount of desorbed hydrogen was measured by TDA for specimens subjected to the delayed-fracture test without loading for various periods. Specimens (50 mm in length) immersed in the solution were cut into 20-mm-long segments and subjected to ultrasonic cleaning with acetone for 2 min. Each segment was dried in ambient air and measured. TDA was started 30 min after the removal of a specimen from a solution. A quadrupole mass spectrometer (ULVAC, Kanagawa, Japan) was used to detect hydrogen. Sampling was conducted at 30-s intervals at a heating rate of 100 °C/h.

3. Experimental results

The delayed-fracture test results are shown in Fig. 1 in terms of the time to fracture as a function of applied stress. The arrows in the figure denote a non-fractured specimen at the elapsed time indicated. The time to fracture decreased with increasing applied stress in APF solutions. In the applied stress range higher than 1000 MPa, the time to fracture in the 0.2% APF solution was almost the same as that in the 2.0% APF solution, although the data points were scattered widely in the 0.2% APF solution. In the 0.2% APF solution, no delayed fracture

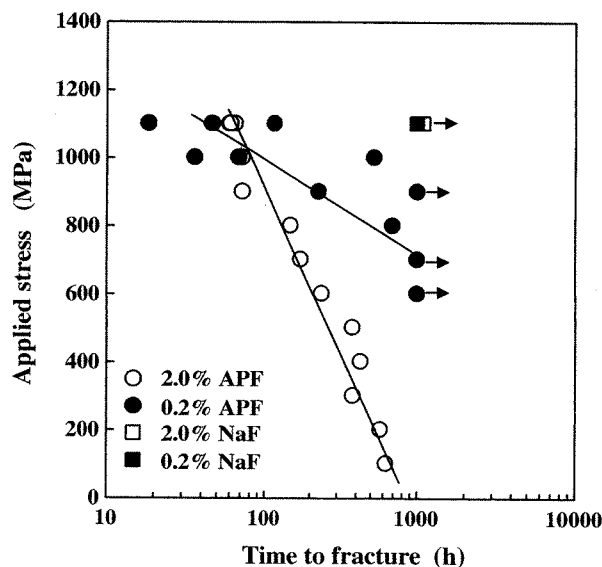


Fig. 1. Plot of time to fracture versus initial applied stress for alpha–beta titanium alloy immersed in APF and NaF solutions.

occurred within 1000 h when the applied stress was lower than 700 MPa. In this experiment, crevice corrosion appeared neither at the contact point of the specimen with the vessel nor in the vicinity of the water plane in both solutions. In the neutral 2.0% and 0.2% NaF solutions, no delayed fracture occurred within the stress range tested, although the surface of each specimen became discolored or corroded after the test.

The fractographs of the specimen fractured by a tensile test in air are shown in Fig. 2. The reduction in area was 21.9%. The fracture surface was relatively ductile and was characterized macroscopically as having a cup–cone morphology (Fig. 2(a)) and microscopically as having small dimples in the central part of the surface (Fig. 2(b)) and shear dimples in the peripheral part of the surface (Fig. 2(c)). On the other hand, Figs. 3(a)–(c) show the fractographs of the specimen in the 2.0% APF solution under an applied stress of 1000 MPa for 72 h. The fracture surface was classified into two areas, namely, a fracture initiation area (Fig. 3(b)) and a crack propagation area in the central part of the surface (Fig. 3(c)). The fracture initiation point could be identified by tracing back the riverlike flows, and the topography of the fracture initiation area was fairly flat. The fracture initiation point was always in the vicinity of the surface followed by radial crack propagation. The feature of the initiation area became clearer with immersion time. For instance, the initiation area fractured in the 2.0% APF solution under an applied stress of 400 MPa for 428 h is shown in Fig. 3(d). The crack propagation area in the central part of the surface appeared as a rough profile, but it hardly exhibited any features of a ductile fracture mode such as dimple morphology. Figs. 4(a)–(c) show the fractographs of the specimen in the 0.2% APF solution under an applied stress of 1000 MPa for 68 h. The fracture surface was characterized macroscopically as having a cup–cone morphology and microscopically as having small dimples and shear dimples. These features of fracture surface in the 0.2% APF solution were observed for all applied stresses and were similar to those observed in tensile tests in air rather than those in the 2.0% APF solution.

On the side surface of specimens before the delayed fracture test, scratches due to SiC paper polishing were observed, as shown in the SEM images in Figs. 5(a) and (b). The side surface of the specimen fractured in the 2.0% APF solution under the applied stress of 1000 MPa for 72 h is shown in Figs. 5(c) and (d). General corrosion and the formation of corrosion products were observed on the surface of the specimens immersed in the 2.0% APF solution, regardless of the time to fracture. Figs. 5(e) and (f) show the side surface of a specimen fractured in the 0.2% APF solution under the applied stress of 1000 MPa for 68 h; the fractured specimens exhibit a microscopically relatively smooth surface, but macroscopically a significantly rougher surface. The scratches on the surface disappeared due to general corrosion, and peeling of the corrosion products was revealed in both APF solutions. The topography of the side surface immersed in the 0.2% APF solution was different from that in the 2.0% APF solution. In the 2.0% NaF solution, the side surface of the delayed-fracture-tested specimen under an applied stress of 1100 MPa, which did not fracture until 1000 h, is shown in Figs. 5(g) and (h). For the specimens tested in NaF

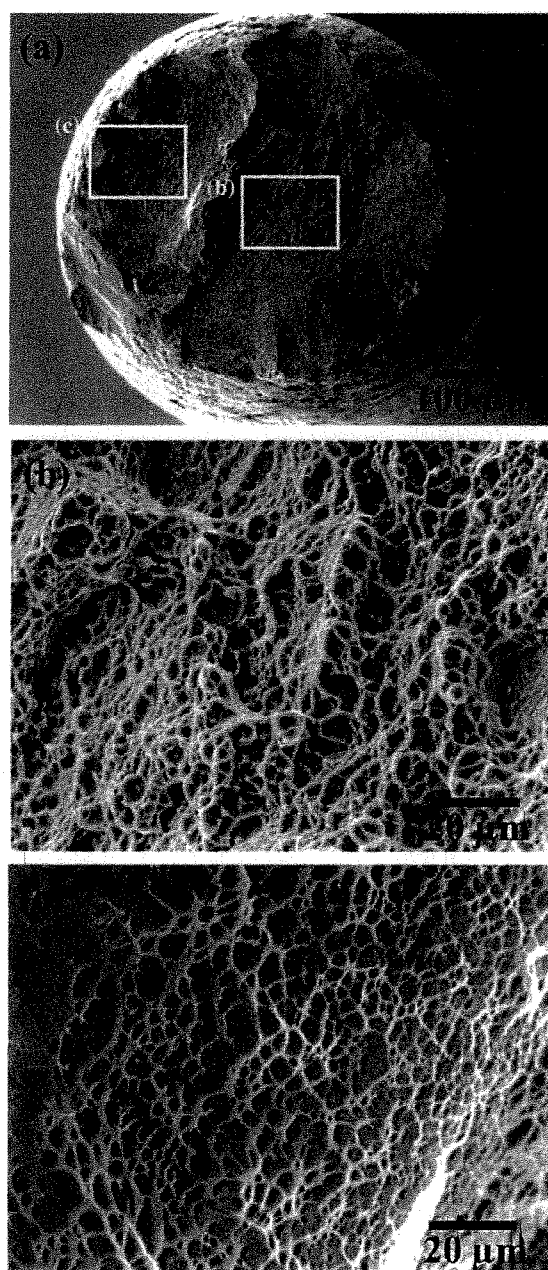


Fig. 2. SEM images of a typical fracture surface after the tensile test in air: (a) general view, (b) dimple area in the center of the specimen, and (c) shear dimple area in the peripheral part of the specimen.

solutions, the scratches from SiC paper polishing disappeared as a result of the general corrosion.

The X-ray diffraction (XRD) pattern of the side surface of the nonimmersed specimen is shown in Fig. 6(a). Similarly, the XRD patterns of specimens immersed in 2.0% and 0.2% APF solutions for 24 h are shown in Figs. 6(b) and (c), respectively. Sodium titanium fluoride, Na_3TiF_6 (monoclinic; $a = 0.5543$ nm, $b = 0.5748$ nm, $c = 0.8002$ nm, $\beta = 90.29^\circ$), was confirmed on the surface of the specimen immersed in the 2.0% APF solutions. For the specimen immersed in

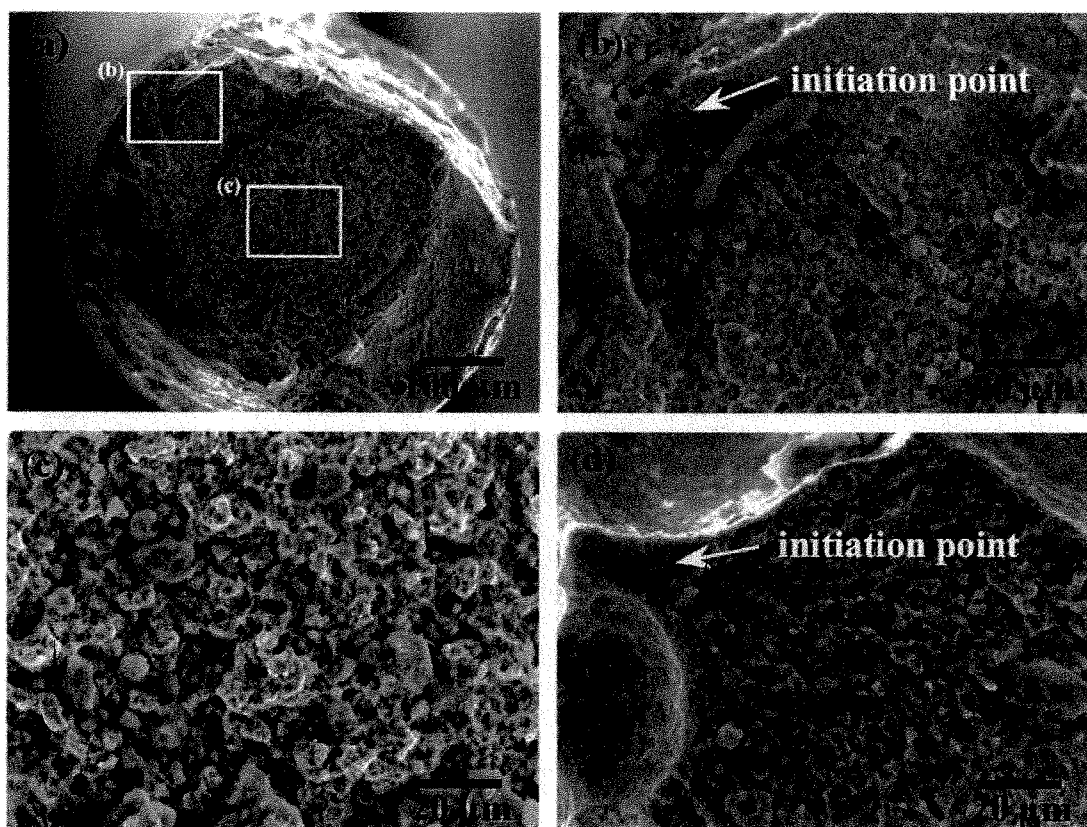


Fig. 3. SEM images of the delayed fracture surface under an applied stress of 1000 MPa in 2.0% APF solution: (a) general view, (b) fracture initiation site, and (c) crack propagation area. (d) Fracture initiation site of the delayed fracture surface under an applied stress of 400 MPa in 2.0% APF solution.

the 0.2% APF solution, sodium aluminum fluoride, Na_3AlF_6 (monoclinic; $a = 0.7769$ nm, $b = 0.5593$ nm, $c = 0.5404$ nm, $\beta = 90.18^\circ$) was detected. Figs. 6(d) and (e) show the XRD patterns of the specimens immersed in the 2.0% APF solution for 480 h before and after the removal of their surface layers, respectively; titanium hydride, $\gamma\text{-TiH}$ (tetragonal; $a = 0.4199$ nm, $c = 0.4576$ nm), was identified. The hydride was detected on the specimen immersed in the 2.0% APF solution for more than 480 h.

Fig. 7 shows typical hydrogen thermal-desorption curves for the nonimmersed specimen and specimens immersed in the 2.0% APF solution for various periods without applied stress. After immersion in the 2.0% APF solution, the desorption curves exhibited a single desorption peak at approximately 550 °C; the desorption temperature ranged from 400 to 700 °C. The progress of hydrogen entry into the alloy was indicated by increased peak intensity relative to immersion time. The total amounts of hydrogen desorbed up to 800 °C for the specimens immersed in 2.0% and 0.2% APF solutions are shown as functions of immersion time in Fig. 8. For the nonimmersed specimen, the amount of desorbed hydrogen, i.e., the concentration of predissolved hydrogen, was 96 mass ppm. Thus, the amount of hydrogen absorbed during the immersion test was calculated by

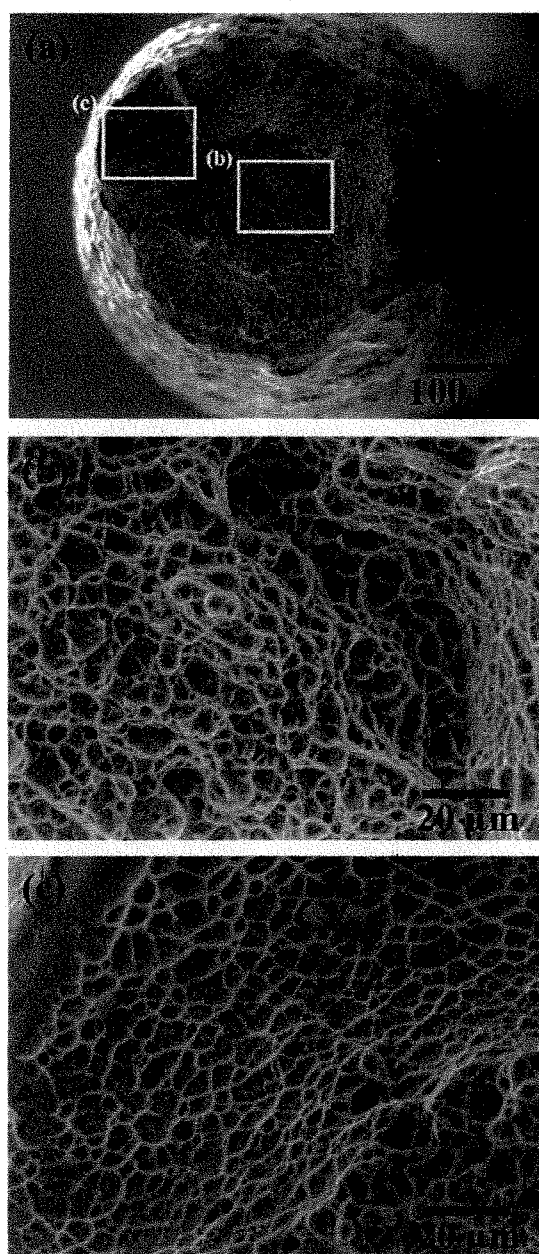


Fig. 4. SEM images of the delayed-fracture surface under an applied stress of 1000 MPa in 0.2% APF solution: (a) general view, (b) small dimple area in the center of the specimen, and (c) shear dimple area in the peripheral part of the specimen.

subtracting the predissolved hydrogen content from the amount of desorbed hydrogen. For specimens immersed in the 2.0% APF solution, the amount of absorbed hydrogen increased with immersion time, and particularly at the later stage of immersion, the hydrogen absorption was enhanced. The amounts of absorbed hydrogen for 24 and 600 h were approximately 200 and 9000 mass ppm, respectively. In contrast, the amount of hydrogen absorbed in the 0.2% APF solution barely increased with immersion time. The amounts of hydrogen

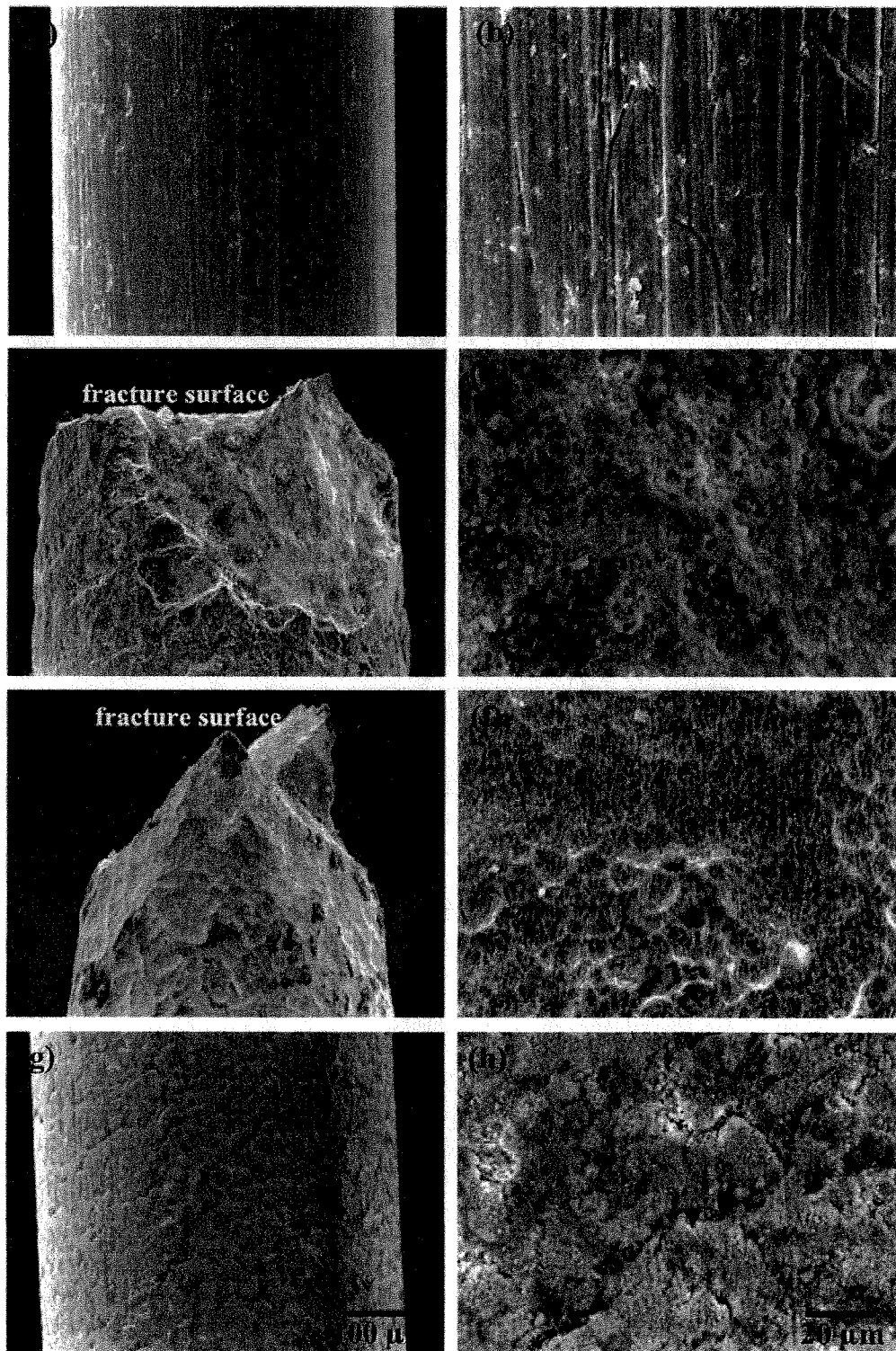


Fig. 5. SEM images of a typical side surface before delayed-fracture test: (a) general and (b) magnified views; after delayed-fracture test under an applied stress of 1000 MPa in 2.0% APF solution for 72 h: (c) general and (d) magnified views; under an applied stress of 1000 MPa in 0.2% APF solution for 68 h: (e) general and (f) magnified views; and under an applied stress of 1100 MPa in 2.0% NaF solution for 1000 h: (g) general and (h) magnified views.

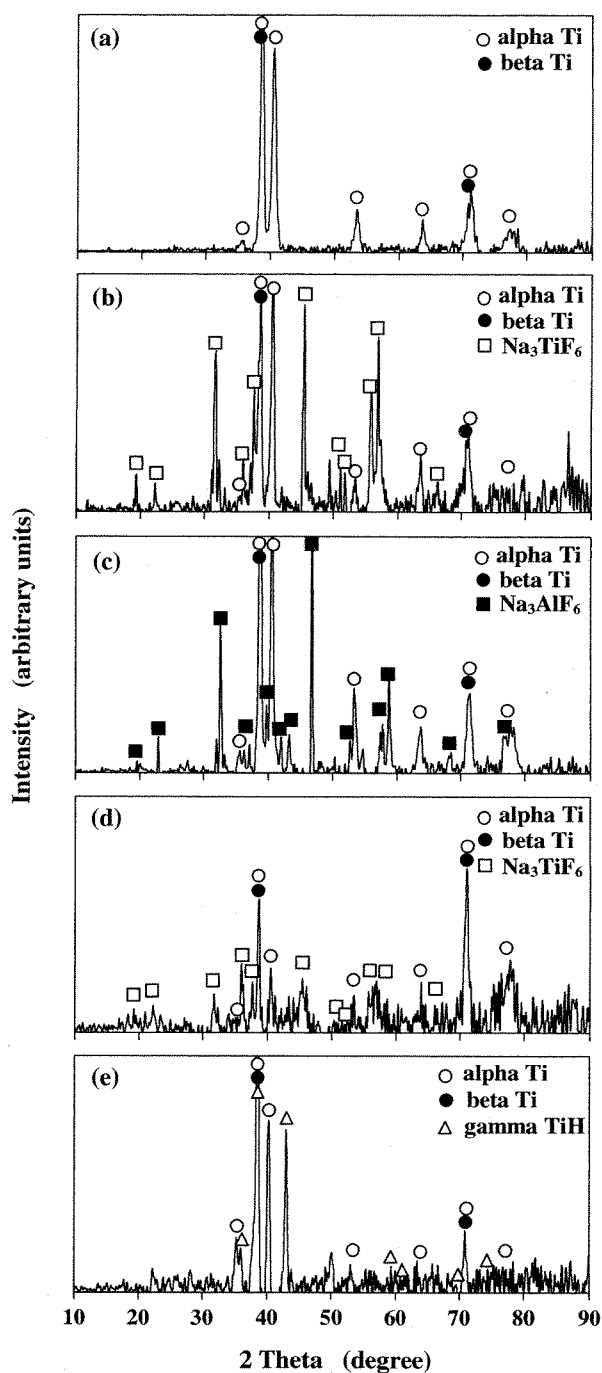


Fig. 6. XRD patterns for the surface of (a) a nonimmersed specimen, (b) a specimen immersed in 2.0% APF solution for 24 h, (c) a specimen immersed in 0.2% APF solution for 24 h, (d) before and (e) after removal of corrosion products from the surface of specimens immersed in 2.0% APF solution for 480 h.

absorbed for 24 and 600 h were approximately 30 and 50 mass ppm, respectively; they were considerably less than those in the 2.0% APF solution. In the case of the specimens immersed in the NaF solutions, the increment in hydrogen desorption was negligible.

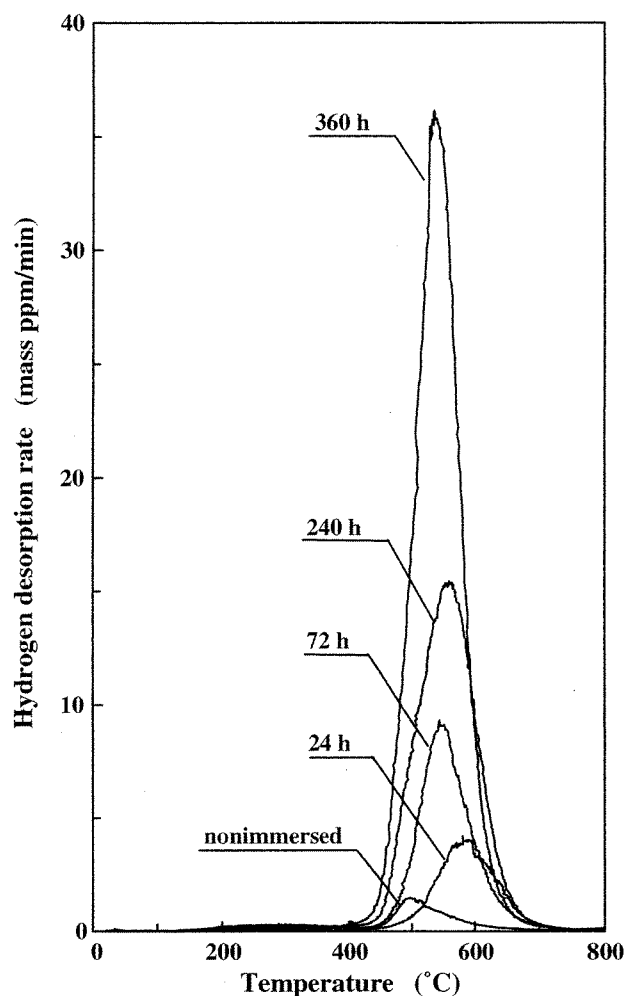


Fig. 7. Hydrogen thermal desorption curves from specimens immersed in 2.0% APF solution without applied stress for various periods.

4. Discussion

One noteworthy finding in this study is that the delayed fracture of alpha–beta titanium alloy occurs in association with hydrogen absorption in APF solutions, which is similar to that of our previous studies of alpha titanium, i.e., commercial pure titanium [38,39], and beta titanium alloy [40,41]. Hence, we mainly compare these results with others in the literature.

The time to fracture of the alpha–beta titanium alloy was longer than those of the previously tested alpha titanium [38] and beta titanium alloy [40] under the same applied stress in the 2.0% APF solution. For instance, in the case of an applied stress of 600 MPa, the times to fracture of alpha titanium [38], and the beta titanium [40] and alpha–beta titanium alloys were approximately 16, 35 and 240 h, respectively. The time to fracture of the alpha–beta titanium alloy was 60–70 h even under an applied stress greater than the yield strength. It is likely that the susceptibility to

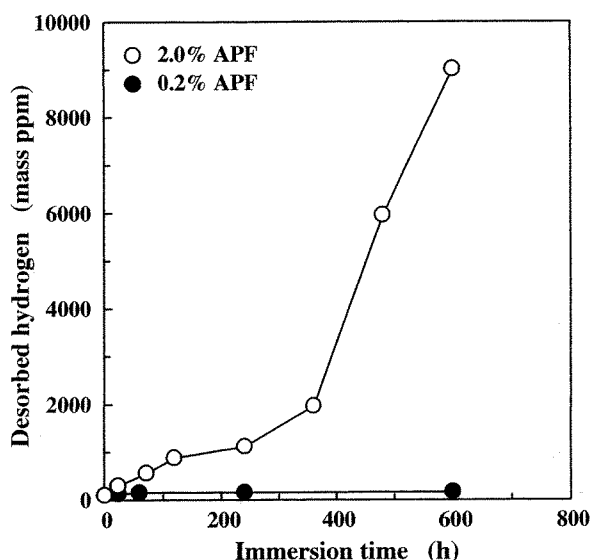


Fig. 8. Amounts of desorbed hydrogen from thermal desorption analysis of specimens immersed in 2.0% and 0.2% APF solutions as a function of immersion time.

delayed fracture in the 2.0% APF solution of the alpha–beta titanium alloy is lower than those of alpha titanium and the beta titanium alloy.

The amounts of absorbed hydrogen in alpha titanium [39], and the beta titanium [41] and alpha–beta titanium alloys were approximately 200, 3800 and 200 mass ppm, respectively, in the 2.0% APF solution for 24 h without applied stress. The mechanical properties of alpha–beta titanium alloys begin to degrade when the amount of absorbed hydrogen exceeds a few hundreds mass ppm [42–49]. Furthermore, the mechanical properties are markedly weakened due to hydrogen absorption of a few thousands mass ppm. In this experiment, the amount of hydrogen absorbed from the 2.0% APF solution at longer immersion times was sufficient to lead to the pronounced degradation of mechanical properties. In fact, the ductility loss of specimens tested in the 2.0% APF solution was revealed from the results of fractography shown in Fig. 3. Since applied stress generally enhances hydrogen absorption [41], the amount of hydrogen absorbed under applied stress is probably larger than that observed in this study. Consequently, the delayed fracture in the 2.0% APF solution of the alpha–beta titanium alloy is attributed to hydrogen embrittlement.

Various mechanisms have been proposed for hydrogen embrittlement of alpha–beta titanium alloys [50–53]. One of the mechanisms is that a brittle hydride forms and cracks. The formation of the hydride results in the compression of the surrounding titanium lattice and is considered to play an important role in the fracture of titanium alloys [54–59]. The hydride precipitates at boundaries between the alpha and beta phases and inside the alpha phase, when alpha–beta titanium alloys absorb hydrogen at a level greater than 650 mass ppm [42]. At low hydrogen levels, hydrogen is concentrated primarily in the beta phase [42]. However, no conclusive evidence has been given that supports the occurrence of hydrogen embrittlement due to hydride formation. For beta titanium alloys, the hydride is not formed by hydrogen

absorption, because the alloys have a high solubility limit. When the amount of absorbed hydrogen exceeds several thousands mass ppm, the tensile strength of beta titanium alloy decreases abruptly below the initial yield strength [60–66]. This phenomenon is often explained by hydrogen-enhanced dislocation mobility [53] or hydrogen-induced decohesion [51]. In addition, hydrogen absorption causes the ductile-to-brittle transition temperature of beta titanium alloys to rise above room temperature [66]. As shown in Fig. 6(e), the hydride was detected by XRD measurements for the alpha–beta titanium alloy immersed in the 2.0% APF solution, when the immersion time exceeded 480 h, which corresponded to the rapid increase in hydrogen absorption. It appears that the hydride did not form to any appreciable extent during the early stage of immersion. Therefore, the effects of the hydride on hydrogen embrittlement of alpha–beta titanium alloy are perhaps small in this delayed fracture test. At room temperature, hydrogen readily diffuses in beta titanium alloys, while hydrogen diffusion is prevented in alpha titanium because of hydride formation [57]. As shown in Fig. 3(c), the fracture mode of the alpha–beta titanium alloy changed over the entire fracture surface, indicating that the absorbed hydrogen diffused to the central parts of the specimen. Since hydrogen is preferentially absorbed in the beta phase of the alpha–beta titanium alloy [42], hydrogen might be able to diffuse to the central parts of the specimen. Thus, the mechanism of hydrogen embrittlement of alpha–beta titanium alloys involves those of alpha titanium and beta titanium alloys in a complicated manner. The operating mechanism may differ in accordance with the microstructures of alloys, environmental conditions and testing methods, but a detailed discussion is beyond the scope of this study.

The thermal desorption of hydrogen from alpha titanium immersed in 2.0% APF solution [38,39] takes place with the primary desorption at 400–700 °C and the secondary desorption at 150–400 °C. As the immersion time increases, the amount of absorbed hydrogen in alpha titanium increases linearly and saturates at approximately 800–900 mass ppm. For the beta titanium alloy immersed in 2.0% APF solution [41], a single desorption peak appears at 400–700 °C; the amount of absorbed hydrogen linearly increased above 10000 mass ppm with immersion time. The hydrogen desorption from the alpha–beta titanium alloy immersed in the 2.0% APF solution appeared in the range from 400 to 700 °C as shown in Fig. 7, implying that hydrogen is trapped strongly or is occluded. The desorption temperature and the amount of desorption give important clues to the states of hydrogen in materials, such as the relative strength of the forces trapping it in defects, or its presence in atomic/molecular form or as a hydride [67–71]. Concerning hydrogen desorption from titanium alloys immersed in the APF solutions, our results will be reported separately. With regard to hydrogen absorption, it is notable that hydrogen absorption of the alpha–beta titanium alloy accelerates at the later stage of immersion.

In the 0.2% APF solution for 24 h, the amounts of absorbed hydrogen in alpha titanium [39], and the beta titanium [41] and alpha–beta titanium alloys were approximately 200, 500 and 30 mass ppm, respectively. For the alpha–beta titanium alloy immersed in 0.2% APF solution, the amount of absorbed hydrogen was an order of magnitude smaller than those for alpha titanium and the beta titanium alloy and increased minimally with immersion time. This result suggests that the amount

of absorbed hydrogen is not sufficient to lead to the pronounced degradation of the mechanical properties of the alpha–beta titanium alloy. As shown in Fig. 5, the decrease in the diameter of immersed specimens resulted from the peeling of the surface layers and dissolution in APF solutions. The peeling of the surface layers is due to the formation of corrosion products. The passive film on titanium and its alloys undergoes a reaction in fluoride solutions, resulting in the formation of titanium fluoride, titanium oxide fluoride, or sodium titanium fluoride on the surface of the alloys [8–26]. Huang [24] detected sodium titanium fluoride, i.e., Na_2TiF_6 , on the Ti–6Al–4V alloy surface after applying a potential of 0 V versus a saturated calomel electrode, which is a passive region in the 0.1% NaF-containing media for X-ray photoelectron spectrometry. In this study, on the basis of XRD measurements and the observation of side surfaces, the corrosion products on the surfaces of the specimens differed between 2.0% and 0.2% APF solutions in both type and morphology. The differences in the type and morphology of the corrosion products related to the concentration of the APF solution are also observed for alpha titanium [39] and the beta titanium alloy [41]. Relationships between the APF solution content and the corrosion products, and the effects of the corrosion products on the peeling of the surface layers should be investigated. In addition to the peeling of the surface layers, the fracture surface in the 0.2% APF solution exhibited a cup–cone morphology similar to that in the tensile test in air. Accordingly, the primary cause of the delayed fracture in the 0.2% APF solution is probably the reduction in cross-sectional area, although the degradation of mechanical properties associated with hydrogen absorption is not excluded.

Under the delayed fracture test in neutral 2.0% NaF solution in our previous studies, the alpha titanium fractured [38], whereas the beta titanium alloy did not fracture within 1000 h [40]. In this experiment, the alpha–beta titanium alloy did not fracture in neutral NaF solutions within 1000 h. However, it should be noted that general corrosion was observed on the surface of specimens tested in neutral NaF solutions as shown in Figs. 5(g) and (h). This result suggests that the delayed fracture of the alpha–beta titanium alloy possibly occurs in neutral NaF solutions after longer immersion times.

5. Conclusions

The fracture of alpha–beta titanium alloy has been examined in a sustained tensile-loaded test in acid and neutral fluoride solutions from the viewpoint of hydrogen embrittlement. Delayed fracture occurs in 2.0% and 0.2% APF solutions, whereas it does not occur within 1000 h in neutral NaF solutions, in which general corrosion is observed. In the 2.0% APF solution, the alloy absorbs sufficient amounts of hydrogen, leading to a pronounced degradation in mechanical properties. In the 0.2% APF solution, the amount of absorbed hydrogen is 30–50 mass ppm; delayed fracture is mainly caused by the reduction in cross-sectional area due to peeling of the corrosion products. The time to fracture of alpha–beta titanium alloy is much longer than those of the alpha titanium and beta titanium alloy tested previously under the same

applied stress in 2.0% APF solution. We conclude that the susceptibility to delayed fracture of alpha–beta titanium alloy is lower than that of alpha titanium and beta titanium alloy in acid and neutral fluoride solutions.

Acknowledgments

The authors thank Mr. K. Kaneko for assistance with the experiments. This study was supported in part by a Grant-in-Aid for Young Scientists (B) (14771090) from the Ministry of Education, Culture, Sports, Science and Technology, Japan.

References

- [1] R.J. Solar, S.R. Pollack, E. Korostoff, *J. Biomed. Mater. Res.* 13 (1979) 217–250.
- [2] M. Pourbaix, *Biomaterials* 5 (1984) 122–134.
- [3] M.A. Khan, R.L. Williams, D.F. Williams, *Biomaterials* 17 (1996) 2117–2126.
- [4] Y. Okazaki, S. Rao, T. Tateishi, Y. Ito, *Mater. Sci. Eng. A* 243 (1998) 250–256.
- [5] M.A. Khan, R.L. Williams, D.F. Williams, *Biomaterials* 20 (1999) 631–637.
- [6] M. Aziz-Kerrzo, K.G. Conroy, A.M. Fenelon, S.T. Farrell, C.B. Breslin, *Biomaterials* 22 (2001) 1531–1539.
- [7] A.J. Sutton, P.M. Rogers, *J. Prosthodont.* 10 (2001) 102–104.
- [8] J. Lausmaa, B. Kasemo, S. Hansson, *Biomaterials* 6 (1985) 23–27.
- [9] H.S. Siirilä, M. Könönen, *Int. J. Oral Maxillofac. Implants* 6 (1991) 50–54.
- [10] L. Pröbster, W. Lin, H. Hüttemann, *Int. J. Oral Maxillofac. Implants* 7 (1992) 390–394.
- [11] B.I. Johansson, B. Bergman, *Dent. Mater.* 11 (1995) 41–46.
- [12] M.H.O. Könönen, E.T. Lavonius, J.K. Kivilahti, *Dent. Mater.* 11 (1995) 269–272.
- [13] G. Boere, *J. Appl. Biomater.* 6 (1995) 283–288.
- [14] F. Toumelin-Chemla, F. Rouelle, G. Burdairon, *J. Dentistry* 24 (1996) 109–115.
- [15] H. Mimura, Y. Miyagawa, *Jpn. J. Dent. Mater. Dev.* 15 (1996) 283–295.
- [16] Y. Oda, E. Kawada, M. Yoshinari, K. Hasegawa K, T. Okabe, *Jpn. J. Dent. Mater. Dev.* 15 (1996) 317–322.
- [17] L. Reclaru, J.-M. Meyer, *Biomaterials* 19 (1998) 85–92.
- [18] M. Nakagawa, S. Matsuya, T. Shiraishi, M. Ohta, *J. Dent. Res.* 78 (1999) 1568–1572.
- [19] M. Nakagawa, S. Matsuya, K. Udoh, *Dent. Mater. J.* 20 (2001) 305–314.
- [20] M. Nakagawa, S. Matsuya, K. Udoh, *Dent. Mater. J.* 21 (2002) 83–92.
- [21] H.-H. Huang, *Biomaterials* 23 (2002) 59–63.
- [22] H.-H. Huang, *Electrochim. Acta* 47 (2002) 2311–2318.
- [23] N. Schiff, B. Grosgeat, M. Lissac, F. Dalard, *Biomaterials* 23 (2002) 1995–2002.
- [24] H.-H. Huang, *Biomaterials* 24 (2003) 275–282.
- [25] K. Ide, M. Hattori, M. Yoshinari, E. Kawada, Y. Oda, *Dent. Mater. J.* 22 (2003) 359–370.
- [26] N. Horasawa, M. Marek, *J. Dent. Res.* 80 (2001) 546 (abstract no. 0153).
- [27] A. Piattelli, A. Scarano, M. Piattelli, E. Vaia, S. Matarasso, *J. Periodontol.* 69 (1998) 185–189.
- [28] M.J. Morgan, D.F. James, R.M. Pilliar, *Int. J. Oral Maxillofac. Implants.* 8 (1993) 409–414.
- [29] A. Piattelli, M. Piattelli, A. Scarano, L. Montesani, *Int. J. Oral Maxillofac. Implants.* 13 (1998) 561–564.
- [30] A. Piattelli, A. Scarano, M. Piattelli, E. Vaia, S. Matarasso, *Biomaterials* 20 (1999) 485–489.
- [31] K. Yokoyama, T. Ichikawa, H. Murakami, Y. Miyamoto, K. Asaoka, *Biomaterials* 23 (2002) 2459–2465.
- [32] K. Yokoyama, K. Hamada, K. Asaoka, *Mater. Trans.* 42 (2001) 141–144.
- [33] K. Yokoyama, K. Hamada, K. Moriyama, K. Asaoka, *Biomaterials* 22 (2001) 2257–2262.

- [34] K. Asaoka, K. Yokoyama, M. Nagumo, *Metall. Mater. Trans. A* 33A (2002) 495–501.
- [35] K. Yokoyama, K. Kaneko, K. Moriyama, K. Asaoka, J. Sakai, M. Nagumo, *J. Biomed. Mater. Res.* 65A (2003) 182–187.
- [36] K. Kaneko, K. Yokoyama, K. Moriyama, K. Asaoka, J. Sakai, *Angle Orthod.* 74 (2004) 487–495.
- [37] K. Yokoyama, K. Kaneko, K. Moriyama, K. Asaoka, J. Sakai, M. Nagumo, *J. Biomed. Mater. Res.* 69A (2004) 105–113.
- [38] K. Yokoyama, K. Kaneko, Y. Miyamoto, K. Asaoka, J. Sakai, M. Nagumo, *J. Biomed. Mater. Res.* 68A (2004) 150–158.
- [39] K. Yokoyama, T. Ogawa, K. Asaoka, J. Sakai, *Mater. Sci. Eng. A* 384 (2004) 19–25.
- [40] K. Kaneko, K. Yokoyama, K. Moriyama, K. Asaoka, J. Sakai, M. Nagumo, *Biomaterials* 24 (2003) 2113–2120.
- [41] T. Ogawa, K. Yokoyama, K. Asaoka, J. Sakai, *Biomaterials* 25 (2004) 2419–2425.
- [42] G.F. Pittinato, S.F. Frederick, *Metall. Trans.* 1 (1970) 3241–3243.
- [43] H.G. Nelson, D.P. Williams, J.E. Stein, *Metall. Trans.* 3 (1972) 469–475.
- [44] G.F. Pittinato, W.D. Hanna, *Metall. Trans.* 3 (1972) 2905–2909.
- [45] D.A. Meyn, *Metall. Trans.* 5 (1974) 2405–2414.
- [46] D.N. Williams, *Mater. Sci. Eng.* 24 (1976) 53–63.
- [47] H.G. Nelson, *Metall. Trans. A* 7A (1976) 621–627.
- [48] G.Y. Gao, S.C. Dexter, *Metall. Trans. A* 18A (1987) 1125–1130.
- [49] D. Hardie, S. Ouyang, *Corros. Sci.* 41 (1999) 155–177.
- [50] D.G. Westlake, *Trans. ASM* 62 (1969) 1000–1006.
- [51] R.A. Oriani, P.H. Josephic, *Acta Metall.* 22 (1974) 1065–1074.
- [52] C.D. Beachem, *Metall. Trans.* 3 (1972) 437–451.
- [53] H.K. Birnbaum, P. Sofronis, *Mater. Sci. Eng. A* 176 (1994) 191–202.
- [54] D.N. Williams, *J. Inst. Metals* 91 (1962) 147–152.
- [55] G.A. Lenning, C.M. Craighead, R.I. Jaffee, *Trans. AIME* 200 (1954) 367–376.
- [56] I.I. Phillips, P. Poole, L.L. Shreir, *Corros. Sci.* 12 (1972) 855–866.
- [57] I.I. Phillips, P. Poole, L.L. Shreir, *Corros. Sci.* 14 (1974) 533–542.
- [58] D.S. Shih, I.M. Robertson, H.K. Birnbaum, *Acta Metall.* 36 (1988) 111–124.
- [59] Z.F. Wang, C.L. Briant, K.S. Kumar, *Corrosion* 54 (1998) 553–560.
- [60] R.J. Lederich, D.S. Schwartz, S.M.L. Sastry, in: D. Eylon, R.R. Boyer, D.A. Koss (Eds.), *Beta Titanium Alloys in the 1990's*, TMS, Warrendale, PA, 1993, pp. 159–169.
- [61] G.A. Young Jr., J.R. Scully, *Scripta Metall. Mater.* 28 (1993) 507–512.
- [62] G.A. Young Jr., J.R. Scully, *Corrosion* 50 (1994) 919–933.
- [63] G. Itoh, M. Kanno, N. Niwa, *Mater. Sci. Eng. A* 213 (1996) 93–97.
- [64] M.A. Gaudett, J.R. Scully, *Scripta Mater.* 36 (1997) 565–572.
- [65] B.G. Pound, *Acta Mater.* 45 (1997) 2059–2068.
- [66] D.F. Teter, I.M. Robertson, H.K. Birnbaum, *Acta Mater.* 49 (2001) 4313–4323.
- [67] W.Y. Choo, J.Y. Lee, *Metall. Trans. A* 13A (1982) 135–140.
- [68] K. Ono, M. Meshii, *Acta Metall. Mater.* 40 (1992) 1357–1364.
- [69] A. Takasaki, Y. Furuya, K. Ojima, Y. Taneda, *J. Alloy. Comp.* 224 (1995) 269–273.
- [70] Y. Hirohata, T. Nakamura, Y. Aihara, T. Hino, *J. Nucl. Mater.* 266–269 (1999) 831–836.
- [71] M. Nagumo, M. Nakamura, K. Takai, *Metall. Mater. Trans. A* 32A (2001) 339–347.

Hydrogen embrittlement of Ni–Ti superelastic alloy in ethanol solution containing hydrochloric acid

Toshio Ogawa^a, Ken'ichi Yokoyama^{b,*}, Kenzo Asaoka^b, Jun'ichi Sakai^a

^a Department of Materials Science and Engineering, Waseda University,
3-4-1 Okubo, Shinjuku-ku, Tokyo 169-8555, Japan

^b Department of Biomaterials and Bioengineering, Institute of Health Biosciences, The University of Tokushima
Graduate School, 3-18-15 Kuramoto-cho, Tokushima 770-8504, Japan

Received 2 June 2004; received in revised form 7 October 2004; accepted 15 October 2004

Abstract

The hydrogen embrittlement of the Ni–Ti superelastic alloy in ethanol solution containing 0.1 mass% hydrochloric acid (HCl) has been investigated using a tensile test (after immersion) and hydrogen thermal desorption analysis (TDA). Upon immersion, the alloy absorbed substantial amounts of hydrogen associated with localized corrosion. The maximum amounts of absorbed hydrogen after immersion for 120 and 600 h were 260 and 1200 mass ppm, respectively. The hydrogen thermal desorption of the immersed specimens appeared as two peaks at approximately 150 and 350 °C. As immersion time increased, the amount of desorbed hydrogen at the lower temperatures increased markedly. When the amount of absorbed hydrogen exceeded 200–400 mass ppm, a marked reduction in tensile strength occurred. The fracture mode of specimens that absorbed hydrogen changed from ductile behavior to brittle behavior; the peripheral parts of the fracture surface exhibited a quasi-cleavage-like topography. The hydrogen embrittlement characteristic of the Ni–Ti superelastic alloy in ethanol solution containing 0.1% HCl was not always in accordance with those of the same alloy in other solutions such as the methanol solution containing 0.1% HCl reported previously.

© 2004 Elsevier B.V. All rights reserved.

Keywords: Ni–Ti; Hydrogen embrittlement; Thermal desorption analysis; Corrosion; Ethanol solution

1. Introduction

The mechanical properties of the Ni–Ti superelastic alloy are susceptible to hydrogen. The effects of hydrogen on the mechanical properties of this alloy have been investigated after cathodic hydrogen-charging in various electrolytic solutions [1–9]. The authors have reported that critical stress for martensite transformation increases slightly and fracture is associated with martensite transformation when the amount of absorbed hydrogen is higher than 50–200 mass ppm [10,11]. Simultaneously, we have emphasized that not only total hydrogen content but also the state of hydrogen, e.g., hydride, weakly trapped at defects and in solution, in

the alloy is an important factor controlling hydrogen embrittlement [9–11].

The hydrogen embrittlement of the Ni–Ti superelastic alloy is an important issue in the practical application of this alloy. In dentistry, Ni–Ti superelastic orthodontic wires absorb substantial amounts of hydrogen in the presence of fluorides such as NaF, which is contained in toothpastes and prophylactic agents owing to its cariostatic effect, thereby causing the degradation of the mechanical properties or fracture of the wires in the oral cavity [10,12]. The hydrogen embrittlement of the alloy must be investigated under various environmental conditions, because the alloy has a wide range of applications. Recently, we have found that the Ni–Ti superelastic alloy absorbs substantial amounts of hydrogen in methanol solution containing 0.1% hydrochloric acid (HCl) [11]. In this case, the thermal desorption of hydrogen appears as a single peak

* Corresponding author. Tel.: +81 88 633 7334; fax: +81 88 633 9125.
E-mail address: yokken@dent.tokushima-u.ac.jp (K. Yokoyama).

at approximately 400 °C. With prolonged immersion, a small second peak appears at approximately 200 °C. The desorption behavior provides information on the state of hydrogen or hydrogen trap sites in materials. However, the association between the desorption behavior and the hydrogen embrittlement of Ni–Ti superelastic alloy is not yet elucidated.

In regard to the environmental effects of methanol solution containing HCl, the stress corrosion cracking of commercial pure titanium was first reported by Mori et al. [13]. Subsequently, it was revealed that titanium absorbs hydrogen in methanol solution containing HCl [14–17]. In ethanol solution containing HCl, Mori et al. [13] also demonstrated that the stress corrosion cracking of commercial pure titanium does not occur. In the larger the molecular weight of alcohol such as ethanol and n-butanol, the cracking of titanium is not observed [13]. However, since the corrosion resistance of Ni–Ti alloys is generally lower than that of pure titanium in environments such as NaCl solution [18–20], corrosion and hydrogen absorption possibly occur in ethanol solution. If Ni–Ti alloys absorb substantial amounts of hydrogen in ethanol solution, it is the first observation for alloys with titanium oxides film. Therefore, it is necessary to confirm experimentally whether hydrogen embrittlement takes place in ethanol solution.

The objective of the present study is to examine the hydrogen embrittlement of the Ni–Ti superelastic alloy in ethanol solution containing 0.1% HCl by hydrogen thermal desorption analysis (TDA). For evaluating the degradation of the mechanical properties of the alloy, a tensile test was conducted.

2. Experimental procedures

A commercial Ni–Ti (Ni: 55 mass%, Ti: balance) superelastic wire alloy with a diameter of 0.50 mm was cut into 50 mm long specimens. Percent in this paper means mass percent, unless otherwise stated. The phase transformation temperatures and mechanical properties of the alloy are listed in Table 1, in which M_s and M_f are the starting and final temperatures, respectively, for martensite transformation on cooling. Similarly, A_s and A_f indicate the starting and final temperatures, respectively, for the reverse transformation on heating. The phase transformation temperatures of the specimen were determined by differential scanning calorimetry (DSC) at a scan rate of 10 °C/min. The critical stress for martensite transformation and the tensile strength at room temperature

Table 1
Mechanical properties and transformation temperatures of tested Ni–Ti superelastic alloy

Critical stress (MPa)	Tensile strength (MPa)	Reduction in area (%)	Transformation temperature (°C)			
			A_f	A_s	M_s	M_f
535 ± 1.4	1425 ± 12.6	54.6	7.5	–26.0	2.5	–38.5

(25 ± 2 °C) were 535 and 1425 MPa, respectively. The specimens were polished with #600-grit SiC papers and ultrasonically washed in acetone for 5 min.

The specimens were separately immersed in 10 ml of ethanol solution with 0.1% HCl at 37 °C for various periods. This immersion test was performed more than five times under the same conditions. Mass loss in the immersed specimens with immersion time was measured using a microbalance. The amount of desorbed hydrogen was measured by TDA with the specimens subjected to the immersion test. Both ends of each specimen (50 mm in length) immersed in the solution, were cut into 20 mm long segment and subjected to ultrasonic cleaning with acetone for 2 min. The segment was dried in ambient air and used for measurement. TDA was carried out 30 min after the removal of the specimen from the solution. A quadrupole mass spectrometer (ULVAC, Kanagawa, Japan) was used for hydrogen detection. Data sampling was conducted at 30 s intervals at a heating rate of 100 °C/h.

The side surfaces of the nonimmersed and immersed specimens were observed using scanning electron microscopy (SEM) and examined using X-ray diffraction (XRD) analysis with Cu K α radiation of wavelength $\lambda = 1.54056 \text{ \AA}$ in the 2θ angle range from 30 to 90° operated at 40 kV and 30 mA.

Tensile tests on the nonimmersed and immersed specimens were carried out at room temperature at a strain rate of $8.33 \times 10^{-4} \text{ s}^{-1}$ within a few min after the removal of the specimens from the test solution. The gauge length of each specimen was 10 mm. The fracture surface of the tensile-tested specimens was observed by SEM.

Vickers microhardness tests were carried out at room temperature on the immersed specimens from the surface to the center of the cross section of the wire at 0.05 mm intervals. The specimens were embedded in epoxy resin and polished, and then subjected to hardness tests 24 h after their removal from the solution. These tests were performed under an applied load of 0.98 N with an applied time of 15 s.

3. Experimental results

Fig. 1 shows the mass loss of the specimens subjected to the immersion test as a function of immersion time. The mass loss had a tendency to increase with immersion time, although the data points were scattered widely. The maximum mass losses after immersion for 120 and 600 h were 0.014 and 0.035 mg/mm², respectively. However, the mass-unchanged specimens, i.e., a mass loss of less than 0.001 mg/mm², were sometimes observed irrespective of immersion time.

The representative TDA curves for the mass-changed specimens immersed for up to 600 h is shown in Fig. 2. The thermal desorption of hydrogen appeared as two peaks at approximately 150 and 350 °C. As the total amount of desorbed hydrogen increased, i.e., as immersion time increased, the amount of desorbed hydrogen at the lower temperature increased remarkably, whereas that at the higher temperature

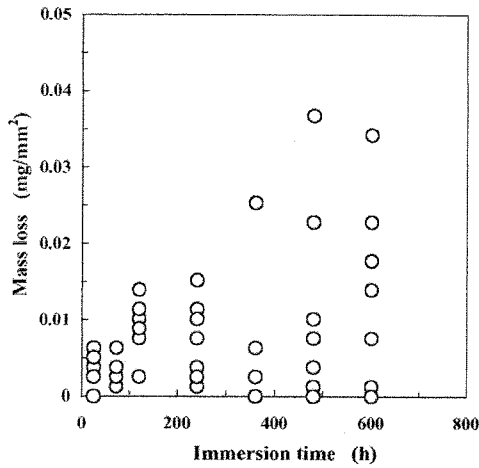


Fig. 1. Mass loss of Ni-Ti superelastic alloy immersed in ethanol solution containing 0.1% HCl as function of immersion time.

hardly changed. Fig. 3(a) shows the total amount of desorbed hydrogen up to 600 °C as a function of immersion time. The amount of desorbed hydrogen, i.e., the amount of hydrogen absorbed during the immersion test, tended to increase with immersion time, although it varied widely. The maximum amounts of absorbed hydrogen after immersion for 120

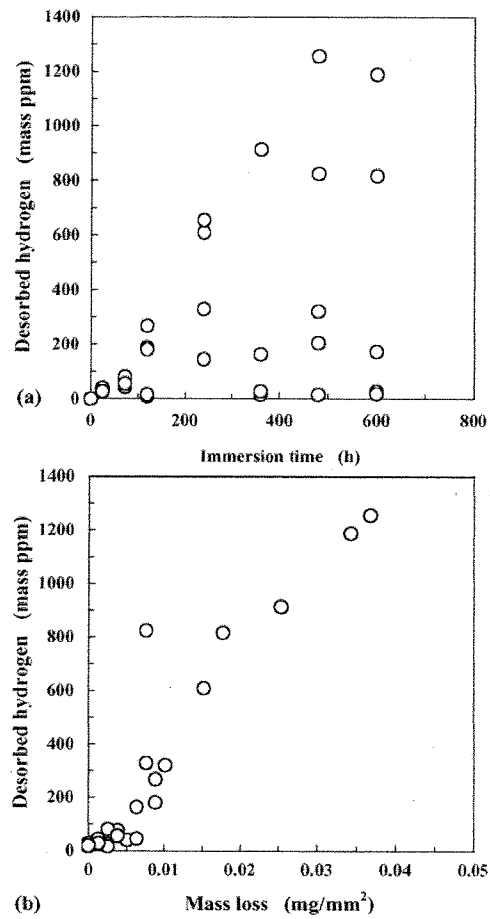


Fig. 3. Amount of desorbed hydrogen from TDA of immersed specimens as function of (a) immersion time and (b) mass loss.

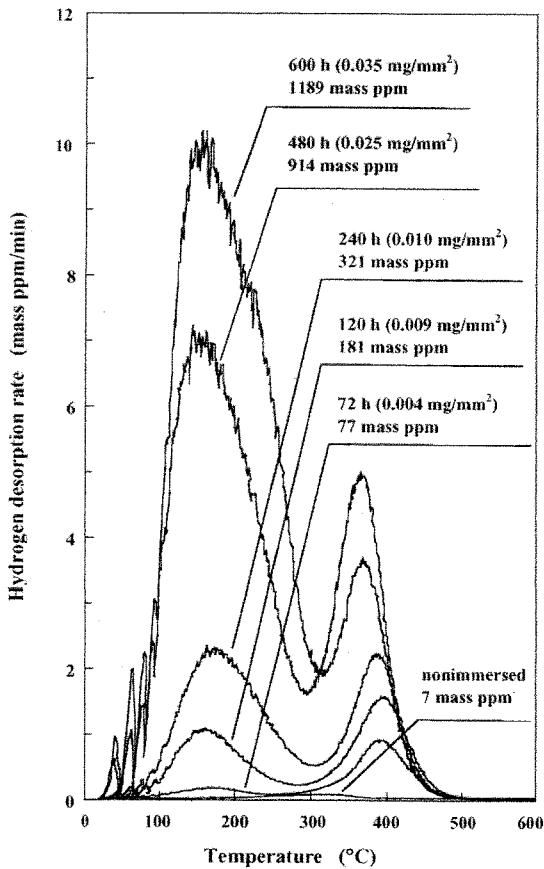


Fig. 2. Hydrogen thermal desorption curves for mass-changed specimens immersed in ethanol solution containing 0.1% HCl for various periods.

and 600 h were 260 and 1200 mass ppm, respectively. The amount of absorbed hydrogen increased linearly with mass loss, as shown in Fig. 3(b). The amounts of absorbed hydrogen were approximately 200–400 and 1100–1300 mass ppm at the mass losses of 0.010 and 0.035 mg/mm². For the mass-unchanged specimens, an increment in the amount of desorbed hydrogen was hardly observed.

On the side surface of the nonimmersed specimen, scratches due to SiC paper polishing were observed as shown in the SEM micrographs in Fig. 4(a and b). The side surfaces of the mass-changed specimens (0.010 and 0.025 mg/mm² immersed for 120 and 480 h, respectively) are shown in Fig. 4(c–f). Localized corrosion was revealed; the area subjected to corrosion increased with immersion time. Very slight corrosion was observed on the side surface of the mass-unchanged specimens immersed for various periods.

The XRD analysis results for the side surfaces of the nonimmersed specimen and the mass-changed specimen (0.035 mg/mm² immersed for 600 h) are shown in Fig. 5(a and b), respectively. The diffraction peaks of both specimens correspond to the B2 structure of the Ni-Ti alloy. No diffraction peaks corresponding to corrosion products or hydrides

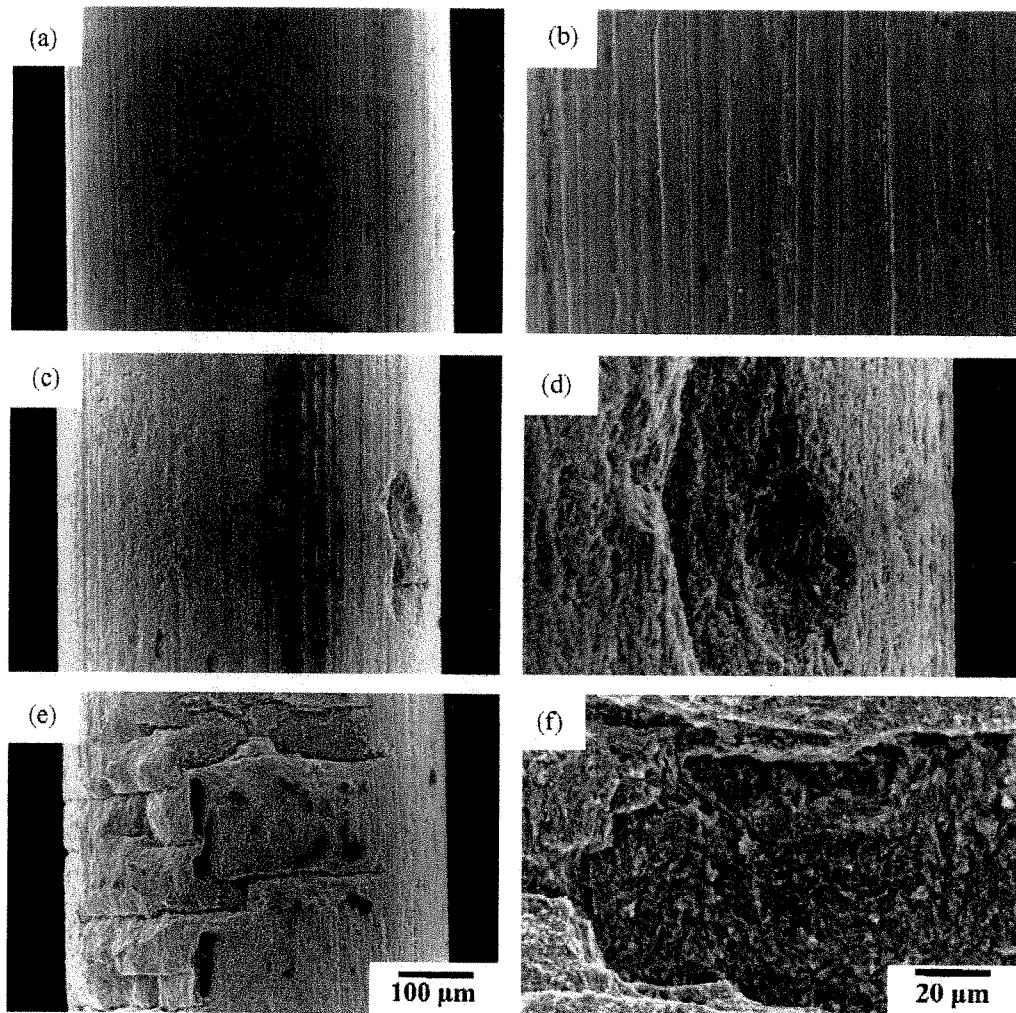


Fig. 4. SEM micrographs of typical side surfaces of (a) nonimmersed specimen, (b) magnified view of (a), (c) mass-changed specimen (0.010 mg/mm^2) immersed for 120 h, (d) magnified view of corrosion area in (c), (e) mass-changed specimen (0.025 mg/mm^2) immersed for 480 h, and (f) magnified view of corrosion area in (e).

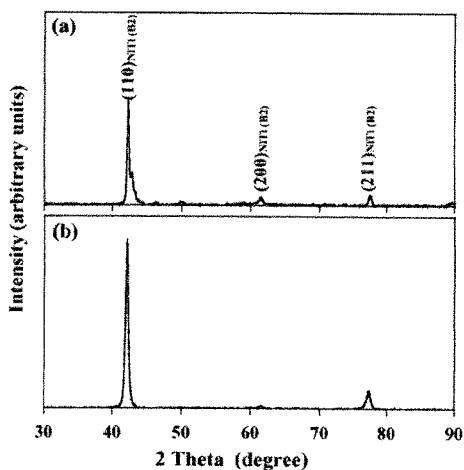


Fig. 5. XRD patterns of the surfaces of (a) nonimmersed specimen and (b) mass-changed specimen (0.035 mg/mm^2) immersed for 600 h.

were detected on the surface of the immersed specimens regardless of mass loss.

Fig. 6 shows representative tensile stress–strain curves for the nonimmersed specimen and the mass-changed specimens immersed for 120 and 600 h. The mass-changed specimens fractured before yielding or the stress-induced martensite transformation. The critical stress for the martensite transformation of the immersed specimens hardly changed. The tensile strengths of all the tested specimens as functions of immersion time and mass loss are shown in Fig. 7(a and b), respectively. The tensile strength tended to decrease with immersion time, although the data points were scattered widely. The tensile strength abruptly decreased when the mass loss exceeded 0.010 mg/mm^2 , corresponding to a hydrogen content of 200–400 mass ppm. The immersed specimens with a mass loss of 0.010 mg/mm^2 fractured without necking, although the tensile strength hardly decreased. At a mass loss below 0.010 mg/mm^2 , the tensile properties of the immersed

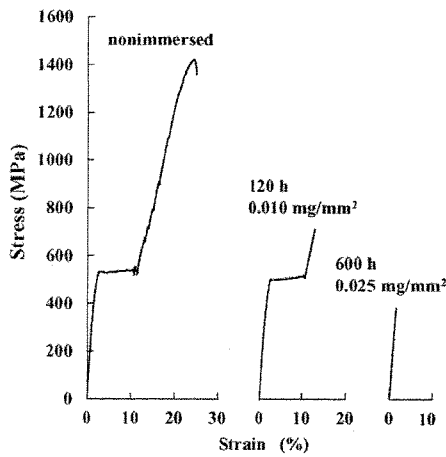


Fig. 6. Typical stress–strain curves for nonimmersed and mass-changed specimens immersed for 120 and 600 h. Strain was calculated from elongation (displacement of crosshead) and the initial gauge length.

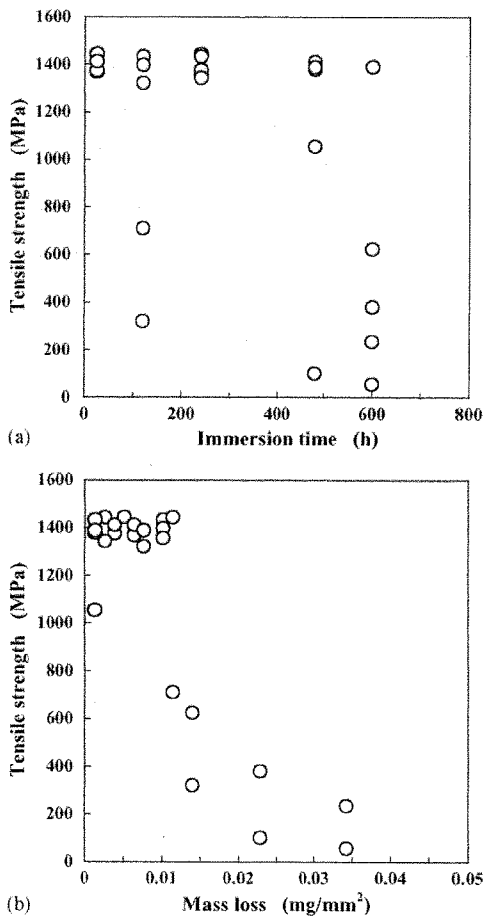


Fig. 7. Tensile strength of immersed specimens in solution as function of (a) immersion time and (b) mass loss.

specimens did not change with only one exceptional specimen.

The fracture surface of the nonimmersed specimen subjected to the tensile test is shown in Fig. 8(a–c). The surface was ductile and was characterized macroscopically with a cup-cone morphology and was composed of microscopic primary and secondary dimples. For the mass-changed specimen (0.010 mg/mm^2) immersed for 120 h, the fracture surface exhibited no reduction in area, as shown in Fig. 8(d). The peripheral parts (Fig. 8(e)) of the fracture surface showed a quasi-cleavage-like topography, whereas the central parts (Fig. 8(f)) of the fracture surface showed both a quasi-cleavage-like topography and shallow dimples. The quasi-cleavage area spread toward the center with increases in mass loss, i.e., hydrogen content, and immersion time. In the mass loss range lower than 0.010 mg/mm^2 , the fracture surfaces of the specimens immersed for various periods were similar to that of the nonimmersed specimen.

Fig. 9 shows the Vickers microhardnesses along the diameter of the cross section of the nonimmersed specimen and the mass-changed specimens (0.015 and 0.035 mg/mm^2) immersed for 240 and 600 h, respectively. The increment in hardness was confirmed at the peripheral parts of the cross-sectional area of the mass-changed specimens.

4. Discussion

Noteworthy findings in the present study are as follows: (1) the Ni–Ti superelastic alloy absorbs substantial amounts of hydrogen in ethanol solution containing 0.1% HCl, thereby causing hydrogen embrittlement and (2) the association between the reduction in tensile strength and hydrogen desorption behavior differs from those obtained in previous studies such as those involving immersion in 0.2% acidulated phosphate fluoride (APF) solution [10] and methanol solution containing 0.1% HCl [11]. We previously demonstrated that the Ni–Ti superelastic alloy absorbs substantial amounts of hydrogen associated with the occurrence of localized corrosion in methanol solution containing 0.1% HCl [11]. In such methanol solution, hydrogen absorption always occurs and the scattering of hydrogen content is relatively small. In contrast, in ethanol solution containing 0.1% HCl, the alloy sometimes undergoes localized corrosion, suggesting that the conditions used in the present experiment are critical for the occurrence of corrosion and hydrogen absorption. Haruna et al. [21] pointed out that the strict control of moisture content and/or dissolved oxygen concentration in methanol solution for the evaluation of the environment-assisted cracking of titanium is necessary. One reason for the scattering of the present results may be the moisture content in ethanol solution.

The hydrogen absorption rate of the alloy in ethanol solution containing 0.1% HCl was slower than that in methanol solution containing 0.1% HCl [11]. For instance, the amounts of absorbed hydrogen in ethanol and methanol solutions were

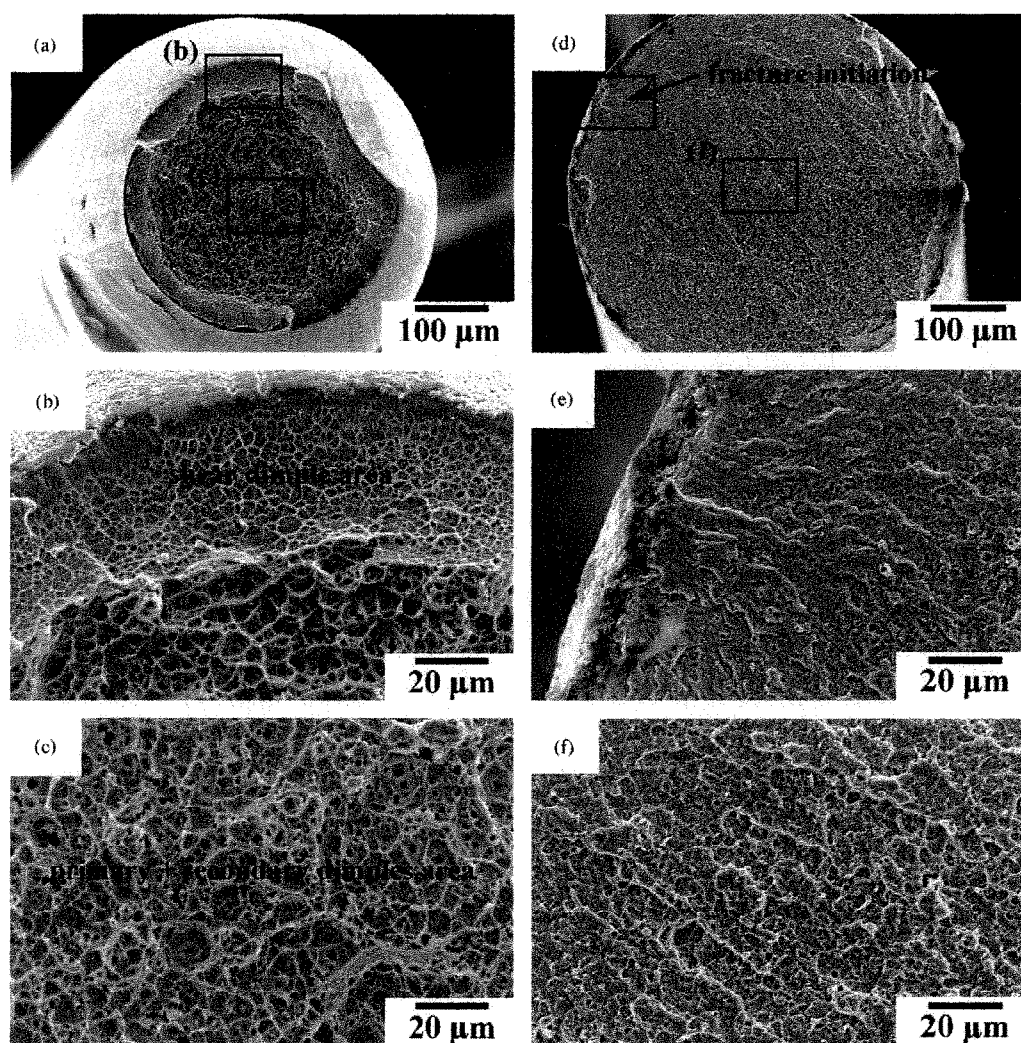


Fig. 8. SEM micrographs of typical fracture surfaces: (a) general view of nonimmersed specimen, (b) magnified view of shear dimple area in the peripheral part of (a), (c) magnified view of primary and secondary dimples area in the center of (a), (d) general view of mass-changed specimen (0.010 mg/mm^2) immersed for 120 h, (e) magnified view of peripheral part in (d), and (f) magnified view of central part in (d).

260 maximum and 500 mass ppm after immersion for 120 h, respectively. Ethanol solution, compared with methanol solution, is considered to be less corrosive to the Ni–Ti superelastic alloy.

In our recent findings [10,11], when the amount of absorbed hydrogen exceeds 50–200 mass ppm, a pronounced reduction in the tensile strength of the Ni–Ti superelastic alloy takes place. Total hydrogen content often has been used as a criterion for the occurrence of embrittlement. In the present study, however, the reduction in the tensile strength did not necessarily occur despite the absorption of 50–200 mass ppm hydrogen, corresponding to a mass loss of $0.003\text{--}0.010 \text{ mg/mm}^2$, as indicated in Figs. 3(b) and 7(b). Moreover, the increment in critical stress for martensite transformation was hardly recognized. The increment in critical stress for martensite transformation is interpreted to be the result of the suppressed martensite transformation due to ab-

sorbed hydrogen [22]. These findings imply that the hydrogen embrittlement characteristic of the Ni–Ti superelastic alloy is closely related to not only total hydrogen content but also the state of hydrogen.

The state of hydrogen in materials can be estimated from the hydrogen thermal desorption behavior [23–26]. In general, hydrogen desorption results from the decomposition of hydride or dissociation of hydrogen from trapping sites. For the Ni–Ti superelastic alloy immersed in methanol solution containing 0.1% HCl, the thermal desorption of hydrogen appeared as a single desorption peak at approximately 400°C [11]; when the amount of absorbed hydrogen exceeded 400 mass ppm, an other smaller desorption peak appeared at 200°C . In the case of the alloy immersed in 0.2% APF solution, the desorption appeared as a single peak at 400 to 500°C irrespective of hydrogen content [10,12]. On the other hand, the desorption of the alloy immersed in ethanol

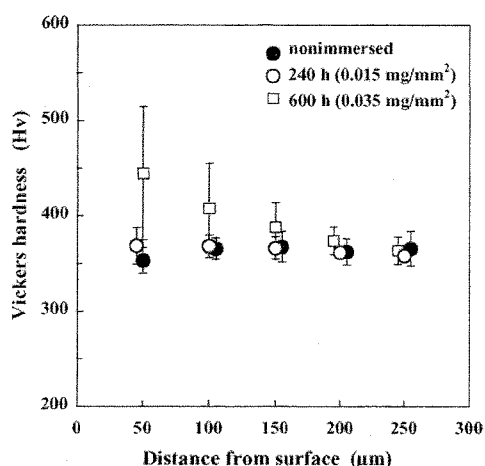


Fig. 9. Vickers microhardnesses of nonimmersed and immersed specimens. Hardness was measured at 0.05 mm intervals and standard deviation was calculated from eight indentations.

solution appeared as two distinct peaks at approximately 150 and 350 °C, as shown in Fig. 2. This result clearly shows that there are different trap sites of hydrogen in the Ni–Ti superelastic alloy immersed in ethanol solution. Moreover, it should be noted that the state of hydrogen in the alloy is changed by the type of solution used in the immersion test. The desorption at higher temperatures is probably ascribed to strongly trapped hydrogen, because hydride formation was not observed by SEM or XRD analysis on the surface of the specimens immersed in ethanol solution. When immersion time increased, the increment in the amount of desorbed hydrogen at higher temperatures was small, whereas that at lower temperatures was remarkable. This implies that hydrogen desorption at lower temperatures reduces the tensile strength of the Ni–Ti superelastic alloy. For steel, the desorption of weakly trapped hydrogen at lower temperatures significantly influences their mechanical properties [27]. The effects of hydrogen desorption at lower temperatures on the mechanical properties of the Ni–Ti superelastic alloy is an important issue for further clarification.

The amount of absorbed hydrogen obtained from TDA is the average amount of absorbed hydrogen for an immersed specimen; the distribution of hydrogen in a given specimen is not known. The amount of absorbed hydrogen depended on mass loss as shown in Fig. 1(b). This indicates that hydrogen absorption results from localized corrosion, and the hydrogen content at the area subjected to corrosion is higher than that obtained by TDA. The distribution and/or state of hydrogen in a given specimen can be determined by fractography, because the fracture surface reflects fracture processes influenced by hydrogen including crack initiation and propagation. As shown in Fig. 8(e), the fracture always initiated at the peripheral parts of the specimens immersed in ethanol solution; the fracture initiation point could be identified by tracing back the chevron-like flows. In addition, the harden-

ing induced by hydrogen absorption was observed at the peripheral parts of the specimen, as shown in Fig. 9. Therefore, it is essential to investigate the brittle area at the peripheral parts of the fracture surface. In our previous studies, the peripheral parts of the fracture surface of specimens immersed in APF solution [10] or cathodic hydrogen-charged with a high current density [6] were fairly flat. No fracture initiation associated with the cracking of brittle hydride was observed. The flat surface implies that the type of crack propagation is independent of the presence of microstructures such as grain boundaries. Cohesive strength or ductility might be reduced by hydrogen atoms in the lattice [28]. In contrast, the peripheral parts of the fracture surface of the specimens immersed in ethanol solution exhibited a quasi-cleavage-like topography as well as those of the specimens immersed in methanol solution containing 0.1% HCl [11] or cathodic hydrogen-charged with a low current density [6]; however, not all details of the topography were identical. That is, when hydrogen absorption occurred slowly, the peripheral parts of the fracture surface tended to show a quasi-cleavage-like topography. In the present study, as immersion time increased, the brittle area at the peripheral parts of the fracture surface extended to the center parts associated with hydrogen diffusion, similar to those observed in previous studies [6,10,29]. Since hydrogen diffusion in the Ni–Ti alloy with the B2 structure is not adequately fast for a limited period at around room temperature [30], it is likely that hydrogen content at the peripheral parts of the cross section of the specimen is much higher than that at the central parts, particularly for rapid hydrogen absorption. When rapid hydrogen absorption occurs, the thermal desorption of hydrogen sometimes shifts at lower temperatures [31], suggesting the change in hydrogen state. It is possible that the hydrogen enrichment at the peripheral parts of the cross section of the specimen induces the change in hydrogen state, resulting in the different fracture surfaces in various solutions.

5. Conclusions

We have demonstrated that the hydrogen absorption of the Ni–Ti superelastic alloy occurs in ethanol solution containing 0.1% HCl, thereby causing hydrogen embrittlement. The relationship between the amount of absorbed hydrogen and tensile strength for the alloy immersed in ethanol solution is not in agreement with those for the alloys immersed in other solutions such as methanol solution containing 0.1% HCl and APF solution. The hydrogen absorption rate in ethanol solution, at most, is one-half that in methanol solution for the same HCl concentration. The thermal desorption of hydrogen appears as two peaks at approximately 150 and 350 °C for the alloy immersed in ethanol solution. The present results indicate that the hydrogen trapping in the Ni–Ti superelastic alloy depends on the conditions of hydrogen absorption, and that total hydrogen content is not necessarily the sole criterion for hydrogen embrittlement.

Acknowledgements

This study was supported in part by a Grant-in-Aid for Young Scientists (B) (14771090) and a Grant-in-Aid for Scientific Research (C) (15560632) from the Ministry of Education, Culture, Sports, Science and Technology, Japan.

References

- [1] N. Wade, Y. Adachi, Y. Hosoi, *Scripta Metall. Mater.* 24 (1990) 1051.
- [2] Y. Adachi, N. Wade, Y. Hosoi, *Jpn. Inst. Metals.* 54 (1990) 525.
- [3] T. Hoshiya, S. Den, H. Katsuta, H. Ando, *Jpn. Inst. Met.* 56 (1992) 747.
- [4] T. Asaoka, T. Kamimura, H. Saito, Y. Ishida, *Jpn. Inst. Met.* 56 (1992) 1111.
- [5] K. Yokoyama, K. Hamada, K. Moriyama, K. Asaoka, *Biomaterials* 22 (2001) 2257.
- [6] K. Yokoyama, K. Hamada, K. Asaoka, *Mater. Trans.* 42 (2001) 141.
- [7] K. Yokoyama, S. Watabe, K. Hamada, J. Sakai, K. Asaoka, M. Nagumo, *Mater. Sci. Eng. A* 341 (2003) 91.
- [8] J.Y. He, K.W. Gao, Y.J. Su, L.J. Qiao, W.Y. Chu, *Mater. Sci. Eng. A* 364 (2004) 333.
- [9] K. Yokoyama, T. Eguchi, K. Asaoka, M. Nagumo, *Mater. Sci. Eng. A* 374 (2004) 177.
- [10] K. Yokoyama, K. Kaneko, K. Moriyama, K. Asaoka, J. Sakai, M. Nagumo, *J. Biomed. Mater. Res.* 65A (2003) 182.
- [11] K. Yokoyama, T. Ogawa, K. Asaoka, J. Sakai, M. Nagumo, *Mater. Sci. Eng. A* 360 (2003) 153.
- [12] K. Yokoyama, K. Kaneko, K. Moriyama, K. Asaoka, J. Sakai, M. Nagumo, *J. Biomed. Mater. Res.* 69A (2004) 105.
- [13] K. Mori, A. Takamura, T. Shimose, *Corrosion* 22 (1966) 29.
- [14] I.A. Menzies, A.F. Averill, *Electrochimica. Acta* 13 (1968) 807.
- [15] J.C. Scully, T.A. Adepoju, *Corros. Sci.* 17 (1977) 789.
- [16] K. Ebtehaj, D. Hardie, R.N. Parkins, *Corros. Sci.* 25 (1985) 415.
- [17] A.C. Hollis, J.C. Scully, *Corros. Sci.* 34 (1993) 821.
- [18] Y. Oshida, S. Miyazaki, *Zairyo-to-Kankyo* 40 (1991) 834.
- [19] G. Rondelli, B. Vicentini, *J. Biomed. Mater. Res.* 51 (2000) 47.
- [20] S.A. Shabalovskaya, *Int. Mater. Rev.* 46 (2001) 233.
- [21] T. Haruna, M. Yamamoto, T. Shibata, *J. Jpn. Inst. Met.* 63 (1999) 977.
- [22] A. Biscarini, R. Campanella, B. Coluzzi, G. Mazzolai, L. Trotta, A. Tuissi, F.M. Mazzolai, *Acta Mater.* 47 (1999) 4525.
- [23] W.Y. Choo, J.Y. Lee, *Metall. Trans. A* 13A (1982) 135.
- [24] K. Ono, M. Meshii, *Acta. Metall. Mater.* 40 (1992) 1357.
- [25] A. Takasaki, Y. Furuya, K. Ojima, Y. Taneda, *J. Alloys Comp.* 224 (1995) 269.
- [26] T. Nishiue, Y. Kaneno, H. Inoue, T. Takasugi, *Intermetallics* 11 (2003) 817.
- [27] K. Takai, R. Watanuki, *ISIJ Int.* 43 (2003) 520.
- [28] R.A. Oriani, P.H. Josephic, *Acta. Metall.* 22 (1974) 1065.
- [29] K. Asaoka, K. Yokoyama, M. Nagumo, *Metall. Mater. Trans. A* 33A (2002) 495.
- [30] R. Schmidt, M. Schlereth, H. Wipf, W. Assmus, M. Müllner, *J. Phys. Condens. Matter* 1 (1989) 2473.
- [31] K. Yokoyama, K. Kaneko, T. Ogawa, K. Moriyama, K. Asaoka, J. Sakai, *Biomaterials* 26 (2005) 101.



Hydrogen embrittlement of work-hardened Ni–Ti alloy in fluoride solutions

Ken'ichi Yokoyama^{a,*}, Kazuyuki Kaneko^b, Toshio Ogawa^c, Keiji Moriyama^b,
Kenzo Asaoka^a, Jun'ichi Sakai^c

^aDepartment of Dental Engineering, School of Dentistry, The University of Tokushima, 3-18-15 Kuramoto-cho, Tokushima 770-8504, Japan

^bDepartment of Orthodontics, School of Dentistry, The University of Tokushima, 3-18-15 Kuramoto-cho, Tokushima 770-8504, Japan

^cDepartment of Materials Science and Engineering, Waseda University, 3-4-1 Okubo, Shinjuku-ku, Tokyo 169-8555, Japan

Received 15 December 2003; accepted 4 February 2004

Abstract

Hydrogen embrittlement of work-hardened Ni–Ti alloy has been examined in acidulated phosphate fluoride (APF) solutions. Upon immersion in a 2.0% APF solution with a pH of 5.0, tensile strength decreased markedly with immersion time. Moreover, the fracture mode changed from ductile to brittle due to brittle layer formation at the peripheral part of the cross section of the specimen. The amount of absorbed hydrogen increased linearly with immersion time, and it reached above 5000 mass ppm after 24 h. The hydrogen desorption temperature of the immersed specimens shifted from 450°C to a lower temperature with immersion time. As the amount of absorbed hydrogen was larger than 500 mass ppm, the degradation of mechanical properties was recognized. Although the tensile properties and fracture mode scarcely change in a 0.2% APF solution, the slight reduction in hardness and hydrogen absorption of several hundreds mass ppm were observed. The results of the present study imply that work-hardened Ni–Ti alloy is less sensitive to hydrogen embrittlement compared with Ni–Ti superelastic alloy.

© 2004 Elsevier Ltd. All rights reserved.

Keywords: Ni–Ti; Hydrogen embrittlement; Corrosion; Fluoride

1. Introduction

Ni–Ti alloy was first introduced as a material for orthodontic wire by Andreasen and Hilleman in the early 1970s [1]. This Ni–Ti orthodontic wire is of the work-hardened type and has an excellent springback property. The wire is now marketed under the brand name of Nitinol Classic (3M Unitek, Monrovia, CA, USA). On the other hand, another Ni–Ti orthodontic wire, namely, Ni–Ti superelastic alloy, was subsequently applied in the mid-1980s [2,3]. The superelasticity of this wire is induced through reversible-stress-induced martensite transformation by loading and unloading [4,5]. The superelastic orthodontic wire allows the teeth to move under almost constant force over a long treatment period. Furthermore, since the work-hardened and superelastic types of Ni–Ti alloys exhibit good corrosion

resistance, mechanical properties and biocompatibility [6–11], they are used widely in orthodontic wires currently.

However, the corrosion resistance of the above Ni–Ti orthodontic wires is not always adequate in the oral environment. The corrosion and discoloration in the oral cavity of these wires have been reported by several researchers [12–14]. In addition, the degradation of the performance and the fracture of these wires during clinical use have been recognized [15–18]. In several recent articles [18–22], we have insisted that the primary reason for the degradation of Ni–Ti superelastic alloy is hydrogen absorption in the oral cavity. In particular, in the presence of fluoride-containing prophylactic agents or toothpastes, the hydrogen absorption of Ni–Ti superelastic alloys as well as titanium and its alloys [23–25] often occurs. The mechanical properties of Ni–Ti superelastic or shape memory alloys are affected considerably by the absorbed hydrogen [26–30]. When the amount of absorbed hydrogen exceeds 50–200 mass ppm, the tensile strength decreases abruptly and brittle

*Corresponding author. Tel.: +81-88-633-7334; fax: +81-88-633-9125.

E-mail address: yokken@dent.tokushima-u.ac.jp (K. Yokoyama).

fracture occurs associated with stress-induced martensite transformation [20,31]. On the other hand, the hydrogen embrittlement of work-hardened Ni–Ti alloy has not yet been revealed. The degradation of the mechanical properties due to hydrogen absorption leads to a reduction in appropriate orthodontic force, thereby causing delayed straightening of irregular teeth. It is therefore necessary to investigate whether the hydrogen embrittlement of work-hardened Ni–Ti alloy takes place in the presence of fluoride.

The objective of the present study is to examine the hydrogen embrittlement of work-hardened Ni–Ti alloy in fluoride solutions. For the evaluation of the hydrogen embrittlement susceptibility, a tensile test and hydrogen thermal desorption analysis (TDA) were performed after immersion tests.

2. Materials and methods

Work-hardened Ni–Ti wires (Nitinol Classic; Unitek/3M Corp., Monrovia, CA) with a diameter of 0.50 mm were cut as specimens of 50 mm length and ultrasonically cleaned in acetone for 5 min. The mechanical properties of the specimens are given in Table 1. The tensile strength was 1700 MPa at room temperature ($25 \pm 2^\circ\text{C}$).

The specimens were immersed individually in 10 ml of 2.0% or 0.2% acidulated phosphate fluoride (APF; 2.0 mass % NaF + 1.7 mass % H_3PO_4 or 0.2 mass % NaF + 0.17 mass % H_3PO_4) aqueous solution with a pH 5.0 at 37°C for various periods. The concentrations of the fluoride were 9000 and 900 mass ppm, corresponding to those in prophylactic agents and toothpastes, respectively. Tensile tests on the immersed specimens were carried out using a Shimadzu Autograph AG-100A machine at a strain rate of $8.33 \times 10^{-4}/\text{s}$ within a few minutes after removal of the specimens from the solution. The gauge length of the specimens was 10 mm. The mass loss of the immersed specimens after the immersion tests was measured, and the standard deviation was calculated from the results obtained from five specimens. To perform hardness tests, the immersed wires were embedded in epoxy resin and polished. After 24 h from the removal of the specimens from the solution, Vickers microhardness tests were carried out on the transverse cross section from the periphery to the center of the wire at 0.05-mm intervals. Measurements

Table 1
Mechanical properties of the tested work-hardened Ni–Ti alloy

Yield stress (MPa)	Tensile strength (MPa)	Reduction in area (%)
1487 ± 34	1701 ± 12	51.4 ± 1.7

were performed under an applied load of 0.98 N for 15 s. The side surface and fracture surface of the tensile-tested specimens were observed by scanning electron microscopy (SEM). The side surfaces of the immersed specimens were examined to identify the corrosion products using an X-ray diffractometer with $\text{Cu K}\alpha$ radiation with a wavelength $\lambda = 1.54056 \text{ \AA}$ at a $2^\circ/\text{min}$ sweep rate operated at 40 kV and 30 mA.

The amount of desorbed hydrogen was measured using TDA by immersing the specimens for various periods. After the immersion test, the specimens (50 mm in length) were cut into 20-mm long segments and subjected to ultrasonic cleaning with acetone for 2 min. The segments were dried in ambient air and subjected to TDA. The waiting time for TDA after the removal of a specimen from the solution was 30 min. A quadrupole mass spectrometer (ULVAC, Kanagawa, Japan) was employed for the hydrogen detection. Data sampling was conducted at a 30-s interval at a heating rate of $100^\circ\text{C}/\text{h}$.

3. Experimental results

Tensile strength of the specimens immersed in the 2.0% APF solution as a function of immersion time is shown in Fig. 1. The tensile strength of the specimens immersed in the 2.0% APF solution decreased with increasing immersion time, when the immersion time was longer than 4 h. The nonimmersed specimen always fractured after necking. In contrast, the 2-h immersed specimen often fractured before necking. The 4-h immersed specimen always fractured without necking. The specimens immersed for more than 6 h always fractured before general yielding. For all the specimens immersed in the 0.2% APF solution up to 480 h, their

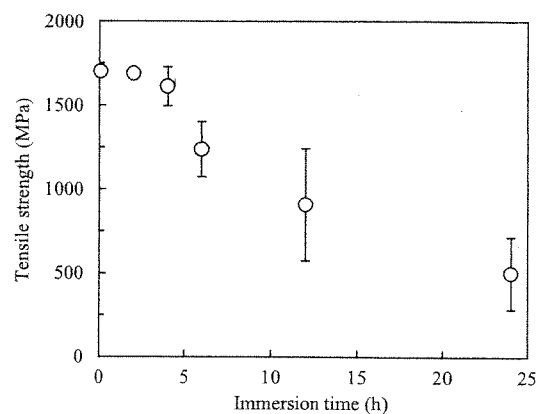


Fig. 1. Tensile strength of immersed specimens in 2.0% APF solution as a function of immersion time. Standard deviation was calculated from the results obtained from five specimens.

tensile properties hardly changed; tensile strength is summarized as a function of immersion time in Table 2.

Figs. 2(a) and (b) show the fractographs of the nonimmersed specimen after the tensile test. The reduction in area was 51%. The fracture surface was characterized macroscopically with a cup-cone morphology and was composed microscopically of primary and secondary dimples. On the other hand, the fracture surface of the specimen immersed in the 2.0% APF solution for 4 h hardly exhibited a reduction in area, as shown in Figs. 2(c) and (d). The peripheral part of the fracture surface was fairly flat while the central part was composed of shallow dimples. Same fractographic features were observed when the immersion times were longer than 2 h. The fraction of the flat area on the fracture surface, namely, the brittle layer, increased with immersion time. As an exception, the shear mode fracture was rarely observed in the specimens immersed in the 2.0% APF solution below 6 h. For the specimens immersed in the 0.2% APF solution, the fracture surface was almost the same as that of the nonimmersed specimen irrespective of immersion time.

The Vickers microhardness values of the specimens subjected to the immersion test in the 2.0% APF

Table 2
Tensile strength of specimens immersed in 0.2% APF solution for various periods

Immersion time (h)	Tensile strength (MPa)
0	1701 ± 12
24	1719 ± 30
60	1686 ± 14
240	1704 ± 13
480	1694 ± 7

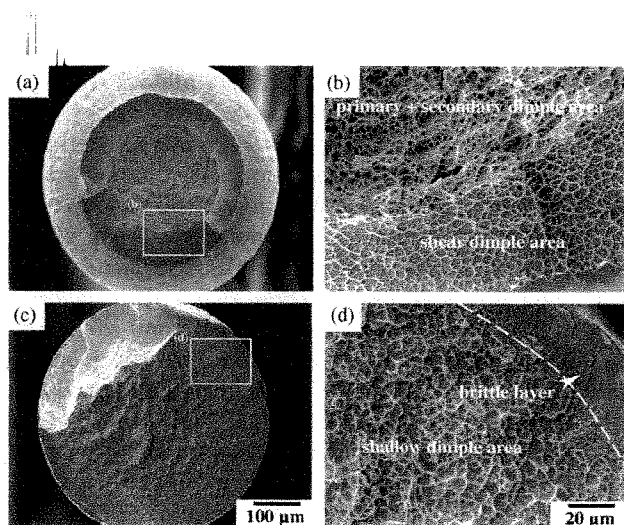


Fig. 2. SEM micrographs of a typical fracture surface: (a) non-immersed specimen; (b) magnified view of dimples in (a); (c) immersed in 2.0% APF solution for 4 h; and (d) magnified view of peripheral part in (c).

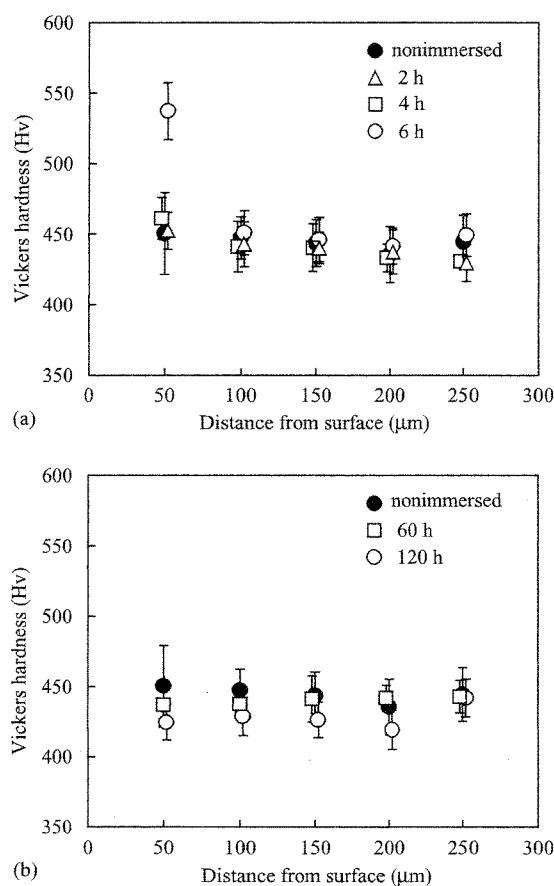


Fig. 3. Vickers microhardness of nonimmersed specimen and specimens immersed for various periods in (a) 2.0% APF solution and (b) 0.2% APF solution. Standard deviation was calculated from eight indentations.

solution for various periods are shown in Fig. 3(a). The hardness of the nonimmersed specimen was approximately 450 throughout the specimen whereas that of the immersed specimens increased near the surface, i.e., at the peripheral part of the cross section. At 6-h immersion, the hardness value at the peripheral part of the cross section was as high as 540. Although accurate measurement was difficult, even for the specimen immersed for 2 h, hardening was estimated at the immediate vicinity of the surface. The hardness of the specimens immersed in the 0.2% APF solution slightly decreased from the surface to the center of the specimen as shown in Fig. 3(b). The hardness decreased in the center of the specimen with immersion time.

The typical SEM micrographs of the side surface of the nonimmersed specimen indicate that surface defects are associated with the wire drawing, electropolishing or pickling procedures performed during the manufacturing process, as shown in Figs. 4(a) and (b). For the surface of the specimen immersed in the 2.0% APF solution for 2 h, as shown in Figs. 4(c) and (d), general

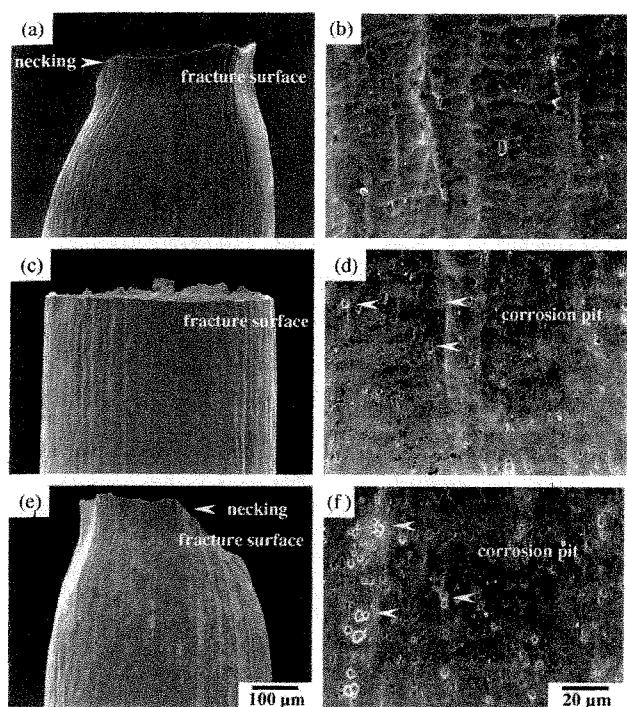


Fig. 4. SEM micrographs of a typical side surface at fracture area: (a) general and (b) magnified views of a nonimmersed specimen, (c) general and (d) magnified views of a specimen immersed in 2.0% APF solution for 2 h, and (e) general and (f) magnified views of a specimen immersed in 0.2% APF solution for 24 h.

corrosion and numerous corrosion pits were observed; macroscopic surface roughness was smaller than that of the nonimmersed specimen. The number of corrosion pits increased with increasing immersion time. The surface feature of the specimen immersed in the 0.2% APF solution for 24 h, as shown in Figs. 4(e) and (f), was similar to that of the specimen immersed in the 2.0% APF solution. As seen from the cross-section of the fracture surface, the fracture mode of the specimen immersed in the 0.2% APF solution was similar to that of the nonimmersed specimen.

The X-ray diffraction (XRD) peaks of work-hardened Ni–Ti alloy correspond to the B2 structure of Ni–Ti alloy, however, diffraction peaks related to corrosion products or hydrides were not detected on the surface of specimens immersed for various periods.

The corrosion rates in terms of the mass loss of the specimens immersed in 2.0% and 0.2% APF solutions are shown in Figs. 5(a) and (b), respectively. Mass loss increased linearly with immersion time in the case of the 2.0% APF solution while it saturated in the case of the 0.2% APF solution. The mass loss of the specimens immersed in the 0.2% APF solution was less than half that in the 2.0% APF solution.

Figs. 6(a) and (b) show the thermal desorption curves for the specimens immersed in 2.0% and 0.2% APF

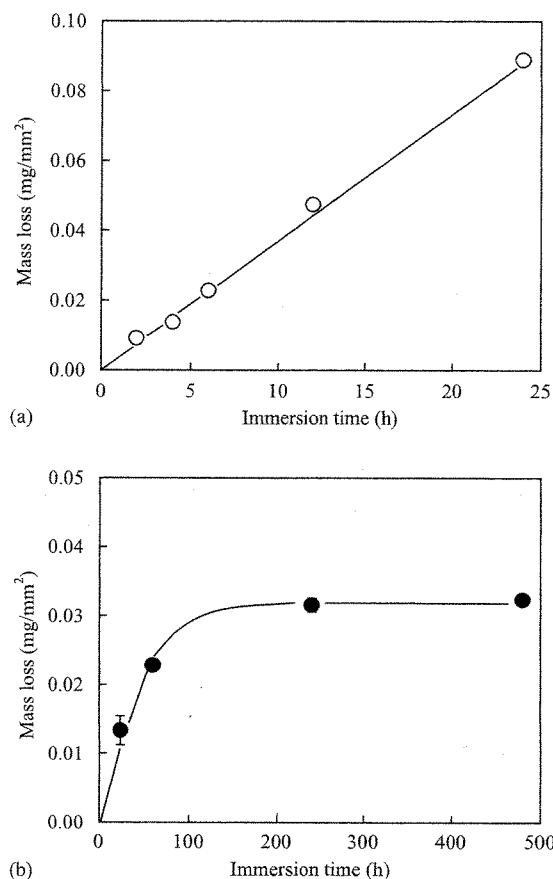


Fig. 5. Mass loss as a function of immersion time of immersed specimen in (a) 2.0% APF solution and (b) 0.2% APF solution. Standard deviation was calculated from the results of five specimens.

solutions for various immersion periods, respectively. In the 2.0% APF solution for 2-h immersion, the thermal desorption of hydrogen appeared with a single desorption peak at approximately 450°C. When the immersion time was longer than 4 h, another peak appeared at lower temperatures. For more than 12 h of immersion, the peak at 450°C disappeared and a broad peak located from room temperature to 350°C appeared. In contrast, a single peak at approximately 450°C appeared for the specimens immersed in the 0.2% APF solution irrespective of immersion time. The progress of hydrogen entry into the specimen was denoted by the increase in total desorbed hydrogen, defined as the integrated peak intensity, relative to immersion time. The total amounts of hydrogen desorbed at up to 600°C for the specimens immersed in 2.0% and 0.2% APF solutions are shown as functions of immersion time in Figs. 7(a) and (b), respectively. The amount of desorbed hydrogen, i.e., hydrogen absorbed during the immersion test, increased linearly with immersion time for the 2.0% APF solution. The amounts of hydrogen absorbed for 2 and 24 h were approximately 500 and 5300 mass ppm, respectively. On the other hand, the amount of hydrogen absorbed in the

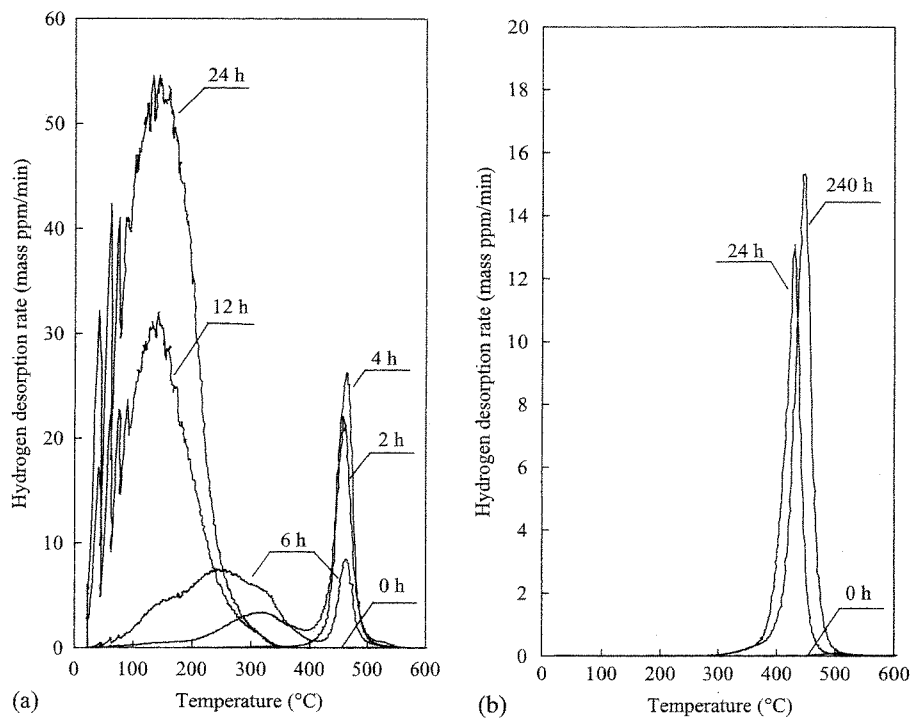


Fig. 6. Hydrogen thermal desorption curves for specimens immersed for various periods in (a) 2.0% APF solution and (b) 0.2% APF solution.

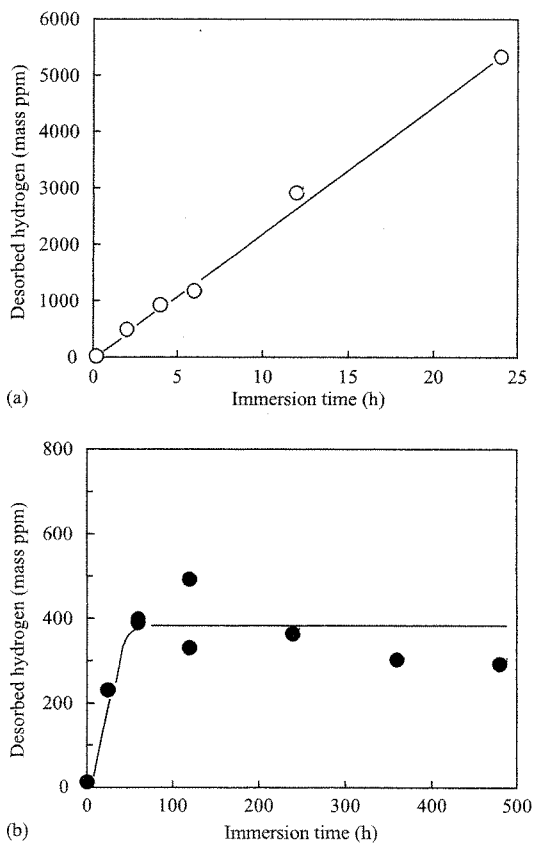


Fig. 7. Amount of desorbed hydrogen from thermal desorption analysis as a function of immersion time of specimens immersed in (a) 2.0% APF solution and (b) 0.2% APF solution.

0.2% APF solution increased with immersion time up to 60 h, above which it saturated at approximately 300–500 mass ppm. The amount of hydrogen absorbed in the 0.2% APF solution was one order in magnitude smaller than that in the 2.0% APF solution.

4. Discussion

One noteworthy finding in the present study is that the degradation of mechanical properties due to hydrogen absorption in work-hardened Ni–Ti alloy occurs in the 2.0% APF solution, similar to that in Ni–Ti superelastic alloy in our previous studies [20,21]. After the immersion in the 2.0% APF solution for 2 h, the work-hardened Ni–Ti alloy often fractured without necking, suggesting that the amount of hydrogen absorbed for 2 h, i.e., approximately 500 mass ppm, was the critical value for the ductility loss. However, it should be noted that hydrogen content does not always give an indication of occurrence of hydrogen embrittlement, although the presence of hydrogen is a premise for the degradation. The distribution and states of hydrogen, e.g., hydride, weakly trapped at defects or occluded interstitially, in the materials are essential issues for hydrogen embrittlement [32]. When Ni–Ti superelastic or shape memory alloys absorb hydrogen beyond the solubility limit, hydride forms, which can be confirmed by XRD measurements [22,26,27]. In the present study, however, hydride was not identified from the

hydrogen-absorbed work-hardened Ni–Ti alloy by XRD measurements. It is likely that hydride hardly formed for the work-hardened Ni–Ti alloy immersed in the 2.0% APF solution.

Absorbed hydrogen diffuses towards the center of the specimen with time. The diffusion coefficient of hydrogen in Ni–Ti alloy with a B2 structure at 37°C reported by Schmidt et al. [33], i.e., $D = 7.3 \times 10^{-15} \text{ m}^2/\text{s}$, is not sufficiently fast to diffuse from the surface to the center of the specimen during a limited time. Using this diffusion coefficient, the diffusion distance of hydrogen in Ni–Ti alloy is calculated to be 15 μm in 2 h. As a consequence, at the peripheral part of the cross section of the specimen immersed in the 2.0% APF solution, the hydrogen concentration is probably much higher than that at the center of the specimen. At the peripheral part of the cross section corresponding to the hydrogen diffusion distance, the brittle fracture mode was observed as shown in Fig. 2(d) and the increase in hardness was revealed for the specimens immersed in the 2.0% APF solution. These findings indicate that the fracture was initiated at the hardened peripheral part of the cross section. The hardening at the peripheral part might be due to the supersaturated solid solution of hydrogen. Therefore, one of the reasons for the ductility loss and the reduction in the tensile strength of the work-hardened Ni–Ti alloy immersed in the 2.0% APF solution is the brittle layer formation at the peripheral part of the cross section associated with rapid hydrogen absorption.

The fact that hydrogen thermal desorption shifted to lower temperatures with immersion time and the desorption peak broadened for the specimens immersed in the 2.0% APF solution, as shown in Fig. 6(a), suggests the existence of several different states of hydrogen. Generally, hydrogen desorption at a high temperature is associated with hydride decomposition. On the basis of our previous studies [20,31,34], the temperature of hydride decomposition is around 300–500°C for the Ni–Ti superelastic alloy. Strongly trapped hydrogen also desorbs in these temperature regions. In the present study, hydrogen desorption at approximately 450°C is interpreted as hydrogen strongly trapped or irreversible to solid solution. The relationship between desorption behavior and hydrogen states must be investigated in detail in the future. The desorption at around 200°C often appears for Ni–Ti superelastic alloy with cathodic hydrogen charging [34] and with immersion in methanol solution containing hydrochloric acid [31]. The origins of hydrogen desorption at lower temperatures are probably diffusive hydrogen, i.e., hydrogen weakly trapped and reversible to solid solution. For steel, hydrogen desorbed at lower temperatures greatly affects their mechanical properties compared with that at higher temperatures [35]. In the present study, the pronounced degradation of tensile

properties was consistent with the appearance of desorption at lower temperatures. However, applying the concept proposed for steel to Ni–Ti alloy should be discussed carefully. The effects of hydrogen desorbed at lower temperatures on the degradation of the mechanical properties will be reported in a later paper.

In our previous study of Ni–Ti superelastic alloy immersed in the 0.2% APF solution [20], when the immersion time exceeded 3 h, the amount of absorbed hydrogen was more than 100 mass ppm and the tensile strength decreased markedly. When the immersion time exceeded 6 h, the tensile strength decreased to the critical stress level for martensite transformation. The amount of hydrogen absorbed in the 0.2% APF solution for 24 h was more than 900 mass ppm. In addition, the critical stress for martensite transformation was increased from 530 to 600 MPa by hydrogen absorption. For the Ni–Ti superelastic alloy, even a small amount of absorbed hydrogen is considered to prevent the transformation from parent to martensite phases [29,30], thereby causing a reduction in tensile strength and increment in critical stress for martensite transformation.

The amount of absorbed hydrogen in the work-hardened Ni–Ti alloy was smaller than that in the Ni–Ti superelastic alloy [20] in the 0.2% APF solution. The amount of mass loss of work-hardened Ni–Ti alloy was approximately equal to that of the Ni–Ti superelastic alloy [20], although the rate of mass loss of the work-hardened Ni–Ti alloy was lower than that of the Ni–Ti superelastic alloy. As shown in Figs. 5 and 7, the increment in the amount of hydrogen coincided with the increment in the mass loss. The hydrogen absorption process in the APF solutions of work-hardened Ni–Ti alloy is probably common in those of Ni–Ti superelastic alloy [20] as well as titanium and its alloys, as reported elsewhere [23,25]. That is, the breakdown of protective film on the surface readily takes place in fluoride solutions [36–41] leading to the dissolution of the alloy and hydrogen absorption because of the high affinity of titanium. However, the hydrogen absorption behavior differs from material factors including alloying elements, microstructure, grain size, the second phase, defects and dislocation density. It is necessary to investigate the effects of these material factors on hydrogen absorption behavior.

For the work-hardened Ni–Ti alloy immersed in the 0.2% APF solution, even though the amount of absorbed hydrogen exceeded several hundreds mass ppm, the degradation of tensile properties hardly occurred. The reason for this is the lack of brittle-layer formation at the peripheral part of the cross section of the specimen because hydrogen is slowly absorbed from the surface and diffuses inwards in the 0.2% APF solution. As evidence of hydrogen diffusion to the center of specimen, there is a slight reduction in hardness at the center of the specimens immersed in the 0.2% APF

solution, as shown in Fig. 3(b). This reduction in hardness is ascribed to the hydrogen-enhanced dislocation mobility or hydrogen-induced decohesion [42–44]. A similar reduction in hardness caused by hydrogen absorption was observed for beta-titanium alloy [23]. These results indicate that the susceptibility of work-hardened Ni–Ti alloy to hydrogen embrittlement is lower than that of Ni–Ti superelastic alloy in the 0.2% APF solution. However, since hydrogen absorption is enhanced by applied stress [24], plastic deformation [45] and electrochemical potential [46–48], the reduction in tensile strength or the ductility loss of the work-hardened Ni–Ti alloy may occur in practice.

5. Conclusions

In the present study, we have demonstrated that the hydrogen embrittlement of work-hardened Ni–Ti alloy occurs in acid fluoride solutions, similar to that of Ni–Ti superelastic alloy reported previously. The amount of absorbed hydrogen in the embrittlement of work-hardened Ni–Ti alloy is several times larger than that of Ni–Ti superelastic alloy. The degradation of the mechanical properties of work-hardened Ni–Ti alloy in the 2.0% APF solution is caused by brittle-layer formation associated with rapid hydrogen absorption. Upon immersion in the 0.2% APF solution, reduction in the tensile strength or ductility loss hardly occurs, although a slight reduction in hardness and a hydrogen absorption of 300–500 mass ppm are observed. Considering the degradation of mechanical properties, work-hardened Ni–Ti alloy, compared with Ni–Ti superelastic alloy, is less sensitive to hydrogen embrittlement.

Acknowledgements

This study was supported in part by a Grant-in-Aid for Young Scientists (B) (14771090) from the Ministry of Education, Culture, Sports, Science and Technology, Japan.

References

- [1] Andreasen GF, Hilleman TB. An evaluation of 55 cobalt substituted nitinol wire for orthodontics. *J Am Dent Assoc* 1971;82:1373–5.
- [2] Burstone CJ, Qin B, Morton JY. Chinese NiTi wire—a new orthodontic alloy. *Am J Orthod* 1985;87:445–52.
- [3] Miura F, Mogi M, Ohura Y, Hamanaka H. The super-elastic property of the Japanese NiTi alloy wire for use in orthodontics. *Am J Orthod Dentofac Orthop* 1986;90:1–10.
- [4] Miyazaki S, Otsuka K, Suzuki Y. Transformation pseudoelasticity and deformation behavior in a Ti–50.6 at% Ni alloy. *Scripta Metall* 1981;15:287–92.
- [5] Otsuka K, Shimizu K. Pseudoelasticity and shape memory effects in alloys. *Int Met Rev* 1986;31:93–114.
- [6] Roncelli G, Vicentini B, Cigada A. The corrosion behaviour of nickel–titanium shape memory alloys. *Corros Sci* 1990;30:805–12.
- [7] Oshida Y, Sachdeva R, Miyazaki S, Fukuyo S. Biological and chemical evaluation of TiNi alloys. *Mater Sci Forum* 1990; 56–58:705–10.
- [8] Rondelli G. Corrosion resistance tests on NiTi shape memory alloy. *Biomaterials* 1996;17:2003–8.
- [9] Wever DJ, Veldhuizen AG, Vries de J, Busscher HJ, Uges DRA, Horn van JR. Electrochemical and surface characterization of a nickel–titanium alloy. *Biomaterials* 1998;19:761–9.
- [10] Thierry B, Tabrizian M, Trepanier C, Savadogo O, Yahia L'H. Effect of surface treatment and sterilization processes on the corrosion behavior of NiTi shape memory alloy. *J Biomed Mater Res* 2000;51:685–93.
- [11] Shabalovskaya SA. Physicochemical and biological aspects of Nitinol as a biomaterial. *Int Mater Rev* 2001;46:233–50.
- [12] Edie JW, Andreasen GF, Zaytoun MP. Surface corrosion of nitinol and stainless steel under clinical conditions. *Angle Orthod* 1981;51:319–24.
- [13] Grimsdottir MR, Hensten-Pettersen A. Surface analysis of nickel–titanium archwire used in vivo. *Dent Mater* 1997;13:163–7.
- [14] Eliades T, Eliades G, Athanasiou AE, Bradley TG. Surface characterization of retrieved NiTi orthodontic archwires. *Eur J Orthod* 2000;22:317–26.
- [15] Harris EF, Newman SM, Nicholson JA. Nitinol arch wire in a simulated oral environment; changes in mechanical properties. *Am J Orthod Dentofac Orthop* 1988;93:508–13.
- [16] Hudgins JJ, Bagby MD, Erickson LC. The effect of long-term deflection on permanent deformation of nickel–titanium archwires. *Angle Orthod* 1990;60:283–8.
- [17] Mohlin B, Müller H, Ödman J, Thilander B. Examination of Chinese NiTi wire by a combined clinical and laboratory approach. *Eur J Orthod* 1991;13:386–91.
- [18] Yokoyama K, Hamada K, Moriyama K, Asaoka K. Degradation and fracture of Ni–Ti superelastic wire in an oral cavity. *Biomaterials* 2001;22:2257–62.
- [19] Asaoka K, Yokoyama K, Nagumo M. Hydrogen embrittlement of nickel–titanium alloy in biological environment. *Metall Mater Trans A* 2002;33A:495–501.
- [20] Yokoyama K, Kaneko K, Moriyama K, Asaoka K, Sakai J, Nagumo M. Hydrogen embrittlement of Ni–Ti superelastic alloy in fluoride solution. *J Biomed Mater Res* 2003;65A:182–7.
- [21] Kaneko K, Yokoyama K, Moriyama K, Asaoka K, Sakai J. Degradation in performance of orthodontic wires caused by hydrogen absorption during short-term immersion in 2.0% acidulated phosphate fluoride solution. *Angle Orthod* 2004;74:487–95.
- [22] Yokoyama K, Kaneko K, Moriyama K, Asaoka K, Sakai J, Nagumo M. Delayed fracture of Ni–Ti superelastic alloys in acidic and neutral fluoride solutions. *J Biomed Mater Res* 2004;69A:105–13.
- [23] Kaneko K, Yokoyama K, Moriyama K, Asaoka K, Sakai J, Nagumo M. Delayed fracture of beta titanium orthodontic wire in fluoride aqueous solutions. *Biomaterials* 2003;24:2113–20.
- [24] Ogawa T, Yokoyama K, Asaoka K, Sakai J. Hydrogen absorption behavior of beta titanium alloy in acid fluoride solutions. *Biomaterials* 2004;25:2419–25.
- [25] Yokoyama K, Kaneko K, Miyamoto Y, Asaoka K, Sakai J, Nagumo M. Fracture associated with hydrogen absorption of sustained tensile-loaded titanium in acid and neutral fluoride solutions. *J Biomed Mater Res* 2004;68A:150–8.

- [26] Wade N, Adachi Y, Hosoi Y. A role of hydrogen in shape memory effect of Ti–Ni alloys. *Scripta Metall Mater* 1990;24:1051–5.
- [27] Adachi Y, Wade N, Hosoi Y. Effect of hydrogen on the shape memory effect and transformation behavior of Ti–Ni alloy. *J Japan Inst Metals* 1990;54:525–31.
- [28] Hoshiya T, Den S, Katsuta H, Ando H. Effect of hydrogen on transformation characteristics and deformation behavior in a TiNi shape memory alloy. *J Japan Inst Metals* 1992;56:747–56.
- [29] Asaoka T, Yamashita H, Saito H, Ishida Y. Effect of a small amount of hydrogen on pseudo-elastic properties of Ti–Ni alloy. *J Japan Inst Metals* 1993;57:1123–9.
- [30] Biscarini A, Campanella R, Coluzzi B, Mazzolai G, Trotta L, Tuissi A, Mazzolai FM. Martensitic transitions and mechanical spectroscopy of Ni_{50.8}Ti_{49.2} alloy containing hydrogen. *Acta Mater* 1999;47:4525–33.
- [31] Yokoyama K, Ogawa T, Asaoka K, Sakai J, Nagumo M. Degradation of tensile strength of Ni–Ti superelastic alloy due to hydrogen absorption in methanol solution containing hydrochloric acid. *Mater Sci Eng A* 2003;360:153–9.
- [32] Nagumo M. Function of hydrogen in embrittlement of high-strength steels. *ISIJ Int* 2001;41:590–8.
- [33] Schmidt R, Schlereth M, Wipf H, Assmus W, Müllner M. Hydrogen solubility and diffusion in the shape-memory alloy NiTi. *J Phys Condens Matter* 1989;1:2473–82.
- [34] Yokoyama K, Watabe S, Hamada K, Sakai J, Asaoka K, Nagumo M. Susceptibility to delayed fracture of Ni–Ti superelastic alloy. *Mater Sci Eng A* 2003;341:91–7.
- [35] Takai K, Watanuki R. Hydrogen in trapping states innocuous to environmental degradation of high-strength steels. *ISIJ Int* 2003;43:520–6.
- [36] Lausmaa J, Kasemo B, Hansson S. Accelerated oxide grown on titanium implants during autoclaving caused by fluorine contamination. *Biomaterials* 1985;6:23–7.
- [37] Könönen MHO, Lavonius ET, Kivilahti JK. SEM observations on stress corrosion cracking of commercially pure titanium in a topical fluoride solution. *Dent Mater* 1995;11:269–72.
- [38] Reclaru L, Meyer J-M. Effects of fluorides on titanium and other dental alloys in dentistry. *Biomaterials* 1998;19:85–92.
- [39] Nakagawa M, Matsuya S, Shiraishi T, Ohta M. Effect of fluoride concentration and pH on corrosion behavior of titanium for dental use. *J Dent Res* 1999;78:1568–72.
- [40] Huang H-H. Effects of fluoride concentration and elastic tensile strain on the corrosion resistance of commercially pure titanium. *Biomaterials* 2002;23:59–63.
- [41] Schiff N, Grosgeat B, Lissac M, Dalard F. Influence of fluoride content and pH on the corrosion resistance of titanium and its alloys. *Biomaterials* 2002;23:1995–2002.
- [42] Beachem CD. A new model for hydrogen-assisted cracking (hydrogen “embrittlement”). *Metall Trans* 1972;3:437–51.
- [43] Birnbaum HK, Sofronis P. Hydrogen-enhanced localized plasticity—a mechanism for hydrogen-related fracture. *Mater Sci Eng A* 1994;176:191–202.
- [44] Oriani RA, Josephic PH. Equilibrium aspects of hydrogen-induced cracking of steels. *Acta Metall* 1974;22:1065–74.
- [45] Nagumo M, Takai K, Okuda N. Nature of hydrogen trapping sites in steels induced by plastic deformation. *J Alloy Comp* 1999;293–295:310–6.
- [46] Nagumo M, Uyama H, Yoshizawa M. Accelerated failure in high strength steel by alternating hydrogen-charging potential. *Scripta Mater* 2001;44:947–52.
- [47] Phillips II, Poole P, Shreir LL. Hydride formation during cathodic polarization of Ti–I. Effect of current density on kinetics of growth and composition of hydride. *Corros Sci* 1972;12:855–66.
- [48] Wang ZF, Briant CL, Kumar KS. Electrochemical, galvanic, and mechanical responses of grade 2 titanium in 6% sodium chloride solution. *Corrosion* 1999;55:128–38.

Hydrogen absorption of titanium in acidic fluoride solutions

Ken'ichi Yokoyama^{a,*}, Toshio Ogawa^b, Kenzo Asaoka^a, Jun'ichi Sakai^b

^a Department of Dental Engineering, School of Dentistry, The University of Tokushima, 3-18-15 Kuramoto-cho, Tokushima 770-8504, Japan

^b Department of Materials Science and Engineering, Waseda University, 3-4-1 Okubo, Shinjuku-ku, Tokyo 169-8555, Japan

Received 25 March 2004; received in revised form 30 April 2004

Abstract

Hydrogen absorption of commercial pure titanium in acidulated phosphate fluoride (APF) solutions of various concentrations has been examined by hydrogen thermal-desorption analysis. In immersion in the 2.0% APF solution of pH 5.0 at 25 °C, the amount of absorbed hydrogen increased with immersion time and then saturated at approximately 800–900 mass ppm. During the early stage of the 24 h immersion, the amount of hydrogen absorbed in the 0.2% APF solution was almost the same as that in the 2.0% APF solution, i.e., 200 mass ppm, whereas it saturated at 300 mass ppm with longer immersion time. For the specimen immersed in the 2.0% APF solution for 24 h, hydrogen desorption was observed with a peak at approximately 550 °C. As the immersion time increased, the second desorption appeared in the range from 150 to 400 °C. In contrast, for the specimens immersed in the 0.2% APF solution, the desorption peak temperature tended to shift from 550 to 450 °C with immersion time. Hydrogen absorption was hardly observed in the specimen immersed in the 0.02% APF solution. The concentration of the APF solutions also affected the type of corrosion product and the surface topography of the immersed specimens. The results of the present study clearly indicate that the degradation of the mechanical properties or fracture of titanium caused by hydrogen absorption occurs in acidic fluoride solutions.

© 2004 Elsevier B.V. All rights reserved.

Keywords: Titanium; Corrosion; Hydrogen embrittlement; Fluoride; Thermal-desorption analysis

1. Introduction

Titanium is widely used in dental implants or devices because of its high biocompatibility and corrosion resistance. The high corrosion resistance of titanium is due to a thin passive film, mainly TiO₂, on the surface. However, it is considered that the corrosion resistance of titanium is not always satisfactory in the oral environment. It has been reported [1–16] that there is pronounced reduction in the corrosion resistance of titanium in the presence of fluorides such as NaF, which is added to prophylactic agents and toothpastes, owing to the cariostatic effect. Generally, the caries-preventing prophylactics contain 0.02–2.0% NaF with a pH value between 3.5 and neutral. According to these results, the breakdown of the passive film occurs readily in fluoride solutions. Furthermore, we have recently found that the degradation of the mechanical properties and fracture of titanium and its alloys are associated with hydrogen absorption in acidulated

phosphate fluoride (APF) solutions [17–22]. Since titanium has closer affinity with hydrogen, the breakdown of the passive film possibly leads to hydrogen absorption.

The susceptibility of titanium to hydrogen embrittlement has been investigated extensively under suitable laboratory testing conditions such as cathodic hydrogen charging [23–26], immersion in methanol solution containing hydrochloric acid [27–30] and exposure to gaseous hydrogen [31,32]. The solubility limit of hydrogen in alpha titanium is at most a few tens mass ppm at room temperature. When the amount of absorbed hydrogen exceeds a few hundreds mass ppm, the mechanical properties of titanium markedly degrade in relation to brittle hydride formation [33,34]. However, how much hydrogen is absorbed in fluoride solutions and the hydrogen absorption behavior have not yet been clarified. If titanium absorbs substantial amounts of hydrogen in fluoride solutions for a short term, hydrogen embrittlement will be a serious issue regarding the use of titanium in the dental field.

The purpose of the present study is to evaluate the hydrogen absorption of titanium in APF solutions of various concentrations by hydrogen thermal-desorption analysis (TDA),

* Corresponding author. Tel.: +81 88 633 7334; fax: +81 88 633 9125.
E-mail address: yokken@dent.tokushima-u.ac.jp (K. Yokoyama).

Table 1

Chemical composition of the commercial pure titanium tested (mass%)	
C	0.003
H	0.0010
O	0.107
N	0.003
Fe	0.026
Ti	Balance

which is a powerful tool for analyzing the content and states of hydrogen in various materials.

2. Materials and methods

Commercial pure titanium wire of 0.50 mm diameter was cut into specimens of 50 mm length. The nominal chemical composition of the wire is given in Table 1. Percent in this paper means mass percent, unless otherwise stated. The specimens were carefully polished with 600-grit SiC paper and ultrasonically washed in acetone for 5 min. The specimens were immersed separately in 50 ml of an aqueous solution of 2.0% APF (2.0% NaF + 1.7% H₃PO₄) with pH 5.0 at room temperature (25 ± 2 °C). For evaluation of solution concentration, 0.2 and 0.02% APF solutions were prepared by dilution of the 2.0% APF solution. The NaF contents in the 2.0, 0.2 and 0.02% APF solutions correspond to that in commercial prophylactic agents, toothpastes and dental rinses, respectively.

The amount of desorbed hydrogen was measured by TDA for the immersed specimens. The immersed specimens were cut at both ends and subjected to ultrasonic cleaning with acetone for 2 min. Subsequently, the specimens were dried in ambient air and then subjected to measurement. TDA was started 30 min after the removal of specimens from the test solutions. A quadrupole mass spectrometer (ULVAC, Kanagawa, Japan) was used for hydrogen detection. Sampling was conducted at 30 s intervals at a heating rate of 100 °C/h.

The side surface of the immersed specimens was observed by scanning electron microscopy (SEM). The corrosion products on the surface of the immersed specimens and the surfaces after removal of the corrosion products were examined using an X-ray diffractometer with Cu K α radiation of wavelength $\lambda = 1.54056 \text{ \AA}$ in the 2θ angle range from 30 to 80° operated at 40 kV and 30 mA. To remove the corrosion products from the surfaces, 600-grit SiC paper was employed. The mass change and diameter of the specimens were measured using a microbalance and a micrometer caliper, respectively. Standard deviations were calculated from the results obtained for five specimens.

3. Experimental results

The representative hydrogen thermal-desorption curves of the specimens immersed in the 2.0 and 0.2% APF solutions for various periods are shown in Figs. 1 (a) and (b), respectively. For the specimen immersed in the 2.0% APF solution

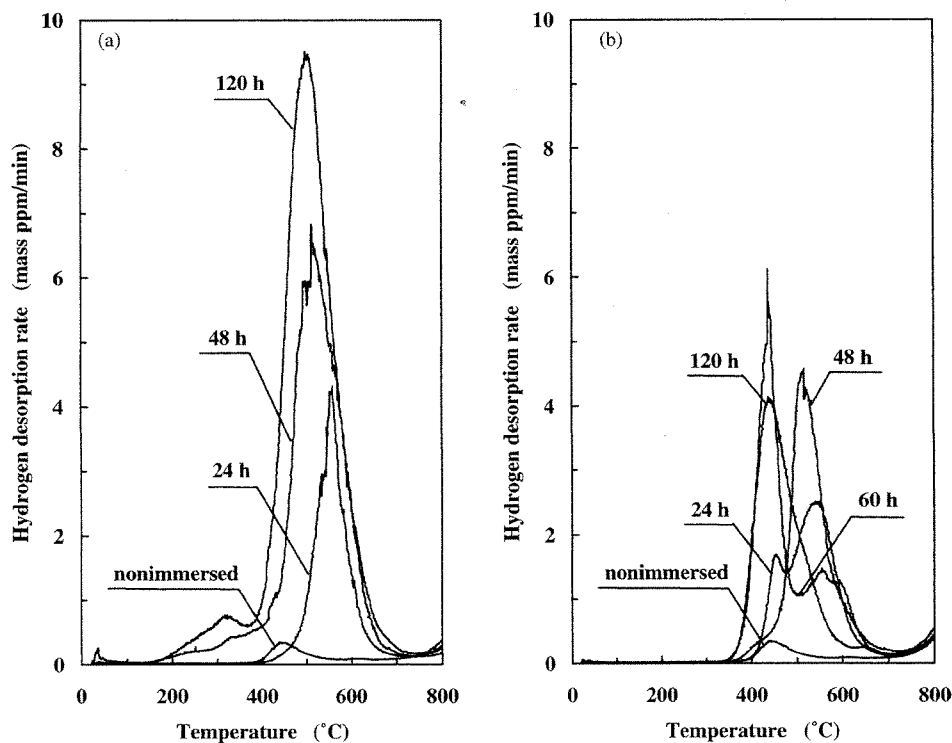


Fig. 1. Hydrogen thermal-desorption curves for specimens immersed for various periods in (a) 2.0% and (b) 0.2% APF solutions.

for 24 h, a single desorption peak was observed at around 550 °C. As the immersion time increased, other desorptions appeared at lower temperatures. In the case of the specimen immersed in the 0.2% APF solution, the desorption peak at 550 °C tended to shift to that at 450 °C with longer immersion time. The amount of desorbed hydrogen was calculated by integrating desorption peak intensity up to 800 °C. The amount of desorbed hydrogen, i.e., the amount of hydrogen absorbed during the immersion test, is shown in Fig. 2 for the specimens immersed in the 2.0, 0.2 or 0.02% APF solutions. The figure clearly shows that titanium absorbed substantial amounts of hydrogen in the 2.0 and 0.2% APF solutions. The hydrogen content of the non-immersed specimen obtained from TDA, that is, pre-dissolved hydrogen content, was 42 mass ppm. Hence, the amount of hydrogen absorbed during the immersion test was calculated by subtracting the pre-dissolved hydrogen content from the amount of desorbed hydrogen. The amount of absorbed hydrogen increased with immersion time during the early stage of immersion in the 2.0% APF solution, and then saturated to approximately 800–900 mass ppm after 72 h. In the later stage of the immersion, the surface layer tended to peel off the specimen. The reduction in the hydrogen content of specimens immersed longer than 150 h is probably due to this peeling off of the surface layer. In immersion in the 0.2% APF solution for more than 48 h, the amount of absorbed hydrogen saturated up to approximately 300 mass ppm. It should be emphasized that the amount of hydrogen absorbed for 24 h, i.e., 200 mass ppm, was almost the same in both the 2.0 and 0.2% APF solutions. After the immersion in the 0.02% APF solution, the increment in hydrogen content was scarcely confirmed.

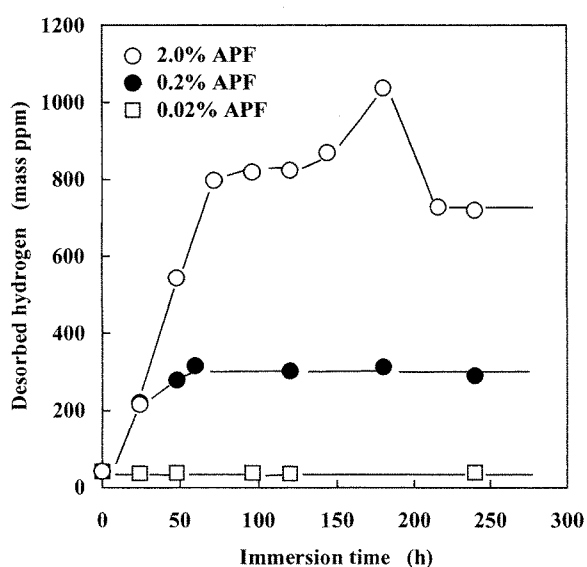


Fig. 2. Amounts of desorbed hydrogen obtained from thermal-desorption analysis of specimens immersed in 2.0, 0.2 and 0.02% APF solutions as functions of immersion time.

On the side surface of the non-immersed specimen, scratches due to SiC paper polishing were observed, as shown in the SEM micrographs in Figs. 3 (a) and (b). The small white spots were SiC particles embedded in the surface. Upon the 24 h immersion in the 2.0% APF solution, corrosion products uniformly deposited on the surface of the specimen, as observed on a macroscopic scale in Fig. 3 (c). The corrosion products were granular and approximately 10 μm in diameter, as shown in Fig. 3 (d); they readily peeled off the surface. On the other hand, general corrosion was observed on the surface of the specimen immersed in the 0.2% APF solution for 24 h, as shown in Figs. 3 (e) and (f). The surface was shown microscopically to have a number of shallow depressions. Figs. 3 (g) and (h) show the surface of the specimen immersed in the 0.02% APF solution for 24 h. The white spots observed in Figs. 3 (a) and (b) disappeared and very slight corrosion was observed, although scratches due to SiC paper polishing remained. The observed topographic features on the surface of specimens immersed in all the test solutions hardly changed with longer immersion time.

Fig. 4 (a) shows the results of X-ray diffraction (XRD) measurements of the side surface of the non-immersed specimen, i.e., alpha titanium. The XRD patterns of the specimen immersed in the 2.0% APF solution for 24 h before and after removal of corrosion products are shown in Figs. 4 (b) and (c), respectively. Sodium titanium fluoride, i.e., Na_3TiF_6 (monoclinic; $a = 0.5543$ nm, $b = 0.5748$ nm, $c = 0.8002$ nm, and $\beta = 90.29^\circ$), was revealed on the surface of the immersed specimen before removal of the surface layer. On the surface of the immersed specimen after removal of the corrosion products, titanium hydride, i.e., TiH_2 (tetragonal; $a = 0.312$ nm, $c = 0.418$ nm), was confirmed. For the surface of the specimen immersed in the 0.2% APF solution for 24 h before and after removal of the surface layer, the formation of titanium fluoride, i.e., TiF_2 (cubic; $a = 0.51555$ nm), and the hydride were confirmed, respectively, as indicated in Figs. 4 (d) and (e). Note that the type of corrosion product depended on the concentration of the APF solution. On the surface of the specimen immersed in the 0.02% APF solution, only the alpha titanium peak was detected.

The results of the mass change of specimens immersed in each APF solution are shown in Fig. 5. The mass of specimen increased during the early stage of the immersion in the 2.0% APF solution, and then it decreased after more than 72 h. The mass increase resulting from the corrosion products deposited on the surface of specimen seems to be larger than the mass loss arising from dissolution. After the immersion in the 0.2% APF solution, the mass decreased gradually, and then the mass loss saturated. For the specimens immersed in the 0.02% APF solution, mass change was not detected.

Fig. 6 shows the ratio of diameter change of the specimens immersed in the APF solutions as functions of immersion time. The diameter increased during the early stage of the immersion in the 2.0% APF solution, and then it decreased

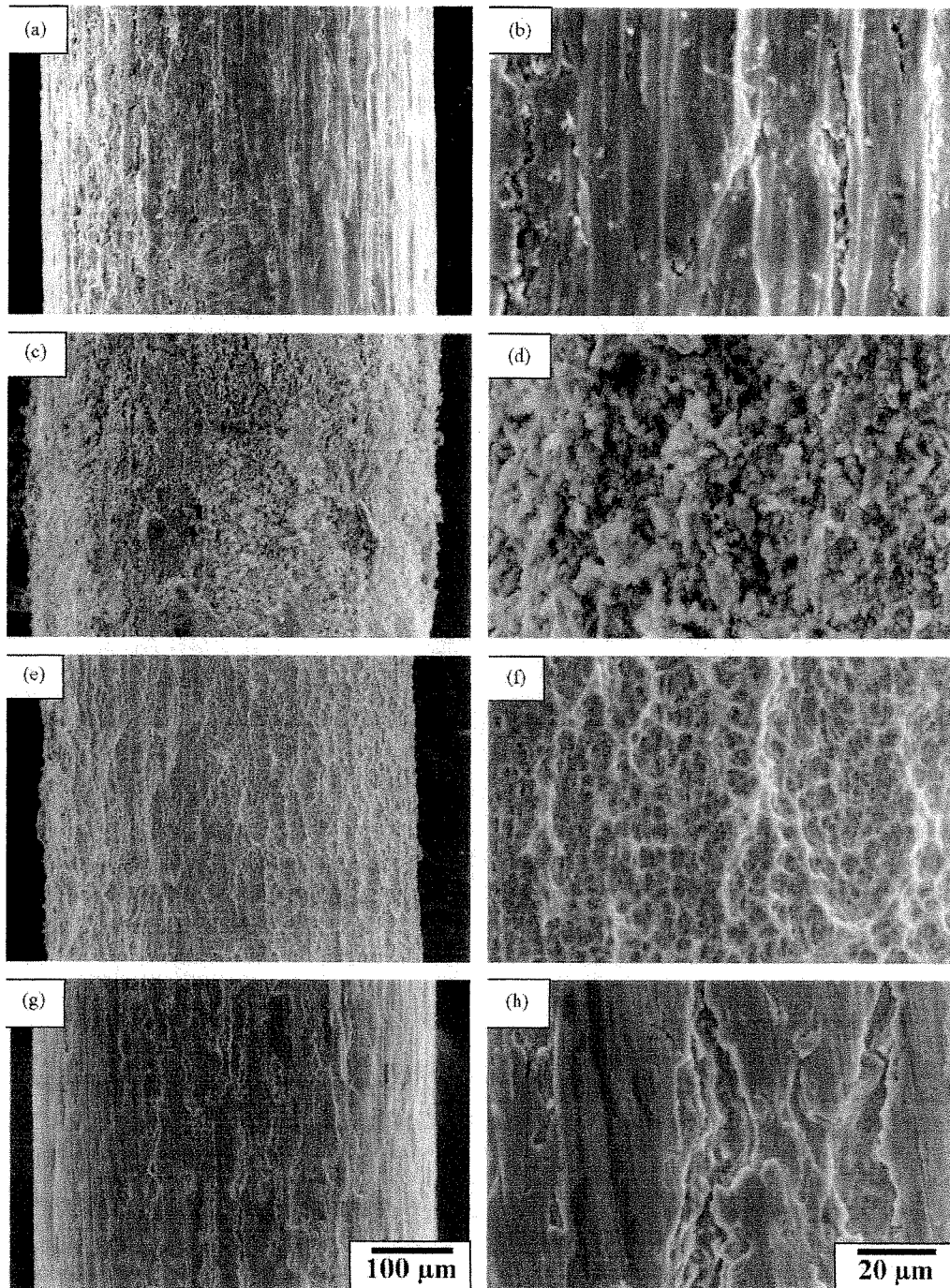


Fig. 3. SEM micrographs of a typical side surface: (a) general and (b) magnified views of a non-immersed specimen; (c) general and (d) magnified views of a specimen immersed in 2.0% APF solution for 24 h; (e) general and (f) magnified views of a specimen immersed in 0.2% APF solution for 24 h; and (g) general and (h) magnified views of a specimen immersed in 0.02% APF solution for 24 h.

after more than 72 h. In the immersion in the 0.2% APF solution, the diameter decreased gradually, and then the decrease in diameter saturated. The diameter change was not observed in the specimens immersed in the 0.02% APF solution. The behavior of diameter change was consistent with that of mass change.

4. Discussion

The above results clearly demonstrate that commercial pure titanium absorbs substantial amounts of hydrogen, which leads to the degradation of the mechanical properties of titanium in 2.0 and 0.2% APF solutions. When

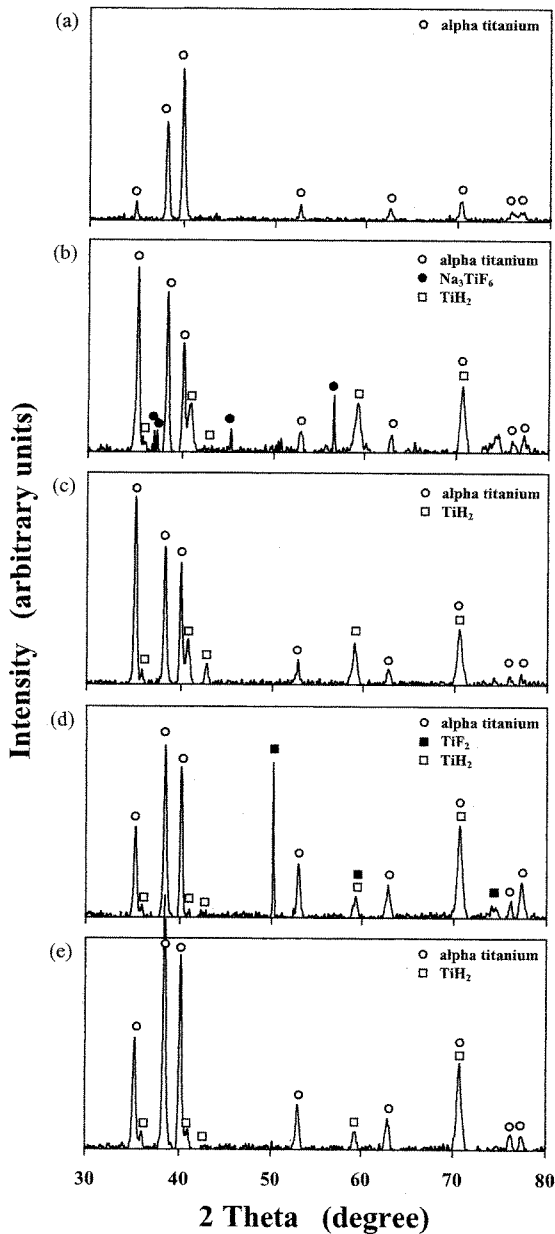


Fig. 4. XRD patterns for the surface of (a) non-immersed specimen, (b) before and (c) after removal of corrosion products from the surface of specimens immersed in 2.0% APF solution for 24 h, and (d) before and (e) after removal of corrosion products from the surface of specimens immersed in 0.2% APF solution for 24 h.

the amount of absorbed hydrogen exceeds a few hundred mass ppm, the pronounced degradation of mechanical properties generally occurs for alpha titanium [23–34]. The authors previously proved that the hydrogen-related failure of commercial pure titanium takes place under a sustained tensile-loading test in a 2.0% APF solution [21]. The time to fracture decreased with increasing applied stress and was in the range from 15 to 220 h. From the present results of TDA as shown in Fig. 2, the amount of hydrogen

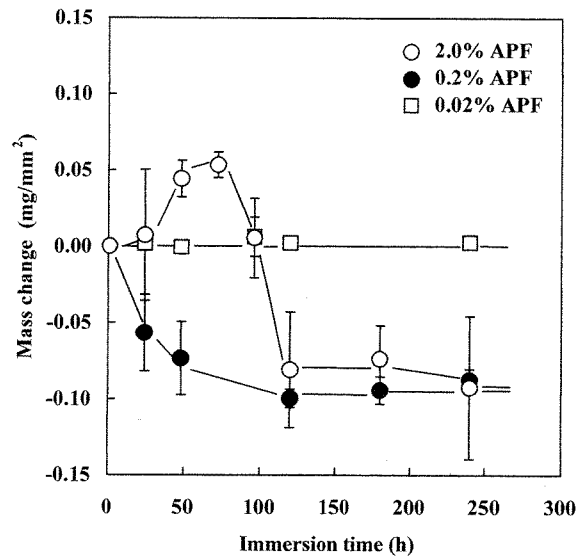


Fig. 5. Mass change of specimens immersed in 2.0, 0.2 and 0.02% APF solutions. Standard deviation was calculated from the results of five specimens.

absorbed in the 2.0% APF solution for 24 h was 200 mass ppm. Thus, the hydrogen content required to initiate the degradation of mechanical properties is estimated to be roughly 100–200 mass ppm, although the enhancement of hydrogen absorption due to applied stress is not reflected. This estimation is in good agreement with that obtained by cathodic hydrogen charging [23–26] or exposure to gaseous hydrogen [31,32].

Hydrogen absorption arises from the breakdown of the thin passive film on the titanium surface in corrosive

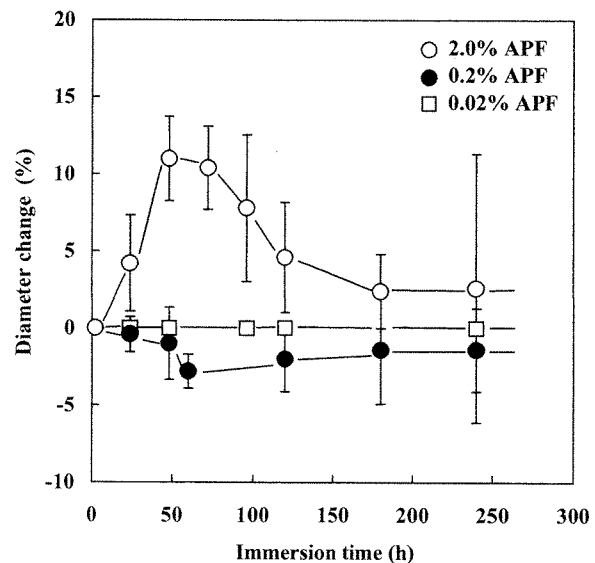


Fig. 6. Diameter change of specimens immersed in 2.0, 0.2 and 0.02% APF solutions. Standard deviation was calculated from the results of five specimens.

environments. Upon the immersion in the APF solutions, film breakdown occurred and corrosion products deposited on the surface of titanium, as shown in Fig. 3. Hydrogen absorption behavior was almost consistent with the progress of corrosion, as indicated in Figs. 2, 5 and 6. Since the corrosion products often prevent the progress of corrosion, it is possible that hydrogen absorption saturated during the later stage of the immersion. For the beta titanium alloy reported previously [22], however, the corrosion products hardly prevent the progress of corrosion and hydrogen absorption. Moreover, the corrosion products tended to peel off, particularly under applied stress [21], causing the reduction in the diameter of the specimen. Therefore, taking into consideration the effect of corrosion prevention by corrosion products and reduction in diameter on the hydrogen-related failure is needed for a detailed discussion.

Various mechanisms of hydrogen embrittlement have been proposed [35–38]. In the case of alpha titanium, the theory of brittle hydride formation and cracking is widely accepted, although there is no direct evidence of fracture associated with hydrides. Because hydrides differ in elastic properties from alpha titanium, cracking of hydrides provides sites for void nucleation even with a low hydride density. In the present study, from the results of XRD measurements in Fig. 4, hydride formation was revealed on the surface of the specimens immersed in 2.0 and 0.2% APF solutions. As shown in Fig. 1, it appears that the higher-temperature desorption of hydrogen is connected with hydride decomposition [39]. However, we must be cautious in applying the embrittlement mechanism of hydride formation and cracking because the mechanical properties are more affected by a lower-temperature desorption of hydrogen, such as hydrogen weakly trapped in defects [40,41]. The present results of TDA indicate that there were different states of hydrogen in titanium immersed in the APF solutions. The states of absorbed hydrogen in titanium will be the key point in elucidating the mechanism of hydrogen embrittlement.

Moreover, the distribution of hydrogen in a specimen plays an important role in the degradation of the mechanical properties of materials. The diffusion coefficient of hydrogen in alpha titanium has been presented by several researchers [42–45]. Using the reported diffusion coefficient at room temperature, e.g., $D = 2 \times 10^{-11} \text{ m}^2/\text{s}$ [45], hydrogen is considered to diffuse to the center of a specimen. In addition, hydrogen is transported by dislocation motion. Conversely, hydride formation at several tens of microns from the surface of the specimen possibly prevents hydrogen diffusion to the center of the specimen at room temperature [23–26]. This hydride also serves as a barrier to further enhance hydrogen absorption. In this case, hydrogen concentration near the surface of a specimen is much higher than that at the center of the specimen. Actually, in our previous study [21], ductility loss was observed at the peripheral part of the fracture surface of commercial pure titanium under the sustained tensile-loading test in the 2.0% APF solution. In the present

study, the amount of hydrogen obtained from TDA was average value over the entire specimen. The distribution of hydrogen in titanium will be reported in detail elsewhere.

As the temperature is raised, hydrogen diffuses to the center of the specimen and the solubility limit of hydrogen increases. For a cathodic hydrogen-charging test, when the solution temperature was increased from 25 to 40 °C, hydrogen absorption was enhanced and the thickness of the hydride layer became almost two times larger [24]. In the present study, immersion tests were performed at 25 °C. If immersion tests are conducted at the test temperature of 37 °C, the amount of absorbed hydrogen will increase markedly.

The amount of absorbed hydrogen was approximately 300 mass ppm in the 0.2% APF solution, as shown in Fig. 2, indicating that the degradation of the mechanical properties of titanium occurs. The hydrogen desorption behavior varied between the 2.0 and 0.2% APF solutions, implying that hydrogen absorption behavior and the states of hydrogen in titanium depend on the concentration of the APF solution. On the basis of the surface analysis, it was found that the type of corrosion product and surface topography of the specimen immersed in the 0.2% APF solution were different from those of the specimen immersed in the 2.0% APF solution. The corrosion products of the specimen immersed in the 0.2% APF solution were hard to peel off the surface compared with those of the specimen immersed in the 2.0% APF solution. The mass and diameter losses are caused by the dissolution of titanium in the 0.2% APF solution. Since there is a possibility that corrosion products slightly affect hydrogen desorption behavior, this effect must be investigated. During the early stage of the immersion, i.e., immersion up to 24 h, the amount of hydrogen absorbed in the 0.2% APF solution was almost the same as that in the 2.0% APF solution. This result implies that the time to fracture does not differ significantly between the 2.0 and 0.2% APF solutions under the sustained tensile-loading test.

In the immersion in 0.02% APF solution, hydrogen absorption and corrosion were hardly observed, suggesting that the critical concentration of APF solution for hydrogen absorption is between 0.2 and 0.02%. However, hydrogen absorption is generally enhanced by environmental conditions including applied stress [22], electrochemical potential [23,25,26], test temperature and pH [24]. It is necessary to examine hydrogen absorption under these conditions in a 0.02% APF solution.

5. Conclusions

Hydrogen absorption of commercially pure titanium has been evaluated in APF solutions of various concentrations at room temperature by TDA. The amount of absorbed hydrogen increases with immersion time and saturates with longer immersion time. The amount of hydrogen absorbed in the 2.0% APF solution (800–900 mass ppm) is three times

larger than that in the 0.2% APF solution (300 mass ppm), although it is the same in both solutions during the early stage of immersion. The hydrogen desorption behavior of the specimens immersed in the 2.0% APF solution is different from that of the specimens immersed in the 0.2% APF solutions. Upon immersion in the 0.02% APF solution, hydrogen absorption and corrosion are scarcely observed. The concentration of the APF solutions affects not only hydrogen absorption, but also the type of corrosion product and the surface topography of the specimens. It is concluded that titanium absorbs sufficient amounts of hydrogen required for the degradation of the mechanical properties or fracture in 2.0 and 0.2% APF solutions.

Acknowledgements

This study was supported in part by a Grant-in-Aid for Young Scientists (B) (14771090) and a Grant-in-Aid for Scientific Research (C) (15560632) from the Ministry of Education, Culture, Sports, Science and Technology, Japan.

References

- [1] J. Lausmaa, B. Kasemo, S. Hansson, *Biomaterials* 6 (1985) 23.
- [2] H.S. Siirilä, M. Könönen, *Int. J. Oral Maxillofac. Implants* 6 (1991) 50.
- [3] L. Pröbster, W. Lin, H. Hüttemann, *Int. J. Oral Maxillofac. Implants* 7 (1992) 390.
- [4] M.H.O. Könönen, E.T. Lavonius, J.K. Kivilahti, *Dent. Mater.* 11 (1995) 269.
- [5] G. Boere, *J. Appl. Biomater.* 6 (1995) 283.
- [6] F. Toumelin-Chemla, F. Rouelle, G. Burdairon, *J. Dentistry* 24 (1996) 109.
- [7] H. Mimura, Y. Miyagawa, *Jpn. J. Dent. Mater. Dev.* 15 (1996) 283.
- [8] Y. Oda, E. Kawada, M. Yoshinari, K. Hasegawa, T. Okabe, *Jpn. J. Dent. Mater. Dev.* 15 (1996) 317.
- [9] L. Reclaru, J.-M. Meyer, *Biomaterials* 19 (1998) 85.
- [10] M. Nakagawa, S. Matsuya, T. Shiraiishi, M. Ohta, *J. Dent. Res.* 78 (1999) 1568.
- [11] M. Nakagawa, S. Matsuya, K. Udoh, *Dent. Mater. J.* 20 (2001) 305.
- [12] M. Nakagawa, S. Matsuya, K. Udoh, *Dent. Mater. J.* 21 (2002) 83.
- [13] H.-H. Huang, *Biomaterials* 23 (2002) 59.
- [14] H.-H. Huang, *Electrochim. Acta* 47 (2002) 2311.
- [15] N. Schiff, B. Grosgeat, M. Lissac, F. Dalard, *Biomaterials* 23 (2002) 1995.
- [16] K. Ide, M. Hattori, M. Yoshinari, E. Kawada, Y. Oda, *Dent. Mater. J.* 22 (2003) 359.
- [17] K. Yokoyama, K. Kaneko, K. Moriyama, K. Asaoka, J. Sakai, M. Nagumo, *J. Biomed. Mater. Res.* 65A (2003) 182.
- [18] K. Kaneko, K. Yokoyama, K. Moriyama, K. Asaoka, J. Sakai, M. Nagumo, *Biomaterials* 24 (2003) 2113.
- [19] K. Kaneko, K. Yokoyama, K. Moriyama, K. Asaoka, J. Sakai, *Angle Orthod.* 74 (2004) 487.
- [20] K. Yokoyama, K. Kaneko, K. Moriyama, K. Asaoka, J. Sakai, M. Nagumo, *J. Biomed. Mater. Res.* 69A (2004) 105.
- [21] K. Yokoyama, K. Kaneko, Y. Miyamoto, K. Asaoka, J. Sakai, M. Nagumo, *J. Biomed. Mater. Res.* 68A (2004) 150.
- [22] T. Ogawa, K. Yokoyama, K. Asaoka, J. Sakai, *Biomaterials* 25 (2004) 2419.
- [23] I.I. Phillips, P. Poole, L.L. Shreir, *Corros. Sci.* 12 (1972) 855.
- [24] I.I. Phillips, P. Poole, L.L. Shreir, *Corros. Sci.* 14 (1974) 533.
- [25] Z.F. Wang, C.L. Briant, K.S. Kumar, *Corrosion* 54 (1998) 553.
- [26] Z.F. Wang, C.L. Briant, K.S. Kumar, *Corrosion* 55 (1999) 128.
- [27] K. Mori, A. Takamura, T. Shimose, *Corrosion* 22 (1966) 29.
- [28] I.A. Menzies, A.F. Averill, *Electrochim. Acta* 13 (1968) 807.
- [29] K. Eftehaj, D. Hardie, R.N. Parkins, *Corros. Sci.* 25 (1985) 415.
- [30] A.C. Hollis, J.C. Scully, *Corros. Sci.* 34 (1993) 821.
- [31] C.F. Clarke, D. Hardie, B.M. Ikeda, *Corros. Sci.* 39 (1997) 1545.
- [32] C.L. Briant, Z.F. Wang, N. Chollocoop, *Corros. Sci.* 44 (2002) 1875.
- [33] G.A. Lenning, C.M. Craighead, R.I. Jaffee, *Trans. AIME* 200 (1954) 367.
- [34] D.N. Williams, *J. Inst. Metals.* 91 (1962) 147.
- [35] D.G. Westlake, *Trans. ASM* 62 (1969) 1000.
- [36] R.A. Oriani, P.H. Josephic, *Acta Metall.* 22 (1974) 1065.
- [37] C.D. Beachem, *Metall. Trans.* 3 (1972) 437.
- [38] H.K. Birnbaum, P. Sofronis, *Mater. Sci. Eng., A* 176 (1994) 191.
- [39] A. Takasaki, Y. Furuya, K. Ojima, Y. Taneda, *J. Alloys Compd.* 224 (1995) 269.
- [40] M. Nagumo, *ISIJ Int.* 41 (2001) 590.
- [41] K. Takai, R. Watanuki, *ISIJ Int.* 43 (2003) 520.
- [42] R.J. Wasilewski, G.L. Kehl, *Metallurgia* 50 (1954) 225.
- [43] T.P. Papazoglou, M.T. Hepworth, *Trans. Metall. Soc. AIME* 242 (1968) 682.
- [44] D.L. Johnson, H.G. Nelson, *Metall. Trans.* 4 (1973) 569.
- [45] E. Brauer, R. Dörr, H. Züchner, *Z. Physik. Chem. N.F.* 100 (1976) 109.



Hydrogen absorption behavior of beta titanium alloy in acid fluoride solutions

Toshio Ogawa^a, Ken'ichi Yokoyama^{b,*}, Kenzo Asaoka^b, Jun'ichi Sakai^a

^aDepartment of Materials Science and Engineering, Waseda University, 3-4-1 Okubo Shinjuku-ku, Tokyo, 169-8555, Japan

^bDepartment of Dental Engineering, School of Dentistry, The University of Tokushima, 3-18-15 Kuramoto-cho, Tokushima, 770-8504, Japan

Received 3 July 2003; accepted 7 September 2003

Abstract

Hydrogen absorption behavior of a beta titanium alloy in acid fluoride solutions has been analyzed by hydrogen thermal desorption. The amount of absorbed hydrogen increased with immersion time in a 2.0% acidulated phosphate fluoride (APF) solution. In the case of an immersion time of 60 h, the amount of absorbed hydrogen exceeded 10 000 mass ppm. In contrast, the amount of hydrogen absorbed in the 0.2% APF solution was several times smaller than that in the 2.0% APF solution for the same immersion time. For immersion in a 0.2% APF solution, hydrogen absorption saturated after 48 h. The surface topography and corrosion products on the surface of the specimen immersed in the 2.0% APF solution were different from those in the 0.2% APF solution. During the later stage of immersion, the amount of absorbed hydrogen markedly increased under higher applied stress, although the applied stress did not enhance hydrogen absorption during the early stage of immersion. These results of hydrogen absorption behavior are consistent with the delayed fracture characteristics of the beta titanium alloy.

© 2003 Elsevier Ltd. All rights reserved.

Keywords: Beta titanium; Corrosion; Delayed fracture; Hydrogen embrittlement; Fluoride; Thermal desorption analysis

1. Introduction

Among biomedical materials, beta titanium alloys show not only excellent specific strength and toughness, but also high corrosion resistance and biocompatibility [1–5]. One problem, however, is that these properties of beta titanium alloys as well as other titanium alloys are adversely affected by hydrogen [6–17]. Hydrogen absorption from the surrounding environments leads to degradation of the mechanical properties of materials. This phenomenon has been referred to as hydrogen embrittlement over the past years. Hydrogen absorption often becomes a problem for high-strength steels even in air [18–20], and it also occurs for titanium in methanol solutions containing hydrochloric acid [21–23]. Consequently, it is necessary to investigate hydrogen absorption under various environmental conditions, because beta titanium alloys may be widely used in the future.

Recently, the authors have revealed that titanium alloys absorb hydrogen in fluoride solutions such as

prophylactic agents [24,25]. For a beta titanium orthodontic wire, a large amount of absorbed hydrogen results in delayed fracture [26]. Upon immersion in a 2.0% acidulated phosphate fluoride (APF) solution, the fracture mode changed from ductile to brittle when the applied stress was lower than 500 MPa, in other words, when the immersion time was longer than 50 h. On the other hand, in the 0.2% APF solution, the alloys did not fracture within 1000 h in the applied stress range below 500 MPa. More details of the delayed fracture behavior of beta titanium alloys have been presented elsewhere [26]. However, hydrogen absorption behavior of beta titanium alloys in acid fluoride solutions is poorly understood. Understanding the connection between hydrogen absorption behavior and delayed fracture is important so that service life can be predicted and controlled.

The purpose of this study is to analyze the delayed fracture of beta titanium alloy in acid fluoride solutions from the viewpoint of hydrogen absorption behavior by hydrogen thermal desorption analysis (TDA). This article focuses on the effects of immersion time and applied stress on hydrogen absorption in 2.0% and 0.2% APF solutions.

*Corresponding author. Tel.: +81-88-633-7334; fax: +81-88-633-9125.

E-mail address: yokken@dent.tokushima-u.ac.jp (K. Yokoyama).

2. Experimental procedures

2.1. Materials

The beta titanium wire (TMA; Ormco Corporation, Glendora, CA) used in this study, which was the same as that used in a previous study [26], had a diameter of 0.45 mm and was cut into 150-mm-long specimens. The specimens were polished with 600-grit SiC paper and ultrasonically washed in acetone for 5 min. The chemical composition and mechanical properties of the specimens are given in Table 1. Tensile tests were carried out at room temperature using an Autograph (Shimadzu) at a strain rate of $8.33 \times 10^{-4} \text{ s}^{-1}$. Standard deviation was calculated from the results obtained from more than five specimens. Hardness tests were performed on the transverse cross section using a Vickers microhardness tester under an applied load of 0.98 N for 15 s. Standard deviation was calculated from the results obtained from more than eight indentations.

2.2. Immersion test

Immersion tests were performed under a sustained-tensile load for various periods at room temperature. The applied stress was in the range of 0–900 MPa and was calculated as the ratio of the applied load to the initial cross-sectional area. The length of each specimen immersed in a solution was 50 mm. The test solutions used were 50 ml each of aqueous solutions of 2.0% and 0.2% APF (2.0% NaF + 1.7% H_3PO_4 and 0.2% NaF + 0.17% H_3PO_4) of pH 5.0. Percent in this article means mass percent, unless otherwise stated. The concentrations of fluoride ions in the 2.0% and 0.2% APF solutions were 9000 and 900 mass ppm, respectively. The side surface of the immersed specimens was observed with a scanning electron microscope (SEM). The corrosion products on the surface of the immersed specimens and the surfaces after removal of the corrosion products were examined using an X-ray diffractometer (XRD) with Cu $\text{K}\alpha$ radiation of wavelength $\lambda = 1.54056 \text{ \AA}$ in the 2θ angle range from 10° to 90° operated at 40 kV and 30 mA. To remove corrosion products from the surfaces, 600-grit SiC paper was employed.

2.3. Thermal desorption analysis

The amount of desorbed hydrogen was measured by TDA for each immersed specimen. The specimens

(50 mm in length) immersed in the solution were cut into 20-mm-long segments and subjected to ultrasonic cleaning with acetone for 2 min. Each segment was dried in ambient air and then measured. TDA was started 30 min after the removal of a specimen from the test solution. A quadrupole mass spectrometer (ULVAC, Kanagawa, Japan) was used for hydrogen detection. Sampling was conducted at 30-s intervals at a heating rate of 100°C/h .

3. Results and discussion

3.1. Effect of immersion time

The hydrogen thermal desorption curves of specimens immersed in the 2.0% APF solution without applied stress for various periods are shown in Fig. 1. A single desorption peak was observed at around $450\text{--}500^\circ\text{C}$, and thermal desorption appeared in the temperature

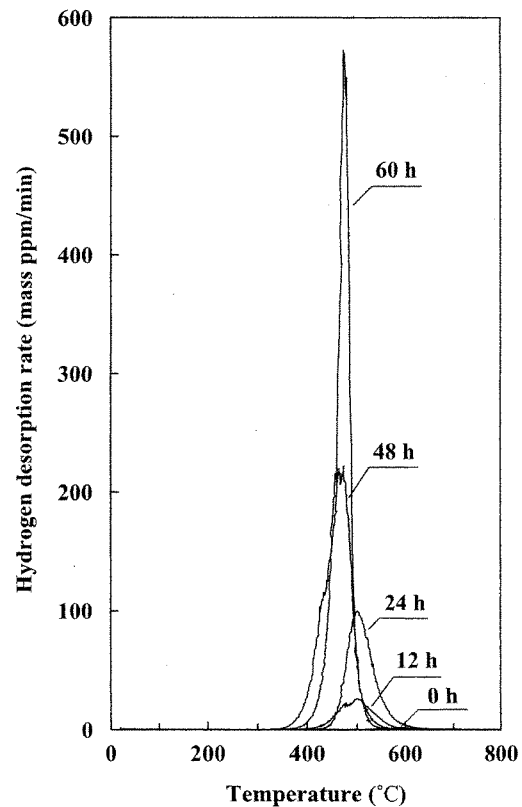


Fig. 1. Hydrogen thermal desorption curves from specimens immersed in 2.0% APF solution for different periods without loading.

Table 1
Chemical composition (mass %) and mechanical properties

Ti	Mo	Zr	Sn	Tensile strength	Vickers microhardness	Reduction in area
77.8	11.3	6.6	4.3	$1154 \pm 18.5 \text{ MPa}$	$288 \pm 13 \text{ Hv}$	87.3%

range from 300°C to 800°C. The desorption temperature gives information on the state of hydrogen in the alloy, but a detailed analysis will be separately reported. The progress of hydrogen entry into the specimen was denoted by an increase in the total amount of desorbed

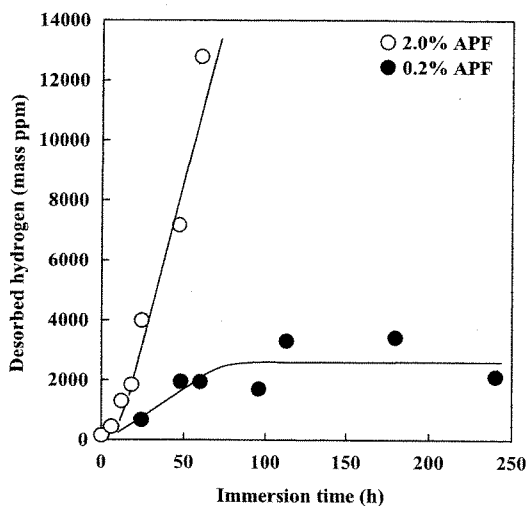


Fig. 2. Amounts of desorbed hydrogen from thermal desorption analysis of specimens immersed in 2.0% and 0.2% APF solutions as functions of immersion time.

hydrogen, defined as the integrated peak intensity. The total amounts of desorbed hydrogen up to 800°C in the 2.0% and 0.2% APF solutions without applied stress are shown as functions of immersion time in Fig. 2. The amount of desorbed hydrogen from the nonimmersed specimens, i.e., the concentration of predissolved hydrogen, was 140 mass ppm. Thus, the amount of hydrogen absorbed during an immersion test was calculated by subtracting the predissolved hydrogen content from the amount of desorbed hydrogen. In the 2.0% APF solution, the amount of desorbed hydrogen increased rapidly with increasing immersion time, although it increased gradually during the early stage of immersion until 18 h. Upon immersion in the 2.0% APF solution for 60 h, the amount of absorbed hydrogen was more than 12000 mass ppm.

In general, beta titanium alloys can absorb a large amount of hydrogen. When the amount of absorbed hydrogen exceeds several thousand mass ppm, the fracture stress decreases due to hydrogen-induced decohesion, and/or the ductile-brittle transition temperature rises in beta titanium alloys [11–17]. In our previous study, the fracture mode of the beta titanium alloy changed from ductile to brittle in the case in which the immersion time was longer than 50 h in the 2.0% APF solution [26]. Hence, the critical amount of absorbed hydrogen for the ductile-brittle transition at

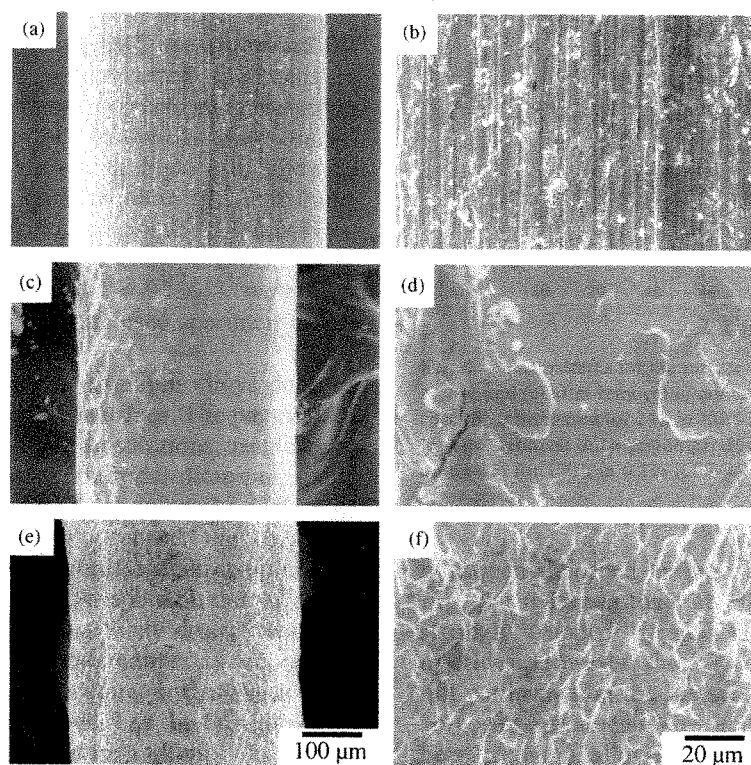


Fig. 3. SEM micrographs of a typical side surface: (a) general and (b) magnified views of a nonimmersed specimen, (c) general and (d) magnified views of a specimen immersed in 2.0% APF solution for 24 h, and (e) general and (f) magnified views of a specimen immersed in 0.2% APF solution for 120 h.

room temperature is estimated to be roughly 10 000 mass ppm in the beta titanium alloy tested.

The amount of desorbed hydrogen in the 0.2% APF solution was several times smaller than that in the 2.0% APF solution for the same immersion time. In the 0.2% APF solution, the amount of absorbed hydrogen saturated up to 2000–3500 mass ppm after 48 h. In our previous study [26], delayed fracture did not occur in the applied stress range below 500 MPa in the 0.2% APF solution. This characteristic of the delayed fracture corresponds to the saturation of hydrogen absorption in the solution.

On the side surface of the specimens before immersion, scratches due to SiC paper polishing were observed, as shown in the SEM micrographs in Figs. 3(a) and (b). After immersion in the 2.0% APF solution for 24 h, as shown in Figs. 3(c) and (d), the specimen exhibited smooth surfaces due to corrosion and peeling of surface layers composed of corrosion products. The immersion time of 24 h in the 2.0% APF solution corresponded to that of 120 h in the 0.2% APF solution in terms of the amount of hydrogen absorbed. Figs. 3(e) and (f) show the side surface after immersion in the 0.2% APF solution for 120 h. Microscopic roughness associated with general corrosion was observed. Noteworthy is that the surface topography of the specimen immersed in the 0.2% APF solution was different from that of the specimen immersed in the 2.0% APF solution.

Fig. 4(a) shows the results of XRD measurements for the side surfaces of the nonimmersed specimen. In contrast, the XRD patterns of the specimen immersed in the 2.0% APF solution for 24 h before and after removal of a surface layer are shown in Figs. 4(b) and (c), respectively. The formation of sodium titanium fluorides, namely, $\text{Na}_5\text{Ti}_3\text{F}_{14}$ (tetragonal; $a = 0.748$ nm, $c = 1.03$ nm) and Na_3TiF_6 (monoclinic; $a = 0.5543$ nm, $b = 0.5748$ nm, $c = 0.8002$ nm, $\beta = 90.29^\circ$), were confirmed on the surface of the immersed specimen before removal of the surface layer.

The corrosion resistance of titanium alloys depends on the thin passive film on their surface. The passive film undergoes a reaction in fluoride solutions, resulting in the formation of titanium fluoride, titanium oxide fluoride, or sodium titanium fluoride on the surface of the alloys [27–37]. As a consequence, the corrosion resistance of those alloys decreases markedly in the solutions. In this study, the passive film on the surface of the beta titanium alloy is most likely destroyed in the 2.0% APF solution in the same manner as reported in previous studies [27–37]. Therefore, hydrogen absorption in the solutions is interpreted as the breakdown of the passive film, because of the high affinity of titanium to hydrogen.

Hydrides are expected to be formed, if titanium alloys absorb hydrogen at their solubility limits. In addition,

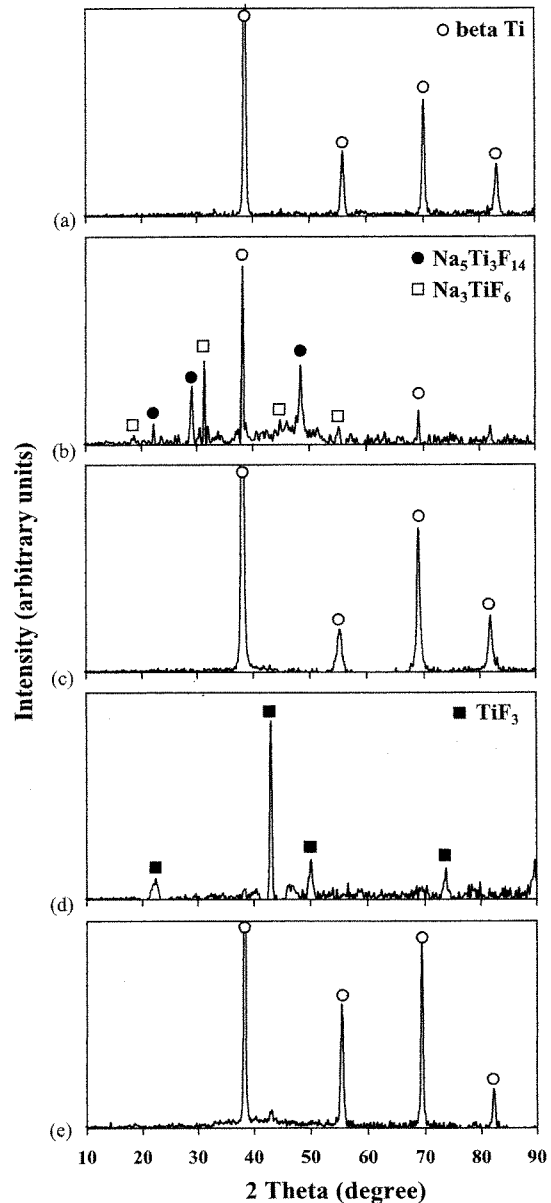


Fig. 4. XRD patterns for the surface of (a) nonimmersed specimen, (b) before and (c) after removal of corrosion products from the surface of specimens immersed for 24 h in 2.0% APF solution, and (d) before and (e) after removal of corrosion products from the surface of specimens immersed for 120 h in 0.2% APF solution.

hydrogen desorbed at high temperatures as shown in Fig. 1, suggesting that the absorbed hydrogen either is strongly trapped by defects, is occluded or formed hydrides. However, the XRD patterns of hydrides were not confirmed on the surface before or after removal of corrosion products. The hydride is hardly formed in beta titanium alloys, although it is formed in alpha titanium alloys [38–40] and in some specific beta titanium alloys such as Ti–30Mo alloy and Ti–13V–11Cr–3Al alloy at high temperatures [41,42]. In this

experiment, the hydride was probably not formed by hydrogen absorption. It is considered that most of the absorbed hydrogen is occluded interstitially and trapped by dislocations, grain boundaries and microvoids. The state of the absorbed hydrogen in the alloy is considered to be in the form of an atom and/or molecule, but a detailed discussion on this is beyond the scope of the present study.

The XRD patterns of the specimens immersed in the 0.2% APF solution for 120 h before and after removal of a surface layer are shown in Figs. 4(d) and (e), respectively. After immersion in the 0.2% APF solution for 120 h, the corrosion product was identified as TiF_3 , similar to the findings in the other report [43]. Note that the corrosion product formed in the 0.2% APF solution was different from that formed in the 2.0% APF solution. This finding and the results of surface observations (Fig. 3) indicate that the corrosion

behavior is different between both solutions. This difference may influence hydrogen absorption, although the correlation between corrosion and the saturation of hydrogen absorption in the 0.2% APF solution is still uncertain. A detailed study of the correlation should be carried out. After immersion in the 0.2% APF solution for 24 h, diffraction peaks were not detected, with the exception of those for beta titanium, because of the small amount of corrosion products, although the formation of corrosion products was observed by SEM.

3.2. Effect of applied stress

The effect of applied stress on the amount of desorbed hydrogen is shown in Figs. 5(a)–(c). After immersion for 6 h in the 2.0% APF solution (Fig. 5(a)), the amount of desorbed hydrogen was approximately 400 mass ppm, regardless of the applied stress. On the other hand, after

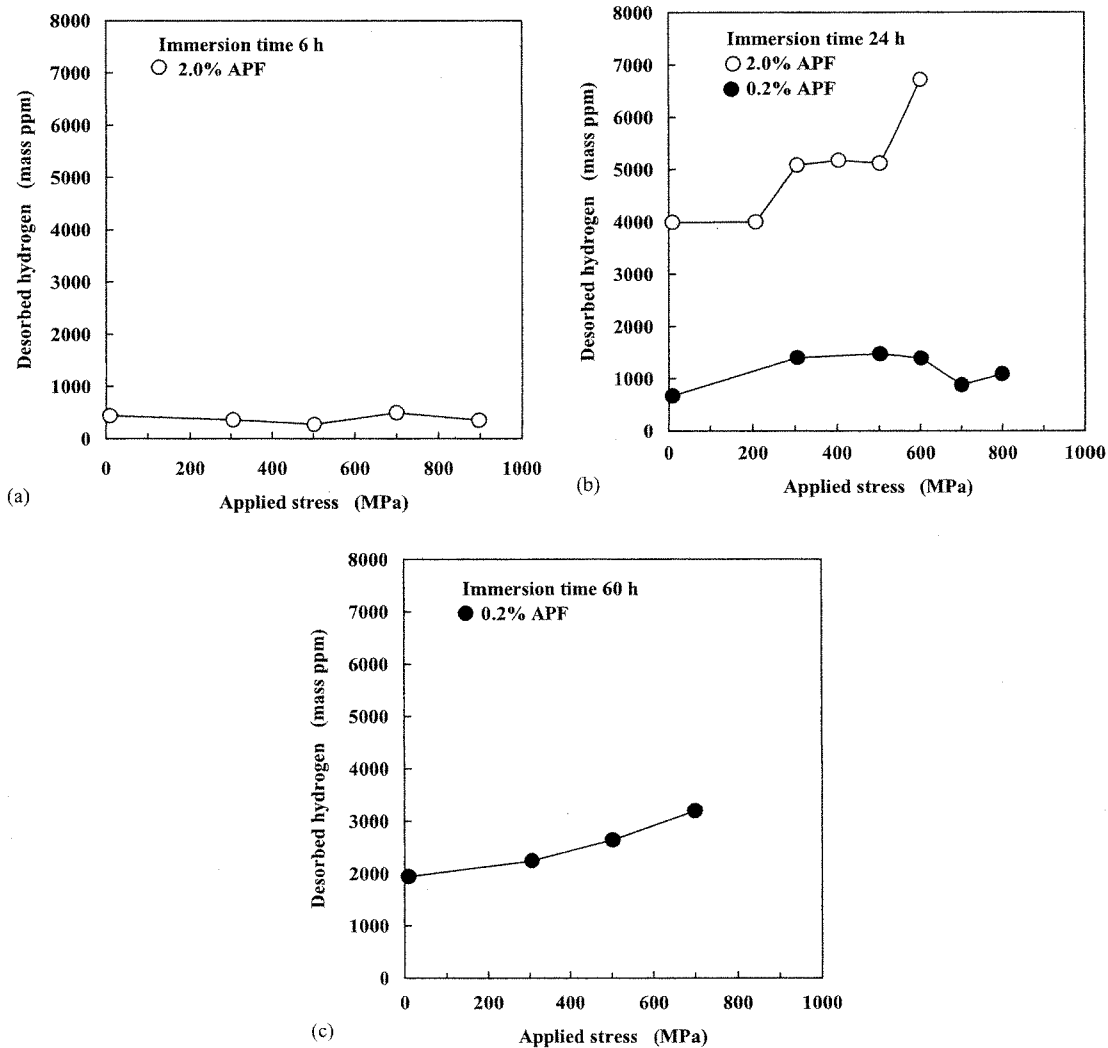


Fig. 5. Amounts of desorbed hydrogen from thermal desorption analysis of specimens immersed in 2.0% and 0.2% APF solutions as functions of applied stress: immersion times of (a) 6 h, (b) 24 h and (c) 60 h.

immersion for 24 h in the 2.0% APF solution as shown in Fig. 5(b), the amount of desorbed hydrogen increased in comparison with that in the case of nonapplied stress. In particular, under an applied stress of 600 MPa, the amount of desorbed hydrogen was approximately 1.7 times larger. In the applied stress range from 500 to 300 MPa, the effect of applied stress on hydrogen absorption was the same. From the results of Figs. 5(a) and (b), the effect of applied stress on hydrogen absorption probably appears when the immersion time becomes longer and/or the applied stress becomes higher. Under the applied stress of 200 MPa, the effect of applied stress on hydrogen absorption might appear with a longer immersion time. In our previous study [26], the time to delayed fracture in the range below 500 MPa in the 2.0% APF solution was 50–60 h and was independent of the applied stress. Thus, this result of hydrogen absorption behavior is almost consistent with the previous result of delayed-fracture characteristics. The amount of desorbed hydrogen from the specimens immersed under an applied stress above 700 MPa could not be measured, because delayed fracture occurred before 24 h in the 2.0% APF solution. From our previous study [26], fracture under an applied stress above 600 MPa, in other words, an immersion time of less than 50 h, is probably explained by the decrease in fracture stress due to hydrogen-induced decohesion.

After immersion in the 0.2% APF solution for 6 h, the increase in the amount of desorbed hydrogen was hardly confirmed to be close to the detectable limit. Upon immersion in the 0.2% APF solution for 24 h, the amount of desorbed hydrogen under the applied stress was slightly larger than that without the applied stress (Fig. 5(b)). However, the amount of desorbed hydrogen was considered to be independent of the applied stress. After immersion for 60 h in the 0.2% APF solution (Fig. 5(c)), the amount of desorbed hydrogen increased with increasing applied stress. Under an applied stress of 700 MPa, the amount of desorbed hydrogen was 1.5 times larger than that without applied stress.

These results indicate that applied stress significantly enhances hydrogen absorption at the later stage of immersion in both solutions, although it hardly enhances hydrogen absorption at the early stage of immersion. At the later stage of immersion immediately before fracture, plastic deformation is presumably induced by the reduction in tensile strength due to hydrogen-induced decohesion and enhances hydrogen absorption.

4. Conclusions

In this study, we examine hydrogen absorption behavior of a beta titanium alloy in 2.0% and 0.2%

APF solutions using TDA. The amount of absorbed hydrogen increased with immersion time in the 2.0% APF solution, while it saturated by immersion in the 0.2% APF solution. For the same immersion time, the amount of hydrogen absorbed in the 2.0% APF solution was several times larger than that in the 0.2% APF solution. At the later stage of immersion, the amount of absorbed hydrogen markedly increased under an applied stress. The hydrogen absorption behavior was in accord with the delayed fracture characteristics of the beta titanium alloy.

Acknowledgements

This study was supported in part by a Grant-in-Aid for Young Scientists (B) (14771090) from the Ministry of Education, Culture, Sports, Science and Technology, Japan.

References

- [1] Goldberg J, Burstone CJ. An evaluation of beta titanium alloys for use in orthodontic appliances. *J Dent Res* 1979;58:593–600.
- [2] Khan MA, Williams RL, Williams DF. In-vitro corrosion and wear of titanium alloys in the biological environment. *Biomaterials* 1996;17:2117–26.
- [3] Niinomi M. Mechanical properties of biomedical titanium alloys. *Mater Sci Eng A* 1998;243:231–6.
- [4] Okazaki Y, Rao S, Tateishi T, Ito Y. Cytocompatibility of various metal and development of new titanium alloys for medical implants. *Mater Sci Eng A* 1998;243:250–6.
- [5] Khan MA, Williams RL, Williams DF. The corrosion behaviour of Ti–6Al–4V, Ti–6Al–7Nb and Ti–13Nb–13Zr in protein solutions. *Biomaterials* 1999;20:631–7.
- [6] Williams DN. The hydrogen embrittlement of titanium alloys. *J Inst Metals* 1962;91:147–52.
- [7] Boyd JD. Precipitation of hydrides in titanium alloys. *Trans ASM* 1969;62:977–88.
- [8] Shih DS, Robertson IM, Birnbaum HK. Hydrogen embrittlement of α titanium: in situ TEM studies. *Acta Metall* 1988;36:111–24.
- [9] Wang ZF, Briant CL, Kumar KS. Hydrogen embrittlement of grade 2 and grade 3 titanium in 6% sodium chloride solution. *Corrosion* 1998;54:553–60.
- [10] Briant CL, Wang ZF, Chollocoop N. Hydrogen embrittlement of commercial purity titanium. *Corros Sci* 2002;44:1875–88.
- [11] Lederich RJ, Schwartz DS, Sastry SML. Effects of internal hydrogen on microstructures and mechanical properties of β 21S and Ti–15–3. In: Eylon D, Boyer RR, Koss DA, editors. *Beta Titanium Alloys in the 1990's*. Warrendale, PA: TMS; 1993. p. 159.
- [12] Young Jr GA, Scully JR. Effects of hydrogen on the mechanical properties of a Ti–Mo–Nb–Al alloy. *Scripta Metall Mater* 1993;28:507–12.
- [13] Young Jr GA, Scully JR. Hydrogen embrittlement of solution heat-treated and aged β -titanium alloys Ti–15%V–3%Cr–3%Al–3%Sn and Ti–15%Mo–3%Nb–3%Al. *Corrosion* 1994;50:919–33.
- [14] Itoh G, Kanno M, Niwa N. Mechanical properties of a Ti–15V–3Cr–3Sn–3Al alloy affected by the impurity hydrogen. *Mater Sci Eng A* 1996;213:93–7.

- [15] Gaudett MA, Scully JR. Effect of pre-dissolved hydrogen on fracture initiation in metastable beta Ti–3Al–8V–6Cr–4Mo–4Zr. *Scripta Mater* 1997;36:565–72.
- [16] Pound BG. Hydrogen trapping in aged β -titanium alloys. *Acta Mater* 1997;45:2059–68.
- [17] Teter DF, Robertson IM, Birnbaum HK. The effects of hydrogen on the deformation and fracture of β -titanium. *Acta Mater* 2001;49:4313–23.
- [18] Hirth JP. Effects of hydrogen on the properties of iron and steel. *Metall Trans A* 1980;11A:861–90.
- [19] Matsuyama S. Delayed fracture of high strength steels. *Tetsu-to-Hagané* 1994;80:679–84.
- [20] Nagumo M. Function of hydrogen in embrittlement of high-strength steels. *ISIJ Int* 2001;41:590–8.
- [21] Mori K, Takamura A, Shimose T. Stress corrosion cracking of Ti and Zr in HCl-Methanol solutions. *Corrosion* 1966;22:29–31.
- [22] Ebtehaj K, Hardie D, Parkins RN. The stress corrosion and pre-exposure embrittlement of titanium in methanolic solutions of hydrochloric acid. *Corros Sci* 1985;25:415–29.
- [23] Hollis AC, Scully JC. The stress corrosion cracking and hydrogen embrittlement of titanium in methanol-hydrochloric acid solutions. *Corros Sci* 1993;34:821–35.
- [24] Yokoyama K, Kaneko K, Moriyama K, Asaoka K, Sakai J, Nagumo M. Hydrogen embrittlement of Ni–Ti superelastic alloy in fluoride solution. *J Biomed Mater Res* 2003;65A:182–7.
- [25] Yokoyama K, Kaneko K, Miyamoto Y, Asaoka K, Sakai J, Nagumo M. Fracture associated with hydrogen absorption of sustained tensile-loaded titanium in acid and neutral fluoride solutions. *J Biomed Mater Res* 2004;68A:150–8.
- [26] Kaneko K, Yokoyama K, Moriyama K, Asaoka K, Sakai J, Nagumo M. Delayed fracture of beta titanium orthodontic wire in fluoride aqueous solutions. *Biomaterials* 2003;24:2113–20.
- [27] Lausmaa J, Kasemo B, Hansson S. Accelerated oxide grown on titanium implants during autoclaving caused by fluorine contamination. *Biomaterials* 1985;6:23–7.
- [28] Siirilä HS, Könönen M. The effect of oral topical fluorides on the surface of commercially pure titanium. *Int J Oral Maxillofac Implant* 1991;6:50–4.
- [29] Pröbster L, Lin W, Hüttemann H. Effect of fluoride prophylactic agents on titanium surfaces. *Int J Oral Maxillofac Implant* 1992;7:390–4.
- [30] Könönen MHO, Lavonius ET, Kivilahti JK. SEM observations on stress corrosion cracking of commercially pure titanium in a topical fluoride solution. *Dent Mater* 1995;11:269–72.
- [31] Boere G. Influence of fluoride on titanium in an acidic environment measured by polarization resistance technique. *J Appl Biomater* 1995;6:283–8.
- [32] Toumelin-Chemla F, Rouelle F, Burdairon G. Corrosive properties of fluoride-containing odontologic gels against titanium. *J Dentistry* 1996;24:109–15.
- [33] Reclaru L, Meyer J-M. Effects of fluorides on titanium and other dental alloys in dentistry. *Biomaterials* 1998;19:85–92.
- [34] Nakagawa M, Matsuya S, Shiraishi T, Ohta M. Effect of fluoride concentration and pH on corrosion behavior of titanium for dental use. *J Dent Res* 1999;78:1568–72.
- [35] Huang H-H. Effects of fluoride concentration and elastic tensile strain on the corrosion resistance of commercially pure titanium. *Biomaterials* 2002;23:59–63.
- [36] Huang H-H. Electrochemical impedance spectroscopy study of strained titanium in fluoride media. *Electrochimica Acta* 2002;47:2311–8.
- [37] Schiff N, Grosgeat B, Lissac M, Dalard F. Influence of fluoride content and pH on the corrosion resistance of titanium and its alloys. *Biomaterials* 2002;23:1995–2002.
- [38] Numakura H, Koiwa M. Hydride precipitation in titanium. *Acta Metall* 1984;32:1799–807.
- [39] Woo OT, Weatherly GC, Coleman CE, Gilbert RW. The precipitation of γ -deuterides (hydrides) in titanium. *Acta Metall* 1985;33:1897–906.
- [40] Numakura H, Koiwa M, Asano H, Murata H, Izumi F. X-ray diffraction study on the formation of γ titanium hydride. *Scripta Metall* 1986;20:213–6.
- [41] Shih DS, Birnbaum HK. Evidence of FCC titanium hydride formation in β titanium alloy: an X-ray diffraction study. *Scripta Metall* 1986;20:1261–4.
- [42] Nakasa K, Liu J. Bending strength of hydrogen-charged Ti–13V–11Cr–3Al alloy. *J Jpn Inst Metals* 1991;55:922–7.
- [43] Vorres KS, Dutton FB. The fluoride of titanium: X-ray powder data and some other observations. *J Am Chem Soc* 1955;77:2019.

Delayed fracture of Ni-Ti superelastic alloys in acidic and neutral fluoride solutions

Ken'ichi Yokoyama,¹ Kazuyuki Kaneko,² Keiji Moriyama,² Kenzo Asaoka,¹ Jun'ichi Sakai,³ Michihiko Nagumo³

¹Department of Dental Engineering, School of Dentistry, The University of Tokushima, 3-18-15 Kuramoto-cho, Tokushima, 770-8504, Japan

²Department of Orthodontics, School of Dentistry, The University of Tokushima, 3-18-15 Kuramoto-cho, Tokushima, 770-8504, Japan

³Department of Materials Science and Engineering, Waseda University, 3-4-1 Okubo, Shinjuku-ku, Tokyo, 169-8555, Japan

Received 16 May 2003; revised 28 October 2003; accepted 7 November 2003

Abstract: Hydrogen-related degradation of the mechanical properties of a Ni-Ti superelastic alloy has been examined by means of delayed fracture tests in acidic and neutral fluoride solutions and hydrogen thermal desorption analysis. Delayed fracture took place in both solutions; the time to fracture was shorter in the acidic solutions than in the neutral solutions with the same fluoride concentration. The time to fracture was reduced in both solutions when applied stress exceeded the critical stress for martensite transformation. In the acidic solutions, Ni-Ti superelastic alloy underwent general corrosion and absorbed substantial amounts of hydrogen. Fractographic features suggested that the delayed fracture in the acidic solutions was attributable to hydrogen embrittlement, whereas in the neutral solutions, a different

fracture mode appeared associated with localized corrosion only in the vicinity of the fracture initiation area. In the neutral solutions, the amount of absorbed hydrogen was much less than that in the acidic solutions, and the delayed fracture was likely to be induced by active path corrosion accompanying hydrogen absorption. The results of the present study imply that the hydrogen-related degradation of performance of Ni-Ti superelastic alloys occurs in the presence of fluoride. © 2004 Wiley Periodicals, Inc. *J Biomed Mater Res* 69A: 105–113, 2004

Key words: Ni-Ti; delayed fracture; hydrogen embrittlement; corrosion; fluoride

INTRODUCTION

Corrosion of Nitinol and Ni-Ti superelastic alloys used as orthodontic wires has been widely observed in the oral cavity, eventually resulting in fracture of the wire.^{1–6} Moreover, dentists consider on the basis of intuition that the flexibility of the wires is lost after clinical use, implying some degradation of mechanical properties. The mechanism might be the product of several events in the oral cavity. One is the embrittlement of the alloys due to the introduction of hydrogen from the surrounding environment.^{7–10} Hydrogen embrittlement is often represented as a reduction in ten-

sile stress, strain, and reduction in area associated with a change in the fracture mode.

The effect of hydrogen on the mechanical properties of Ni-Ti superelastic alloys has been studied in cathodic hydrogen charging^{7–9,11–13} and immersion in solutions such as acidulated phosphate fluoride (APF) solution.¹⁰ As the alloys absorb hydrogen, the tensile strength and reduction in area decrease considerably, and fracture takes place before stress-induced martensite transformation when the amount of absorbed hydrogen is substantially increased. Furthermore, the effects of a corrosive environment on mechanical properties become remarkably distinct when the applied stress exceeds the critical stress for martensite transformation.¹⁴ Therefore, for evaluation of the degradation of mechanical properties of Ni-Ti superelastic alloys in various solutions, it is necessary to take into consideration the effect of applied stress (e.g., by using a sustained load, delayed fracture testing).

The delayed fracture test is particularly important

Correspondence to: K. Yokoyama; e-mail: yokken@dent.tokushima-u.ac.jp

Contract grant sponsor: Ministry of Education, Culture, Sports, Science, and Technology, Japan; contract grant number: Grant-in-Aid for Young Scientists (B) 14771090

© 2004 Wiley Periodicals, Inc.

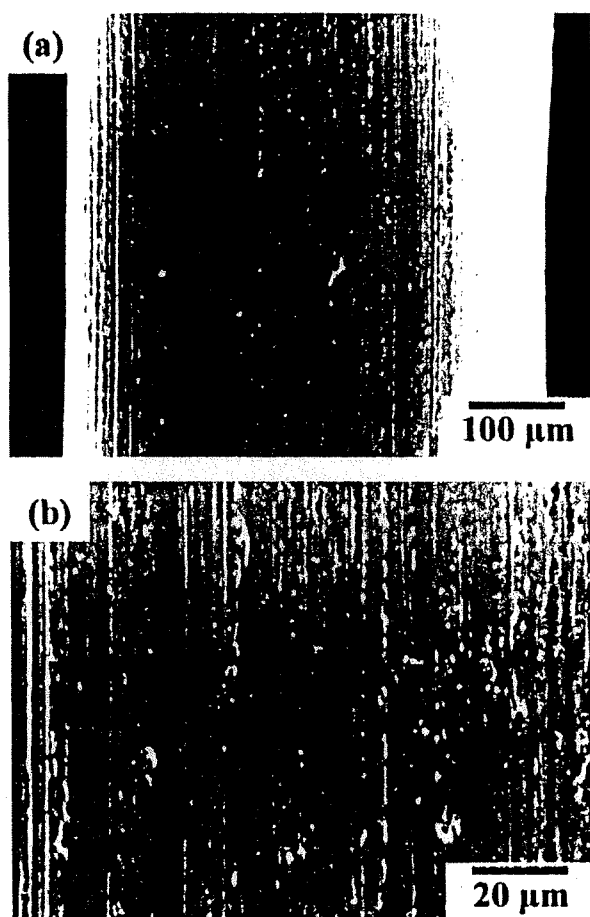


Figure 1. SEM micrographs of the side surface of a specimen polished with SiC paper. (a) General and (b) magnified views of the surface.

for characterizing the susceptibility of high-strength steels to hydrogen.¹⁵⁻²² Although delayed fracture life is one of the important properties of Ni-Ti alloys used in biomedical applications, their susceptibility to environmental conditions has rarely been studied. In acidic fluoride solutions including prophylactic agents, the corrosion resistance of titanium and its alloys is remarkably reduced.²³⁻³⁶ The breakdown of the oxide film on the surface of the alloy is expected to lead to hydrogen absorption in various solutions. In actuality, Ni-Ti superelastic alloys absorb a considerable amount of hydrogen in a 0.2% APF solution,¹⁰ causing delayed fracture in the solution. In a milder environment, such as neutral fluoride solutions, the alloys are barely affected by corrosion. However, the delayed fracture may occur even in neutral solutions because of an accelerated corrosion of the alloys due to applied stress.¹⁴

The purpose of the present study is to examine the delayed fracture of a Ni-Ti superelastic alloy in acidic and neutral fluoride solutions. On the basis of hydrogen thermal desorption analysis (TDA) and fracto-

graphic examination, the characteristics of delayed fracture are discussed.

EXPERIMENTAL PROCEDURES

Materials

Commercial Ni-Ti superelastic alloy wires with a diameter of 0.50 mm were cut into 150-mm-long specimens. The specimens were polished with 600-grit SiC paper and ultrasonically cleaned with acetone for 5 min; the scanning electron microscope (SEM) micrographs of the surfaces are shown in Figure 1(a,b). The martensite to austenite transformation temperatures and the mechanical properties of the specimens are given in Table I. The phase transformation temperatures of the specimens were determined by an electric resistance method. Here, M_s and M_f indicate the start and finish temperatures for the martensite transformation, respectively, on cooling. Similarly, A_s and A_f indicate the start and finish temperatures, respectively, for the reverse transformation on heating. The critical stress for the martensite transformation and the tensile strength were 530 and 1250 MPa, respectively. The tensile test data were measured at room temperature ($25 \pm 2^\circ\text{C}$) on an Instron-type machine (Autograph AG-100A, Shimadzu) at a strain rate of $8.33 \times 10^{-4}/\text{s}$. The standard deviation was calculated from the results for more than five specimens. The microstructure of the specimen on a cross-sectional area was observed by means of optical microscopic examination using an etching solution consisting of hydrofluoric, nitric, and acetic acids (7:7:10 volume ratio), as shown in Figure 2. The microstructure of the specimen exhibits a typical lathlike structure.

Delayed fracture test

The delayed fracture test (i.e., a sustained tensile-loading test in solution) was conducted at room temperature with specimens 50 mm in length immersed in 50 mL of solution. Applied stress was varied to determine the delayed fracture life characteristics. The test solutions used were aqueous solutions of 0.2 or 2.0% acidulated phosphate fluoride (APF; 0.2% NaF + 0.17% H_3PO_4 or 2.0% NaF + 1.7% H_3PO_4) with pH 5.0 and 0.2 or 2.0% NaF with pH 6.5. The fluoride concentrations in the 0.2 and 2.0% solutions were 900 and 9000 ppm, respectively. Percent in this article indicates mass percent, unless otherwise stated. Immediately after fracture, the specimens were taken from the solutions, cleaned with

TABLE I
Mechanical Properties and Transformation Temperatures of the Ni-Ti Superelastic Alloy

Critical Stress (MPa)	Tensile Strength (MPa)	Reduction in Area (%)	Transformation Temperature ($^\circ\text{C}$)			
			A_f	A_s	M_s	M_f
530 ± 16.7	1250 ± 7.2	54.7	-4	-26	-3	-27

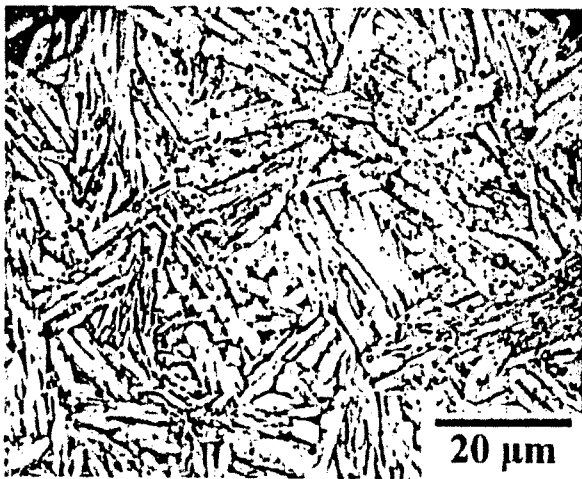


Figure 2. Optical micrograph of Ni-Ti superelastic alloy.

acetone, and dried in ambient air. The test was terminated when no delayed fracture occurred after >1000 h. The side surface and fracture surface of the tested specimens were examined with SEM. The corrosion products on the surface were examined by using an X-ray diffractometer (XRD) operated at 40 kV and 30 mA, using Cu K_α radiation of wavelength λ = 1.54056 Å for 2θ angles ranging from 30 to 80°.

Thermal desorption analysis

The amount of absorbed hydrogen was measured before fracture for specimens subjected to the delayed fracture test. Specimens (50 mm in length) immersed in the solution were cut into 20-mm-long segments and subjected to ultrasonic cleaning with acetone for 2 min. The segments were dried in ambient air and measured. The starting time of TDA after the removal from the solution was 30 min. A quadrupole mass spectrometer (ULVAC) was used for the detection of hydrogen. Sampling was conducted at 30-s intervals at a heating rate of 100°C/h.

RESULTS AND DISCUSSION

Delayed fracture test in APF solutions

The delayed fracture test results are plotted in Figure 3 in terms of the time to fracture as a function of the applied stress, in 0.2 and 2.0% APF solutions. The arrows in the figure indicate nonfractured specimens at the indicated elapsed time. The time to fracture decreased with increasing applied stress. The slope of the linear dependence changed at the critical stress for martensite transformation in the 0.2% APF solution. In the 2.0% APF solution, the line defining the relationship of the applied stress versus time to fracture broke

at the critical stress. This result suggests that the strength of the Ni-Ti superelastic alloys is very susceptible to the environment when the applied stress exceeds the critical stress for martensite transformation. This result agrees with that of a delayed fracture test using cathodic charging in a 0.9% NaCl solution, as reported previously.¹⁴ For the same applied stress, the time to fracture in the 2.0% APF solution was shorter than that in the 0.2% APF solution, implying an effect of fluoride concentration.

SEM micrographs of the side surface of a specimen subjected to the delayed fracture test in the 0.2% APF solution under the applied stress of 600 MPa are shown in Figure 4(a,b). General corrosion took place over the immersed area, and scratches due to paper polishing disappeared. The corrosion was observed regardless of the concentration of the solution and the applied stress level.

Figure 5 shows TDA curves of specimens immersed in the 0.2% APF solution for 24 h under applied stresses of 300, 450, 600, and 750 MPa. The thermal desorption of hydrogen appeared with a desorption peak at ~400°C. The progress of hydrogen entry into the alloy was shown as an increase in the total desorbed hydrogen, defined as the integrated peak intensity. In the as-received specimen, the amount of desorbed hydrogen (i.e., the initial concentration of hydrogen) was 7 ppm. The amount of hydrogen absorbed under an applied stress > 600 MPa was ~600 ppm, whereas that absorbed <450 MPa was ~400 ppm. This result suggests that the hydrogen absorption accelerates when the applied stress exceeds the

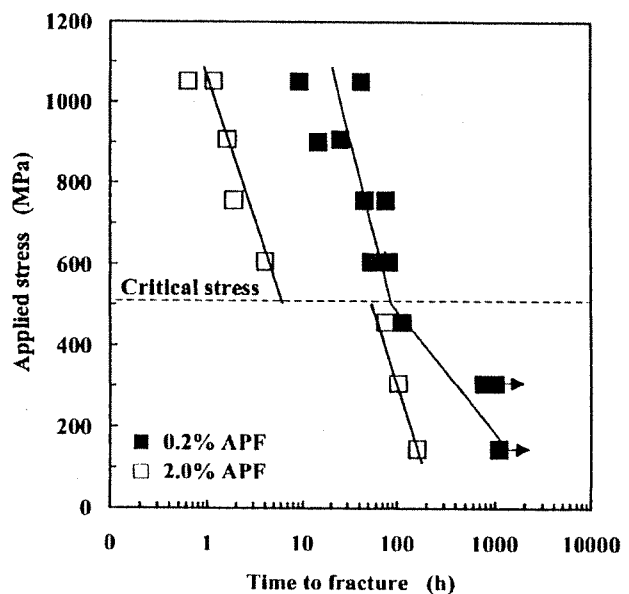


Figure 3. Delayed fracture diagrams of Ni-Ti superelastic alloy in 0.2 and 2.0% APF solutions. Arrows indicate specimens that did not fracture.

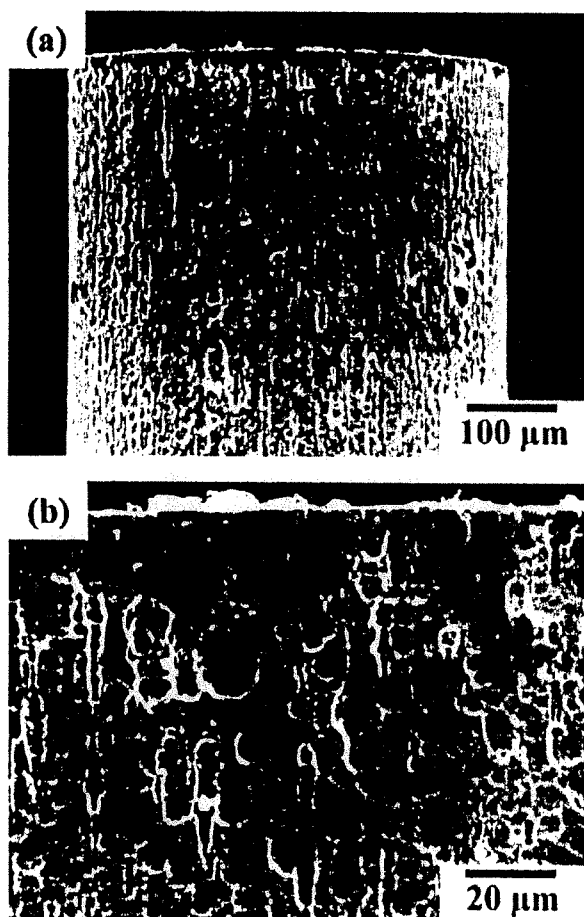


Figure 4. SEM micrographs of the side surface of a specimen subjected to delayed fracture test under the applied stress of 600 MPa in the 0.2% APF solution. (a) General and (b) magnified views.

critical stress of 530 MPa for martensite transformation. Because Figure 5 is for an immersion time of 24 h, the amount of absorbed hydrogen may further increase until the time of fracture at 50–80 h and 80–110 h under applied stresses of 450 and 600 MPa, respectively, as shown in Figure 3.

Figure 6 shows XRD patterns from the side surface of (a) a nonimmersed specimen and (b) before and (c) after the removal of surface corrosion products on specimens immersed in the 0.2% APF solution without loading. The formation of sodium titanium fluoride, Na_2TiF_6 (hexagonal; $a = 0.91974$ nm, $c = 0.51317$ nm), during immersion was evident. The thin passive film on the Ni-Ti alloy surface, mainly TiO_2 , which generally exhibits good corrosion resistance similar to titanium,^{38–40} has been shown to dissolve or react to form titanium fluoride, titanium oxide fluoride, or sodium titanium fluoride in acidic fluoride solutions^{23–36}; this is in agreement with the present results. The breakdown of the film may lead to hydrogen absorption because of a high affinity of the alloy for hydrogen.

Figure 6(b,c) confirms the formation of nickel titanium hydride, TiNiH (tetragonal; $a = 0.6221$ nm, $c = 1.2363$ nm), both before and after removal of corrosion products from the surface, and again, this is coincident with the case of cathodically hydrogen-charged Ni-Ti superelastic alloys.^{41,42} The hydride formed in the APF solution was identical with that formed by cathodic charging.

Figure 7(a) shows fractographic features of a specimen fractured in the 0.2% APF solution under an applied stress of 600 MPa for 82 h. The fracture pattern was roughly classified into two areas; one was a fairly flat area in the peripheral part of the fracture surface as shown in Figure 7(b), and the other was an area of shallow dimples in the central part as shown in Figure 7(c). Both types were observed regardless of the fluoride concentration and the level of the applied stress. These characteristics of the fracture surface were very

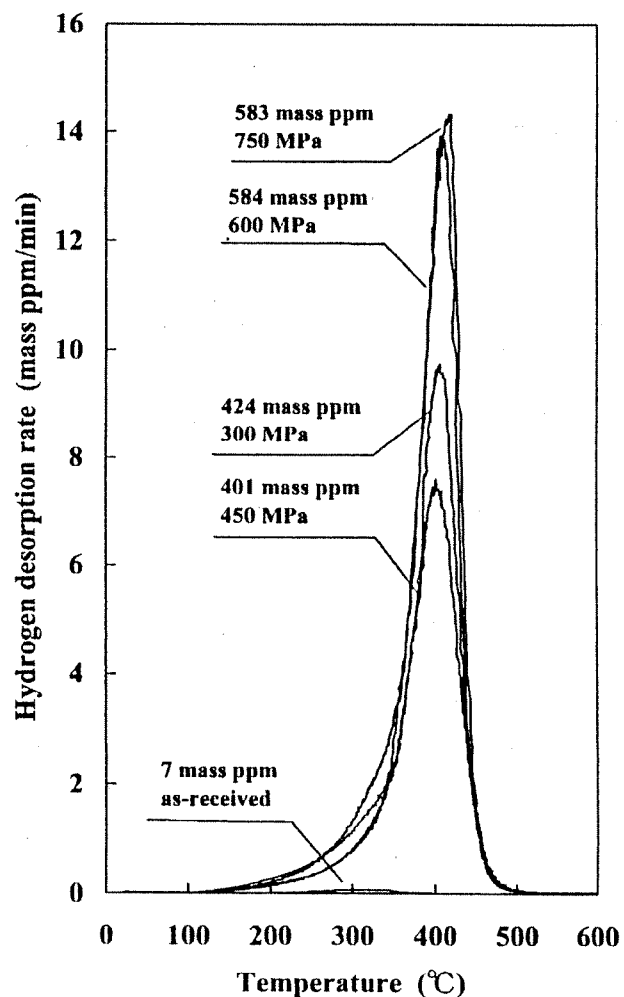


Figure 5. Hydrogen thermal desorption curves from specimens subjected to the delayed fracture test under applied stresses of 300, 450, 600, and 750 MPa in the 0.2% APF solution for 24 h.

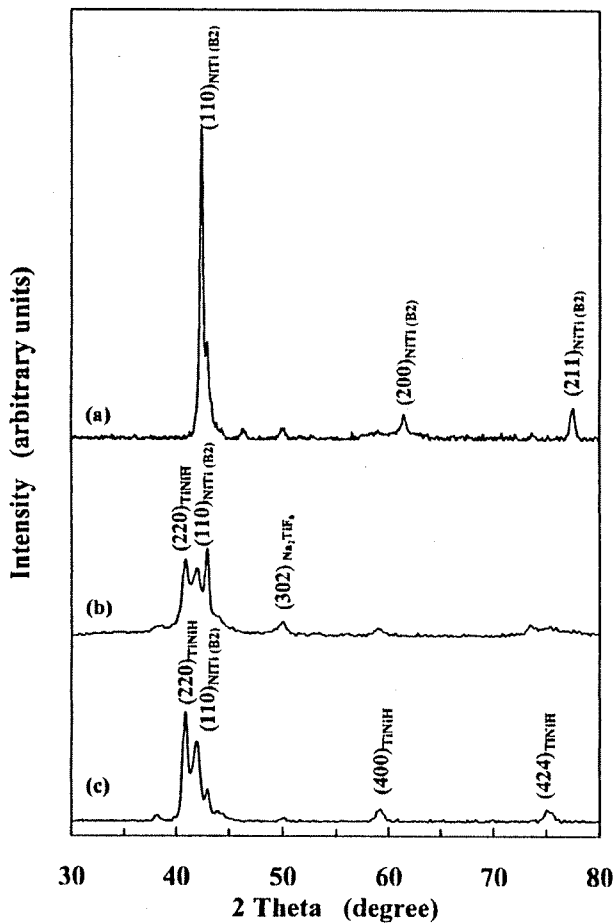


Figure 6. XRD patterns from the surface of (a) a non-immersed specimen, (b) before, and (c) after removal of corrosion products on the surface of specimens immersed in the 0.2% APF solution without loading.

similar to those on specimens tensile tested after immersion in the 0.2% APF solution¹⁰ or cathodic hydrogen charging.^{7,14} The flat area might be due to hydride formation acting as the fracture initiation site, because the hydride is hard and brittle and ready to provide microcrack nucleation. Fractured specimens hardly exhibited any reduction in area in either the 0.2 or 2.0% APF solution.

The fraction of the flat area increased with increasing immersion time as shown in Figure 8. The rate of increase was almost the same in 0.2 and 2.0% APF solutions. The increase is attributable to the diffusion of absorbed hydrogen from the surface. The diffusion coefficient D is described by the Arrhenius relation,

$$D = D_0 \exp(-E/k_B T), \quad (1)$$

where E is the activation energy, D_0 is the preexponential factor, k_B is the Boltzmann constant, and T is absolute temperature. Using the reported diffusion

coefficient of hydrogen in Ni-Ti alloy with a B2 structure at room temperature,⁴³

$$D = 3.6 \times 10^{-15} \text{ m}^2/\text{s}, \quad (2)$$

the diffusion distance of hydrogen in the alloy is calculated to be 65 μm in 80 h, without taking into

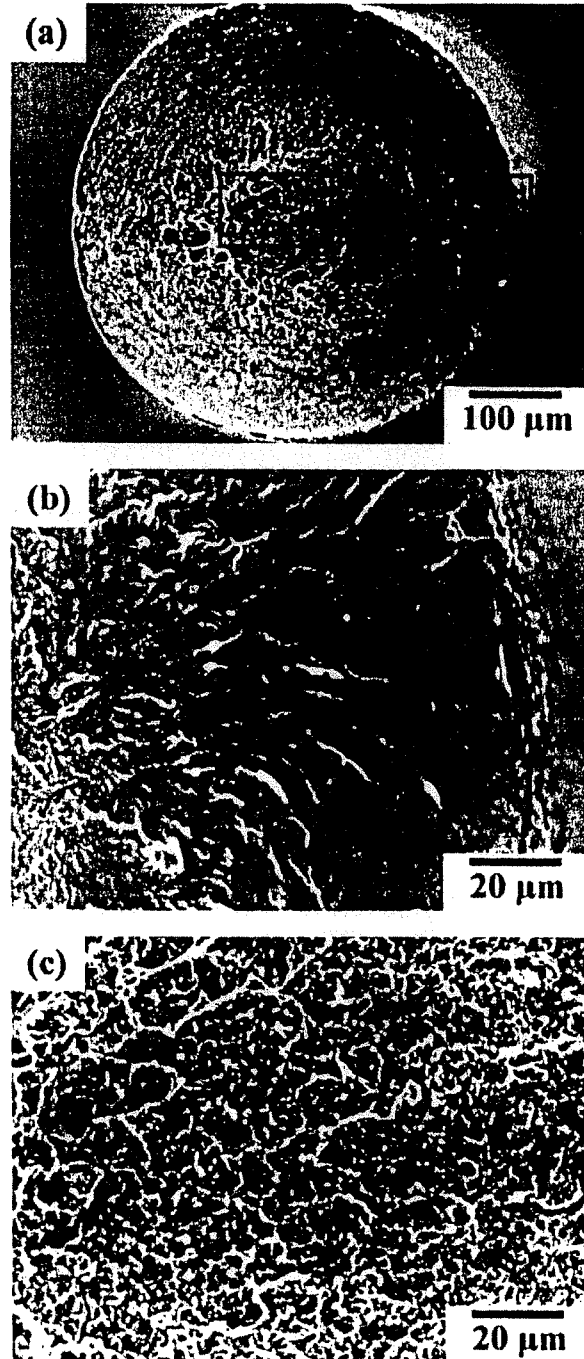


Figure 7. SEM micrographs of the delayed fracture surface under an applied stress of (a) 600 MPa in the 0.2% APF solution, (b) the flat area in a peripheral part, and (c) a shallow dimple area in the central part.

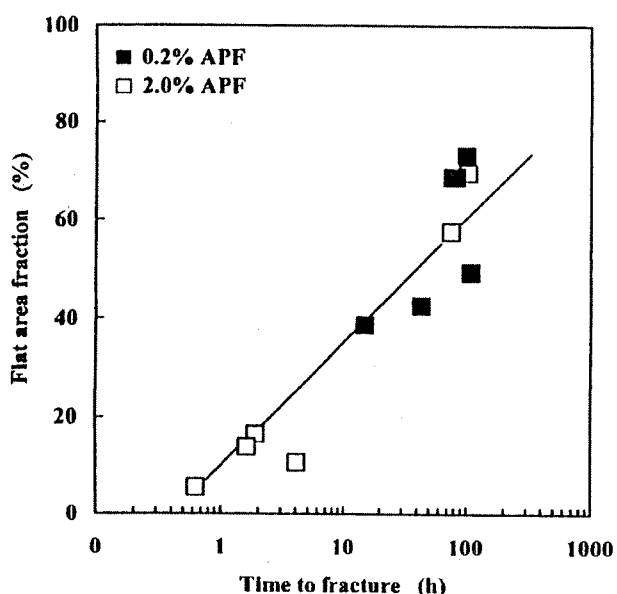


Figure 8. Fraction of flat area on the delayed fracture surface in 0.2 and 2.0% APF solutions as a function of time to fracture.

account the diffusion coefficient in monoclinic martensite with a B19' structure or the effects of applied stress. This calculated value approximates the thickness of the peripheral part (i.e., the flat area) on the fracture surface. Moreover, the increment of the flat area with immersion time agrees with that obtained in the tensile test after immersion in the 0.2% APF solution¹⁰ or cathodic hydrogen charging as reported previously.^{7,14}

Delayed fracture test in neutral NaF solutions

The delayed fracture test results in 0.2 and 2.0% NaF solutions are shown in Figure 9. It is noteworthy that the delayed fracture of Ni-Ti superelastic alloy took place readily even in the neutral NaF solutions. Although the time to fracture was longer than that in APF solutions of the same fluoride concentration, the dependence on fluoride concentration and the change in the slope of the line defining the relationship of applied stress versus time to fracture at the critical stress for martensite transformation were similar to those in APF solutions. Several specimens subjected to the lower range of applied stresses fractured after >1000 h, and the lower limit stress was not discernible in either APF or NaF solutions.

The appearance of the side surface on a specimen subjected to the delayed fracture test under an applied stress of 600 MPa in the 2.0% NaF solution is shown in Figure 10(a,b). In contrast to APF solutions, corrosion

associated with arrested cracks perpendicular to the loading direction was local only near the fracture initiation point in both 0.2 and 2.0% NaF solutions, regardless of the applied stress. In the present experiment, crevice corrosion appeared neither at the contact point of a specimen with the vessel nor in the vicinity of the water plane in NaF solutions or in APF solutions.

Hydrogen absorption in the 2.0% NaF solution was examined by means of TDA. Figure 11 shows TDA curves of hydrogen absorbed in a nonloaded specimen immersed in 10 mL of 2.0% NaF solution at 37°C for a long period. It is apparent that substantial hydrogen absorption occurred, but the desorption temperature range was lower than that in APF solutions, and the desorption peak temperature was ~250°C. The low desorption temperature suggests that absorbed hydrogen is weakly trapped in the alloy. The absorption of hydrogen increased with immersion time, but the amount of desorption was much less than that in APF solutions. An increase in absorption by loading was not confirmed in the 2.0% NaF solution.

Fractographic features in NaF solutions are shown in Figure 12(a) for a specimen fractured in 2.0% NaF solution under an applied stress of 600 MPa. In NaF solutions, the reduction in area was negligible, compared to 54% on tensile testing in air. The fracture mode was different between APF and NaF solutions. For the delayed fracture in NaF solutions, the fracture always initiated in the vicinity of the surface followed by radial crack propagation. The fracture initiation area, as shown in Figure 12(b), could be identified by

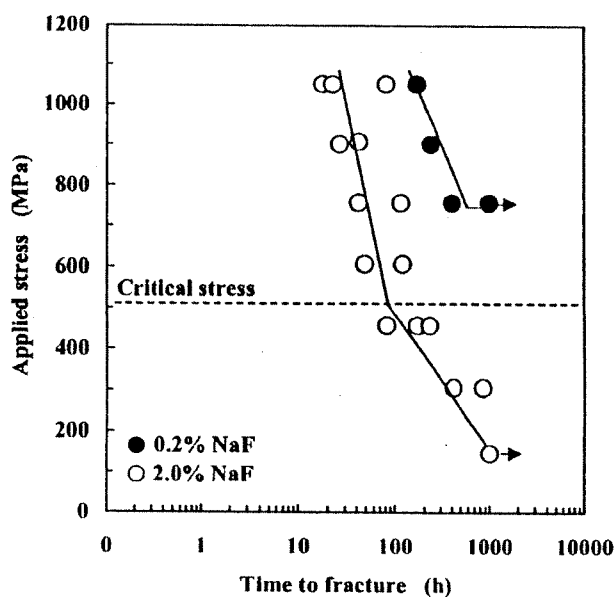


Figure 9. Delayed fracture diagrams of Ni-Ti superelastic alloy in 0.2 and 2.0% NaF solutions. Arrows indicate specimens that did not fracture.

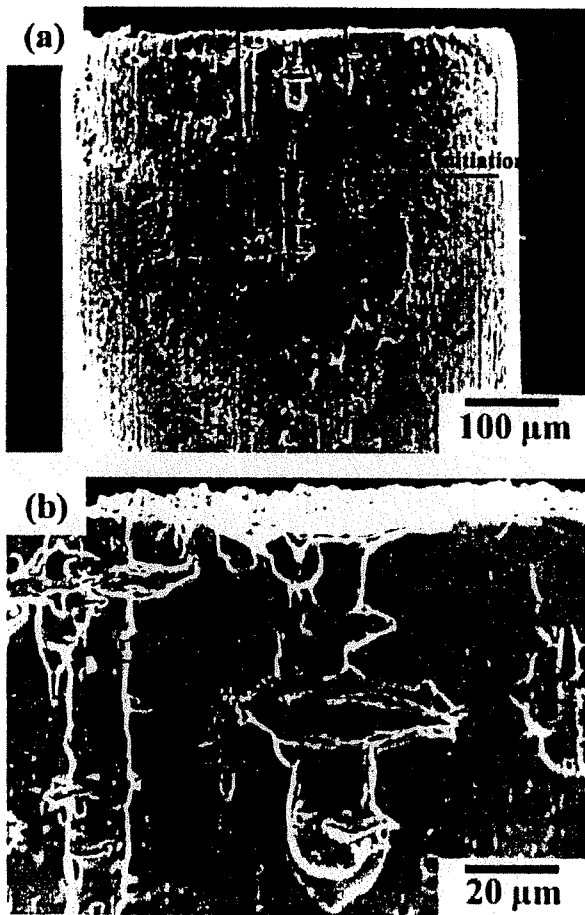


Figure 10. SEM micrographs of the side surface of a specimen subjected to delayed fracture test under an applied stress of 600 MPa in a 2.0% NaF solution. (a) General view near the fracture surface and (b) magnified view near the fracture initiation point.

tracing back the river-like flows. The morphology of the fracture initiation area was fairly flat with a large number of corrosion pits. The corrosion pits possibly affected the fracture initiation. In view of the existence of corrosion pits and the side surface features shown in Figure 10, the flat area is likely the surface of an arrested crack before it extends to the final fracture. In addition, it appears that the flat area exhibits the characteristics of brittle fracture associated with hydrogen absorption, whereas the main crack propagation area was composed of shallow dimples, as shown in Figure 12(c). The fraction of the flat area increased with the time to fracture (i.e., the immersion time or decreased applied stress) prominently in the 2.0% NaF solution as shown in Figure 13.

The present study has revealed that a Ni-Ti superelastic alloy is susceptible to delayed fracture in both APF and neutral NaF solutions. The susceptibility was more prominent in the former solution, accompanied

by a higher hydrogen absorption and general corrosion. In APF solutions, the formation of a hydride on the surface of a specimen and a flat area in the periphery of the fracture surface suggests that hydride formation is a possible cause of embrittlement. However, a stepwise increase in the susceptibility at an applied stress level above the critical stress for martensite transformation (Fig. 3) implies a more complicated function for hydrogen. Further studies will be presented elsewhere.

In neutral NaF solutions, the amount of absorbed hydrogen was much less than that in APF solutions, but the amount was close to 50–200 ppm that affects mechanical properties of Ni-Ti superelastic alloys.^{10,44} The amount of hydrogen in TDA is a mean value over the specimen, and the localized corrosion near the fracture initiation site (Fig. 10) suggests that the hydrogen concentration concerned with fracture is

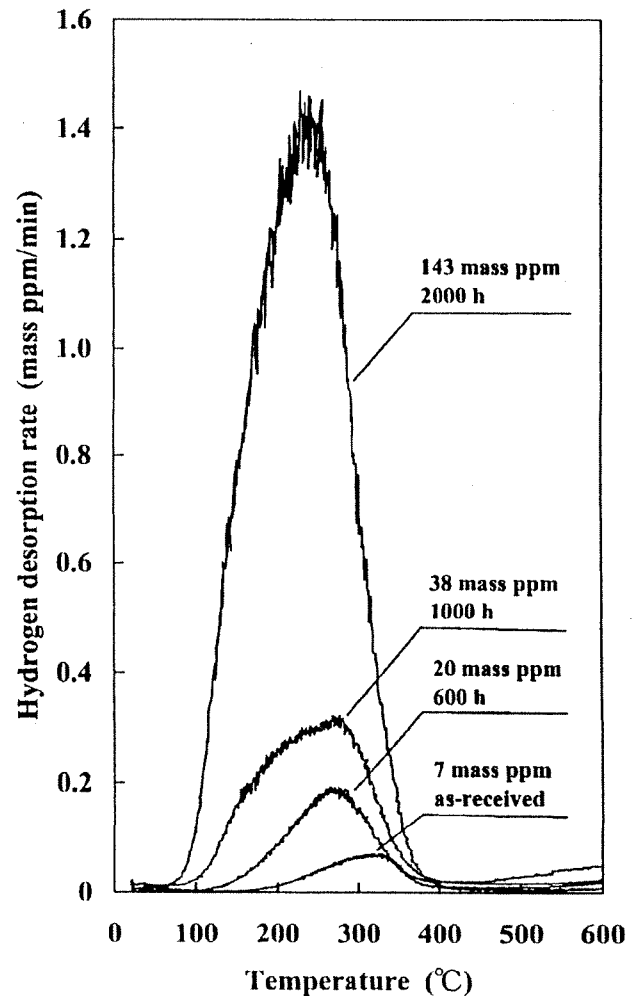


Figure 11. Hydrogen thermal desorption curves from specimens immersed in 2.0% NaF solutions without loading for up to 2000 h at 37°C.

higher. Nonetheless, the fractographic features showed slow crack growth, suggesting active path corrosion as the dominant fracture mode in which an extremely small amount of hydrogen in the vicinity of a crack sometimes plays an important role.^{45,46}

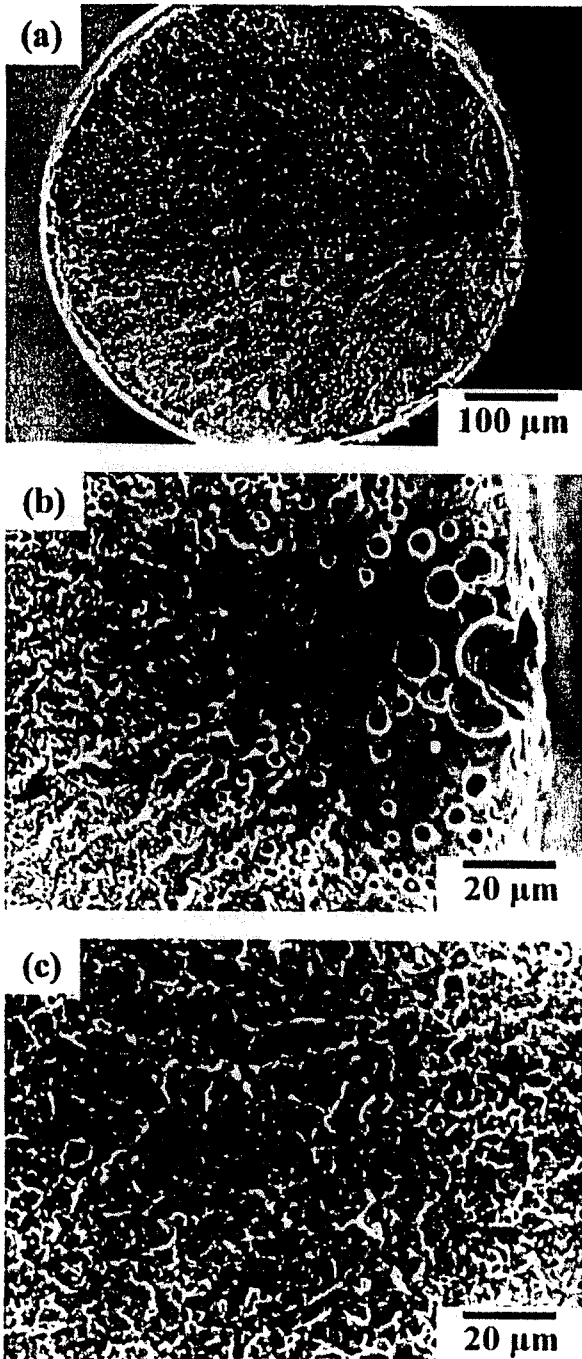


Figure 12. SEM micrographs of the delayed fracture surface under an applied stress of 600 MPa in a 2.0% NaF solution. (a) General view, (b) flat area in fracture initiation site, and (c) shallow dimple in crack propagation area.

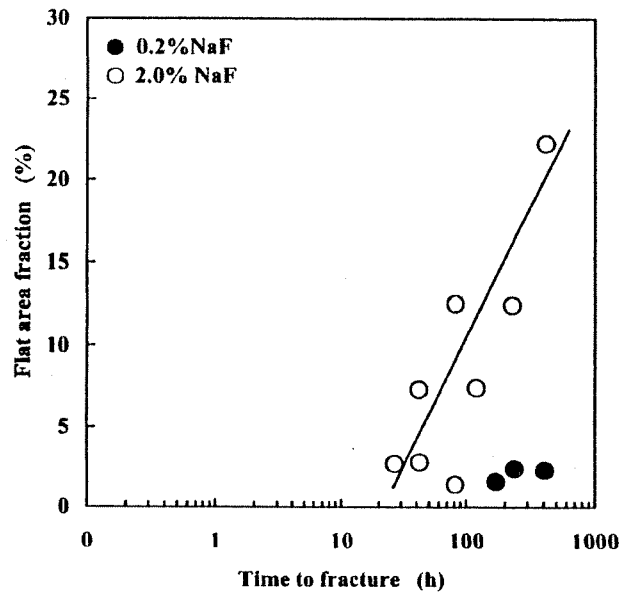


Figure 13. Fraction of flat area in the fracture surface of specimens subjected to the delayed fracture test in 0.2 and 2.0% NaF solutions as a function of time to fracture.

CONCLUSIONS

A Ni-Ti superelastic alloy is susceptible to delayed fracture in both APF and neutral NaF solutions. The susceptibility was more prominent in the former solution accompanied by a higher hydrogen absorption and general corrosion. In APF solutions, the delayed fracture is likely to be caused by hydrogen embrittlement, whereas in NaF solutions, active path corrosion accompanied by hydrogen absorption is thought to be dominant.

References

1. Edie JW, Andreasen GF, Zaytoon MP. Surface corrosion of nitinol and stainless steel under clinical conditions. *Angle Orthod* 1981;51:319-324.
2. Harris EF, Newman SM, Nicholson JA. Nitinol arch wire in a simulated oral environment: changes in mechanical properties. *Am J Orthod Dentofac Orthop* 1988;93:508-513.
3. Hudgins JJ, Bagby MD, Erickson LC. The effect of long-term deflection on permanent deformation of nickel-titanium archwires. *Angle Orthod* 1990;60:283-288.
4. Mohlin B, Müller H, Ödman J, Thilander B. Examination of Chinese NiTi wire by a combined clinical and laboratory approach. *Eur J Orthod* 1991;13:386-391.
5. Grimsdottir MR, Hensten-Pettersen A. Surface analysis of nickel-titanium archwire used *in vivo*. *Dent Mater* 1997;13:163-167.
6. Eliades T, Eliades G, Athanasiou AE, Bradley TG. Surface characterization of retrieved NiTi orthodontic archwires. *Euro J Orthod* 2000;22:317-326.
7. Yokoyama K, Hamada K, Asaoka K. Fracture analysis of hydrogen-charged nickel-titanium superelastic alloy. *Mater Trans* 2001;42:141-144.

8. Yokoyama K, Hamada K, Moriyama K, Asaoka K. Degradation and fracture of Ni-Ti superelastic wire in an oral cavity. *Biomaterials* 2001;22:2257-2262.
9. Asaoka K, Yokoyama K, Nagumo M. Hydrogen embrittlement of nickel-titanium alloy in biological environment. *Metall Mater Trans A* 2002;33A:495-501.
10. Yokoyama K, Kaneko K, Moriyama K, Asaoka K, Sakai J, Nagumo M. Hydrogen embrittlement of Ni-Ti superelastic alloy in fluoride solution. *J Biomed Mater Res* 2003;65A:182-187.
11. Wade N, Adachi Y, Hosoi Y. A role of hydrogen in shape memory effect of Ti-Ni alloys. *Scripta Metall Mater* 1990;24:1051-1055.
12. Adachi Y, Wade N, Hosoi Y. Effect of hydrogen on the shape memory effect and transformation behavior of Ti-Ni alloy. *J Jpn Inst Metals* 1990;54:525-531.
13. Asaoka T, Yamashita H, Saito H, Ishida Y. Effect of a small amount of hydrogen on pseudo-elastic properties of Ti-Ni alloy. *J Jpn Inst Metals* 1993;57:1123-1129.
14. Yokoyama K, Watabe S, Hamada K, Sakai J, Asaoka K, Nagumo M. Susceptibility to delayed fracture of Ni-Ti super-elastic alloy. *Mater Sci Eng A* 2003;341:91-97.
15. Petch J, Stables P. Delayed fracture of metals under static load. *Nature* 1952;169:842-843.
16. Frohberg RP, Barnett WJ, Troiano AR. Delayed failure and hydrogen embrittlement in steel. *Trans ASM* 1955;47:892-925.
17. Steigerwald EA, Schaller FW, Troiano AR. The role of stress in hydrogen induced delayed failure. *Trans TMS AIME* 1960;218:832-841.
18. Beachem CD. A new model for hydrogen-assisted cracking (hydrogen "embrittlement"). *Metall Trans* 1972;3:437-451.
19. Hirth JP. Effects of hydrogen on the properties of iron and steel. *Metall Trans A* 1980;11A:861-890.
20. Matsuyama S. Delayed fracture of high strength steels. *Tetsu-to-Hagané* 1994;80:679-684.
21. Nagumo M, Nakamura M, Takai K. Hydrogen thermal desorption relevant to delayed-fracture susceptibility of high-strength steels. *Metall Mater Trans A* 2001;32A:339-347.
22. Tarui T, Yamasaki S. Evaluation method of delayed fracture property and overcoming techniques of delayed fracture of high strength steels. *Tetsu-to-Hagané* 2002;88:612-619.
23. Lausmaa J, Kasemo B, Hansson S. Accelerated oxide grown on titanium implants during autoclaving caused by fluorine contamination. *Biomaterials* 1985;6:23-27.
24. Siirilä HS, Könönen M. The effect of oral topical fluorides on the surface of commercially pure titanium. *Int J Oral Maxillofac Implants* 1991;6:50-54.
25. Pröbster L, Lin W, Hüttemann H. Effect of fluoride prophylactic agents on titanium surfaces. *Int J Oral Maxillofac Implants* 1992;7:390-394.
26. Boere G. Influence of fluoride on titanium in an acidic environment measured by polarization resistance technique. *J Appl Biomater* 1995;6:283-288.
27. Toumelin-Chemla F, Rouelle F, Burdairon G. Corrosive properties of fluoride-containing odontologic gels against titanium. *J Dent* 1996;24:109-115.
28. Mimura H, Miyagawa Y. Electrochemical corrosion behavior of titanium castings. 1. Effects of degree of surface polishing and kind of solution. *Jpn J Dent Mater Dev* 1996;15:283-295.
29. Oda Y, Kawada E, Yoshinari M, Hasegawa K, Okabe T. The influence of fluoride concentration on the corrosion of titanium and titanium alloys. *Jpn J Dent Mater Dev* 1996;15:317-322.
30. Reclaru L, Meyer J-M. Effects of fluorides on titanium and other dental alloys in dentistry. *Biomaterials* 1998;19:85-92.
31. Nakagawa M, Matsuya S, Shiraiishi T, Ohta M. Effect of fluoride concentration and pH on corrosion behavior of titanium for dental use. *J Dent Res* 1999;78:1568-1572.
32. Nakagawa M, Matsuya S, Udoh K. Corrosion behavior of pure titanium and titanium alloys in fluoride-containing solutions. *Dent Mater J* 2001;20:305-314.
33. Nakagawa M, Matsuya S, Udoh K. Effects of fluoride and dissolved oxygen concentrations on the corrosion behavior of pure titanium and titanium alloys. *Dent Mater J* 2002;21:83-92.
34. Huang H-H. Effects of fluoride concentration and elastic tensile strain on the corrosion resistance of commercially pure titanium. *Biomaterials* 2002;23:59-63.
35. Huang H-H. Electrochemical impedance spectroscopy study of strained titanium in fluoride media. *Electrochimica Acta* 2002;47:2311-2318.
36. Schiff N, Grosogeat B, Lissac M, Dalard F. Influence of fluoride content and pH on the corrosion resistance of titanium and its alloys. *Biomaterials* 2002;23:1995-2002.
37. Nagumo M, Uyama H, Yoshizawa M. Accelerated failure in high strength steel by alternating hydrogen-charging potential. *Scripta Mater* 2001;44:947-952.
38. Chan CM, Trigwell S, Duerig T. Oxidation of an NiTi alloy. *Surf Interface Anal* 1990;15:349-354.
39. Green SM, Grant DM, Wood JV. XPS characterisation of surface modified Ni-Ti shape memory alloy. *Mater Sci Eng A* 1997;224:21-26.
40. Tan L, Crone WC. Surface characterization of NiTi modified by plasma source ion implantation. *Acta Mater* 2002;50:4449-4460.
41. Wu SK, Wayman CM. Interstitial ordering of hydrogen and oxygen in TiNi alloys. *Acta Metall* 1988;36:1005-1013.
42. Nam TH, Shimizu K, Saburi T, Nenno S. Crystal structure of a hydride formed by electrochemical hydrogenation in a Ti-Ni-Al alloy. *Mater Trans JIM* 1989;30:539-548.
43. Schmidt R, Schlereth M, Wipf H, Assmus W, Müllner M. Hydrogen solubility and diffusion in the shape-memory alloy NiTi. *J Phys Condens Matter* 1989;1:2473-2482.
44. Yokoyama K, Ogawa T, Asaoka K, Sakai J, Nagumo M. Degradation of tensile strength of Ni-Ti superelastic alloy due to hydrogen absorption in methanol solution containing hydrochloric acid. *Mater Sci Eng A* 2003;360:153-159.
45. Gest RJ, Troiano AR. Stress corrosion and hydrogen embrittlement in an aluminum alloy. *Corrosion* 1974;30:274-279.
46. Tanguy D, Bayle B, Dif R, Magnin TH. Hydrogen effects during IGSCC of pure Al-5Mg alloy in NaCl media. *Corros Sci* 2002;44:1163-1175.

Degradation in Performance of Orthodontic Wires Caused by Hydrogen Absorption During Short-Term Immersion in 2.0% Acidulated Phosphate Fluoride Solution

Kazuyuki Kaneko, DDS^a; Ken'ichi Yokoyama, PhD^b; Keiji Moriyama, DDS, PhD^c; Kenzo Asaoka, PhD^d; Jun'ichi Sakai, PhD^e

Abstract: The purpose of this study was to investigate the degradation in performance of four major alloys of orthodontic wires, namely nickel-titanium, beta titanium, stainless steel, and cobalt-chromium-nickel, caused by hydrogen absorption during short-term immersion in an acid fluoride solutions. The hydrogen-related degradation of orthodontic wires after immersion in 2.0% acidulated phosphate fluoride solution at 37°C for 60 minutes was evaluated by a tensile test, scanning electron microscope observation, and hydrogen thermal desorption analysis. Upon immersion, the tensile strengths of the nickel-titanium and beta titanium wires decreased. Particularly, the nickel-titanium wire fractured before yielding, and the fracture mode changed from ductile to brittle. The amounts of absorbed hydrogen in the nickel-titanium and beta titanium wires were 200 and 100 mass ppm, respectively. On the other hand, the tensile strengths of the stainless steel and cobalt-chromium-nickel wires were only slightly affected by immersion. The results of this study suggest that degradation in performance of orthodontic wires of titanium alloys occurs because of hydrogen absorption even after a short-term immersion in fluoride solutions. (*Angle Orthod* 2004;74:487-495.)

Key Words: Orthodontic wire; Hydrogen embrittlement; Fluoride; Corrosion

INTRODUCTION

Four major orthodontic alloy wires, namely, nickel-titanium, beta titanium, stainless steel, and cobalt-chromium-nickel wires, exhibit good corrosion resistance, owing to thin protective films on their surface. Films of nickel-titanium or beta titanium alloy are mainly composed of titanium oxide, whereas those of stainless steel or cobalt-chromium-nickel alloy are mainly composed of chromium oxide. These orthodontic wires shows high corrosion resistance in various solutions¹⁻⁸ such as Ringer's solution,^{1,8}

artificial saliva,³ and NaCl solution.⁶ In these solutions, the corrosion resistance of titanium alloys is higher than that of stainless steels or cobalt-based alloys from the viewpoint of film breakdown. In the oral cavity, however, even titanium alloys do not always exhibit high corrosion resistance. Actually, corrosion of orthodontic wires in the oral cavity has been observed.⁹⁻¹³ One reason for this is that the corrosion resistance of titanium alloys decreases in solutions that contain fluoride.¹⁴⁻²⁸ In acid fluoride solutions such as prophylactic agents, the titanium protective film reacts with hydrofluoric acid to form sodium titanium fluoride.^{25,26} The breakdown of the film leads to a decrease in corrosion resistance¹⁴⁻²⁸ because titanium shows intrinsically high activities.

As another serious effect of fluoride on titanium alloys, significant degradation of the mechanical properties of Ni-Ti superelastic and beta titanium alloys caused by hydrogen absorption, ie, hydrogen embrittlement, occurs in fluoride solutions.^{29,30} On the other hand, stress corrosion cracking of stainless steel has been reported in fluoride solutions.³¹⁻³⁵ Stress corrosion cracking and hydrogen embrittlement are closely related. Hydrogen embrittlement of stainless steel³⁶⁻⁴⁰ and cobalt-chromium alloys⁴¹ were investigated by cathodic hydrogen charging. However, the correlation between hydrogen absorption and degradation of stainless steel in fluo-

^a Graduate Student, Department of Orthodontics, School of Dentistry, The University of Tokushima, Tokushima, Japan.

^b Assistant Professor, Department of Dental Engineering, School of Dentistry, The University of Tokushima, Tokushima, Japan.

^c Professor and Chairman, Department of Orthodontics, School of Dentistry, The University of Tokushima, Tokushima, Japan.

^d Professor, Department of Dental Engineering, School of Dentistry, The University of Tokushima, Tokushima, Japan.

^e Professor, Department of Materials Science and Engineering, Waseda University, Tokyo, Japan.

Corresponding author: Ken'ichi Yokoyama, PhD, Department of Dental Engineering, School of Dentistry, The University of Tokushima, 3-18-15 Kuramoto-cho, Tokushima, 770-8504, Japan (e-mail: yokken@dent.tokushima-u.ac.jp).

Accepted: August 2003. Submitted: May 2003.

© 2004 by The EH Angle Education and Research Foundation, Inc.

TABLE 1. Orthodontic Wires Used in the Study

Alloy	Abbreviation	Brand Name	Manufacturer
Nickel-titanium	NiTi	NITI	Ormco
Beta titanium	Beta Ti	TMA	Ormco
Stainless steel	Stainless	Stainless steel	Ormco
Cobalt-chromium-nickel	CoCrNi	Elgiloy blue	Rocky Mountain Orthodontics

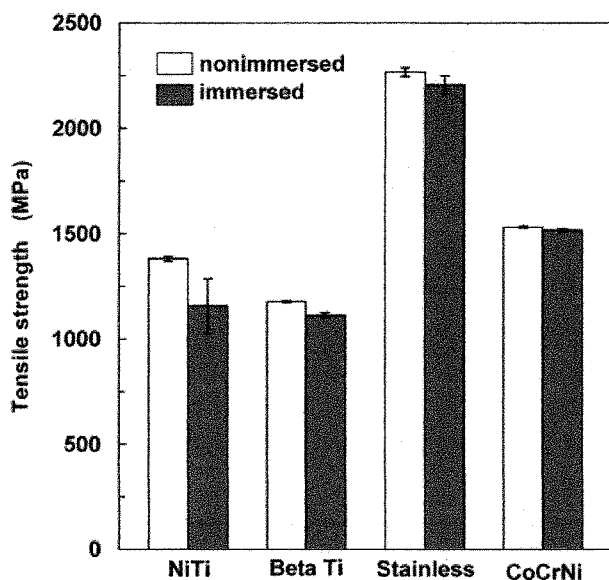


FIGURE 1. Tensile strengths of nonimmersed wires and wires immersed in 2.0% APF solution for 60 minutes. Standard deviation was calculated from the results obtained from five specimens.

ride solutions has not yet been clarified. In addition, it is necessary to confirm whether degradation in performance of orthodontic wires occurs during short-term contact with fluoride solution. The degradation of such wires in the oral cavity leads to a decrease in orthodontic force.

The purpose of the present study was to examine the degradation in performance of four major orthodontic wires after short-term immersion in acid fluoride solution from the viewpoint of hydrogen embrittlement. For the evaluation of the degradation in performance, tensile tests, surface observation by scanning electron microscope, and hydrogen thermal desorption analysis (TDA) were conducted.

MATERIALS AND METHODS

Four major orthodontic wires, namely, nickel-titanium, beta titanium, stainless steel, and cobalt-chromium-nickel wires, were tested in this study. The wire abbreviations, brand names, and manufacturers are listed in Table 1. These 0.40-mm (0.016-inch)-diameter wires were cut as 50-mm-long specimens. The specimens were immersed separately in 10 mL of an aqueous solution of 2.0% acidulated phosphate fluoride (APF; 2.0% NaF + 1.7% H₃PO₄) with pH 5.0 at 37°C for 60 minutes. Percent in solution means mass percent unless otherwise stated.

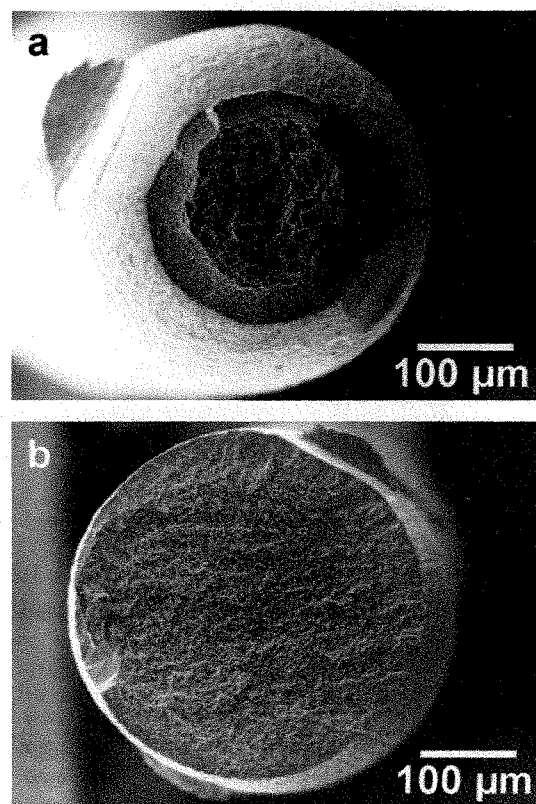


FIGURE 2. SEM micrographs of typical fracture surface of (a) non-immersed and (b) immersed nickel-titanium wires.

Tensile tests on the nonimmersed and immersed specimens were carried out at room temperature ($25 \pm 2^\circ\text{C}$) using a Shimadzu Autograph AG-100A machine at a strain rate of 8.33×10^{-4} /second. The gauge length of the specimens was 10 mm. All the immersed specimens were tested within a few minutes after being taken out of the solution. The mass change of the immersed specimens was measured. The standard deviation of tensile strengths and mass changes was calculated from the results obtained from more than five specimens. The fracture surface and side surface of the specimens were examined using a scanning electron microscope (SEM).

The amount of desorbed hydrogen was measured by hydrogen TDA for the nonimmersed and immersed specimens. TDA was started 30 minutes after removal of specimens from the solution. A quadrupole mass spectrometer (ULVAC, Kanagawa, Japan) was used for hydrogen detec-

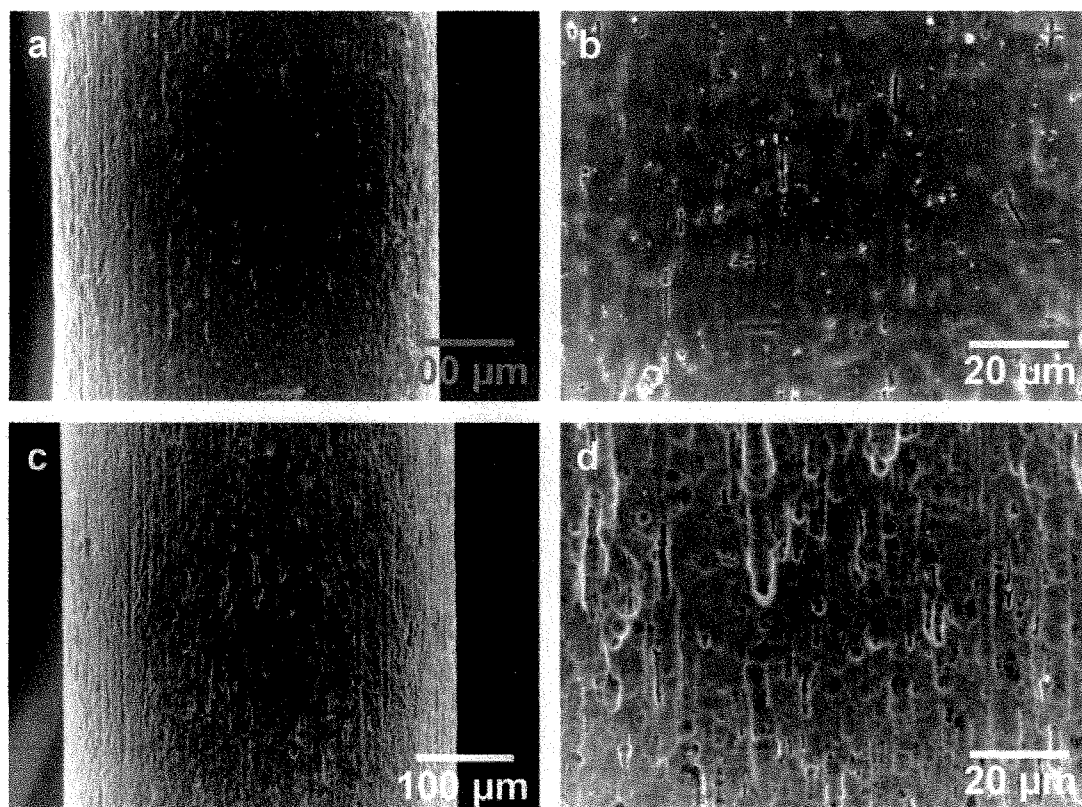


FIGURE 3. SEM micrographs of side surface of nickel-titanium wire: (a) general and (b) magnified views of nonimmersed wire; (c) general and (d) magnified views of immersed wire.

tion. Sampling was conducted at 30-second intervals, and the heating rate was 100°C/hour up to a terminal temperature of 800°C.

RESULTS

The tensile test results for the nonimmersed and immersed specimens are shown in Figure 1. The tensile strength of the immersed nickel-titanium wire decreased from 1380 to 1160 MPa. The reduction in tensile strength was 16.2%. It should be noted that the immersed nickel-titanium wire fractured before yielding. The critical stress for the stress-induced martensite transformation of the immersed nickel-titanium wire increased from 430 to 480 MPa compared with that of the nonimmersed wire. For the beta titanium wire, the tensile strength slightly decreased after immersion, and the reduction in tensile strength was 5.6%. On the other hand, the tensile strength of the immersed stainless steel wire only slightly decreased (reduction in tensile strength, 2.6%), and that of the immersed cobalt-chromium-nickel wire hardly decreased (reduction in tensile strength, 0.9%).

Figure 2 shows the fractographs of the nonimmersed (Figure 2a) and immersed nickel-titanium wires (Figure 2b). The fracture surface of the nonimmersed wire was duc-

tile and was characterized macroscopically with a cup-cone morphology. In contrast, the fracture surface of the immersed wire was fairly flat and exhibited no reduction in area. For the other wires, the fracture surface was not significantly different for the nonimmersed and immersed wires and was characterized macroscopically with a cup-cone morphology.

The SEM micrographs of the side surface of the nonimmersed and immersed nickel-titanium wires are shown in Figure 3. The side surface of the nonimmersed wires indicates that surface defects related to the wire drawing, pickling, or electropolishing procedures performed during the manufacturing process contribute to corrosion. The surface of the immersed nickel-titanium wire became rough because of corrosion, as shown in Figure 3c,d. The side surface of the nonimmersed beta titanium wire is shown in Figure 4a,b. Surface defects and corrosion pits produced by the manufacturing process were observed on the entire surface. For the immersed beta titanium wire, corrosion products uniformly formed on its surface, as shown in Figure 4c,d. The side surface of the nonimmersed stainless steel wire exhibited scratches and pits on its surface, as shown in Figure 5a,b. Upon immersion, corrosion products were distributed inhomogeneously on its surface (Figure 5c,d).

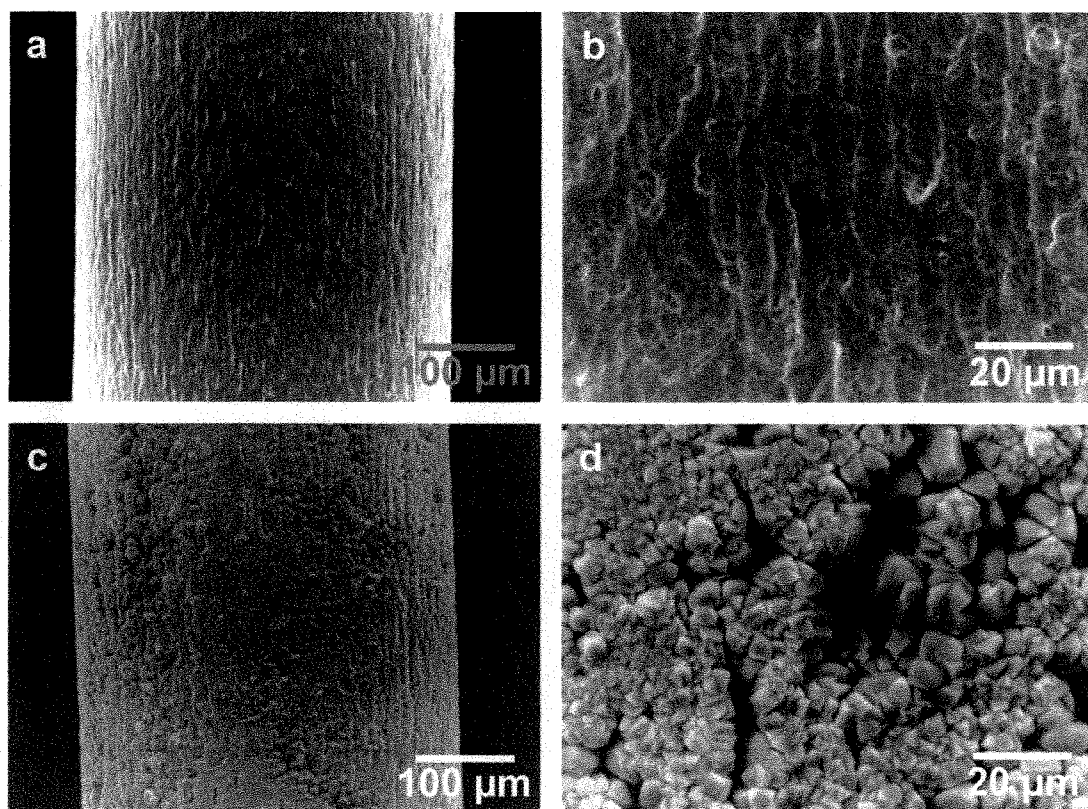


FIGURE 4. SEM micrographs of side surface of beta titanium wire: (a) general and (b) magnified views of nonimmersed wire; (c) general and (d) magnified views of immersed wire.

The side surface wire was not significantly different for the nonimmersed and immersed cobalt-chromium-nickel wires, as shown in Figure 6a through d.

The results of the mass change after immersion are shown in Figure 7. The mass of the nickel-titanium wire decreased, whereas that of the beta titanium wire increased. The mass loss of the nickel-titanium wire is attributable to corrosion during immersion in the solution. For the beta titanium wire, the mass increase resulting from the corrosion products deposited on its surface seems to be larger than the mass loss arising from dissolution. The mass of the stainless steel wire increased slightly because of the deposition of corrosion products on its surface. On the other hand, the mass change of the cobalt-chromium-nickel wire was hardly confirmed.

Figure 8a through d shows the TDA curves for the non-immersed and immersed wires. The progress of hydrogen entry into the wires was denoted by an increase in the total desorbed hydrogen, defined as the integrated peak intensity. The amount of hydrogen that desorbed from the non-immersed wires gives the concentration of predissolved hydrogen. For the immersed nickel-titanium and beta titanium wires, thermal hydrogen desorption appeared with a desorption peak at approximately 400°C and 650°C, respectively. This TDA result clearly indicates that the nickel-

titanium and beta titanium wires absorbed a large amount of hydrogen in the solution even with a 60-minute immersion. The amounts of absorbed hydrogen during the immersion of the nickel-titanium and beta titanium wires were calculated by subtracting the predissolved hydrogen content in each wire and were found to be 227 and 94 mass ppm, respectively. On the other hand, for the immersed stainless steel and cobalt-chromium-nickel wires, no increase in the amount of desorbed hydrogen was confirmed.

DISCUSSION

Orthodontic wires with a titanium protective film degenerated by immersion in 2.0% APF solution for 60 minutes. The nickel-titanium wire absorbed a substantial amount of hydrogen and the fracture mode changed from ductile to brittle, as shown in Figure 2. Furthermore, the increase in critical stress for martensite transformation by immersion might obstruct the generation of an appropriate orthodontic force. The increase in critical stress for martensite transformation is likely ascribable to the effect of hydrogen of preventing martensite transformation because martensite transformation is sensitive to the presence of interstitial atoms.⁴² These results are in good agreement with that obtained by immersion in 0.2% APF solution in our previous

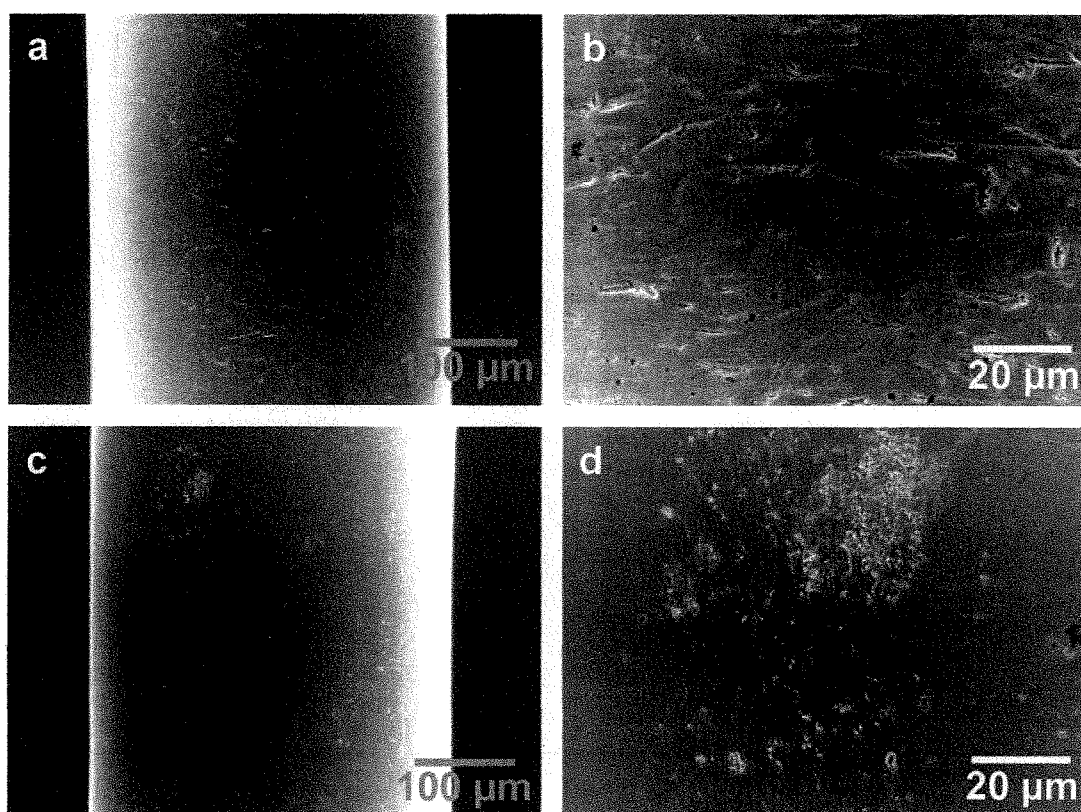


FIGURE 5. SEM micrographs of side surface of stainless steel wire: (a) general and (b) magnified views of nonimmersed wire; (c) general and (d) magnified views of immersed wire.

study.²⁹ In acid fluoride solutions, the breakdown of a titanium protective film occurs readily, and a nickel-titanium alloy absorbs hydrogen because of the high affinity of titanium to hydrogen. When the amount of absorbed hydrogen exceeds 50–200 mass ppm, a pronounced degradation in the performance of nickel-titanium superelastic alloys occurs.^{29,43} As with the findings of previous studies, fracture stress presumably decreases to critical stress for martensite transformation, and a wire fractures before martensite transformation with longer immersion time.

Fracture of nickel-titanium orthodontic wires is often experienced during clinical use in the oral cavity.^{44,45} Its main cause has been considered to be surface defects generated during wire manufacture, fatigue, or corrosion-related phenomena.^{9,46} However, our results clearly indicate that one of the reasons for the fracture is degradation in performance caused by hydrogen absorption in the presence of fluoride in the oral cavity. Various mechanisms have been proposed for hydrogen embrittlement, eg, the stress-induced hydride formation and cleavage mechanism,⁴⁷ hydrogen-induced decohesion theory,⁴⁸ and hydrogen-enhanced localized plasticity model,^{49,50} but a detailed discussion is beyond the scope of the present study.

The beta titanium wire absorbed substantial amounts of

hydrogen like the nickel-titanium wire, although its tensile strength was slightly decreased by immersion in 2.0% APF solution for 60 minutes. In general, the tensile strength of beta titanium alloys decreases considerably with increasing hydrogen content.^{51–57} When hydrogen content is larger than several thousand mass ppm, pronounced degradation, such as ductile-to-brittle transition, occurs. Moreover, the delayed fracture of beta titanium alloys takes place because of hydrogen absorption in APF solutions.³⁰ Therefore, a marked degradation in performance of beta titanium orthodontic wires will occur with longer immersion times.

The absorbed hydrogen in titanium alloys diffuses from the surface inward even at room temperature, and diffusion distance depends on the coefficient of hydrogen diffusion in materials. Hence, for thinner nickel-titanium and beta titanium wires, degradation in performance caused by hydrogen absorption probably occurs for a short immersion time in comparison with the results of the present study.

In the current study, hydrogen contents in the nonimmersed nickel-titanium and beta titanium wires were relatively large, as shown in Figure 8a,b, suggesting that hydrogen was introduced by manufacturing processes such as electropolishing. Wu and Wayman⁵⁸ have reported that nickel-titanium alloys absorb hydrogen during electropol-

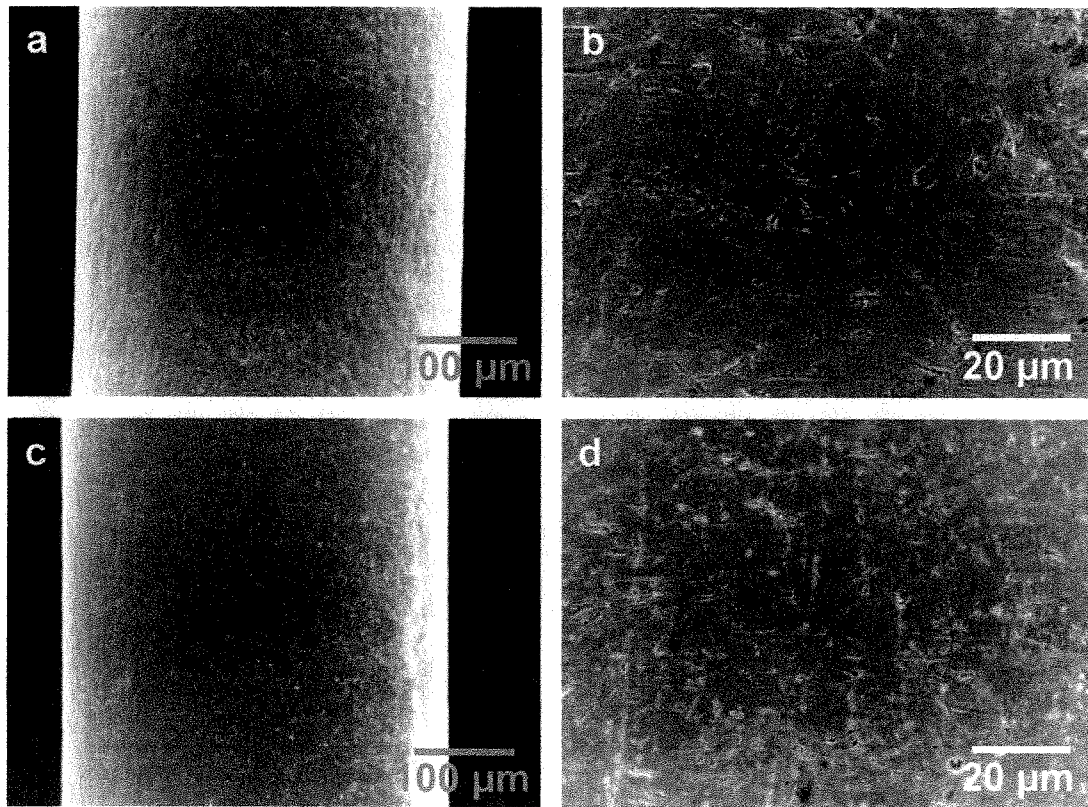


FIGURE 6. SEM micrographs of side surface of cobalt-chromium-nickel wire: (a) general and (b) magnified views of nonimmersed wire; (c) general and (d) magnified views of immersed wire.

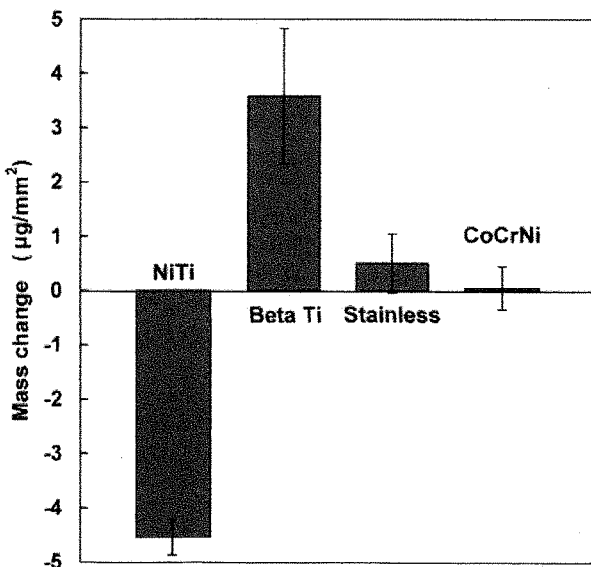


FIGURE 7. Mass change after immersing wires. Standard deviation was calculated from the results of more than five measurements.

ishing in the preparation of transmission electron microscopy specimens. Diminution of the hydrogen content by the manufacturer will help improve the clinical performance of wires.

The tensile strength of the orthodontic wire with a chromium protective film was only slightly reduced by immersion in 2.0% APF solution for 60 minutes. For the stainless steel wire, the effect of immersion was recognized on the basis of the results of SEM observation and mass change measurement. However, the increase in the amount of desorbed hydrogen was not confirmed. It should be noted that local hydrogen density was not measured in the present experiment of TDA because the amount of absorbed hydrogen was taken as the mean value over the immersed wire.

Hydrogen embrittlement of stainless steels³⁶⁻⁴⁰ and cobalt-based alloys⁴¹ has been examined by cathodic hydrogen charging. When stainless steels and cobalt-based alloys absorb hydrogen, a degradation of their mechanical properties results, ie, there is reduced tensile strength and ductility. The stress corrosion cracking of stainless steels in the presence of fluoride has been reported by several authors,³¹⁻³⁵ although the involvement of hydrogen absorption has not been mentioned. In the case of stress corrosion cracking in

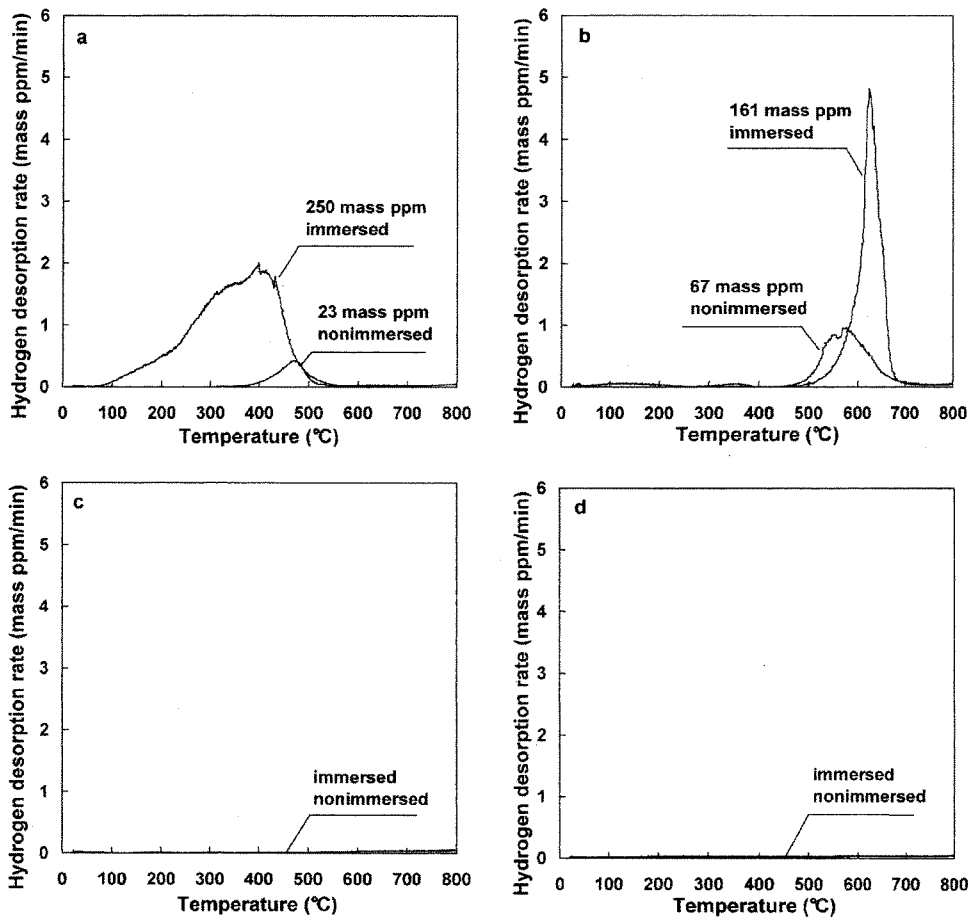


FIGURE 8. Hydrogen thermal desorption curves for nonimmersed wires and wires immersed in 2.0% APF solution for 60 minutes: (a) nickel-titanium, (b) beta titanium, (c) stainless steel, and (d) cobalt-chromium-nickel wires.

acid solutions, crack growth is accompanied by anodic dissolution and cathodic hydrogen generation at the crack tip. The breakdown of the protective film at the crack tip often leads to hydrogen absorption. Even an extremely small amount of hydrogen in the vicinity of the crack can sometimes play an important role in stress corrosion cracking.^{59,60} Therefore, that the slight degradation of stainless steel is attributable to a small amount of hydrogen should not be excluded, although hydrogen desorption was not detected in the present study. Nonetheless, for a short immersion time without loading, we provisionally consider that the serious degradation of orthodontic wires with a chromium protective film caused by hydrogen absorption does not occur in a 2.0% APF solution. Local hydrogen absorption and long-term immersion tests should be investigated in the future.

CONCLUSIONS

The degradation in performance of four major orthodontic wires caused by hydrogen absorption was investigated

by immersion in a 2.0% APF solution for 60 minutes. Upon immersion, the nickel-titanium and beta titanium wires absorbed substantial amounts of hydrogen and degenerated, whereas the performance of the stainless steel and cobalt-chromium-nickel wires was only slightly affected. In APF solutions, the degradation resistance of wires with a titanium protective film is considered to be lower than that of wires with a chromium protective film. Clinically, the present results suggest that orthodontists should, as much as possible, avoid placing wires with a titanium protective film in contact with prophylactic agents, toothpastes, or dental rinses that contain fluoride.

ACKNOWLEDGMENT

This study was supported in part by a Grant-in-Aid for Young Scientists (B) (14771090) from the Ministry of Education, Culture, Sports, Science, and Technology, Japan.

REFERENCES

1. Bundy KJ, Vogelbaum MA, Desai VH. The influence of static stress on the corrosion behavior of 316L stainless steel in Ringer's solution. *J Biomed Mater Res.* 1986;20:493-505.

2. Rondelli G, Vicentini B, Cigada A. The corrosion behavior of nickel titanium shape memory alloys. *Corros Sci*. 1990;30:805-812.
3. Rondelli G. Corrosion resistance tests on NiTi shape memory alloy. *Biomaterials*. 1996;17:2003-2008.
4. Wever DJ, Veldhuizen AG, de Vries J, Busscher HJ, Uges DRA, van Horn JR. Electrochemical and surface characterization of a nickel-titanium alloy. *Biomaterials*. 1998;19:761-769.
5. Rondelli G, Vicentini B. Localized corrosion behavior in simulated human body fluids of commercial Ni-Ti orthodontic wires. *Biomaterials*. 1999;20:785-792.
6. Rondelli G, Vicentini B. Evaluation by electrochemical tests of the passive film stability of equiatomic Ni-Ti alloy also in presence of stress-induced martensite. *J Biomed Mater Res*. 2000;51:47-54.
7. Thierry B, Tabrizian M, Trepanier C, Savadogo O, Yahia L'H. Effect of surface treatment and sterilization processes on the corrosion behavior of NiTi shape memory alloy. *J Biomed Mater Res*. 2000;51:685-693.
8. Montero-Ocampo C, Lopez H, Salinas Rodriguez A. Effect of compressive straining on corrosion resistance of a shape memory Ni-Ti alloy in ringer's solution. *J Biomed Mater Res*. 1996;32:583-591.
9. Edie JW, Andreasen GF, Zaytoon MP. Surface corrosion of nitinol and stainless steel under clinical conditions. *Angle Orthod*. 1981;51:319-324.
10. Harris EF, Newman SM, Nicholson JA. Nitinol arch wire in a simulated oral environment; Changes in mechanical properties. *Am J Orthod Dentofacial Orthop*. 1988;93:508-513.
11. Hudgins JJ, Bagby MD, Erickson LC. The effect of long-term deflection on permanent deformation of nickel-titanium archwires. *Angle Orthod*. 1990;60:283-288.
12. Grimsdottir MR, Hensten-Petersen A. Surface analysis of nickel-titanium archwire used in vivo. *Dent Mater*. 1997;13:163-167.
13. Eliades T, Eliades G, Athanasiou AE, Bradley TG. Surface characterization of retrieved NiTi orthodontic archwires. *Eur J Orthod*. 2000;22:317-326.
14. Lausmaa J, Kasemo B, Hansson S. Accelerated oxide grown on titanium implants during autoclaving caused by fluorine contamination. *Biomaterials*. 1985;6:23-27.
15. Siirilä HS, Könönen M. The effect of oral topical fluorides on the surface of commercially pure titanium. *Int J Oral Maxillofac Implants*. 1991;6:50-54.
16. Pröbster L, Lin W, Hüttemann H. Effect of fluoride prophylactic agents on titanium surfaces. *Int J Oral Maxillofac Implants*. 1992;7:390-394.
17. Boere G. Influence of fluoride on titanium in an acidic environment measured by polarization resistance technique. *J Appl Biomater*. 1995;6:283-288.
18. Könönen MHO, Lavonius ET, Kivilahti JK. SEM observations on stress corrosion cracking of commercially pure titanium in a topical fluoride solution. *Dent Mater*. 1995;11:269-272.
19. Toumelin-Chemla F, Rouelle F, Burdairon G. Corrosive properties of fluoride-containing odontologic gels against titanium. *J Dent*. 1996;24:109-115.
20. Mimura H, Miyagawa Y. Electrochemical corrosion behavior of titanium castings. Part 1. Effects of degree of surface polishing and kind of solution. *Jpn J Dent Mater Dev*. 1996;15:283-295.
21. Oda Y, Kawada E, Yoshinari M, Hasegawa K, Okabe T. The influence of fluoride concentration on the corrosion of titanium and titanium alloys. *Jpn J Dent Mater Dev*. 1996;15:317-322.
22. Reclaru L, Meyer J-M. Effects of fluorides on titanium and other dental alloys in dentistry. *Biomaterials*. 1998;19:85-92.
23. Nakagawa M, Matsuya S, Shiraiishi T, Ohta M. Effect of fluoride concentration and pH on corrosion behavior of titanium for dental use. *J Dent Res*. 1999;78:1568-1572.
24. Nakagawa M, Matsuya S, Udoh K. Corrosion behavior of pure titanium and titanium alloys in fluoride-containing solutions. *Dent Mater J*. 2001;20:305-314.
25. Nakagawa M, Matsuya S, Udoh K. Effects of fluoride and dissolved oxygen concentrations on the corrosion behavior of pure titanium and titanium alloys. *Dent Mater J*. 2002;21:83-92.
26. Huang H-H. Effects of fluoride concentration and elastic tensile strain on the corrosion resistance of commercially pure titanium. *Biomaterials*. 2002;23:59-63.
27. Huang H-H. Electrochemical impedance spectroscopy study of strained titanium in fluoride media. *Electrochim Acta*. 2002;47:2311-2318.
28. Schiff N, Grosgeat B, Lissac M, Dalard F. Influence of fluoride content and pH on the corrosion resistance of titanium and its alloys. *Biomaterials*. 2002;23:1995-2002.
29. Yokoyama K, Kaneko K, Moriyama K, Asaoka K, Sakai J, Nagumo M. Hydrogen embrittlement of Ni-Ti superelastic alloy in fluoride solution. *J Biomed Mater Res*. 2003;65A:182-187.
30. Kaneko K, Yokoyama K, Moriyama K, Asaoka K, Sakai J, Nagumo M. Delayed fracture of beta titanium orthodontic wire in fluoride aqueous solutions. *Biomaterials*. 2003;24:2113-2120.
31. Takemoto M, Shonohara T, Shirai M, Shinogaya T. External stress corrosion cracking (ESCC) of austenitic stainless steel. *Mater Perf*. 1985;24:26-32.
32. Zucchi F, Trabanelli G, Demertzis G. The intergranular stress corrosion cracking of a sensitized AISI 304 in NaF and NaCl solutions. *Corros Sci*. 1988;28:69-79.
33. Shibata T, Haruna T, Oki T. Initiation and growth of intergranular stress corrosion cracks for sensitized 304 stainless steel depending on NaF concentration of aqueous solution. *Tetus-to-Hagané*. 1993;79:721-725.
34. Yamazaki O. Effect of fluoride ion on the crevice corrosion for type 304 stainless steel in neutral NaCl solution. *Zairyo-to-Kankyo*. 1996;45:365-359.
35. Bastidas JM, Fosca C, Chico B, Otero E. Weight loss and electrochemical results for two super-austenitic stainless steels in chloride-fluoride mixtures. *Corros Sci*. 1996;38:559-563.
36. Whiteman MB, Troiano AR. Hydrogen embrittlement of austenitic stainless steel. *Corrosion*. 1965;21:53-56.
37. Holzworth ML. Hydrogen embrittlement of type 304L stainless steel. *Corrosion*. 1969;25:107-115.
38. Rozenak P, Eliezer D. Effects of metallurgical variables on hydrogen embrittlement in AISI type 316, 321 and 347 stainless steels. *Mater Sci Eng*. 1983;61:31-41.
39. Ulmer DG, Altstetter CJ. Hydrogen-induced strain localization and failure of austenitic stainless steels at high hydrogen concentrations. *Acta Metall Mater*. 1991;39:1237-1248.
40. Herms E, Olive JM, Puiggali M. Hydrogen embrittlement of 316L type stainless steel. *Mater Sci Eng A*. 1999;272:279-283.
41. Edwards BJ, Louthan MR Jr, Sisson RD Jr. Hydrogen embrittlement of Zimaloy: a cobalt-chromium-molybdenum orthopedic implant alloy. In: Fraker AC, Griffin CD, eds. *Corrosion and Degradation of Implant Materials: Second Symposium, ASTM STP 859*. Philadelphia, Pa: American Society for Testing and Materials; 1983:11-29.
42. Biscarini A, Campanella R, Coluzzi B, Mazzolai G, Trotta L, Tuissi A, Mazzolai FM. Martensitic transitions and mechanical spectroscopy of Ni_{40.8}Ti_{59.2} alloy containing hydrogen. *Acta Mater*. 1999;47:4525-4533.
43. Yokoyama K, Ogawa T, Asaoka K, Sakai J, Nagumo M. Degradation of tensile strength of Ni-Ti superelastic alloy due to hydrogen absorption in methanol solution containing hydrochloric acid. *Mater Sci Eng A*. In press.
44. Mohlin B, Müller H, Ödman J, Thilander B. Examination of Chinese NiTi wire by a combined clinical and laboratory approach. *Eur J Orthod*. 1991;13:386-391.

45. Yokoyama K, Hamada K, Moriyama K, Asaoka K. Degradation and fracture of Ni-Ti superelastic wire in an oral cavity. *Biomaterials*. 2001;22:2257-2262.
46. Schwaninger B, Sarkar NK, Foster BE. Effect of long-term immersion corrosion on the flexural properties of nitinol. *Am J Orthod*. 1982;82:45-49.
47. Westlake DG. A generalized model for hydrogen embrittlement. *Trans ASM*. 1969;62:1000-1006.
48. Oriani RA, Josephic PH. Equilibrium aspects of hydrogen-induced cracking of steels. *Acta Metall*. 1974;22:1065-1074.
49. Beachem CD. A new model for hydrogen-assisted cracking (hydrogen "embrittlement"). *Metall Trans*. 1972;3:437-451.
50. Birnbaum HK, Sofronis P. Hydrogen-enhanced localized plasticity—a mechanism for hydrogen-related fracture. *Mater Sci Eng A*. 1994;176:191-202.
51. Lederich RJ, Schwartz DS, Sastry SML. Effects of internal hydrogen on microstructures and mechanical properties of β 21S and Ti-15-3. In: Eylon D, Boyer RR, Koss DA, eds. *Beta Titanium Alloys in the 1990's*. Warrendale, Pa: TMS; 1993:159-169.
52. Young GA Jr, Scully JR. The effects of hydrogen on the room temperature mechanical properties of Ti-15V-3Cr-3Al-3Sn and Ti-15Mo-3Nb-3Al. In: Eylon D, Boyer RR, Koss DA, eds. *Beta Titanium Alloys in the 1990's*. Warrendale, PA: TMS; 1993:147-158.
53. Young GA Jr, Scully JR. Effects of hydrogen on the mechanical properties of a Ti-Mo-Nb-Al alloy. *Scripta Metall Mater*. 1993;28:507-512.
54. Young GA Jr, Scully JR. Hydrogen embrittlement of solution heat-treated and aged β -titanium alloys Ti-15%V-3%Cr-3%Al-3%Sn and Ti-15%Mo-3%Nb-3%Al. *Corrosion*. 1994;50:919-933.
55. Itoh G, Kanno M, Niwa N. Mechanical properties of a Ti-15V-3Cr-3Sn-3Al alloy affected by the impurity hydrogen. *Mater Sci Eng A*. 1996;213:93-97.
56. Gaudett MA, Scully JR. Effect of pre-dissolved hydrogen on fracture initiation in metastable beta Ti-3Al-8V-6Cr-4Mo-4Zr. *Scripta Mater*. 1997;36:565-572.
57. Teter DF, Robertson IM, Birnbaum HK. The effects of hydrogen on the deformation and fracture of β -titanium. *Acta Mater*. 2001;49:4313-4323.
58. Wu SK, Wayman CM. Interstitial ordering of hydrogen and oxygen in TiNi alloys. *Acta Metall*. 1988;36:1005-1013.
59. Gest RJ, Troiano AR. Stress corrosion and hydrogen embrittlement in an aluminum alloy. *Corrosion*. 1974;30:274-279.
60. Tanguy D, Bayle B, Dif R, Magnin Th. Hydrogen effects during IGSCC of pure Al-5Mg alloy in NaCl media. *Corros Sci*. 2002;44:1163-1175.

Fracture of nickel–titanium superelastic alloy in sodium hypochlorite solution

Ken'ichi Yokoyama^{a,*}, Kazuyuki Kaneko^b, Eiji Yabuta^c, Kenzo Asaoka^a, Jun'ichi Sakai^c

^a Department of Dental Engineering, School of Dentistry, The University of Tokushima, 3-18-15 Kuramoto-cho, Tokushima 770-8504, Japan

^b Department of Orthodontics, School of Dentistry, The University of Tokushima, 3-18-15 Kuramoto-cho, Tokushima 770-8504, Japan

^c Department of Materials Science and Engineering, Waseda University, 3-4-1 Okubo Shinjuku-ku, Tokyo 169-8555, Japan

Received 11 June 2003; received in revised form 6 October 2003

Abstract

Fracture of the Ni–Ti superelastic alloy for endodontic instruments such as files was investigated with a sustained tensile-loading test in sodium hypochlorite (NaOCl) solution of various concentrations. It was found that the time to fracture was reduced when the applied stress exceeded the critical stress for martensite transformation. When the applied stress was higher than the critical stress, the 0.3 mm diameter wires of the Ni–Ti superelastic alloy sometimes fractured within 60 min. From the results of observations of the fracture surface using a scanning electron microscope, it was revealed that the fracture of the Ni–Ti superelastic alloy is significantly influenced by corrosion when the applied stress was higher than the critical stress for martensite transformation. The results of the present study suggest that one of the causes of the fracture of Ni–Ti files during clinical use is corrosion under the applied stress above the critical stress for martensite transformation in NaOCl solution.

© 2003 Elsevier B.V. All rights reserved.

Keywords: Ni–Ti; Superelastic alloy; Fracture; Corrosion; Sodium hypochlorite

1. Introduction

The biomedical applications of the Ni–Ti superelastic alloy are increasing. In the dental field, the superelastic effect of this alloy is mainly used in orthodontic wires and endodontic instruments. Endodontic instruments such as files made of the alloy were first introduced by Walia et al. in 1988 [1], because the alloy has excellent mechanical properties including flexibility and high torsion strength [2–6]. In addition, the Ni–Ti superelastic alloy exhibits good corrosion resistance in saliva and saline solutions [7–10]. However, the corrosion of endodontic instruments made of Ni–Ti superelastic alloy in sodium hypochlorite (NaOCl) solutions has been reported by Haikel et al. [11] and Busslinger et al. [12].

NaOCl solution is irrigated into root canals as disinfecting and/or complexing agent during chemomechanical shaping and cleaning. Ni–Ti endodontic instruments are often used

in contact with the solution. It is therefore important to investigate the corrosion behavior and degradation of the mechanical properties of the Ni–Ti superelastic alloy in NaOCl solution. Haikel et al. [11] and Busslinger et al. [12] also suggested that NaOCl solution has no effect on the mechanical properties of Ni–Ti files such as flexibility and torsion strength at a short immersion time. However, the effect of the applied stress on the corrosion behavior of the Ni–Ti alloy has not been investigated in NaOCl solution.

Actually, Ni–Ti files frequently fracture inside the root canal during clinical use. This unexpected fracture and high cost are the weak points of Ni–Ti endodontic instruments. Bonetti Filho et al. [13] strongly recommended that small Ni–Ti instruments should be discarded after five uses. Several workers reported that the major cause of the fracture of Ni–Ti files is overload operation, because the torsional properties of Ni–Ti files are lower than those of traditional stainless steel files [2,3]. Kuhn et al. [14] also indicated that the manufacture of Ni–Ti alloys by machining in files promotes work hardening, which contributes to the degradation of their mechanical properties. On the other hand, we have demonstrated that the Ni–Ti superelastic alloy is more

* Corresponding author. Tel.: +81-88-633-7334;

fax: +81-88-633-9125.

E-mail address: yokken@dent.tokushima-u.ac.jp (K. Yokoyama).

susceptible to environmental conditions when the applied stress is higher than the critical stress for martensite transformation [15]. The effects of environmental conditions such as chemical species in solutions like NaOCl solution on the fracture of the alloy under an applied stress cannot be disregarded. It is therefore necessary to confirm experimentally whether or not the fracture of the Ni–Ti superelastic alloy under an applied stress occurs in NaOCl solution.

The objective of the present study is to examine the fracture of the Ni–Ti superelastic alloy in NaOCl solution of various concentrations during a sustained tensile-loading test. The mechanism of fracture was investigated by characterizing fractographic features and measuring corrosion potential.

2. Experimental procedures

2.1. Materials

A commercial Ni–Ti (Ni: 55 mass%, Ti: balance) superelastic wire of 0.5 mm diameter was used. Percent in this paper means mass percent, unless otherwise stated. In order to investigate the effect of the diameter of the wire on the time to fracture, a 0.3 mm diameter wire was also used. The surfaces of the specimens were carefully polished using #600-grid SiC paper to eliminate accretions, followed by cleaning with acetone and drying in ambient air. The transformation temperatures and the mechanical properties of the Ni–Ti superelastic alloy are given in Table 1. The transformation temperatures were measured by an electrical resistance method. Here, M_s and M_f indicate the start and finish temperatures for martensite transformation, respectively, during cooling. Similarly, A_s and A_f indicate the start and finish temperatures, respectively, for reverse transformation. The critical stress for martensite transformation and the tensile strength at room temperature ($25 \pm 2^\circ\text{C}$) are 530 and 1250 MPa, respectively.

2.2. Sustained tensile-loading test

A sustained tensile-loading test in solutions of 0.1, 1.0 and 5.0% NaOCl was carried out at room temperature. The

Table 1
Transformation temperatures and mechanical properties of the tested Ni–Ti superelastic alloy

Parameter	Value
Transformation temperature ($^\circ\text{C}$)	
A_f	-4
A_s	-26
M_s	-3
M_f	-27
Critical stress (MPa)	530 ± 16.7
Tensile strength (MPa)	1250 ± 7.2
Reduction in area (%)	54.7

applied stress was calculated as the ratio of the applied load to the initial cross-sectional area and was varied to determine the fracture life characteristics. The pH values of these solutions were 10.9, 11.9 and 12.4, respectively. The immersed length of the specimen in each solution was 50 mm and the volume of the test solution was 50 ml. Immediately after fracture, the specimens were taken out from the solution, followed by cleaning with acetone and drying in ambient air. The fracture surface of the specimens was observed using a scanning electron microscope (SEM).

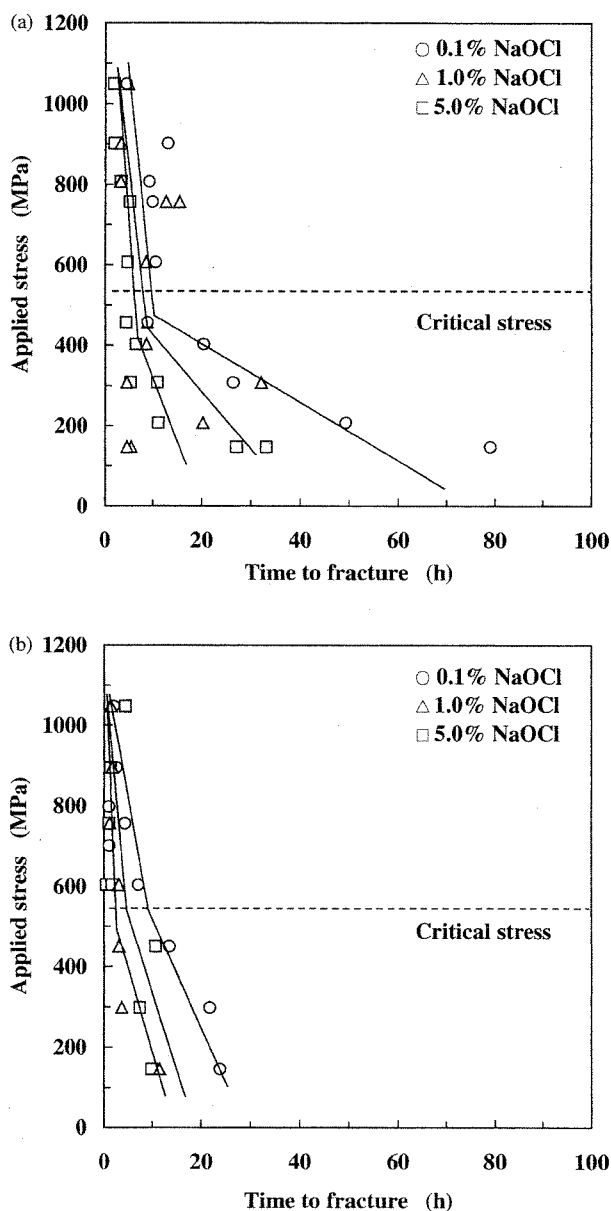


Fig. 1. Effect of the applied stress on time to fracture of the Ni–Ti superelastic alloy in 0.1, 1.0 and 5.0% NaOCl solutions. The specimens of 0.5 mm (a) and 0.3 mm (b) diameter.

2.3. Analysis of corrosion products

Corrosion products, which precipitated in the NaOCl solutions, were filtered, dried, and washed with distilled water several times in order to remove any impurities. For comparison with the corrosion products of the Ni–Ti superelastic alloy, pure nickel (99.9%) and commercial pure titanium (99.8%) were individually immersed in the NaOCl solutions in additional experiments. The corrosion products were examined using a SEM and an X-ray diffractometer (XRD; RIGAKU RINT-TTR) with Cu K α radiation of $\lambda = 1.54056 \text{ \AA}$ wavelength for the 2θ angle range from 10 to 80° at 50 kV and 200 mA. The mass ratio of the principal component in corrosion products was analyzed by energy dispersive spectroscopy (EDS).

2.4. Corrosion test

Corrosion potentials of the alloy without the applied stress were measured at room temperature in the NaOCl

solutions under open-air conditions. The counter and reference electrodes were a platinum electrode and a saturated calomel electrode (SCE), respectively. The measurements were started 10 s after immersion in the test solution.

3. Experimental results

The sustained tensile-loading test results are presented in Fig. 1 in terms of the time to fracture as a function of the initial applied stress. Figs. 1(a) and (b) show specimens of 0.5 and 0.3 mm diameter, respectively. In general, NaOCl concentration is used clinically during root canal therapy between 0.5 and 5.5%. In the present study, it is found that the alloys fractured even at a low concentration of 0.1%. Although the measurement conditions varied widely, the time to fracture tended to increase with decreasing NaOCl concentration. The time to fracture also increased with decreasing applied stress. The slope of the linear dependence changed around the critical stress for martensite

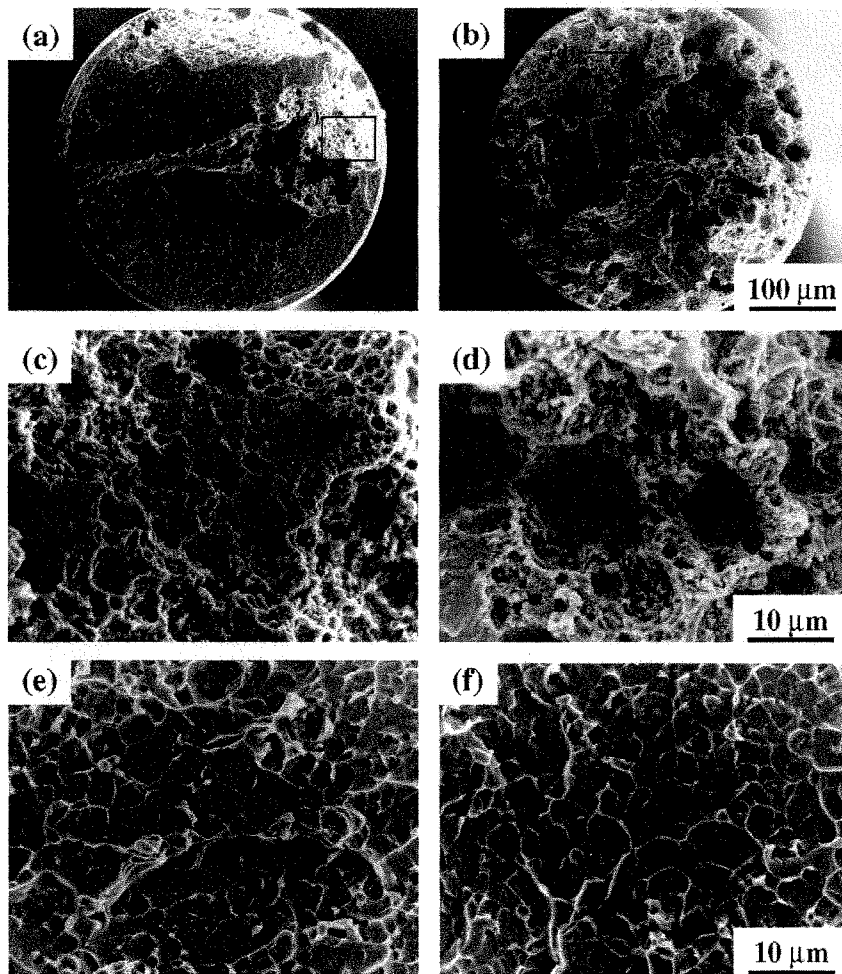


Fig. 2. SEM micrographs of the macroscopic fracture surface of the 0.5 mm diameter specimen in 5.0% NaOCl solution under applied stresses of 750 MPa (a) and 150 MPa (b). Magnified views of the corrosion area under applied stresses of 750 MPa (c) and 150 MPa (d), and the shallow-dimple pattern area under applied stresses of 750 MPa (e) and 150 MPa (f).

transformation. Moreover, the time to fracture decreased with decreasing diameter of specimen. It should be noted that the 0.3 mm diameter specimen under the applied stress above 530 MPa sometimes fractured within 60 min. The shortest time to fracture was only 30 min in this experiment.

The fracture surfaces of the 0.5 mm diameter specimens in 5.0% NaOCl solution for applied stresses of 750 and 150 MPa are shown in Figs. 2(a) and (b), respectively. On the basis of SEM observations, fracture surface patterns can be classified into two areas: the corrosion area (Figs. 2(c) and (d)) and the shallow-dimple pattern area (Figs. 2(e) and (f)). Regardless of the concentration of NaOCl solution, the fracture surface patterns were similar to those mentioned above. Fig. 3 shows a fraction of the shallow-dimple pattern area, i.e., the non-corrosion area, in a cross-section as a function of the applied stress in 0.5 mm-diameter specimens. At an applied stress higher than the critical stress for martensite transformation, the shallow-dimple pattern area decreased gradually with decreasing applied stress. On the other hand, in the applied stress range lower than the critical stress, the shallow-dimple pattern area decreased abruptly. Thus, when the applied stress was higher than the critical stress for martensite transformation, the Ni–Ti superelastic alloy fractured by slight corrosion. This result indicates that the fracture of Ni–Ti superelastic alloy is accelerated at an applied stress higher than the stress for stress-induced martensite transformation. In addition, the dimple pattern area tends to decrease with increasing concentration of NaOCl solution.

The side surfaces of the fractured samples with 0.5 mm diameter in 5.0% NaOCl solution under applied stresses of 750 and 150 MPa are shown in Figs. 4(a) and (b), respectively. A marked corrosion was observed in the periphery of the fracture surface, but not in other immersed areas. No crevice corrosion occurred at the point of contact with the

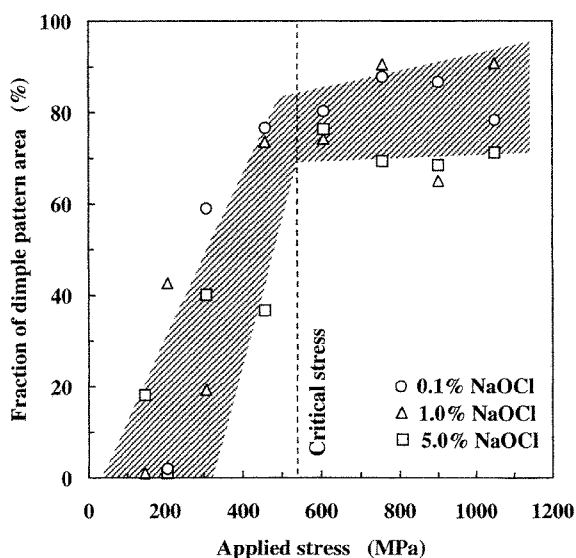


Fig. 3. Fraction of dimple pattern area in the fracture surface as a function of applied stress in 0.1, 1.0 and 5.0% NaOCl solutions.

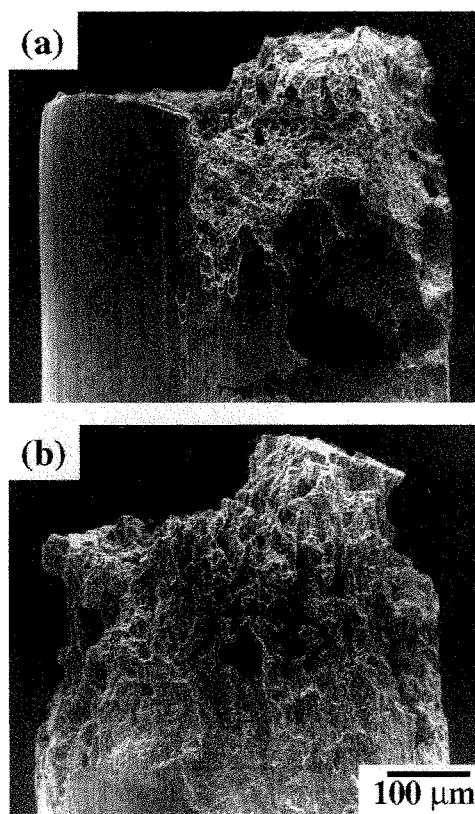


Fig. 4. SEM micrographs of the surface in 5.0% NaOCl solution under applied stresses of 750 MPa (a) and 150 MPa (b).

vessel and in the vicinity of the water plane in this experiment.

The features of the corrosion products, which precipitated in 5.0% NaOCl solution, are shown in Fig. 5. The sizes of the corrosion products of the Ni–Ti superelastic alloy (Figs. 5(a) and (b)) and pure nickel (Figs. 5(c) and (d)) were approximately 50–200 μm . Both corrosion products were black, as observed by the naked eye. In the case of commercial pure titanium, no corrosion products precipitated in the NaOCl solutions. The XRD profiles of the corrosion products are shown in Fig. 6. The corrosion products of the Ni–Ti superelastic alloy were identified as those of β -NiOOH (hexagonal; $a = 0.281 \text{ nm}$, $c = 0.484 \text{ nm}$) and NiTi (cubic; $a = 0.2998 \text{ nm}$), as shown in Fig. 6(a). Nickel and titanium, which were contained in the corrosion products of the Ni–Ti superelastic alloy, were in the mass ratio of 65 and 35 (atomic ratio of 60 and 40) from results of EDS analysis. For the corrosion products of pure nickel (Fig. 6(b)), all the major peaks were identified as those of Ni(OH)₂ (hexagonal; $a = 0.3114 \text{ nm}$, $c = 0.4617 \text{ nm}$).

Fig. 7 shows the changes in the corrosion potentials of the Ni–Ti superelastic alloy in the NaOCl solutions under open-air conditions. The corrosion potential shifted in the noble direction up to +0.5 V during the early stage of immersion and rapidly dropped to $\pm 0 \text{ V}$ approximately 10 min

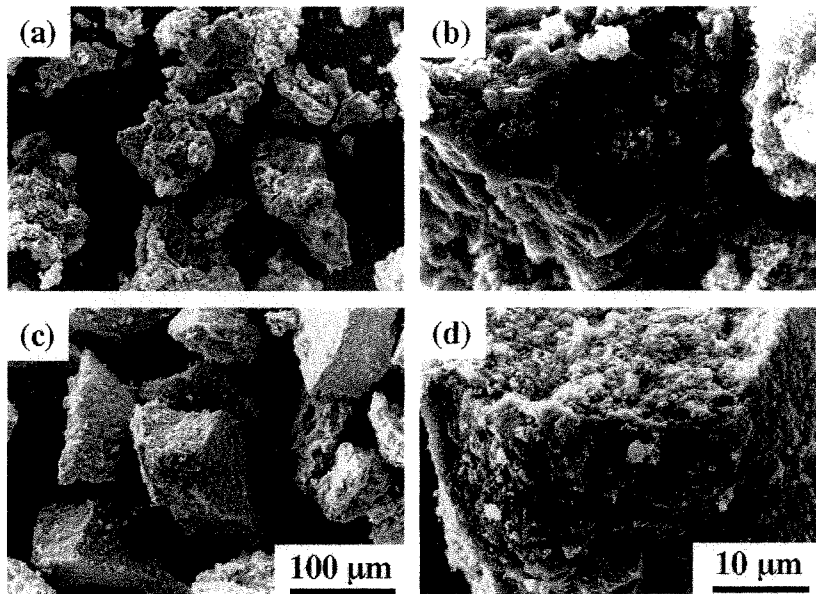


Fig. 5. SEM micrographs of corrosion products which precipitated in 5.0% NaOCl solution of: (a) Ni-Ti superelastic alloy; (b) magnified view of (a); (c) pure nickel; (d) magnified view of (c).

after immersion. The time to the potential drop reduced with increasing concentration of NaOCl solution. The fluctuation behavior of the potential was observed after the potential drop. In 5.0% NaOCl solution, the potential again increased up to +0.5 V and dropped to ±0 V.

4. Discussion

One important finding in the present study is that the fracture of the Ni-Ti superelastic alloy occurs in a very short time under an applied stress in NaOCl solution. Titanium

surface is covered with a thin passive film such as TiO₂ of uniform thickness. This oxide film is chemically stable in alkaline solutions such as NaOCl solution. On the other hand, nickel forms nickel hydroxide including Ni(OH)₂ in alkaline solutions [16,17]. In the present case of pure nickel, Ni(OH)₂ precipitated in NaOCl solution, as shown in Fig. 6. The reaction is presumably:

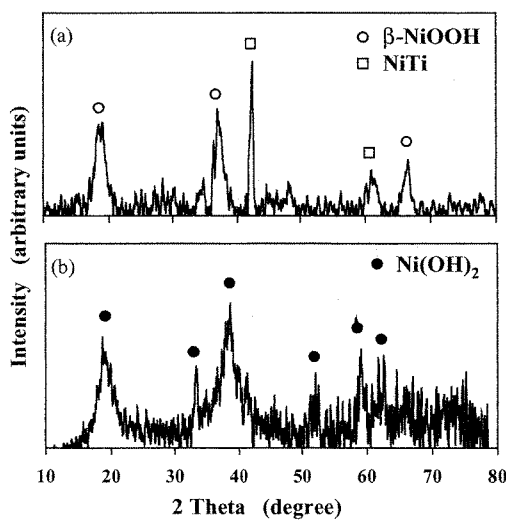


Fig. 6. XRD patterns of corrosion products which precipitated in 5.0% NaOCl solution of: (a) Ni-Ti superelastic alloy; (b) pure nickel.

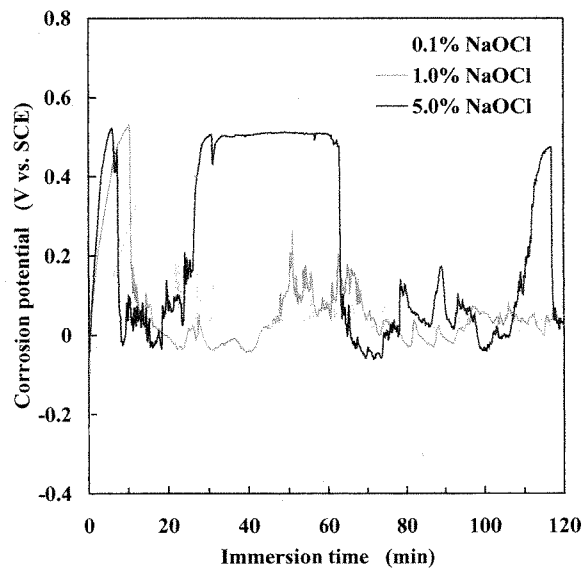


Fig. 7. Changes in the corrosion potential of Ni-Ti superelastic alloy in 0.1, 1.0 and 5.0% NaOCl solutions.

Cl^- ion in solution accelerates the breakdown of nickel hydroxide. Chan et al. [18] proved by means of XPS, SEM and Auger electron spectroscopy that the surface film of the Ni–Ti alloy is composed of TiO_2 , TiO_x , NiO and nickel which remained metallic. In the present study, corrosion products of the Ni–Ti superelastic alloy were identified as those of β -NiOOH and NiTi, making it clearer that nickel preferentially dissolves in NaOCl solution based on results of EDS analysis. For the Ni–Ti superelastic alloy in the NaOCl solutions, therefore, the breakdown of the surface film seems to result in selective dissolution of nickel.

The time to fracture of the Ni–Ti superelastic alloy and the time to breakdown of the surface film decreased with increasing concentration of NaOCl solution, as shown in Figs. 1 and 7. This result suggests that the local breakdown of the surface film decreases the time to fracture. The time to breakdown of the film was only 10 min in 5.0% NaOCl solution even in the case of without the applied stress. The applied stress generally accelerates the breakdown of the surface film in various solutions. The corrosion behavior of the Ni–Ti superelastic alloy is not known for a large strain such as in the present experiment, although Rondelli and Vicentini [10] reported that the presence of stress-induced martensite does not appreciably modify the localized corrosion resistance of the Ni–Ti alloy under 4% strain. The effects of the applied stress on the corrosion potential in NaOCl solution will be revealed in future research.

In the present study, the fracture of the Ni–Ti superelastic alloy was caused by a decrease in the cross-sectional area due to corrosion under an applied stress in NaOCl solution, as shown in Fig. 2. The corrosion area in the fracture surface, as shown in Figs. 2(c) and (d), is probably due to the above-mentioned selective dissolution of nickel. Under the same corrosion conditions, the fracture of 0.3 mm diameter specimen seems to be more affected by the decrease of the cross-sectional area than that of 0.5 mm diameter specimen. Hence, it follows that the time to fracture decreases with decreasing diameter of specimen.

Formerly, the service life of Ni–Ti superelastic files was expected from the results of immersion tests without an applied stress. Busslinger et al. [12] reported that no significant corrosion was found even after an immersion time of 60 min in 1% NaOCl solution. Certainly, when the applied stress was lower than the critical stress for martensite transformation, it took a fairly long time before the Ni–Ti superelastic alloy fractured in the present experiment. However, for higher applied stress, the fracture of the alloy occurred in a shorter time than expected. Our recent finding [15] that Ni–Ti superelastic alloy was more affected by corrosive environments, when the applied stress exceeded the critical stress for martensite transformation. This tendency of the alloy was clearly exhibited in 0.1% NaOCl solution in the present study, as shown in Fig. 1. Therefore, taking into consideration the effect of the applied stress, the service life of Ni–Ti superelastic files should be evaluated under corrosive environments, particularly under mildly corrosive

environments. For higher concentrations of NaOCl solution in the applied stress range lower than the critical stress, the main cause of early fracture is presumed to be that the alloy is greatly influenced by corrosion.

Furthermore, one should note that in the present study, the time to fracture of the Ni–Ti superelastic alloy was evaluated by a sustained tensile-loading test in NaOCl solutions. Ni–Ti endodontic instruments are subjected to load fluctuation and concentration change of solutions during clinical use. The load and potential fluctuations accelerate the fracture in the case of high-strength steel [19–22]. Therefore, the service life of Ni–Ti endodontic instruments in practice probably becomes shorter than that in this experiment.

5. Conclusions

The fracture of Ni–Ti superelastic alloy in 0.1, 1.0 and 5.0% NaOCl solutions has been examined by a sustained tensile-loading test. The time to fracture was reduced when the applied stress exceeded the critical stress for martensite transformation. The fracture of the alloy occurred in a short time even when the concentration of the solution was low. It was revealed that the fracture was mainly caused by the preferential dissolution of nickel in the solution. One of the reasons for the fracture of Ni–Ti instruments during clinical use is corrosion under the applied stress above the critical stress for martensite transformation in NaOCl solutions.

References

- [1] H. Walia, W.A. Brantley, H. Gerstein, *J. Endod.* 14 (1988) 346.
- [2] J.J. Camps, W.J. Pertot, *Int. Endod. J.* 28 (1995) 239.
- [3] M.B. Rowan, J.I. Nicholls, J. Steiner, *J. Endod.* 22 (1996) 341.
- [4] E.S. Marsicovetere, J.O. Burgess, D.J. Clement, C.E. del Rio, *J. Endod.* 22 (1996) 681.
- [5] J. Wolcott, T. Himel, *J. Endod.* 23 (1997) 217.
- [6] J.P. Pruett, D.J. Clement, D.L. Carnes Jr., *J. Endod.* 23 (1997) 77.
- [7] G. Rondelli, B. Vicentini, A. Cigada, *Corros. Sci.* 30 (1990) 805.
- [8] Y. Oshida, S. Miyazaki, *Zairyo-to-Kankyo* 40 (1991) 834.
- [9] G. Rondelli, *Biomaterials* 17 (1996) 2003.
- [10] G. Rondelli, B. Vicentini, *J. Biomed. Mater. Res.* 51 (2000) 47.
- [11] Y. Haïkel, R. Serfaty, P. Wilson, J.M. Speisser, C. Allemann, *J. Endod.* 24 (1998) 731.
- [12] A. Busslinger, B. Sener, F. Barbakow, *Int. Endod. J.* 31 (1998) 290.
- [13] I. Bonetti Filho, R. Miranda Esberard, R. de Toledo Leonardo, C.E. del Rio, *J. Endod.* 24 (1998) 461.
- [14] G. Kuhn, B. Tavernier, L. Jordan, *J. Endod.* 27 (2000) 516.
- [15] K. Yokoyama, S. Watabe, K. Hamada, J. Sakai, K. Asaoka, M. Nagumo, *Mater. Sci. Eng. A* 341 (2003) 91.
- [16] W. Visscher, E. Barendrecht, *Surf. Sci.* 135 (1983) 436.
- [17] R.E. Hummel, R.J. Smith, E.D. Verink Jr., *Corros. Sci.* 27 (1987) 803.
- [18] C.M. Chan, S. Trigwell, T. Duerig, *Surf. Interface Anal.* 15 (1990) 349.
- [19] K. Izutsu, K. Takai, M. Nagumo, *Tetsu-to-Hagané* 83 (1997) 371.
- [20] K. Nakasa, M. Kato, *Tetsu-to-Hagané* 85 (1999) 479.
- [21] M. Nagumo, H. Uyama, M. Yoshizawa, *Scripta Mater.* 44 (2001) 947.
- [22] M. Nagumo, *ISIJ Int.* 41 (2001) 590.

Fracture associated with hydrogen absorption of sustained tensile-loaded titanium in acid and neutral fluoride solutions

Ken'ichi Yokoyama,¹ Kazuyuki Kaneko,² Youji Miyamoto,³ Kenzo Asaoka,¹ Jun'ichi Sakai,⁴ Michihiko Nagumo⁴

¹Department of Dental Engineering, School of Dentistry, The University of Tokushima, 3-18-15 Kuramoto-cho, Tokushima, 770-8504, Japan

²Department of Orthodontics, School of Dentistry, The University of Tokushima, 3-18-15 Kuramoto-cho, Tokushima, 770-8504, Japan

³First Department of Oral and Maxillofacial Surgery, School of Dentistry, The University of Tokushima, 3-18-15 Kuramoto-cho, Tokushima, 770-8504, Japan

⁴Department of Materials Science and Engineering, Waseda University, 3-4-1 Okubo Shinjuku-ku, Tokyo, 169-8555, Japan

Received 31 January 2003; revised 26 June 2003; accepted 22 August 2003

Abstract: The fracture of commercial pure titanium in acid and neutral fluoride solutions has been examined by a sustained tensile-loading test and hydrogen thermal desorption analysis. It was found that the fracture of titanium occurred in neutral 2.0% NaF solution as well as in 2.0% acidulated phosphate fluoride (APF) solution. The time to fracture decreased with increasing applied stress in both 2.0% APF and 2.0% NaF solutions. In the case of the same applied stress, the time to fracture in the 2.0% APF solution was shorter than that in the 2.0% NaF solution. General corrosion was exhibited on the side surface of the tested specimens. The formation of sodium titanium fluoride was observed on the

surface of the immersed specimens in the 2.0% APF solution. Hydrogen desorption of the tested specimen in the 2.0% APF solution was observed with a peak at approximately 600°C. The amount of absorbed hydrogen was >300 mass ppm in the 2.0% APF solution under an applied stress for 24 h. The results of the present study imply that applying stress to titanium by immersing in fluoride solutions leads to the degradation of its mechanical properties. © 2003 Wiley Periodicals, Inc. *J Biomed Mater Res* 68A: 150–158, 2004

Key words: titanium; fracture; hydrogen embrittlement; corrosion; fluoride

INTRODUCTION

Titanium has been widely used as a material in dental devices including dental implants because of its high biocompatibility and corrosion resistance. The high corrosion resistance is attributed to a thin oxide film, mainly TiO₂, on the surface. In fluoride solutions, however, the breakdown of the oxide film has been reported in several articles.^{1–13} According to these results, the corrosion resistance of titanium is reduced markedly in acid fluoride solutions, whereas it re-

mains unchanged in neutral fluoride solutions. Fluorides such as NaF, Na₂PO₃F, and SnF₂ are added in toothpaste, prophylactic agents, and dental rinse, and exert a cariostatic effect. Caries-preventing prophylactics generally contain 100–10,000 ppm F and have pHs between about 3.5 and neutral.

Moreover, titanium implants sometimes fracture in the oral cavity after a long period of use.^{14–20} The mechanism of such fracture can hardly be identified because it involves several factors such as fatigue, fretting corrosion, biomechanical overload, and defects in implant design in a complicated way. Könönen et al.²¹ have suggested that the stress corrosion cracking of titanium in fluoride solution with a pH of 5.5 is one cause of implant failure. However, we have insisted that one reason for the degradation of the mechanical properties and fracture of titanium and its alloys is hydrogen absorption in a biological environment.^{22–26} For example, a Ni-Ti superelastic alloy

Correspondence to: K. Yokoyama; e-mail: yokken@dent.tokushima-u.ac.jp

Contract grant sponsor: Ministry of Education, Culture, Sports, Science, and Technology of Japan; contract grant number: 14771090

© 2003 Wiley Periodicals, Inc.

absorbs substantial amounts of hydrogen in 0.2% acidulated phosphate fluoride (APF) solution.²⁶ Hydrogen embrittlement of pure titanium, an important matter from the industrial point of view, has been investigated with cathodically hydrogen charging,^{27,28} exposure to gaseous hydrogen,²⁹ and immersion in methanol solution containing HCl.³⁰⁻³² However, it has not yet been confirmed whether or not hydrogen absorption of titanium occurs in fluoride solutions. If the hydrogen absorption takes place in fluoride solutions, hydrogen embrittlement of titanium will be a serious problem for its use in the dental field. Furthermore, the effect of applied stress on the fracture of titanium in fluoride solutions should be examined.

The purpose of the present study was to examine the fracture of sustained tensile-loaded titanium in acid and neutral fluoride solutions and the associated behavior of hydrogen absorption by means of hydrogen thermal desorption analysis (TDA).

EXPERIMENTAL PROCEDURES

Materials

Work-hardened commercial pure titanium wire with a diameter of 0.50 mm was cut into specimens of 150-mm length. The chemical composition is given in Table 1. Percent in this article means mass percent, unless otherwise stated. The specimens were polished with 600-grit SiC paper and ultrasonically washed in acetone for 5 min. Tensile tests were performed at room temperature on an Instron-type machine (Autograph AG-100A; Shimadzu) at a strain rate of 8.33×10^{-4} /s. The microstructure of the specimens in a cross-sectional area was examined by optical microscopy, after etching using a solution of hydrofluoric, nitric, and acetic acids. To clarify grain boundaries, the hard etching was performed.

Sustained tensile-loading test

A sustained tensile-loading test in fluoride solutions was performed at room temperature. Figure 1 shows the scheme of the apparatus. The applied stress was calculated as the ratio of the applied load to the initial cross-sectional area and was varied to determine the

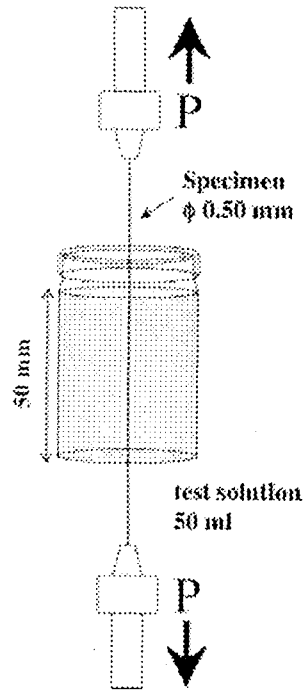


Figure 1. Schematic of sustained tensile-loading test apparatus.

fracture life characteristics. The immersed length of the specimens in the solution was 50 mm. The time to fracture of the specimens was measured, and the test was terminated when no fracture occurred after >1000 h of immersion. The test solutions used were 50 mL of 2.0% aqueous APF (2.0% NaF + 1.7% H₃PO₄) solution with pH 5.0 or 2.0% aqueous NaF solution with pH 6.5. The fluoride concentration in the solutions was 9000 ppm. The fracture surface and the side surface were examined with a scanning electron microscope (SEM). The corrosion products on the surface were examined using an X-ray diffractometer (XRD) operated at 30 kV and 15 mA with Cu K_α radiation of wavelength $\lambda = 1.54056 \text{ \AA}$ for 2θ angles ranging from 10 to 80°.

Corrosion test

The corrosion potentials of the specimens without the applied stress were measured at room temperature in 2.0% APF and 2.0% NaF solutions under open-air conditions. The counter and reference electrodes used were a platinum electrode and a saturated calomel electrode (SCE), respectively. The measurements were started 10 s after immersion in the test solutions.

TABLE I
Chemical Composition of the Tested Commercial Pure Titanium (Mass %)

C	H	O	N	Fe	Ti
0.01	0.001	0.06	0.004	0.03	Balance

TABLE II
Mechanical Properties of Tested Titanium

Yield Stress (MPa)	Tensile Strength (MPa)	Reduction in Area (%)
702 ± 22.3	777 ± 10.5	69.2 ± 1.7

TDA

The amount of desorbed hydrogen was measured using TDA by subjecting the specimens to the sustained tensile-loading test for 24 h. Both ends of a specimen (50 mm in length) immersed in the solution were cut into 20-mm-long segments and subjected to ultrasonic cleaning with acetone for 2 min. The segments were dried in ambient and subjected to TDA. The starting time of TDA after the removal of a specimen from the solution was 30 min. A quadrupole mass spectrometer (ULVAC, Kanagawa, Japan) was used for hydrogen detection. Data sampling was conducted at 30-s intervals at a heating rate of 100°C/h.

EXPERIMENTAL RESULTS

The mechanical properties of the specimen are given in Table II. The standard deviation was calculated from the results obtained from more than five specimens. Yield stress, tensile strength, and reduction in area of the specimen were 702 MPa, 777 MPa, and 69%, respectively. The microstructure of a representative specimen is shown in Figure 2. The grains were approximately 20 μm in size. These grains were equiaxial in shape. The sustained tensile-loading test result is plotted in Figure 3 in terms of the time to fracture as

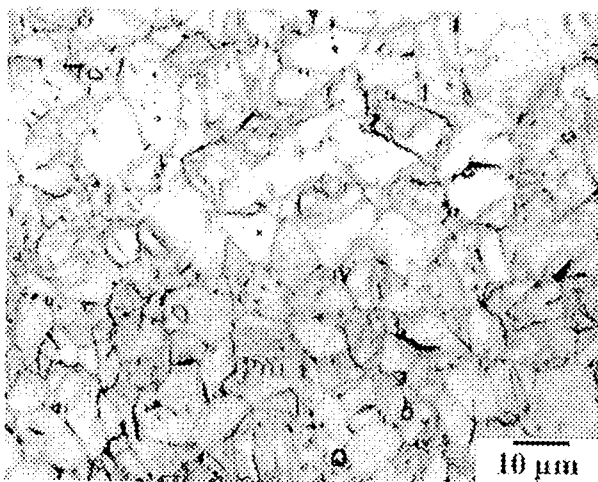


Figure 2. Light optical metallography of titanium showing general microstructure.

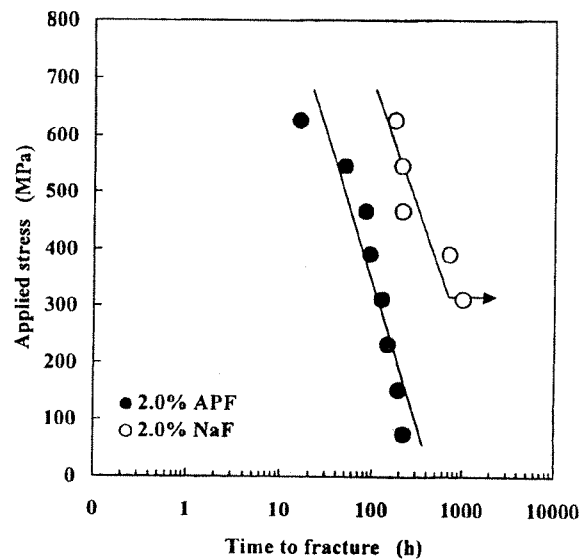


Figure 3. Plot of time to fracture versus initial applied stress for titanium immersed in 2.0% APF and 2.0% NaF solutions.

a function of the initial applied stress. Note that fracture occurred in both the neutral 2.0% NaF and 2.0% APF solutions. The time to fracture decreased with increasing applied stress in both solutions. For the same applied stress, the time to fracture in the 2.0% APF solution was shorter than that in the 2.0% NaF solution, in which fracture did not occur within 1000 h when the applied stress was lower than 320 MPa. The arrow in the figure denotes the nonfractured specimen at the indicated elapsed time. In this experiment, crevice corrosion appeared neither at the contact point of the specimen with the vessel nor in the vicinity of the water plane in both solutions.

The fractographs of the specimen fractured by a tensile test in air are shown in Figure 4(a,b). The fracture surface was ductile and was characterized macroscopically with a double cup morphology and microscopically with small shallow dimples. The fracture surface in the 2.0% APF solution under the applied stress of 470 MPa for 82 h and 11 min is shown in Figure 4(c,d). The microscopic characteristic of the fracture surface consisted mainly of small shallow dimples similar to that in air. Nonmetallics or inclusions were not observed in the bottom of the dimples. In the 2.0% NaF solution under the applied stress of 470 MPa for 209 h and 19 min, the fracture surface was similar to that in 2.0% APF solution, as shown in Figure 4(e,f). However, the macroscopic characteristics of the fracture surface in both solutions were different from that in air. In particular, the decrease in the extent of plastic deformation was observed at the periphery of the fracture surface in both solutions.

On the side surface of the specimen tensile-frac-

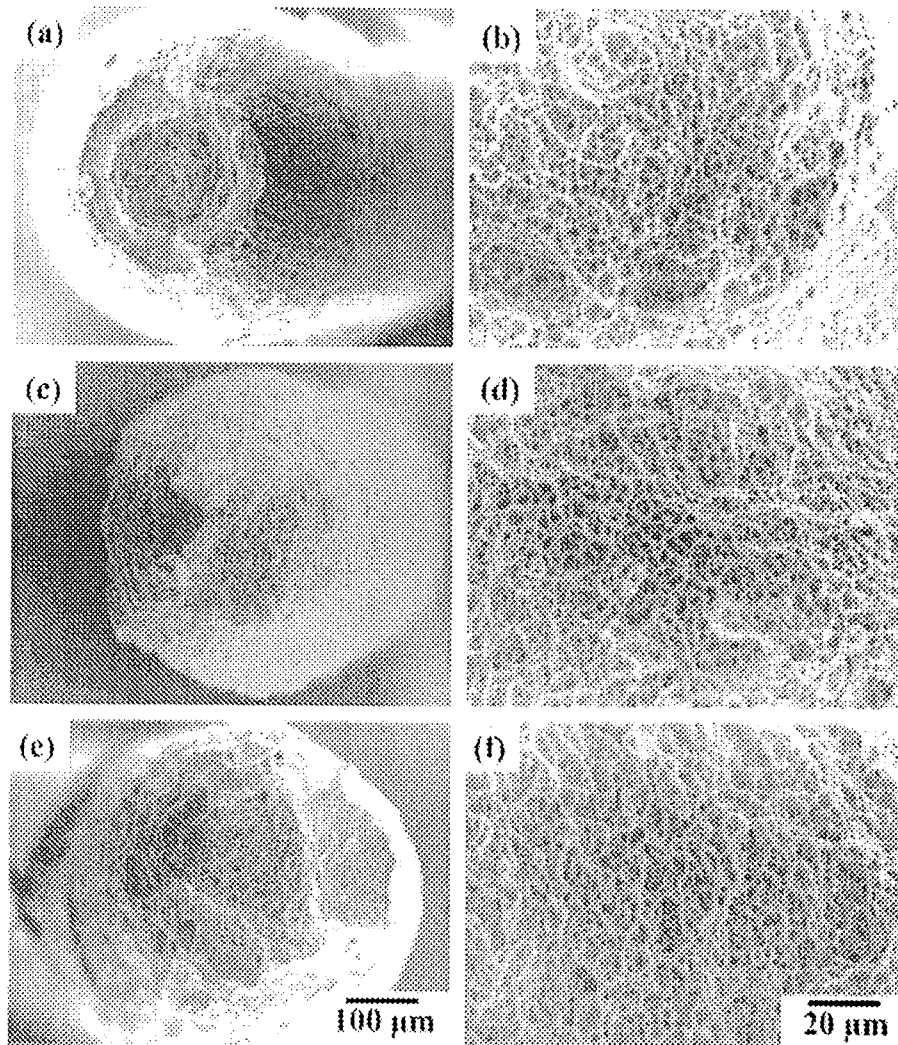


Figure 4. SEM micrographs of a typical fracture surface: after tensile test in air, (a) general and (b) magnified views; after sustained tensile-loading test under the applied stress of 470 MPa in 2.0% APF solution, (c) general and (d) magnified views; and under the applied stress of 470 MPa in 2.0% NaF solution, (e) general and (f) magnified views.

tured in air, scratches due to SiC paper polishing were observed, as shown in the SEM micrographs of Figure 5(a,b). The side surface after fracture in the 2.0% APF solution under the applied stress of 470 MPa is shown in Figure 5(c,d). In the 2.0% APF solution, the scratches on the surface disappeared due to general corrosion and the peeling off of surface layers such as corrosion products, regardless of the applied stress. The side surface after fracture in the 2.0% NaF solution under the applied stress of 470 MPa is shown in Figure 5(e,f), where the fractured specimens exhibited a microscopically smooth, but macroscopically significantly rough surface.

Figure 6(a) shows the reduction in area including peeled-off surface layers as a function of the applied stress in both solutions. The dashed line in the figure denotes the reduction in area for the tensile test in air.

The percentage reduction in area increased with decreasing applied stress. In the case of low applied stress, that is, in the case of long immersion time, the reduction in area mainly resulted from the peeling off of the surface layers as well as corrosion. Note that the percentage reduction in area at high applied stress became lower than that in the case of the tensile-fractured specimen in air. Figure 6(b) shows an example of the decrease in the percentage reduction in area in the fracture surface under the applied stress of 630 MPa in the 2.0% APF solution.

Figure 7 shows the XRD results for the side surfaces of the nonimmersed and 24-h-immersed specimens without loading. The formation of sodium titanium fluoride, Na_3TiF_6 (monoclinic; $a = 0.5543$ nm, $b = 0.5748$ nm, $c = 0.8002$ nm, and $\beta = 90.29^\circ$), was confirmed on the surface of the specimen immersed in the

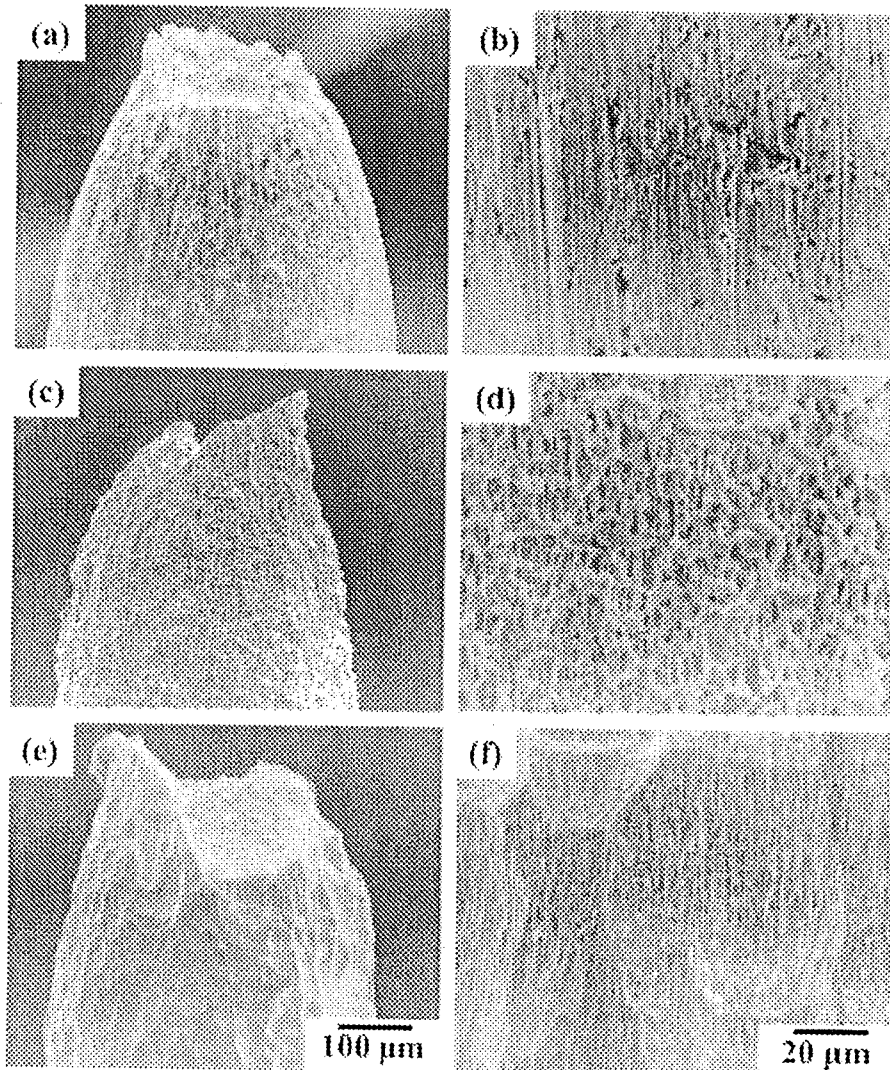


Figure 5. SEM micrographs of a typical side surface: after tensile test in air, (a) general and (b) magnified views; after sustained tensile-loading test under the applied stress of 470 MPa in 2.0% APF solution, (c) general and (d) magnified views; and under the applied stress of 470 MPa in 2.0% NaF solution, (e) general and (f) magnified views.

2.0% APF solution, whereas no formation of corrosion products was confirmed in the 2.0% NaF solution.

The changes in the corrosion potentials in the 2.0% APF and 2.0% NaF solutions under the open-air conditions without loading are shown in Figure 8. The corrosion potential decreased in the early stage of immersion in the 2.0% NaF solution and the final value was -0.6 V. However, in the 2.0% APF solution, the final value of corrosion potential was approximately -1.0 V.

Figure 9 shows the TDA curves for the specimens after the sustained tensile-loading test under the applied stress of 470 MPa in the 2.0% APF and 2.0% NaF solutions for 24 h. In the figure, the TDA curve of the original specimen is also included. In the original as-received specimen, the amount of desorbed hydrogen, that is, the concentration of predissolved hydrogen,

was 38 mass ppm. The desorption temperature ranged from 400 to 800°C. However, after the sustained tensile-loading test in the 2.0% APF solution for 24 h, the desorption curves exhibited a single desorption peak at approximately 600°C. The total amount of desorbed hydrogen up to 800°C was 360 mass ppm. Thus, the amount of absorbed hydrogen during the sustained tensile-loading test was 322 mass ppm. In immersion in the 2.0% NaF solution for 24 h, no increase in the hydrogen desorption was confirmed.

DISCUSSION

Important findings in the present study are that titanium fractures under a sustained tensile-loading

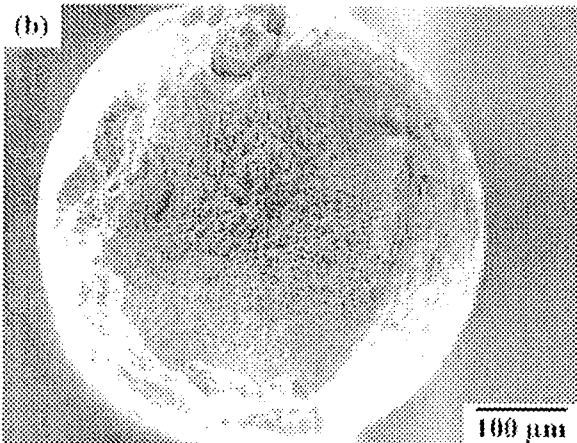
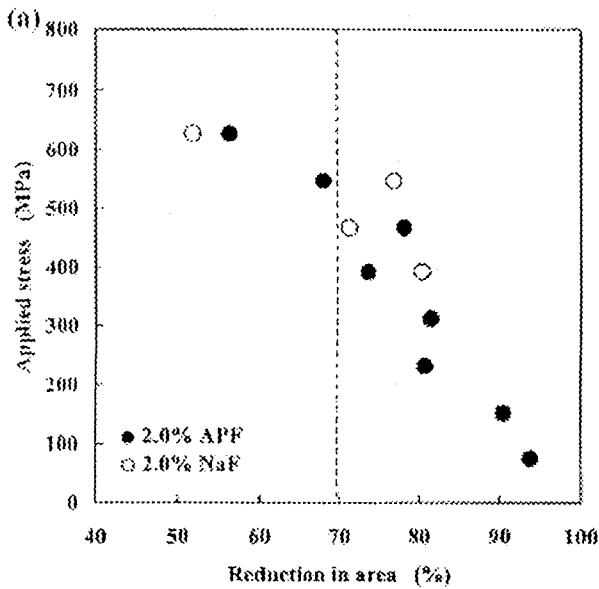


Figure 6. (a) Reduction in area of specimen as a function of applied stress for titanium immersed in 2.0% APF and 2.0% NaF solutions. (b) SEM micrographs of the fracture surface under the applied stress of 630 MPa in 2.0% APF solution.

test even in a neutral NaF solution and that the fracture is associated with hydrogen absorption in an APF solution. Previously, the effects of fluoride solutions on the fracture of titanium and its alloys have been investigated from the viewpoint of corrosion or discoloration.¹⁻¹³ The corrosion behavior of titanium depends on an oxide film on its surface composed of mainly TiO₂, which spontaneously covers the surface in the presence of oxygen. In acid fluoride solutions, the oxide film undergoes a reaction, forming titanium fluoride, titanium oxide fluoride, or sodium titanium fluoride,^{7,12} and the loss of the oxide film leads to the reduction of the corrosion resistance of titanium in fluoride solutions. In the present study, the formation of sodium titanium fluoride on the surface and the reduction in corrosion potential were confirmed in the

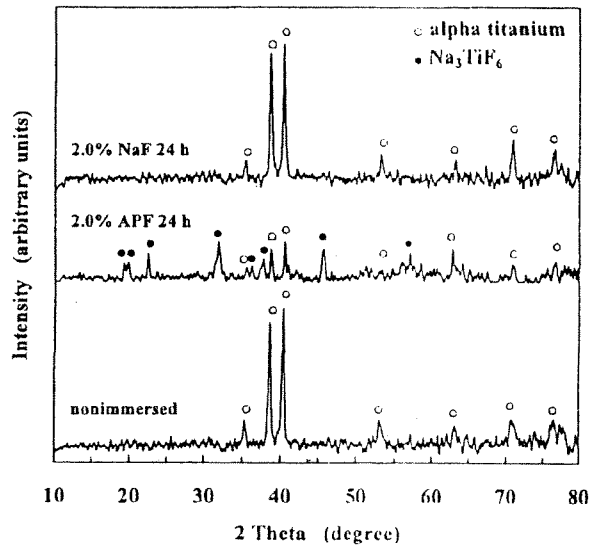


Figure 7. XRD patterns for the surface of nonimmersed and 24-h-immersed specimens in 2.0% APF and 2.0% NaF solutions.

2.0% APF solution, as shown in Figures 7 and 8. It has also been reported that the corrosion behavior of titanium is markedly affected by the pH and concentration of fluoride solutions,⁹⁻¹¹ and no titanium corrosion has been observed in neutral fluoride solution. In the present study, no corrosion was observed in the neutral 2.0% NaF solution without loading, as shown in Figures 7 and 8. However, when stress was applied, corrosion and fracture of titanium occurred readily in the 2.0% NaF solution, indicating a strong effect of the applied stress on corrosion. Therefore, taking into con-

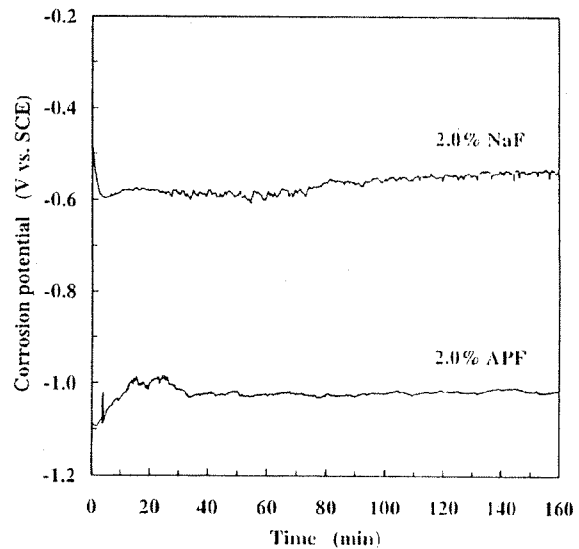


Figure 8. Changes in corrosion potential of titanium under open-air conditions without loading in 2.0% APF and 2.0% NaF solutions.

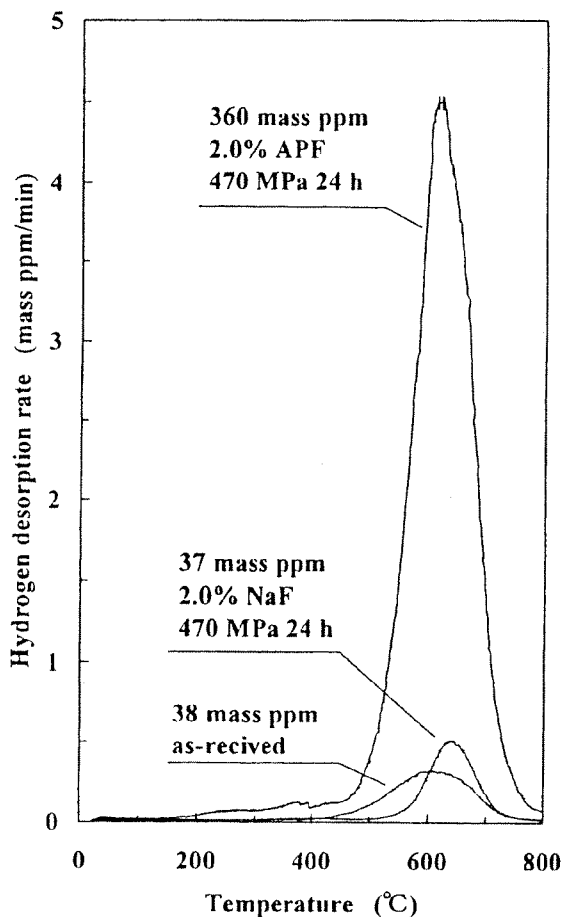


Figure 9. Hydrogen thermal desorption curves for as-received specimen and specimens subjected to sustained tensile-load test in 2.0% APF and 2.0% NaF solutions under the applied stress of 470 MPa for 24 h.

sideration the effect of the applied stress, the corrosion resistance and service life of titanium should be evaluated under mildly corrosive environments.

In the present study, the fracture of titanium might be attributed to the reduction of the cross-sectional area due to the peeling off of the surface layers and corrosion. However, closer analysis reveals that the effects of hydrogen absorption are another factor for the degradation of the mechanical properties of titanium. Titanium is a highly active metal with a high affinity for hydrogen. The breakdown of the oxide film on its surface may lead to hydrogen absorption in various solutions. For example, hydrogen absorption occurs readily in titanium in a methanol solution containing HCl.³⁰⁻³² The absorbed hydrogen diffuses from the surface inwards. Using the reported diffusion constant of hydrogen in titanium at room temperature,³³

$$D = 2 \times 10^{-11} \text{ m}^2/\text{s} \quad (1)$$

diffusion of hydrogen to the center of a specimen is approximately enough in 82 h, which is the time required for titanium to fracture under the applied stress of 470 MPa in the 2.0% APF solution. Because the amount of absorbed hydrogen in the 2.0% APF solution was >300 mass ppm under the applied stress of 470 MPa for 24 h, the amount of absorbed hydrogen may further increase until fracture. In general, when the amount of absorbed hydrogen exceeds 200 mass ppm, the ductility of titanium is markedly reduced.³⁴⁻³⁷ In the present study, the time to fracture was reduced in the 2.0% APF solution compared with that in the 2.0% NaF solution, as shown in Figure 3. The decrease in the percentage reduction in area associated with the increase in the applied stress, shown in Figure 6(a), is primarily due to the peeling off and corrosion of the surface layer, but the dependences were almost similar between the two solutions. However, the high hydrogen absorption in the 2.0% APF solution revealed in Figure 9 is in accordance with the effect of hydrogen absorption on the prominent reduction in the time to fracture. Although the effect of the peeling off and corrosion of the surface layer could not be ruled out, the fracture is likely to be associated with hydrogen absorption in the 2.0% APF solution.

As a mechanism of hydrogen embrittlement of titanium, hydride formation has been proposed.³⁴⁻³⁷ Three types of hydrides can form in titanium matrix: δ , ϵ , and γ hydrides.³⁸⁻⁴⁰ The δ hydride has an fcc unit cell of CaF_2 type with the hydrogen atoms occupying the tetrahedral sites randomly. At higher hydrogen concentrations, the δ hydride transforms into ϵ hydride which has an fct structure ($c/a < 1$) at low temperatures. However, at low hydrogen concentrations, the metastable γ hydride, which has an fct structure ($c/a > 1$) with an ordered arrangement of hydrogen, forms. Because these hydrides are brittle and have different elastic properties from titanium, cracking of hydrides provides sites of void nucleation even with a low density of hydrides. The thermal desorption behavior gives information about hydrogen trapping sites and hydride decomposition based on the temperature profile and the amount of desorption.⁴¹ The decomposition behavior of electrochemically formed titanium hydrides has been investigated using TDA, XRD, and differential thermal analysis.⁴² In the present study, the thermal desorption behavior agrees with that obtained by Takasaki et al.,⁴² suggesting the formation of hydrides in 2.0% APF solution, although hydride formation was not confirmed by XRD. The dimple morphology of the fractographic features shown in Figure 4 is rather contrary to the cracking of hydrides being the dominating mechanism of fracture. Details on the effect of hydrogen should be further studied.

Conversely, in immersion in the 2.0% NaF solution for 24 h, hydrogen absorption was hardly confirmed

under the applied stress of 470 MPa, despite the decrease in the percentage reduction in area similar to that observed in the 2.0% APF solution, as shown in Figure 6. This finding suggests that hydrogen is not related to the failure. However, it is noticed that an extremely small amount of hydrogen at the vicinity of a crack can sometimes have an important role in stress corrosion cracking.⁴⁵ In the present study, the local density of hydrogen could not be measured because the amount of absorbed hydrogen was taken as the mean value over the immersed area of a specimen. Details of the fracture morphologies as well as the examination of the local hydrogen concentration in the NaF solution should also be further studied.

CONCLUSIONS

Fracture of titanium in acid and neutral fluoride solutions has been examined by a sustained tensile-loading test from the viewpoint of hydrogen embrittlement. The time to fracture decreased with increasing applied stress in both 2.0% APF and 2.0% NaF solutions. In the case of the same applied stress, the time to fracture in the 2.0% APF solution was shorter than that in the 2.0% NaF solution associated with a similar decrease in the percentage reduction in area in both solutions. In the 2.0% APF solution, titanium absorbed a substantial amount of hydrogen. One of the causes of the fracture of titanium devices in the oral cavity is possibly hydrogen embrittlement in the presence of fluoride.

References

1. Lausmaa J, Kasemo B, Hansson S. Accelerated oxide grown on titanium implants during autoclaving caused by fluorine contamination. *Biomaterials* 1985;6:23-27.
2. Siirila HS, Könönen M. The effect of oral topical fluorides on the surface of commercially pure titanium. *Int J Oral Maxillofac Implants* 1991;6:50-54.
3. Prebster L, Lin W, Hüttermann H. Effect of fluoride prophylactic agents on titanium surfaces. *Int J Oral Maxillofac Implants* 1992;7:390-394.
4. Boere G. Influence of fluoride on titanium in an acidic environment measured by polarization resistance technique. *J Appl Biomater* 1995;6:283-288.
5. Toumelin-Chemla F, Rouelle F, Burdairon G. Corrosive properties of fluoride-containing odontologic gels against titanium. *J Dent* 1996;24:109-115.
6. Mimura H, Miyagawa Y. Electrochemical corrosion behavior of titanium castings. Part I. Effects of degree of surface polishing and kind of solution. *Jpn J Dent Mater Dev* 1996;15:283-295.
7. Oda Y, Kawada E, Yoshinari M, Hasegawa K, Okabe T. The influence of fluoride concentration on the corrosion of titanium and titanium alloys. *Jpn J Dent Mater Dev* 1996;15:317-322.
8. Reclaru L, Meyer J-M. Effects of fluorides on titanium and other dental alloys in dentistry. *Biomaterials* 1998;19:85-92.

9. Nakagawa M, Matsuya S, Shiraisli T, Ohta M. Effect of fluoride concentration and pH on corrosion behavior of titanium for dental use. *J Dent Res* 1999;78:1566-1572.
10. Nakagawa M, Matsuya S, Udoh K. Corrosion behavior of pure titanium and titanium alloys in fluoride-containing solutions. *Dent Mater J* 2001;20:305-314.
11. Nakagawa M, Matsuya S, Udoh K. Effects of fluoride and dissolved oxygen concentrations on the corrosion behavior of pure titanium and titanium alloys. *Dent Mater J* 2002;21:83-92.
12. Huang H-H. Effects of fluoride concentration and elastic tensile strain on the corrosion resistance of commercially pure titanium. *Biomaterials* 2002;23:59-63.
13. Schiff N, Grosogeat B, Lissac M, Dalard F. Influence of fluoride content and pH on the corrosion resistance of titanium and its alloys. *Biomaterials* 2002;23:1995-2002.
14. Morgan MJ, James DF, Pilliar RM. Fractures of the fixture component of an osseointegrated implant. *Int J Oral Maxillofac Implants* 1993;8:409-414.
15. Rangert B, Krogh PHJ, Langer B, Roedel NV. Bending overload and implant fracture: a retrospective clinical analysis. *Int J Oral Maxillofac Implants* 1995;10:326-334.
16. Balshi TJ. An analysis and management of fractured implant: a clinical report. *Int J Oral Maxillofac Implants* 1996;11:660-666.
17. Piattelli A, Scarano A, Piattelli M, Vaia E, Matarasso S. Hollow implants retrieved for fracture: a light and scanning electron microscope analysis of 4 cases. *J Periodontol* 1998;69:185-189.
18. Piattelli A, Piattelli M, Scarano A, Montesani L. Light and scanning electron microscopic report of four fractured implants. *Int J Oral Maxillofac Implants* 1998;13:561-564.
19. Piattelli A, Scarano A, Piattelli M, Vaia E, Matarasso S. A microscopical evaluation of 24 retrieved failed hollow implants. *Biomaterials* 1999;20:485-489.
20. Yokoyama K, Ichikawa T, Murakami H, Miyamoto Y, Asaoka K. Fracture mechanisms of retrieved titanium screw thread in dental implant. *Biomaterials* 2002;23:2459-2465.
21. Könönen MHO, Lavonius ET, Kivilahti JK. SEM observations on stress corrosion cracking of commercially pure titanium in a topical fluoride solution. *Dent Mater* 1995;11:269-272.
22. Yokoyama K, Hamada K, Asaoka K. Fracture analysis of hydrogen-charged nickel-titanium superelastic alloy. *Mater Trans* 2001;42:141-144.
23. Yokoyama K, Hamada K, Moriyama K, Asaoka K. Degradation and fracture of Ni-Ti superelastic wire in an oral cavity. *Biomaterials* 2001;22:2257-2262.
24. Asaoka K, Yokoyama K, Nagumo M. Hydrogen embrittlement of nickel-titanium alloy in biological environment. *Metall Mater Trans A* 2002;33A:495-501.
25. Yokoyama K, Watabe S, Hamada K, Sakai J, Asaoka K, Nagumo M. Susceptibility to delayed fracture of Ni-Ti superelastic alloy. *Mater Sci Eng A* 2003;341:91-97.
26. Yokoyama K, Kaneko K, Moriyama K, Asaoka K, Sakai J, Nagumo M. Hydrogen embrittlement of Ni-Ti superelastic alloy in fluoride solution. *J Biomed Mater Res* 2003;65A:182-187.
27. Phillips II, Poole P, Shreir LL. Hydride formation during cathodic polarization of Ti. I. Effect of current density on kinetics of growth and composition of hydride. *Corros Sci* 1972;12:855-866.
28. Phillips II, Poole P, Shreir LL. Hydride formation during cathodic polarization of Ti. II. Effect of temperature and pH of solution on hydride growth. *Corros Sci* 1974;14:533-542.
29. Briant CL, Wang ZF, Chollacoop N. Hydrogen embrittlement of commercial purity titanium. *Corros Sci* 2002;44:1875-1888.
30. Mori K, Takamura A, Shimose T. Stress corrosion cracking of Ti and Zr in HCl-methanol solutions. *Corrosion* 1966;22:29-31.
31. Ebtehaj K, Hardie D, Parkins RN. The stress corrosion and pre-exposure embrittlement of titanium in methanolic solutions of hydrochloric acid. *Corros Sci* 1985;25:415-429.

32. Hollis AC, Scully JC. The stress corrosion cracking and hydrogen embrittlement of titanium in methanol-hydrochloric acid solutions. *Corros Sci* 1993;34:821-835.
33. Brauer E, Dörr R, Züchner H. Hydrogen diffusion in titanium. *Z Physik Chem NF* 1976;100:109-112.
34. Lenning GA, Craighead CM, Jaffee RI. Constitution and mechanical properties of titanium-hydrogen alloys. *Trans AIME* 1954;200:367-376.
35. Williams DN. The hydrogen embrittlement of titanium alloys. *J Inst Metals* 1962;91:147-152.
36. Shih DS, Robertson IM, Birnbaum HK. Hydrogen embrittlement of α titanium: *in situ* TEM studies. *Acta Metall* 1988;36:111-124.
37. Wang ZF, Briant CL, Kumar KS. Hydrogen embrittlement of grade 2 and grade 3 titanium in 6% sodium chloride solution. *Corrosion* 1998;54:553-560.
38. Numakura H, Koiwa M. Hydride precipitation in titanium. *Acta Metall* 1984;32:1799-1807.
39. Woo OT, Weatherly GC, Coleman CE, Gilbert RW. The precipitation of γ -deuterides (hydrides) in titanium. *Acta Metall* 1985;33:1897-1906.
40. Numakura H, Koiwa M, Asano H, Murata H, Izumi F. X-ray diffraction study on the formation of γ titanium hydride. *Scripta Metall* 1986;20:213-216.
41. Choo WY, Lee JY. Thermal analysis of trapped hydrogen in pure iron. *Metall Trans A* 1982;13A:135-182.
42. Takasaki A, Furuya Y, Ojima K, Taneda Y. Hydrogen dissociation and hydrogen evolution behavior of electrochemically charged pure titanium. *J Alloy Comp* 1995;224:269-273.
43. Tanguy D, Bayle B, Dif R, Magnin Th. Hydrogen effects during IGSCC of pure Al-5Mg alloy in NaCl media. *Corros Sci* 2002; 44:1163-1175.

Degradation of tensile strength of Ni–Ti superelastic alloy due to hydrogen absorption in methanol solution containing hydrochloric acid

Ken'ichi Yokoyama^{a,*}, Toshio Ogawa^b, Kenzo Asaoka^a, Jun'ichi Sakai^b,
Michihiko Nagumo^b

^a Department of Dental Engineering, School of Dentistry, The University of Tokushima, 3-18-15 Kuramoto-cho, Tokushima 770-8504, Japan

^b Department of Materials Science and Engineering, Waseda University, 3-4-1 Okubo Shinjuku-ku, Tokyo 169-8555, Japan

Received 19 December 2002; received in revised form 8 May 2003

Abstract

Degradation of tensile strength of a Ni–Ti superelastic alloy due to hydrogen absorption has been studied in methanol solution containing 0.1 mass % hydrochloric acid (HCl). The amount of absorbed hydrogen from the solution was measured by thermal desorption analysis (TDA). Hydrogen desorption of immersed specimens appeared in the temperature range from 100 to 600 °C. The amounts of absorbed hydrogen of immersed specimens were in the range of 50–500 mass ppm when immersed in the solution for 8–120 h. Tensile strength of immersed specimens decreased abruptly up to immersion time of 24 h. In the immersion time range from 24 to 120 h, the tensile strength was coincident with the critical stress for martensite transformation. It was concluded that the degradation of tensile strength of a Ni–Ti superelastic alloy is caused by hydrogen absorption in methanol solution containing HCl. © 2003 Elsevier B.V. All rights reserved.

Keywords: Ni–Ti; Hydrogen embrittlement; Thermal desorption analysis; Corrosion; Methanol solution

1. Introduction

There have been increasing numbers of industrial and medical applications of Ni–Ti alloys due to their unique shape memory as well as their superelastic effect, excellent ductility and good fatigue life. Moreover, the alloys exhibit good corrosion resistance and biocompatibility [1–5]. However, it has been reported that Ni–Ti superelastic alloys deteriorate in corrosive environments, such as the oral cavity [6–8]. Ni–Ti orthodontic arch wires often fracture in the oral cavity after a few months from setting [9–11]. Recently, we have proved that the primary cause of the fracture is hydrogen embrittlement in the oral cavity [11–14]. These are good examples of the immersed Ni–Ti superelastic alloy in fluoride solution resulting in the degradation of its mechanical properties due to hydrogen embrittlement

[15]. Fluoride is contained in toothpaste, prophylactic agents and dental rinse, since fluoride exhibits a cariostatic effect.

The degradation of the mechanical properties of Ni–Ti alloys due to hydrogen absorption is an important problem when these alloys are used under corrosive environmental conditions. The effects of hydrogen on the mechanical properties of Ni–Ti alloys have been evaluated with cathodically charged [16–18] or gaseous hydrogen [19]. However, little is known about the degradation of Ni–Ti superelastic alloys due to hydrogen absorption by immersion in various solutions. Ni–Ti alloys possibly absorb hydrogen in other solutions. Titanium and its alloys absorb considerable amounts of hydrogen under corrosive environments. It is known that stress-corrosion cracking of titanium and its alloys occurs by hydrogen absorption in methanol solutions containing hydrochloric acid (HCl) [20–23]. It is necessary to investigate hydrogen absorption of Ni–Ti alloys under various environmental conditions because these alloys may become widely used in the future.

* Corresponding author. Tel.: +81-88-633-7334; fax: +81-88-633-9125.

E-mail address: yokken@dent.tokushima-u.ac.jp (K. Yokoyama).

The purpose of the present study is to examine the effect of hydrogen absorption in methanol solutions containing HCl on the degradation of the tensile strength of Ni–Ti superelastic alloys by thermal desorption analysis (TDA).

2. Experimental procedures

A commercial Ni–Ti (Ni: 55 mass %, Ti: balance) superelastic alloy wire with a diameter of 0.50 mm was cut into specimens of 50 mm length, which were polished with No. 600-grit SiC papers and ultrasonically washed in acetone for 5 min. Percent in this paper means mass percent, unless otherwise stated. The specimens were immersed separately in 10 ml of methanol solution with 0.1% HCl at 37 °C.

The amount of desorbed hydrogen was measured by TDA with the specimens immersed in methanol solutions for various periods. Both ends of each specimen (50 mm in length) immersed in the solution, were cut into 20-mm long pieces and subjected to ultrasonic cleaning with acetone for 2 min. The specimen was dried in ambient and used for measurement. TDA was carried out 30 min after removal of the specimen from the solution. A quadrupole mass spectrometer (ULVAC, Kanagawa, Japan) was used for the detection of hydrogen. Data sampling was conducted at 30-s intervals at a heating rate of 100 °C h⁻¹.

The side surface of the immersed specimens was observed using a scanning electron microscope (SEM). Weight loss of the immersed specimens with time was measured and S.D. was calculated from the results obtained for five specimens.

Hardness tests were carried out at room temperature (25 ± 2 °C) for the immersed specimens from the surface to the center of the wire at intervals of 0.05 mm. The specimens were embedded in epoxy resin and polished, followed by testing 24 h after removal from the solution. Measurements were performed under an applied load of 0.98 N and an applied time of 15 s. Tensile tests of the immersed specimens were carried out at room temperature using a Shimadzu Autograph AG-100A machine at a strain rate of 8.33 × 10⁻⁴ s⁻¹ within a few minutes after removal of the specimens from the solution. The gauge length of each specimen was 10 mm. The fracture surface of the tensile-tested specimens was observed with SEM.

3. Results and discussion

3.1. Hydrogen thermal desorption analysis

Fig. 1 shows TDA curves for the specimens immersed for up to 120 h. The results reveal that the Ni–Ti

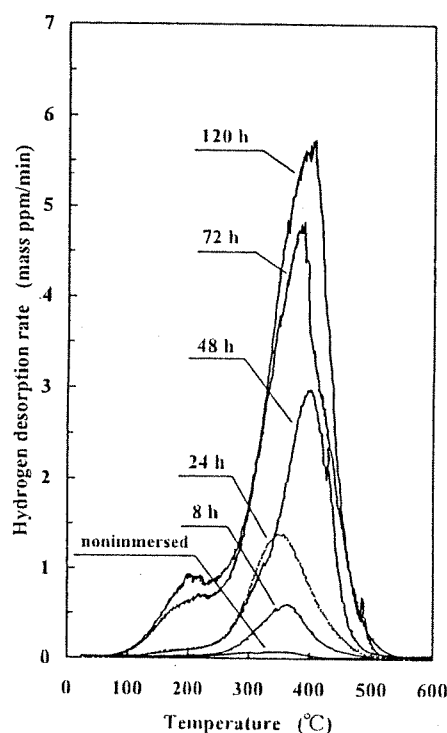


Fig. 1. Hydrogen thermal desorption curves for specimens immersed in methanol solution containing 0.1% HCl for up to 120 h at 37 °C.

superelastic alloy absorbed a large amount of hydrogen in the methanol solution containing 0.1% HCl. The thermal desorption of hydrogen appeared with the desorption peak at approximately 400 °C. For immersion time longer than 72 h, the second peak appeared at approximately 200 °C. The progress of hydrogen entry into the specimen was denoted by the increase in the total desorbed hydrogen, defined as the integrated peak intensity, with immersion time. The total amount of hydrogen desorbed up to 600 °C is shown in Fig. 2 as a function of immersion time. The amount of desorbed hydrogen, i.e. the amount of absorbed hydrogen during the immersion test, increased with increasing immersion time. The thermal desorption behavior gives information on the hydrogen trapping sites and the decomposition of hydrides from the temperature profile and the amount of desorption. The main desorption peak appeared at approximately 400 °C in the present experiment. On the other hand, the desorption peak of the sample immersed in 0.2% acidulated phosphate fluoride (0.2% APF; 0.2% NaF + 0.17% H₃PO₄) solution appeared at approximately 500 °C in our previous study [15]. Moreover, in the case of cathodically hydrogen charging in 0.9% NaCl solution, two desorption peaks appeared at approximately 200 and 300 °C [13,14]. The TDA behavior implies that the states of hydrogen in the alloy are different between the hydrogen-charging conditions. The desorption in the low-temperature range from 100 to 200 °C may be that of diffusive hydrogen,

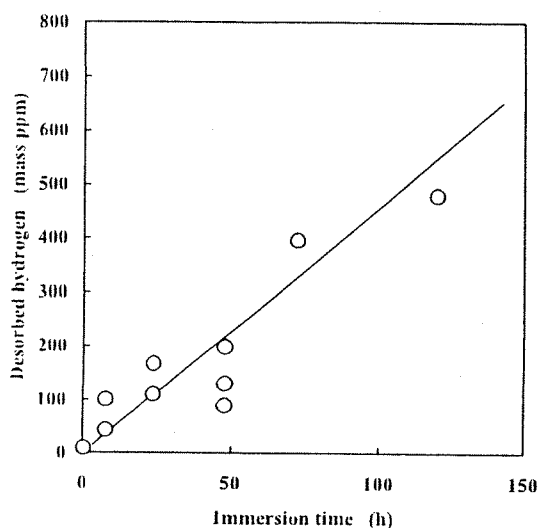


Fig. 2. Amount of desorbed hydrogen as a function of immersion time.

i.e. hydrogen weakly trapped and reversible to solid solution. The temperatures of hydrogen desorption of approximately 500 °C are close to the decomposition temperature of hydrides, suggesting the formation of hydrides at the time of immersion in the methanol solution. In general, it is recognized that hydrides form in titanium alloys when the hydrogen concentration reaches the solubility limits, e.g. in cathodically hydrogen-charged Ni–Ti alloys [16,24,25].

3.2. Weight loss test

SEM micrographs of the side surface of the non-immersed and 24-h immersed specimens are shown in Fig. 3(a–d, respectively). A large amount of localized corrosion was observed on the surface of the immersed specimen, as indicated by arrows in Fig. 3(c). Fig. 4 shows a plot of the weight loss data. The weight loss of the specimens increased linearly with immersion time. The weight loss of the specimens is attributable to localized corrosion during immersion in the solution. A thin passive film of the Ni–Ti alloy mainly consists of titanium oxide. The oxide film is expected to confer on the Ni–Ti alloy good corrosion behavior similar to that of titanium alloys. However, in some severe corrosive environments, such as highly acidified chloride solutions, breakdown of this passive film can occur, then repassivation becomes a difficult and relatively slow process [26]. The loss of the passive film probably leads to the absorption of hydrogen from various solutions because of the high affinity of titanium with hydrogen.

3.3. Degradation of tensile strength

Fig. 5 gives the Vickers microhardness values along a diameter of a cross section of the nonimmersed and the

specimens immersed for 24 h. For the nonimmersed specimen, the hardness was fairly uniform at approximately 360. On the other hand, the hardness of the specimen immersed for 24 h was slightly higher than that of the nonimmersed specimen. The hardness of 380 for the 24-h immersed specimen agrees with that of the cathodically charged specimen in our previous study [14]. The result of the hardening at the inner parts of the specimen indicates that hydrogen entered inside the specimen as well as adsorbed on to the surface of specimen. The original of the hardening might be due to solution hardening by hydrogen or to the formation of hydride [16]. In the present experiment, the size of indentations was approximately 30 μm square under the applied load of 0.98 N, giving roughly 900–1200 MPa that sufficiently exceeds the critical stress for martensite transformation. Then, measured hardness values are considered hardly affected by superelasticity.

The mechanical properties of the nonimmersed specimen are given in Table 1. The critical stress for martensite transformation and tensile strength of the specimen were 530 and 1250 MPa, respectively, at room temperature. Fig. 6 shows typical tensile stress–strain curves of the nonimmersed and immersed specimens tested. The tensile test results after immersion are shown in Fig. 7 in terms of the critical stress for martensite transformation and the tensile strength as functions of immersion time. The tensile strength of the 8-h immersed specimen was slightly higher than that of the nonimmersed specimen. The result is likely to be due to solid-solution hardening by hydrogen absorption. The amount of hydrogen absorbed by the 8-h immersed specimen was approximately 50–100 mass ppm, as shown in Fig. 2, which is similar to the previously observed value [15] during immersion in 0.2% APF solution for 2 h. In the case of the specimen immersed in 0.2% APF solution for 2 h, the tensile strength became slightly higher than that of the nonimmersed specimen, similar to the present case.

In the immersion in methanol solution with 0.1% HCl for 12–16 h, the tensile strengths rapidly decreased and became lower than that of the nonimmersed specimen. The fracture of specimens occurred after stress-induced martensite transformation. In the case of the immersion for 16 h, the fracture sometimes occurred during martensite transformation. The critical stress for martensite transformation increased up to approximately 560 MPa with immersion for 16 h. It was noted that for immersion time exceeding 24 h, the fracture of the immersed specimens occurred at a stress level close, but slightly lower than the extension of the critical stress. This result is consistent with that obtained using hydrogen-precharged specimens under different conditions, such as immersion in 0.2% APF solution [15] or cathodically charging in 0.9% NaCl solution [11,12], although the hydrogen thermal desorption behavior was

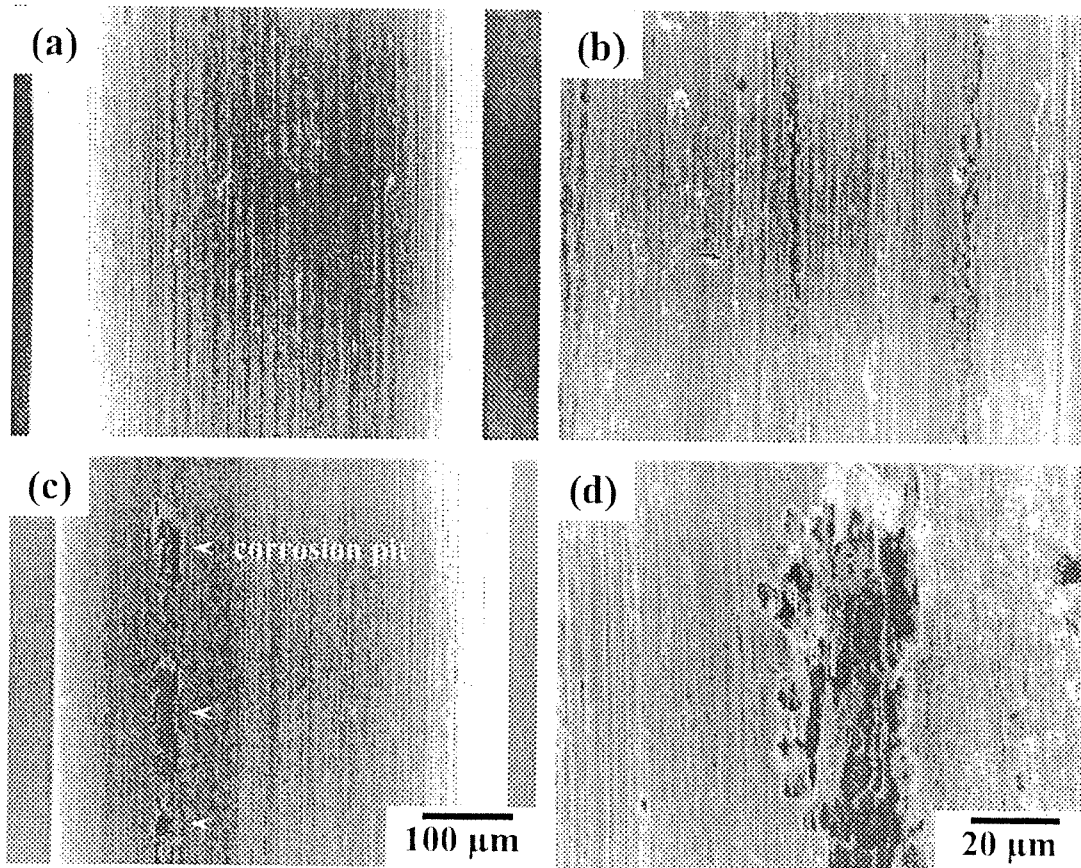


Fig. 3. SEM micrographs of the typical side surface of (a, b) nonimmersed and (c, d) 24-h-immersed specimens; arrows mark corrosion pits.

different from that obtained under different hydrogen-charging conditions. With further extension of the immersion period, the tensile strength was reduced to

a constant value identical to the critical stress for martensite transformation. This result suggests that the degree of the degradation cannot be ascribed to the

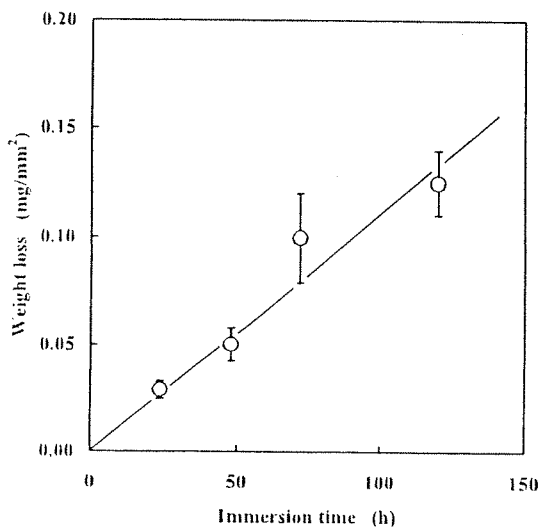


Fig. 4. Weight loss of specimens immersed in methanol solution containing HCl. S.D. was calculated from the results of five measurements.

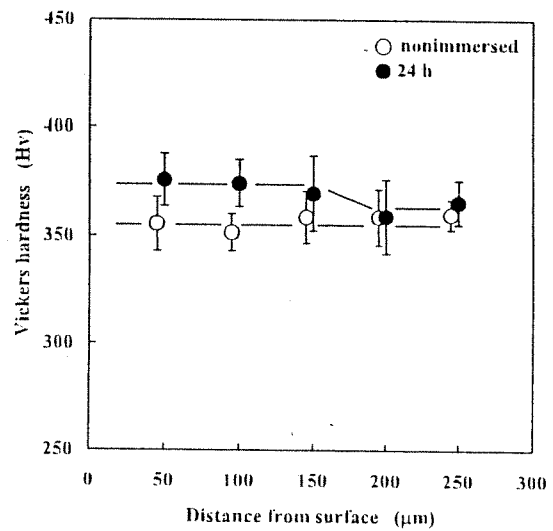


Fig. 5. Vickers microhardness values of nonimmersed and immersed specimens. Hardness was measured at intervals of 0.05 mm and S.D. was calculated from eight indentations.

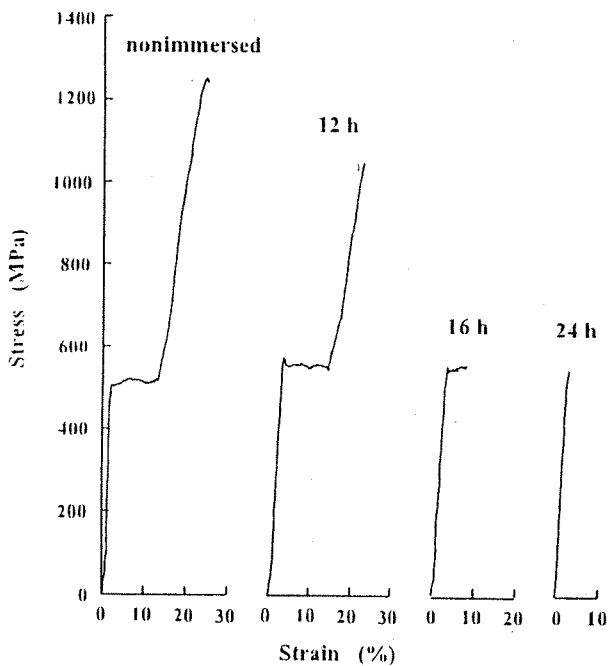


Fig. 6. Typical stress-strain curves of nonimmersed and immersed specimens. Strain was calculated from elongation (displacement of crosshead) and the initial gage length.

amount of absorbed hydrogen. The increase in the critical stress for martensite transformation is most likely attributed to the hydrogen effect of preventing martensite transformation. Martensite transformation is sensitive to the presence of interstitial atoms, such as hydrogen [27]. In the short immersion period, the decrease of tensile strength probably results from the hydrogen-related degradation of martensite. On the other hand, in the long immersion period, some

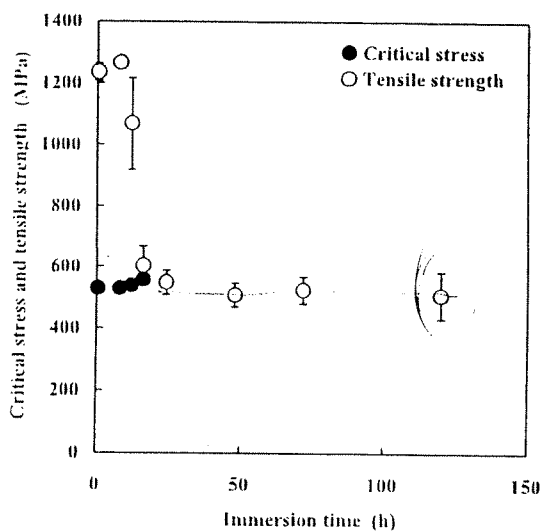


Fig. 7. Tensile strength of immersed specimens in solution as a function of immersion time. S.D. was calculated from results obtained from five to eight specimens.

Table 1

Mechanical properties of the tested Ni-Ti superelastic alloy

Critical stress (MPa)	Tensile strength (MPa)	Reduction of area (%)
530 ± 16.7	1250 ± 7.2	54.7

dynamical effect of hydrogen in martensite transformation is to be considered as well as the formation of hydride. The hydrogen-desorption at around 200 °C observed in Fig. 1 might be associated with the failure with a high hydrogen concentration. Detailed discussion on the effect of the hydrogen in the fracture is for further studies.

Fig. 8 show SEM micrographs of the fracture surface of the immersed specimens. The 8-h immersed specimen was ductile and characterized by cup-cone morphologies, as shown in Fig. 8(a); it consists of deep dimples as shown in the magnified view in Fig. 8(b). The fracture surface of the 8-h immersed specimen was very similar to that of the nonimmersed specimen. On the other hand, on macroscopic scale, the reduction of the area was not observed for an immersion time longer than 12 h. Fig. 8(c) shows the fracture surface of the 24-h immersed specimen, which was characterized by shallow dimples as shown in the magnified view in Fig. 8(d). The characteristics of the fracture surface correspond approximately to those of specimens cathodically hydrogen-precharged in 0.9% NaCl solution [12] and immersed in 0.2% APF solution [15]. The shallow-dimple pattern suggests reduced ductility of the immersed specimen. The area of corrosion pits was observed in the periphery of the fracture surface as indicated by arrows in Fig. 8(c). The diameter of the corrosion pit increased with increasing immersion time. In the 24-h immersed specimen, the diameter of the corrosion pit exceeded 100 μm . A fracture initiation point existed at the vicinity of the corrosion pit edge, as shown in Fig. 8(e). If the formation of corrosion pits was the cause of the decrease in tensile strength, tensile strength should decrease further for immersion time exceeding 24 h. However, the tensile strength of the immersed specimens was independent of the diameter and the number of corrosion pits. The result suggests that a decrease in tensile strength is mainly responsible for interference in the stress-induced martensite transformation by hydrogen absorption as in the case of cathodic hydrogen charging.

4. Conclusions

It has been demonstrated in this study that a reduction of the tensile strength of a Ni-Ti superelastic alloy occurs in methanol solution containing 0.1% HCl due to hydrogen absorption. The total amount of

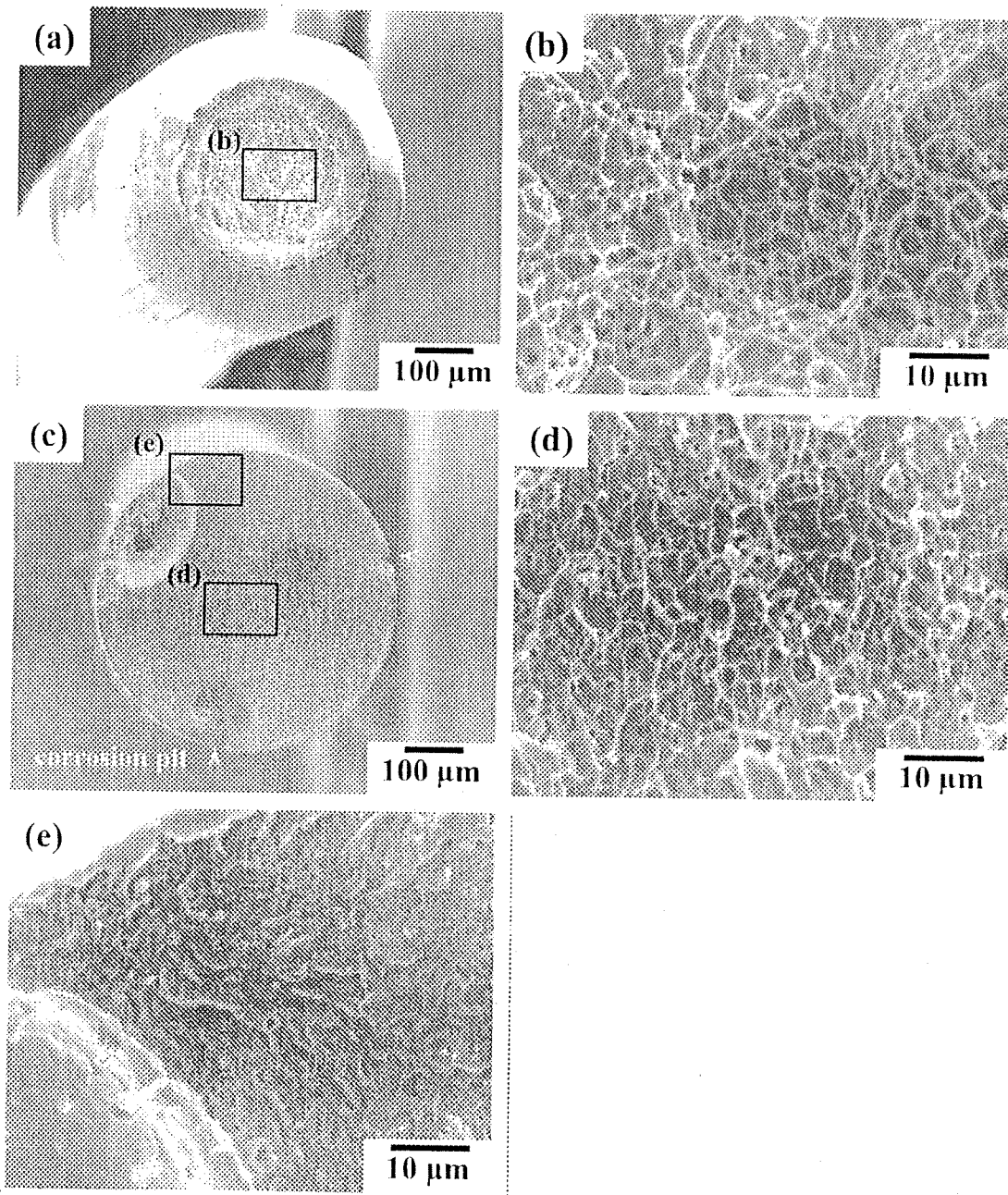


Fig. 8. SEM micrographs of a typical fracture surface: (a) immersed in solution for 8 h; (b) magnified view of dimples in (a); (c) immersed in solution for 24 h, arrows mark corrosion pits; (d) magnified view of shallow dimples in (c); and (e) magnified view of initiation point in (c).

absorbed hydrogen increased with increasing immersion time. When the amount of absorbed hydrogen exceeded 100–200 mass ppm, the tensile strength of the immersed specimen was reduced to and maintained at the critical stress for martensite transformation while hydrogen absorption further proceeded. Hydrogen TDA showed that a desorption peak appeared at approximately 400 °C. The relationship between thermal desorption

behavior and mechanical properties of the Ni–Ti super-elastic alloy will be studied in the future.

References

- [1] K. Otsuka, K. Shimizu, *Int. Met. Rev.* 31 (1986) 93.
- [2] S.A. Shabalovskaya, *Bio-Med. Mater. Eng.* 6 (1996) 267.

- [3] T. Duerig, A. Pelton, D. Stöckel, *Mater. Sci. Eng. A* 273–275 (1999) 149.
- [4] K.N. Melton, O. Mercier, *Acta Metall.* 27 (1979) 137.
- [5] Y. Oshida, R. Sachdeva, S. Miyazaki, S. Fukuyo, *Mater. Sci. Forum* 56–58 (1990) 705.
- [6] J.W. Edie, G.F. Andreasen, M.P. Zaytoun, *Angle Orthod.* 51 (1981) 319.
- [7] M.R. Grimsdottir, A. Hensten-Pettersen, *Dent. Mater.* 13 (1997) 163.
- [8] T. Eliades, G. Eliades, A.E. Athanasiou, T.G. Bradley, *Eur. J. Orthod.* 22 (2000) 317.
- [9] E.F. Harris, S.M. Newman, J.A. Nicholson, *Am. J. Orthod.* 93 (1988) 508.
- [10] B. Mohlin, H. Müller, J. Ödman, B. Thilander, *Eur. J. Orthod.* 13 (1991) 386.
- [11] K. Yokoyama, K. Hamada, K. Moriyama, K. Asaoka, *Biomaterials* 22 (2001) 2257.
- [12] K. Yokoyama, K. Hamada, K. Asaoka, *Mater. Trans.* 42 (2001) 141.
- [13] K. Asaoka, K. Yokoyama, M. Nagumo, *Metall. Mater. Trans. A* 33A (2002) 495.
- [14] K. Yokoyama, S. Watabe, K. Hamada, J. Sakai, K. Asaoka, M. Nagumo, *Mater. Sci. Eng. A* 341 (2003) 91.
- [15] K. Yokoyama, K. Kaneko, K. Moriyama, K. Asaoka, J. Sakai, M. Nagumo, *J. Biomed. Mater. Res.* 65A (2003) 182.
- [16] Y. Adachi, N. Wade, Y. Hosoi, *Jpn. Inst. Metals* 54 (1990) 525.
- [17] N. Wade, Y. Adachi, Y. Hosoi, *Scr. Metall. Mater.* 24 (1990) 1051.
- [18] T. Asaoka, H. Yamashita, H. Saito, Y. Ishida, *Jpn. Inst. Metals* 57 (1993) 1123.
- [19] T. Hoshiya, S. Den, H. Katsuta, H. Ando, *Jpn. Inst. Metals* 56 (1992) 747.
- [20] K. Mori, A. Takamura, T. Shimose, *Corrosion* 22 (1966) 29.
- [21] K. Ebtehaj, D. Hardie, R.N. Parkins, *Corros. Sci.* 25 (1985) 415.
- [22] A.C. Hollis, J.C. Scully, *Corros. Sci.* 34 (1993) 821.
- [23] T. Haruna, M. Yamamoto, T. Shibata, *Jpn. Inst. Metals* 63 (1999) 977.
- [24] S.K. Wu, C.M. Wayman, *Acta Metall.* 36 (1988) 1005.
- [25] T.H. Nam, K. Shimizu, T. Saburi, S. Nenno, *Mater. Trans. JIM* 30 (1989) 539.
- [26] G. Rondelli, *Biomaterials* 17 (1996) 2003.
- [27] A. Biscarini, R. Campanella, B. Coluzzi, G. Mazzolai, L. Trotta, A. Tuissi, F.M. Mazzolai, *Acta Mater.* 47 (1999) 4525.



Delayed fracture of beta titanium orthodontic wire in fluoride aqueous solutions

Kazuyuki Kaneko^a, Ken'ichi Yokoyama^{b,*}, Keiji Moriyama^a, Kenzo Asaoka^b, Jun'ichi Sakai^c, Michihiko Nagumo^c

^a Department of Orthodontics, School of Dentistry, The University of Tokushima, 3-18-15 Kuramoto-cho, Tokushima 770-8504, Japan

^b Department of Dental Engineering, School of Dentistry, The University of Tokushima, 3-18-15 Kuramoto-cho, Tokushima 770-8504, Japan

^c Department of Materials Science and Engineering, Waseda University, 3-4-1 Okubo, Shinjuku-ku, Tokyo 169-8555, Japan

Received 10 October 2002; accepted 13 December 2002

Abstract

Hydrogen embrittlement of a beta titanium orthodontic wire has been examined by means of a delayed-fracture test in acid and neutral fluoride aqueous solutions and hydrogen thermal desorption analysis. The time to fracture increased with decreasing applied stress in 2.0% and 0.2% acidulated phosphate fluoride (APF) solutions. The fracture mode changed from ductile to brittle when the applied stress was lower than 500 MPa in 2.0% APF solution. On the other hand, the delayed fracture did not occur within 1000 h in neutral NaF solutions, although general corrosion was also observed similar to that in APF solutions. Hydrogen desorption of the delayed-fracture-tested specimens was observed with a peak at approximately 500°C. The amount of absorbed hydrogen was 5000–6500 mass ppm under an applied stress in 2.0% APF solution for 24 h. It is concluded that the immersion in fluoride solutions leads to the degradation of the mechanical properties and fracture of beta titanium alloy associated with hydrogen absorption.

© 2003 Elsevier Science Ltd. All rights reserved.

Keywords: Beta titanium; TMA; Orthodontic wire; Delayed fracture; Hydrogen embrittlement; Fluoride

1. Introduction

A beta titanium alloy for orthodontic wire was first introduced by Goldberg and Burstone in 1979 [1]. The alloy is now marketed under the brand name TMA (Ormco Corporation, Glendora, CA), which stands for "titanium–molybdenum alloy". The beta titanium alloy exhibits excellent properties, including low elastic modulus, high springback, high formability and high weldability compared to conventional stainless steel and cobalt–chromium–nickel orthodontic wires [2–9]. Moreover, the advantage of this alloy over other orthodontic wires is that it does not contain nickel. However, the alloy has a known tendency to fracture during clinical use. If this tendency is eliminated, the alloy will be used more widely in the future.

We have proposed that one of the reasons for the fracture of titanium and its alloys is hydrogen embrittlement in the oral cavity [10–15]. The fracture or degradation of mechanical properties caused by hydrogen is generally termed hydrogen embrittlement. This hydrogen embrittlement is often represented as a reduction in both fracture strain and area, and is accompanied by a change in the fracture mode. Hydrogen embrittlement of titanium alloys such as Ni–Ti superelastic alloy in the oral cavity sometimes occurs in the presence of fluoride [15]. Fluoride is added in toothpaste, prophylactic agents, and dental rinse, because of its cariostatic effect. Caries-preventing prophylactics generally contain 100–10000 ppm F, with pH between about 3.5 and neutral. The effects of fluoride on titanium and its alloys have been investigated from the viewpoint of corrosion or discoloration by several workers [16–29]. It was clarified that the corrosion resistance of titanium and its alloys markedly decreases in fluoride solutions. However, the hydrogen embrittlement of the beta titanium alloy in fluoride

*Corresponding author. Tel.: +81-88-633-7334; fax: +81-88-633-9125.

E-mail address: yokken@dent.tokushima-u.ac.jp (K. Yokoyama).

solutions has not been reported previously. It is therefore necessary to confirm experimentally whether or not hydrogen embrittlement of the alloy occurs in fluoride solutions.

The purpose of the present study is to examine the hydrogen embrittlement of a beta titanium orthodontic wire in fluoride solutions and the associated behavior of hydrogen absorption by means of hydrogen thermal desorption analysis (TDA). For the evaluation of hydrogen embrittlement susceptibility, the delayed-fracture test was conducted.

2. Experimental procedures

2.1. Materials

Beta titanium wire (TMA; Ormco Corporation, Glendora, CA) with a diameter of 0.45 mm was cut into specimens of 150 mm length. The specimens were polished with #600-grit SiC paper and ultrasonically washed in acetone for 5 min. Tensile tests were carried out at room temperature using an Instron-type machine (Autograph AG-100A, Shimadzu) at a strain rate of $8.33 \times 10^{-4} \text{ s}^{-1}$. The chemical composition and mechanical properties of the specimens are given in Table 1. Standard deviation was calculated from the results obtained from more than five specimens.

2.2. Delayed-fracture test

The delayed-fracture test, i.e., a sustained tensile-loading test in a solution, was carried out at room temperature. Applied stress was varied to determine the delayed-fracture life characteristics. The length of each specimen immersed in a solution was 50 mm and the time to fracture of the specimens was determined. The test was terminated when no delayed fracture occurred after more than 1000 h. The test solutions used were 50 ml each of the aqueous solutions of 0.2% and 2.0% acidulated phosphate fluoride (APF; 0.2% NaF + 0.17% H_3PO_4 and 2.0% NaF + 1.7% H_3PO_4) with pH 5.0, and 0.2% and 2.0% NaF with pH 6.5. The concentrations of fluoride in 0.2% and 2.0% NaF solutions were 900 and 9000 ppm, respectively. The fracture surface of the delayed-fracture-tested specimens was examined with a scanning electron microscope (SEM). Hardness tests were performed on the transverse cross section from the periphery to the center of the wire

Table 1
Chemical composition (mass%) and mechanical properties

Ti	Mo	Zr	Sn	Tensile strength	Reduction in area
77.8	11.3	6.6	4.3	$1154 \pm 18.5 \text{ MPa}$	87.3%

at intervals of 0.05 mm using a Vickers microhardness tester. Measurements were carried out under an applied load of 0.98 N for 15 s. Standard deviation was calculated from the results obtained from eight indentations. The corrosion products on the surface were examined using an X-ray diffractometer (XRD) with $\text{Cu K}\alpha$ radiation of wavelength $\lambda = 1.54056 \text{ \AA}$ in the 2θ angle range from 10° to 90° operated at 30 kV and 15 mA.

2.3. Thermal desorption analysis

The amount of desorbed hydrogen was measured by TDA for all the specimens, which were subjected to the delayed-fracture test for 24 h. Both sides of each specimen, immersed in a solution (50 mm in length) were cut into 20-mm-long pieces and subjected to ultrasonic cleaning with acetone for 2 min. Each specimen was dried in ambient and used for measurement. TDA was started 30 min after the removal of a specimen from a solution. A quadrupole mass spectrometer (ULVAC, Kanagawa, Japan) was used for hydrogen detection. Sampling was conducted at 30-s intervals at a heating rate of 100°C/h .

3. Experimental results

The delayed-fracture test result is shown in Fig. 1 in terms of the time to fracture as a function of the applied stress. The arrow in the figure denotes the non-fractured specimen at the indicated elapsed time. The time to fracture tended to increase with decreasing applied stress

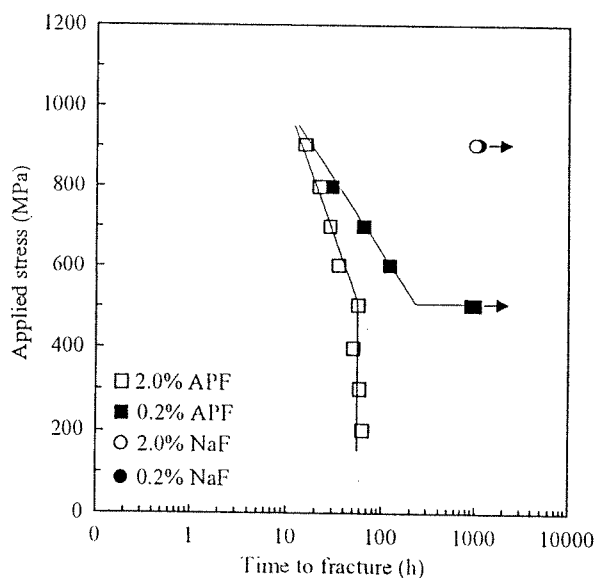


Fig. 1. Delayed-fracture diagrams of beta titanium alloy in APF and NaF solutions.

in APF solutions. For the same applied stress, the time to fracture in 2.0% APF solution was shorter than that in 0.2% APF solution. Note that when the applied stress was lower than 500 MPa, the time to fracture was not affected by the applied stress in 2.0% APF solution, and no delayed fracture occurred within 1000 h in 0.2% APF solution. In this experiment, no crevice corrosion resulted at the point of contact with the vessel in both 2.0% and 0.2% APF solutions. In 2.0% and 0.2% NaF solutions, the surface of each specimen became discolored after immersion, but no delayed fracture occurred within the stress range tested.

Figs. 2(a) and (b) show the fractographs of the specimen in 2.0% APF solution under the applied stress of 600 MPa for 35 h and 5 min. When the applied stress was higher than 600 MPa, the fractures of the specimens in both 2.0% and 0.2% APF solutions were characterized macroscopically based on cup-cone morphologies. The reduction in area was approximately 80% regardless of the applied stress. The fracture surface was composed microscopically of primary and secondary dimples. In contrast, under an applied stress of 500 MPa for 56 h and 17 min, the fracture surface of the specimen in 2.0% APF solution was fairly flat and exhibited no reduction in area, as shown in Figs. 2(c) and (d). The fractures were characterized microscopically based on quasi-cleavage. Noteworthy is that the fracture mode changed to brittle when the applied stress was lower

than 500 MPa for the specimen in 2.0% APF solution. The diameters of the delayed-fracture-tested specimens decreased from 0.45 to 0.35 mm due to the peeling of their peripheral layer in the solutions. Fig. 3 shows the fracture surface of the specimen in 0.2% APF solution under the applied stress of 600 MPa for 121 h and 48 min. The fracture surface consisted of three areas, namely, shear dimple area (Fig. 3(b)), mixed area of primary and secondary dimples (Fig. 3(c)), and quasi-cleavage area (Fig. 3(d)). When the applied stress was higher than 700 MPa in 0.2% APF solution, brittle fractured area was not observed, i.e., the fracture surface consisted of a shear dimple area and a mixed area of primary and secondary dimples.

On the side surface of specimen before the delayed-fracture test, scratches due to SiC paper polishing were observed, as shown in the SEM micrographs of Figs. 4(a) and (b). On the other hand, after the test in 2.0% APF solution under the applied stresses of 600 (Figs. 4(c) and (d)) and 500 MPa (Figs. 4(e) and (f)), the specimens exhibited smooth surfaces due to the peeling off of surface layers composed of corrosion products. Figs. 4(g) and (h) show the side surface after the test in 0.2% APF solution under the applied stress of 600 MPa. From the cross section of the fracture surface, the fracture mode was characterized macroscopically based on shearing due to slip deformation. Moreover, the surface became rough due to general corrosion.

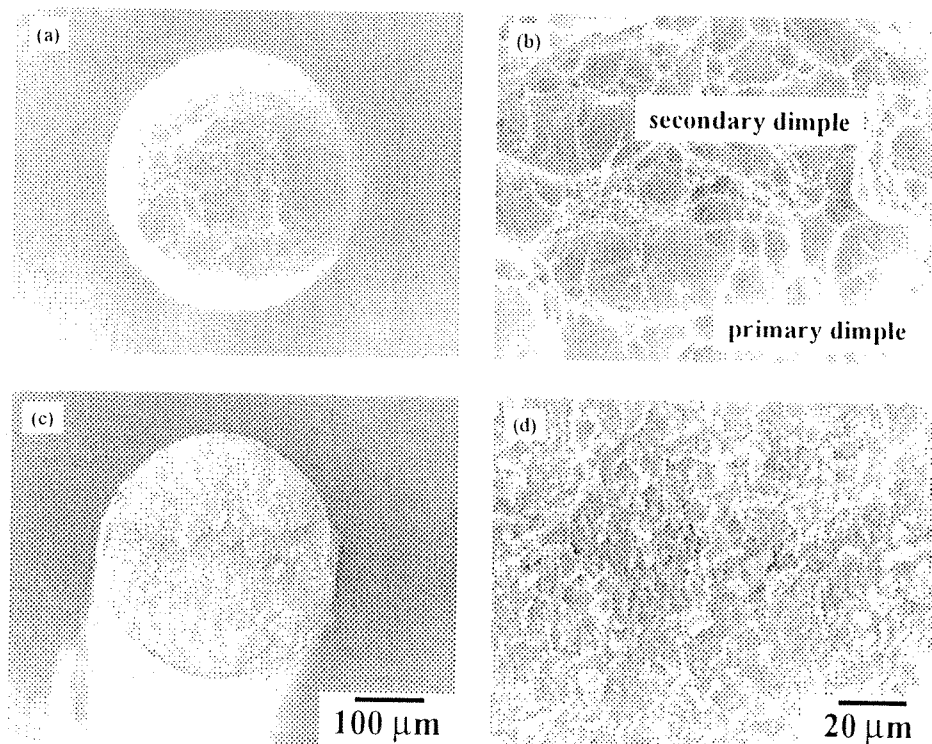


Fig. 2. SEM micrographs of delayed-fracture surface under applied stresses of (a), (b) 600 and (c), (d) 500 MPa in 2.0% APF solution.

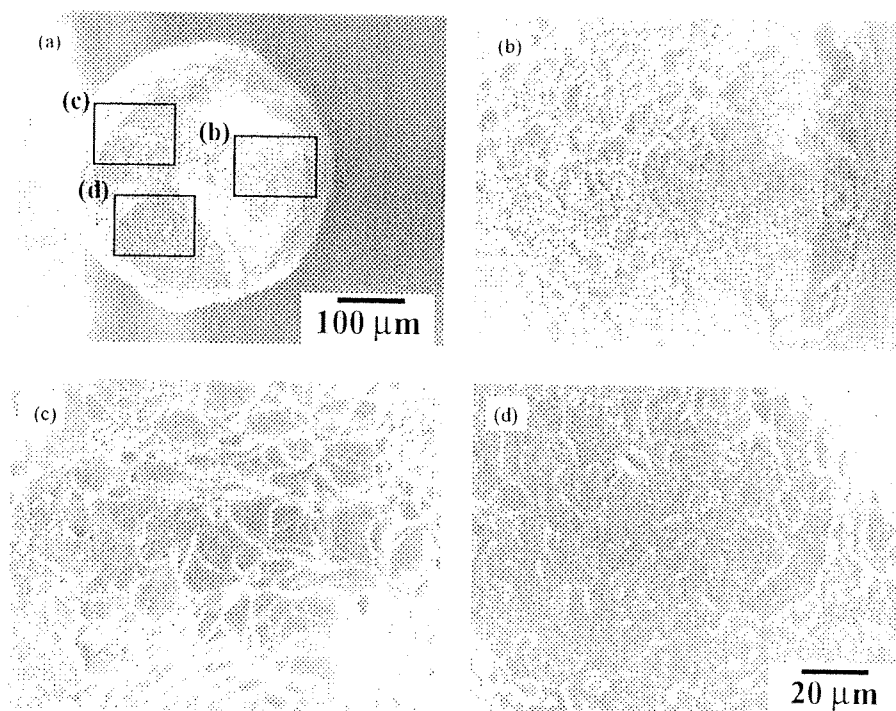


Fig. 3. SEM micrographs of the delayed-fracture surface at applied stress of: (a) 600 MPa in 0.2% APF solution; (b) shear dimple area; (c) mixed area of primary and secondary dimples; and (d) quasi-cleavage area on the fracture surface.

Corrosion was observed on the surface of the specimen, which did not fracture within 1000 h in the applied stress range below 500 MPa. In neutral 2.0% NaF solution, the side surface of a delayed-fracture-tested specimen, which did not fracture until 1000 h, is shown in Figs. 5(a) and (b). In the case of the specimens in NaF solutions, delayed fracture did not occur, but corrosion pits and loss of scratches appeared similar to those in APF solutions.

Fig. 6 shows the XRD results for the surfaces of the non-immersed and immersed specimens in 2.0% APF solution for 24 h. The formation of sodium titanium fluoride, $\text{Na}_5\text{Ti}_3\text{F}_{14}$ (tetragonal; $a = 0.748$ nm, $c = 1.03$ nm), was confirmed on the surface of the immersed specimen.

The Vickers microhardness values of the non-immersed and immersed specimens in 2.0% APF solution for 24 or 48 h without loading are shown in Fig. 7. The hardness of the non-immersed specimen was approximately 290 at any part. On the other hand, the hardness of the immersed specimen was slightly reduced compared with that of the non-immersed specimen.

Fig. 8 shows TDA curves for the specimens before and after the delayed-fracture test under the applied stress of 600 or 500 MPa in 2.0% APF solution for 24 h. The progress of hydrogen entry into the specimen was denoted by the increase in the total desorbed hydrogen, defined as the integrated peak intensity, with immersion time. Before the delayed-fracture test, the amount of

desorbed hydrogen, i.e., concentration of predissolved hydrogen, was 140 mass ppm. The desorption occurred in the temperature range from 400°C to 800°C. On the other hand, after the delayed-fracture test for 24 h, the desorption curves exhibited a single desorption peak at approximately 500°C. The total amounts of desorbed hydrogen up to 800°C under the applied stresses of 600 and 500 MPa were 6709 and 5306 mass ppm, namely, the amounts of absorbed hydrogen during the delayed-fracture test were 6569 and 5166 mass ppm, respectively.

4. Discussion

A noteworthy finding in the present study is that the delayed fracture of the beta titanium alloy occurs in association with hydrogen absorption in APF solutions. The corrosion behavior of beta titanium alloy depends on an oxide film composed of mainly TiO_2 on the surface, which spontaneously covers the surface of titanium and its alloys in the presence of oxygen. The effects of fluoride on the corrosion behavior of titanium and its alloys have been presented by several authors [16–29]. According to their results, the oxide film undergoes a reaction in fluoride solutions, resulting in the formation of titanium fluoride, titanium oxide fluoride, or sodium titanium fluoride on the surface of the alloys. Hence, the corrosion resistance of those alloys decreases markedly in the solutions. In the present

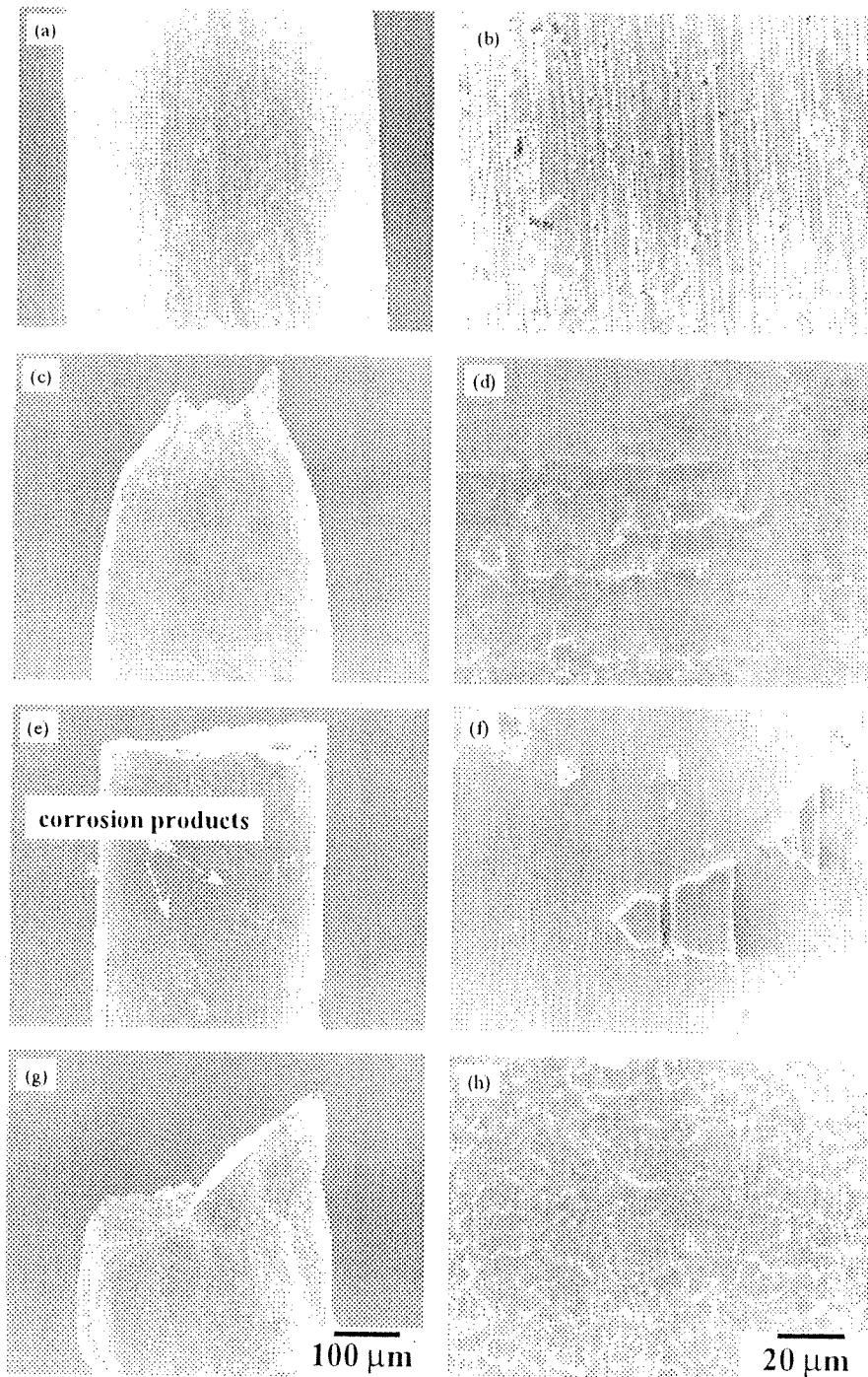


Fig. 4. SEM micrographs of a typical side surface: before delayed-fracture test. (a) General and (b) magnified views; after delayed-fracture test under applied stress of 600 MPa in 2.0% APF solution, (c) general and (d) magnified views; under applied stress of 500 MPa in 2.0% APF solution, (e) general and (f) magnified views; and under applied stress of 600 MPa in 0.2% APF solution, (g) general and (h) magnified views.

study, the oxide film on the surface of the beta titanium alloy is likely destroyed in APF solutions in the same manner as that reported in previous works, as shown in Figs. 4 and 6. The loss of the oxide film may lead to the absorption of hydrogen from various solutions because

of the high affinity of titanium to hydrogen. In NaF solutions, the delayed fracture did not occur within 1000 h, but corrosion pits and the disappearance of scratches were observed on the surface of the tested specimen similar to that in APF solutions, as shown in

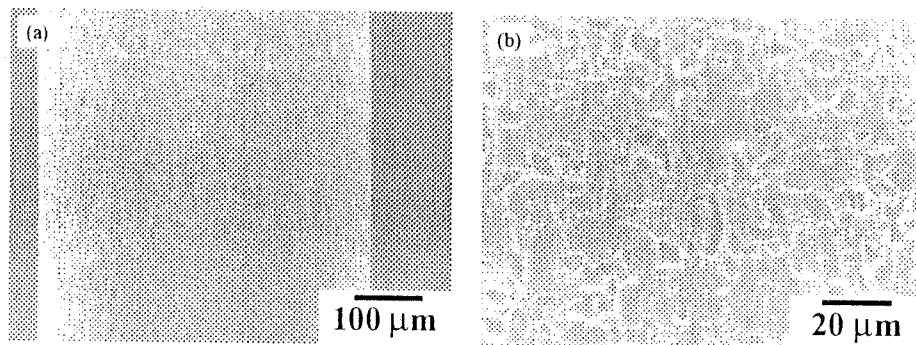


Fig. 5. SEM micrographs of the typical side surface after delayed-fracture-tested specimen in 2.0% NaF solution for 1000 h. (a) General and (b) magnified views of the surface.

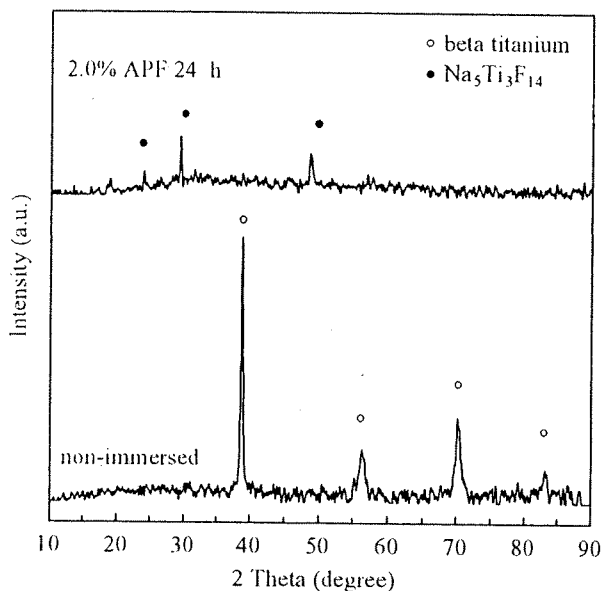


Fig. 6. XRD patterns for the surface of non-immersed specimen and 24-h-immersed specimen in 2.0% APF solution.

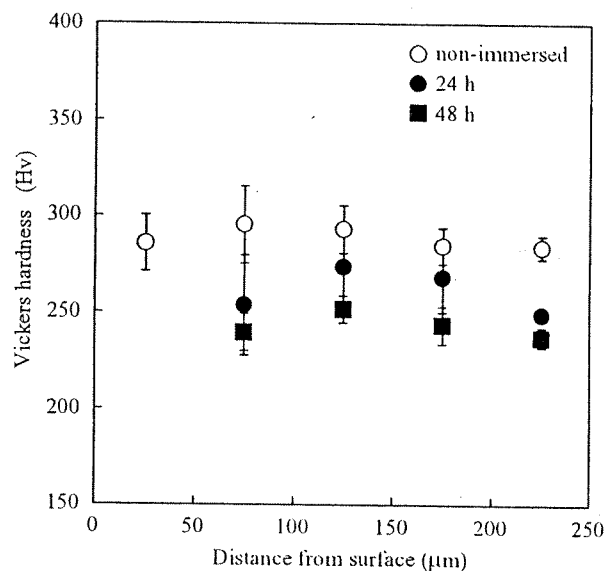


Fig. 7. Vickers microhardness values of non-immersed, 24- and 48-h-immersed specimens. The hardness was measured at intervals of 0.05 mm, and the standard deviation was calculated from eight indentations.

Fig. 5. This result indicates that the oxide film is destroyed and the delayed fracture of the beta titanium alloy might take place in neutral NaF solutions.

Various mechanisms have been proposed for the hydrogen embrittlement of beta titanium alloys [30–37]. Hydride is formed in certain beta titanium alloys such as Ti–30Mo and Ti–13V–11Cr–3Al alloys at high temperatures [30–31]. No direct evidence of the association of hydrides with the brittle fracture of beta titanium alloys has been reported, although the brittle fracture of alpha titanium is caused by hydride formation [38–40]. In a Ti–15% Mo–3% Nb–3% Al alloy, no hydride is formed by hydrogen charging [32–35,37]. In this study, hydride formation was not observed by means of XRD. Furthermore, the hardness of the immersed specimen was reduced, despite the fact that hydride formation

generally leads to hardening of matrix. Hence, it can be considered that hydride formation is not responsible for the delayed fracture observed in the present study. The lattice decohesion theory has also been proposed for beta titanium alloys [37]. In the case of a Ti–15% Mo–3% Nb–3% Al alloy, tensile strength decreases abruptly below the initial yield strength when the amount of absorbed hydrogen exceeds 1000–3000 mass ppm [33–35,37]. Moreover, the rise of the ductile to brittle transition temperature with electrochemical hydrogen precharging and exposure to gaseous hydrogen has been reported [33,36–39]. According to the results, the brittle fracture of hydrogen-charged beta titanium alloys could be expected even at room temperature.

In the present study, the amounts of absorbed hydrogen were 6569 and 5166 mass ppm under the

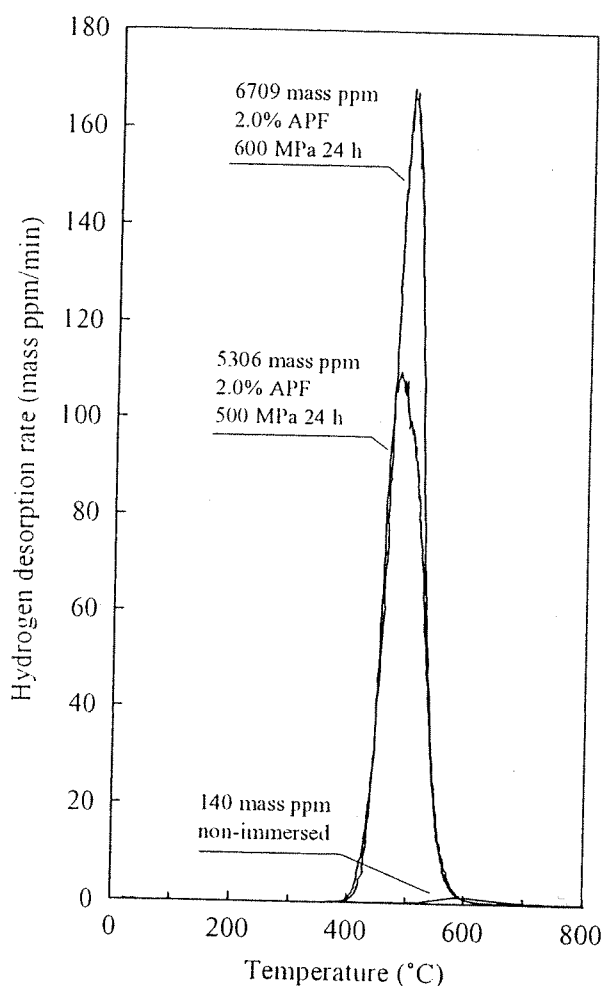


Fig. 8. Hydrogen thermal desorption curves for specimens before and after delayed-fracture test under applied stresses of 600 and 500 MPa in 2.0% APF solution for 24 h.

applied stresses of 600 and 500 MPa in 2.0% APF solution for 24 h, respectively. The times to fracture under these conditions are approximately 35 and 55 h, as shown in Fig. 1. The amount of absorbed hydrogen may further increase before the delayed fracture takes place. If we assume the critical hydrogen concentration is responsible for the failure, the observed hydrogen contents well coincide with the values reported in the literature. However, the amount of absorbed hydrogen in the delayed fracture under the applied stress of 500 MPa probably exceeds that under 600 MPa because of the longer immersion time. This is in contrast to the fact that the time to fracture is almost constant under an applied stress lower than 500 MPa. This implies that hydrogen concentration is not the sole criterion for the failure. The applied stress may affect the stress and strain states in front of incipient cracks as well as the sharpness of a crack. Interactions between hydrogen

and stress/strain states may operate in the failure in a complicated manner. Further studies are needed to clarify their interactions in the studied alloy.

In 0.2% APF solution on the basis of fractographic features, the mechanism of delayed fracture seems to be almost the same as that in 2.0% APF solution. It is, however, presumed that the amount of absorbed hydrogen in 0.2% APF solution is less than that in 2.0% APF solution in the case of the same immersion time. In this case, factors for accelerating hydrogen absorption, such as applied stress, play an important role in 0.2% APF solution. The effect of applied stress is shown clearly as the difference in the slope in the delayed-fracture diagrams shown in Fig. 1 between 2.0% and 0.2% APF solutions in the applied stress range above 600 MPa. Under an applied stress lower than 500 MPa in 0.2% APF solution, factors for accelerating hydrogen absorption are small in comparison with that under an applied stress higher than 600 MPa, and hydrogen absorption may be reduced. From the result of quasi-cleavage on the fracture surface, as shown in Fig. 3(d), delayed fracture will occur in the applied stress range below 500 MPa, if the delayed-fracture test is performed for a long period. The effect of applied stress on hydrogen absorption will be reported elsewhere.

5. Conclusions

Fracture of a beta titanium orthodontic wire in acid and neutral fluoride aqueous solutions has been examined from the viewpoint of hydrogen embrittlement. The delayed fracture occurred in 2.0% and 0.2% APF solutions. The fracture mode changed from ductile to brittle in 2.0% APF solution when the applied stress was lower than 500 MPa, in other words, when the immersion time was longer than 50 h. In 0.2% APF solution, the delayed fracture did not occur within 1000 h in the applied stress range below 500 MPa. The amount of absorbed hydrogen was approximately 5000–6500 mass ppm under an applied stress in 2.0% APF solution for 24 h. On the other hand, the existence of a delayed fracture in neutral NaF solutions is necessary to investigate what under various conditions. It is concluded that one of the reasons for the fracture of the beta titanium alloy during clinical use is hydrogen embrittlement in fluoride solutions.

Acknowledgements

This study was supported in part by a Grant-in-Aid for Young Scientists (B) (14771090) from the Ministry of Education, Culture, Sports, Science and Technology, Japan.

References

- [1] Goldberg J, Burstone CJ. An evaluation of beta titanium alloys for use in orthodontic appliances. *J Dent Res* 1979;58:593–600.
- [2] Burstone CJ, Goldberg AJ. Beta titanium: a new orthodontic alloy. *Am J Orthod* 1980;77:121–32.
- [3] Kusy RP. Comparison of nickel–titanium and beta titanium wire sizes to conventional orthodontic arch wire materials. *Am J Orthod* 1981;79:625–9.
- [4] Goldberg AJ, Morton J, Burstone CJ. The flexure modulus of elasticity of orthodontic wire. *J Dent Res* 1983;62:856–8.
- [5] Goldberg AJ, Shastry CV. Age hardening of orthodontic beta titanium alloys. *J Biomed Mater Res* 1984;18:155–63.
- [6] Donovan MT, Lin JJ, Brantley WA, Conover JP. Weldability of beta titanium arch wires. *Am J Orthod* 1984;85:207–16.
- [7] Nelson KR, Burstone CJ, Goldberg AJ. Optimal welding of beta titanium orthodontic wires. *Am J Orthod Dentofac Orthop* 1987;92:213–9.
- [8] Kusy RP, Stush AM. Geometric and material parameters of a nickel–titanium and a beta titanium orthodontic arch wire alloy. *Dent Mater* 1987;3:207–17.
- [9] Kusy RP, Wilson TW. Dynamic mechanical properties of straight titanium alloy arch wires. *Dent Mater* 1990;6:228–36.
- [10] Yokoyama K, Hamada K, Moriyama K, Asaoka K. Degradation and fracture of Ni–Ti superelastic wire in an oral cavity. *Biomaterials* 2001;22:2257–62.
- [11] Yokoyama K, Hamada K, Asaoka K. Fracture analysis of hydrogen-charged nickel–titanium superelastic alloy. *Mater Trans* 2001;42:141–4.
- [12] Yokoyama K, Ichikawa T, Murakami H, Miyamoto Y, Asaoka K. Fracture mechanisms of retrieved titanium screw thread in dental implant. *Biomaterials* 2002;23:2459–65.
- [13] Asaoka K, Yokoyama K, Nagumo M. Hydrogen embrittlement of nickel–titanium alloy in biological environment. *Metall Mater Trans A* 2002;33A:495–501.
- [14] Yokoyama K, Watabe S, Hamada K, Sakai J, Asaoka K, Nagumo M. Susceptibility to delayed fracture of Ni–Ti superelastic alloy. *Mater Sci Eng A* 2003;341:91–7.
- [15] Yokoyama K, Kaneko K, Moriyama K, Asaoka K, Sakai J, Nagumo M. Hydrogen embrittlement of Ni–Ti superelastic alloy in fluoride solution. *J Biomed Mater Res*, in press.
- [16] Lausmaa J, Kasemo B, Hansson S. Accelerated oxide grown on titanium implants during autoclaving caused by fluorine contamination. *Biomaterials* 1985;6:23–7.
- [17] Sürilä HS, Könönen M. The effect of oral topical fluorides on the surface of commercially pure titanium. *Int J Oral Maxillofac Implants* 1991;6:50–4.
- [18] Pröbster L, Lin W, Hüttemann H. Effect of fluoride prophylactic agents on titanium surfaces. *Int J Oral Maxillofac Implants* 1992;7:390–4.
- [19] Könönen MHO, Lavonius ET, Kivilahti JK. SEM observations on stress corrosion cracking of commercially pure titanium in a topical fluoride solution. *Dent Mater* 1995;11:269–72.
- [20] Boere G. Influence of fluoride on titanium in an acidic environment measured by polarization resistance technique. *J Appl Biomater* 1995;6:283–8.
- [21] Toumelin-Chemla F, Rouelle F, Burdairon G. Corrosive properties of fluoride-containing odontologic gels against titanium. *J Dent* 1996;24:109–15.
- [22] Mimura H, Miyagawa Y. Electrochemical corrosion behavior of titanium castings: Part 1. Effects of degree of surface polishing and kind of solution. *Jpn J Dent Mater Dev* 1996;15:283–5.
- [23] Oda Y, Kawada E, Yoshinari M, Hasegawa K, Okabe T. The influence of fluoride concentration on the corrosion of titanium and titanium alloys. *Jpn J Dent Mater Dev* 1996;15:317–22.
- [24] Reclaru L, Meyer J-M. Effects of fluorides on titanium and other dental alloys in dentistry. *Biomaterials* 1998;19:85–92.
- [25] Nakagawa M, Matsuya S, Shiraishi T, Ohta M. Effect of fluoride concentration and pH on corrosion behavior of titanium for dental use. *J Dent Res* 1999;78:1568–72.
- [26] Nakagawa M, Matsuya S, Udoh K. Corrosion behavior of pure titanium and titanium alloys in fluoride-containing solutions. *Dent Mater J* 2001;20:305–14.
- [27] Nakagawa M, Matsuya S, Udoh K. Effects of fluoride and dissolved oxygen concentrations on the corrosion behavior of pure titanium and titanium alloys. *Dent Mater J* 2002;21:83–92.
- [28] Huang H-H. Effects of fluoride concentration and elastic tensile strain on the corrosion resistance of commercially pure titanium. *Biomaterials* 2002;23:59–63.
- [29] Schiff N, Grosogeat B, Lissac M, Dalard F. Influence of fluoride content and pH on the corrosion resistance of titanium and its alloys. *Biomaterials* 2002;23:1995–2002.
- [30] Shih DS, Birnbaum HK. Evidence of FCC titanium hydride formation in β titanium alloy: an X-ray diffraction study. *Scr Metall* 1986;20:1261–4.
- [31] Nakasa K, Liu J. Bending strength of hydrogen-charged Ti–13V–11Cr–3Al alloy. *J Jpn Inst Metals* 1991;55:922–7.
- [32] Lederich RJ, Schwartz DS, Sastry SML. Effects of internal hydrogen on microstructures and mechanical properties of β 21S and Ti–15–3. In: Eylon D, Boyer RR, Koss DA, editors. *Beta titanium alloys in the 1990s*. Warrendale, PA: TMS, 1993. p. 159–69.
- [33] Young Jr GA, Scully JR. The effects of hydrogen on the room temperature mechanical properties of Ti–15V–3Cr–3Al–3Sn and Ti–15Mo–3Nb–3Al. In: Eylon D, Boyer RR, Koss DA, editors. *Beta titanium alloys in the 1990s*. Warrendale, PA: TMS, 1993. p. 147–58.
- [34] Young Jr GA, Scully JR. Effects of hydrogen on the mechanical properties of a Ti–Mo–Nb–Al alloy. *Scr Metall Mater* 1993;28:507–12.
- [35] Young Jr GA, Scully JR. Hydrogen embrittlement of solution heat-treated and aged β -titanium alloys Ti–15% V–3% Cr–3% Al–3% Sn and Ti–15% Mo–3% Nb–3% Al. *Corrosion* 1994;50:919–33.
- [36] Pound BG. Hydrogen trapping in aged β -titanium alloys. *Acta Mater* 1997;45:2059–68.
- [37] Teter DF, Robertson IM, Birnbaum HK. The effects of hydrogen on the deformation and fracture of β -titanium. *Acta Mater* 2001;49:4313–23.
- [38] Pardee WJ, Paton NE. Model of sustained load cracking by hydride growth in Ti alloys. *Metall Trans A* 1980;11A:1391–400.
- [39] Shin DS, Robertson IM, Birnbaum HK. Hydrogen embrittlement of β titanium: in situ tem studies. *Acta Metall* 1988;36:111–24.
- [40] Wang ZF, Briant CL, Kumar KS. Hydrogen embrittlement of grade 2 and grade 3 titanium in 6% sodium chloride solution. *Corrosion* 1998;54:553–60.

Hydrogen embrittlement of Ni-Ti superelastic alloy in fluoride solution

Ken'ichi Yokoyama,¹ Kazuyuki Kaneko,² Keiji Moriyama,² Kenzo Asaoka,¹ Jun'ichi Sakai,³ Michihiko Nagumo³

¹Department of Dental Engineering, School of Dentistry, The University of Tokushima, 3-18-15 Kuramoto-cho, Tokushima, 770-8504, Japan

²Department of Orthodontics, School of Dentistry, The University of Tokushima, 3-18-15 Kuramoto-cho, Tokushima, 770-8504, Japan

³Department of Materials Science and Engineering, Waseda University, 3-4-1 Okubo Shinjuku-ku, Tokyo, 169-8555, Japan

Received 3 January 2002; accepted 19 June 2002

Abstract: Hydrogen embrittlement of Ni-Ti superelastic alloy in a fluoride solution (0.2% APF) has been investigated by means of a tensile test (after immersion) and hydrogen thermal desorption analysis. Upon immersion, the tensile strength of the alloy decreased to the critical stress level of martensite transformation. Hydrogen desorption of the immersed specimens appeared with a peak at around 500°C. The amount of absorbed hydrogen in the alloy ranged from 100 to 1000 mass ppm when immersed in the fluoride solution for 2 to 24 h. The immersion in the fluoride solution led

to the degradation of mechanical properties due to hydrogen embrittlement. The results of the present study imply that one reason that Ti and its alloys fracture in the oral cavity is the fact that hydrogen is absorbed in a fluoride solution, such as prophylactic agents. © 2003 Wiley Periodicals, Inc. *J Biomed Mater Res* 65A: 182–187, 2003

Key words: Ni-Ti; hydrogen embrittlement; fluoride; corrosion

INTRODUCTION

Ni-Ti superelastic alloys are used widely in orthodontic wires because of their unique superelastic property, excellent ductility, good fatigue life, good corrosion resistance, and good biocompatibility.^{1–4} However, from a practical point of view, the corrosion and fracture of the alloys in the oral cavity remain important problems.^{5–7}

The corrosion resistance of Ni-Ti superelastic alloys has been investigated mostly by means of electrochemical polarization techniques. The alloys show good corrosion resistance in various test solutions, such as artificial saliva, Ringer's solution, and NaCl solution.^{8–10} However, discoloration or corrosion of the alloy has been widely observed in practice.^{5,11,12} One reason for this that has been reported is that the corrosion resistance of Ti is lost in solutions that contain fluoride.^{13–21} Fluoride is contained in toothpastes,

prophylactic agents, and dental rinses because fluoride has a cariostatic effect. In general, the caries-preventing prophylactics contain 100 to 10,000 ppm of F, with a pH value between about 3.5 and neutral. In addition, foods and drinks such as tea contain fluoride although in very small amounts.

Environmental degradation and fracture should be considered when the alloys are used under severe environmental conditions, such as those in the oral cavity. However, the environmental effects on the deformation and fracture behaviors of the alloys have been the subject of very few studies. In our previous articles, we demonstrated the degradation and fracture of Ni-Ti alloy and Ti caused by hydrogen absorption in the oral cavity or in the human body, both of which provide a saline solution.^{22–25} Stress corrosion cracking of Ti in a topical fluoride solution also was reported.²⁶ However, few studies have been carried out on the hydrogen embrittlement of Ti and its alloys in fluoride solutions.

The purpose of the present study was to examine the degradation and fracture of a Ni-Ti superelastic alloy in a fluoride solution and the associated behaviors of hydrogen absorption. This was done by means

Correspondence to: K. Yokoyama; e-mail: yokken@dent.tokushima-u.ac.jp

TABLE I
Mechanical Properties and Transformation Temperatures of the Tested Ni-Ti Superelastic Alloy

Critical Stress (MPa)	Tensile Strength (MPa)	Reduction of Area (%)	Transformation Temperature (°C)			
			A_f	A_s	M_s	M_f
530 ± 16.7	1250 ± 7.2	54.7	-4	-26	-3	-27

of hydrogen thermal desorption analysis (TDA) or hydrogen thermal desorption spectroscopy (TDS) applied extensively for the study of hydrogen embrittlement in steel.²⁷⁻²⁹

MATERIALS AND METHODS

Commercial Ni-Ti superelastic alloy wires with a diameter of 0.50 mm were cut as specimens of 50 mm in length. The martensite to austenite transformation temperatures and the mechanical properties of the alloy are given in Table I. The phase transformation temperatures of the alloy were determined by an electrical resistance method. The critical stress of martensite transformation and the tensile strength at room temperature were 530 and 1250 MPa, respectively. The specimens were polished with #600-grit SiC paper and ultrasonically washed in acetone for 5 min. The specimens were immersed separately in 10 mL of a 0.2% acidulated phosphate fluoride (APF; 0.2 mass % NaF + 0.17 mass % H₃PO₄) aqueous solution with pH 5.0 at 37°C for 2 to 24 h. The concentration of the fluoride was 900 ppm F and was similar to that used in toothpastes.

Tensile tests of the immersed alloys were carried out at room temperature on a Shimadzu Autograph AG-100A machine at a strain rate of 8.33×10^{-4} /s within a few minutes after removal from the solution. The gauge length of the specimens was 10 mm. Weight loss of the immersed alloys with time was measured, and the standard deviation was calculated from the results obtained from five specimens. The immersed wires were embedded in an epoxy resin and polished. After 24 h from removal from the solution, hardness tests were carried out on the transverse cross section from the periphery to the center of the wire at intervals of 0.05 mm. Measurements were performed under an applied load of 0.98N for 15 s. The fracture surface of tensile-tested specimens was examined with a scanning electron microscope (SEM).

TDA was conducted with a gas chromatograph at a heating rate of 100°C/h using Ar as the carrier gas at a flow rate of 0.33 mL/s. Measurement of hydrogen concentration at 300-s intervals was started 600 s after removal of the specimen from the solution.

RESULTS

The tensile test results in terms of the critical stress and the tensile strength as a function of the immersion time are shown in Figure 1. The tensile strength

slightly increased with immersion time up to 3 h, then decreased rapidly. The decrease was from 1250 to 600 MPa, after which the tensile strength remained unchanged even after immersion for more than 6 h. The critical stress of martensite transformation gradually increased from 530 to 600 MPa as the immersion time increased up to 5 h. It was observed that the fracture of the immersed alloy took place before martensite transformation when the immersion time was longer than 6 h; that is, the tensile strength agrees with the critical stress at immersion times longer than 6 h.

Figure 2 shows fractographs of a specimen immersed for 24 h. The outer part [Fig. 2(b)] of the fracture surface was fairly flat whereas the central part [Fig. 2(c)] was composed of primary shallow dimples. This suggests that failure was initiated at the outer part of the specimen. In addition, the fracture surfaces did not show reduction in area even when the immersion time was longer than 3 h.

Figure 3 shows the fraction of the dimple pattern area in the fracture surface as a function of the immersion time. The dimple pattern area decreased initially with increasing immersion time, then reached a steady value. In other words, the brittle outer part became up

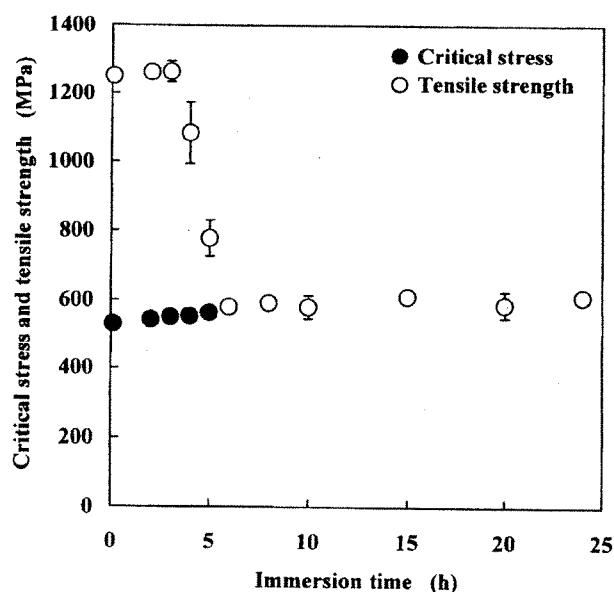


Figure 1. Tensile strength and critical stress of specimens immersed in 0.2% APF solution as a function of immersion time. The standard deviation was calculated from the results obtained from five specimens.

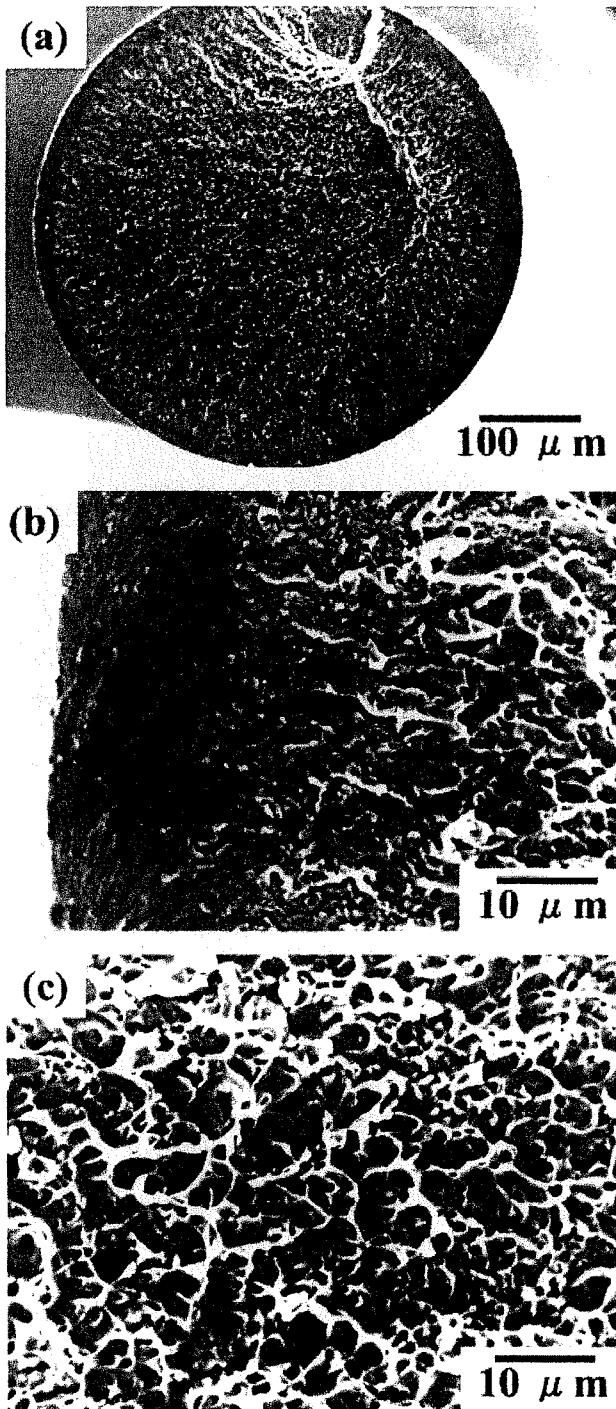


Figure 2. SEM micrographs of typical fracture surface of a specimen immersed in the solution for (a) 24 h. (b) Outer and (c) central parts of the fracture surface.

to 50–100 μm thick when the immersion time exceeded 10 h. The Vickers microhardness of the alloy subjected to the immersion test is shown in Figure 4. The hardness of the as-received alloy was about 350 at any part. It was noted that the hardness number in the outer part had a high value of 400 in the specimen

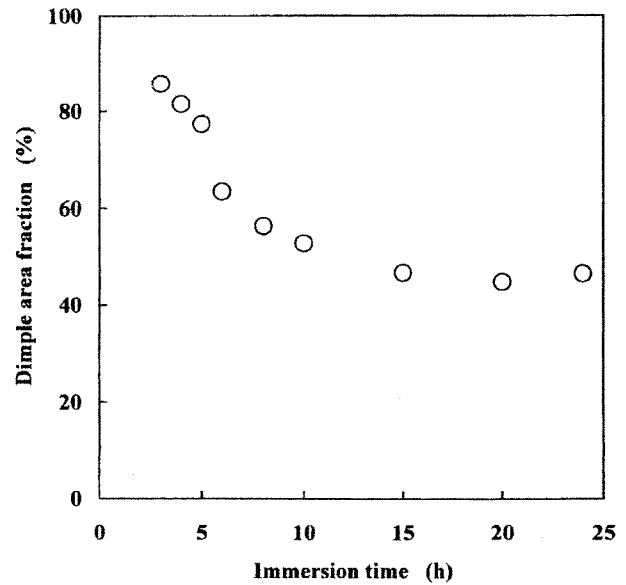


Figure 3. Fraction of dimple pattern area in the fracture surface as a function of immersion time.

immersed for 24 h. Typical SEM micrographs of the outer surface of an as-received and a 24-h immersed specimen are shown in Figure 5(a,b), respectively. The surface after immersion showed general corrosion. The progress of corrosion relative to weight loss, which increased with increasing immersion time, is shown in Figure 6.

The thermal desorption of hydrogen appeared with a desorption-rate peak at around 500°C. Figure 7

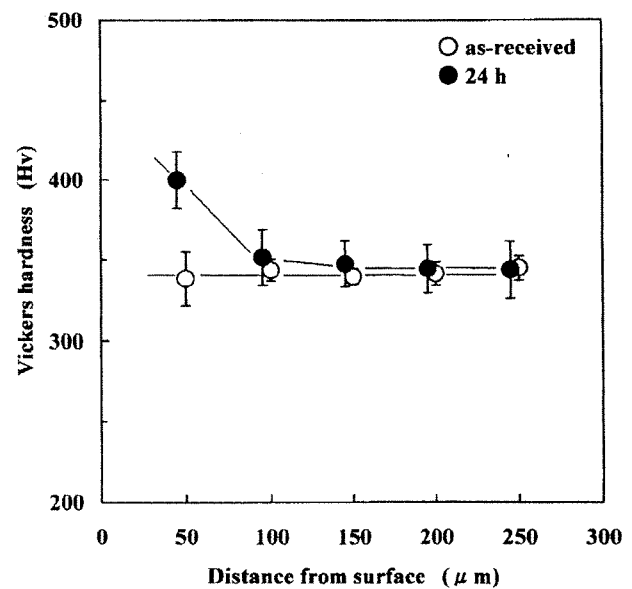


Figure 4. Vickers microhardness of as-received and 24-h immersed specimens. The hardness was measured at intervals of 0.05 mm, and the standard deviation was calculated from eight indentations.

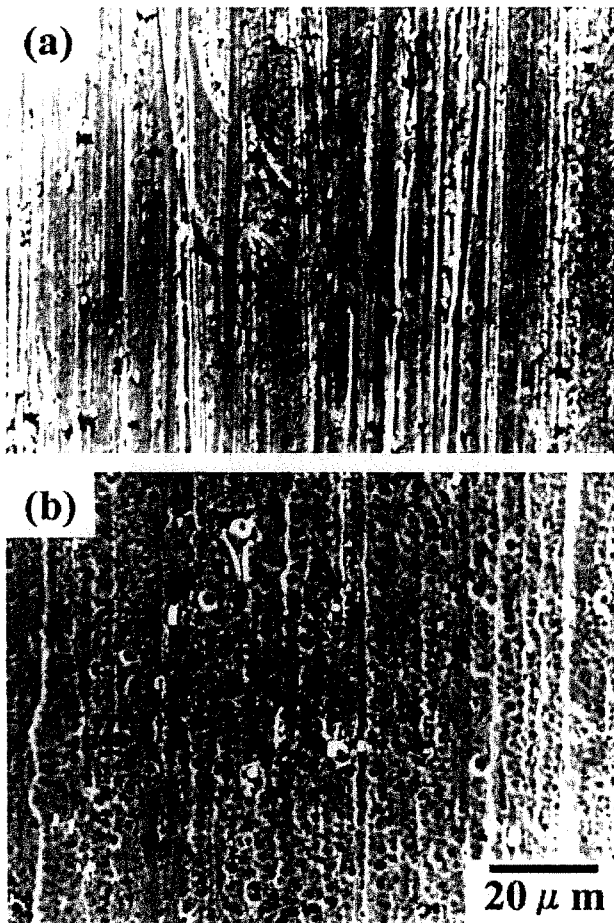


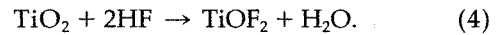
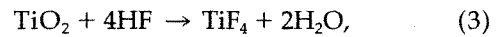
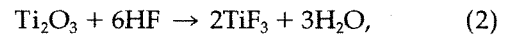
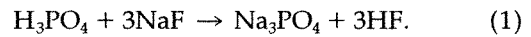
Figure 5. SEM micrographs of the typical surface of (a) as-received and (b) 24-h immersed specimens.

shows TDA curves of specimens immersed for up to 24 h. The progress of hydrogen entry into the alloy was denoted by the increase in the total desorbed hydrogen, defined as the integrated peak intensity, relative to the immersion time. The total amount of hydrogen desorbed up to 600°C is shown as a function of immersion time in Figure 8. The amount of the desorbed hydrogen, that is, hydrogen absorbed during immersion, increased with increasing immersion time.

DISCUSSION

One important finding in the present study is the hydrogen embrittlement of Ni-Ti superelastic alloy in 0.2% APF (0.2 mass % NaF + 0.17 mass % H₃PO₄) aqueous solution. The effects of fluoride ion on the corrosion resistance of Ti and its alloys have been reported by several authors.¹³⁻²¹ It was considered that hydrofluoric acid (HF), which is produced according to the reaction shown in Equation (1), dis-

solves the protective oxide film on the surface of Ti and its alloys, according to Equations (2-4).^{16,19,21}



In the present case, the oxide film on the surface of Ni-Ti superelastic alloy most likely is destroyed in the same manner as the above reactions. The loss of the oxide film may lead to the absorption of hydrogen from various solutions because of the high affinity of Ti with hydrogen.

In previous studies, hydrogen embrittlement of Ni-Ti superelastic alloy was observed under cathodic hydrogen precharging in 0.9% NaCl aqueous solution.²²⁻²⁴ In the tensile test of the alloy that was hydrogen-precharged for various periods, fracture took place before martensite transformation, and the increase in charging time and current density accelerated the failure. The formation of brittle hydrides and the presence of diffusible hydrogen were thought to be the causes. The formation of titanium hydride with a body-centered tetragonal structure by electrochemical charging was reported.^{30,31}

In the present study, the results obtained by immersion in a 0.2% APF solution for various periods are similar to those of the previous study of cathodic hydrogen precharging. The high hardness observed in the outer part of the specimen immersed for 24 h, as

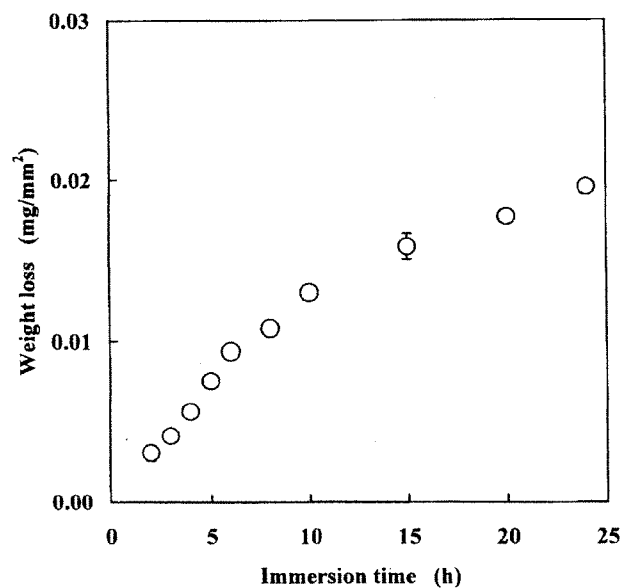


Figure 6. Weight loss of specimens immersed in 10 mL of 0.2% APF solution. The standard deviation was calculated from the results of five measurements.

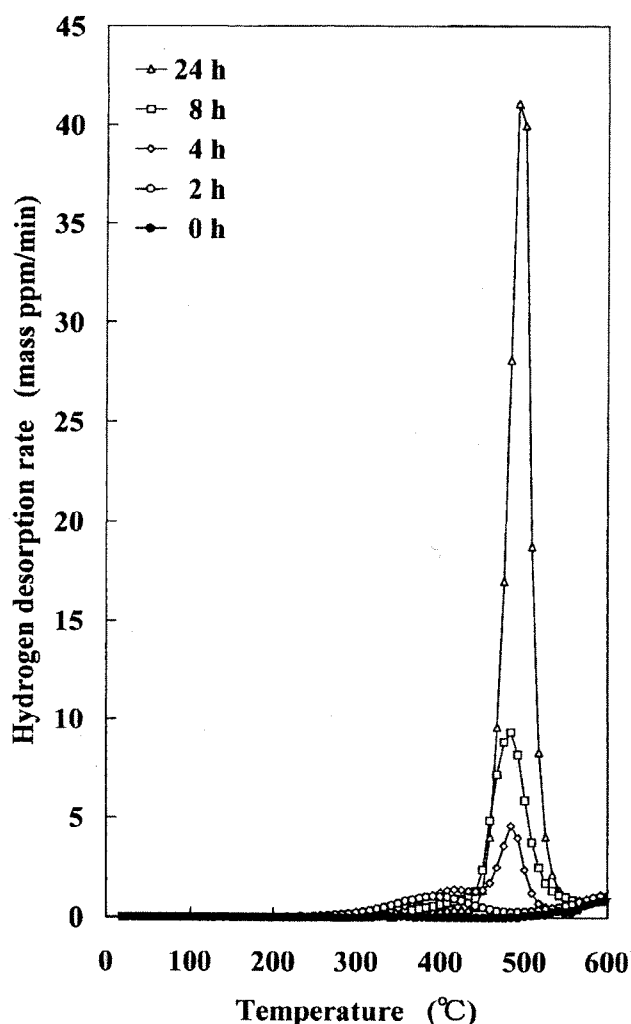


Figure 7. Hydrogen thermal desorption curves from specimens immersed in 0.2% APF solution for up to 24 h at 37°C.

shown in Figure 4, also is similar to the previous result,²⁴ suggesting the formation of hydride.

The thermal desorption behavior gives information relative to the hydrogen trapping sites and the decomposition of hydrides from the temperature profile and the amount of desorption.²⁷ In the present case, a single desorption peak appeared at around 500°C, as shown in Figure 7, in contrast to the case of cathodic hydrogen precharging that gave rise to two desorption peaks at around 200 and 300°C.^{22,24} The peak temperature of 500°C is close to the decomposition temperature of TiH_2 , suggesting the formation of hydrides at the time of immersion in APF solution. The TDA behaviors imply that the states of hydrogen in the alloy are different between the two hydrogen-charging conditions. The details of the desorption behavior of Ni-Ti superelastic alloy will be reported later.

In the present case, hydrogen concentration continuously increased during immersion, as shown in Fig-

ure 8. The total amount of desorbed hydrogen was as much as 1000 mass ppm at 24-h of immersion, which is much higher than 1 mass ppm, the value normally observed in steels. Hydrogen concentration often has been used as a measure of the occurrence of embrittlement, but it is not generally the case. For example, in a sustained-load fracture test of a high-strength martensitic steel, it has been demonstrated that an alternating hydrogen-charging potential accelerated failure with a smaller amount of hydrogen than that in the condition of constant hydrogen-charging potential.³² The dominant role of strain-induced vacancies in the embrittlement coupled with hydrogen was consistent.^{29,32} The mechanism of hydrogen embrittlement may differ depending on the material and the environment. In Ni-Ti superelastic alloys used in environments that contain fluoride ion, the effect of hydride operating in the mechanism of hydrogen embrittlement is not ruled out, and further work is needed to identify hydride formation and its relationship to embrittlement.

CONCLUSIONS

The degradation and fracture of Ni-Ti superelastic alloy in fluoride solution have been investigated from the viewpoint of hydrogen embrittlement. The alloy absorbs substantial amounts of hydrogen in 0.2% APF aqueous solution. Hydrogen TDA showed that a single desorption-rate peak appeared at around 500°C. The amount of total absorbed hydrogen increased with the immersion time. When the amount of ab-

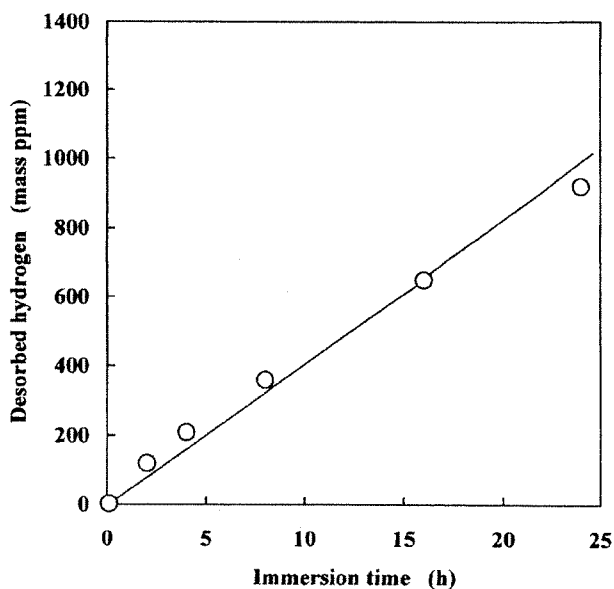


Figure 8. Amount of desorbed hydrogen from thermal desorption analysis as a function of immersion time.

sorbed hydrogen exceeded 200 mass ppm, the tensile strength of immersed alloy was reduced to the critical stress level of martensite transformation. It is concluded that one of the reasons for the fracture of Ti and its alloys in the oral cavity is hydrogen embrittlement in fluoride solution.

References

1. Andreasen GF, Hilleman TB. An evaluation of 55 cobalt substituted nitinol wire for orthodontics. *J Am Dent Assoc* 1971; 82:1373-1375.
2. Miyazaki S, Otsuka K, Suzuki Y. Transformation pseudoelasticity and deformation behavior in a Ti-50.6at% Ni alloy. *Scripta Metallurgica* 1981;15:287-292.
3. Shabalovskaya SA. On the nature of the biocompatibility and on medical applications of NiTi shape memory and superelastic alloys. *Bio-Med Mater Eng* 1996;6:267-289.
4. McKelvey AL, Ritchie RO. Fatigue-crack growth behavior in the superelastic and shape-memory alloy nitinol. *Metallurg Mater Trans A* 2001;32A:731-776.
5. Edie JW, Andreasen GF, Zaytoun MP. Surface corrosion of nitinol and stainless steel under clinical conditions. *Angle Orthod* 1981;51:319-324.
6. Harris EF, Newman SM, Nicholson JA. Nitinol arch wire in a simulated oral environment: Changes in mechanical properties. *Am J Orthod Dentofacial Orthop* 1988;93:508-513.
7. Hudgins JJ, Bagby MD, Erickson LC. The effect of long-term deflection on permanent deformation of nickel-titanium archwires. *Angle Orthod* 1990;60:283-288.
8. Wever DJ, Veldhuizen AG, de Vries J, Busscher HJ, Uges DRA, van Horn JR. Electrochemical and surface characterization of a nickel-titanium alloy. *Biomaterials* 1998;19:761-769.
9. Thierry B, Tabrizian M, Trepanier C, Savadogo O, Yahia L'H. Effect of surface treatment and sterilization processes on the corrosion behavior of NiTi shape memory alloy. *J Biomed Mater Res* 2000;51:685-693.
10. Montero-Ocampo C, Lopez H, Salinas Rodriguez A. Effect of compressive straining on corrosion resistance of a shape memory Ni-Ti alloy in Ringer's solution. *J Biomed Mater Res* 1996; 32:583-591.
11. Grimsdottir MR, Hensten-Pettersen A. Surface analysis of nickel-titanium archwire used in vivo. *Dent Mater* 1997;13: 163-167.
12. Eliades T, Eliades G, Athanasiou AE, Bradley TG. Surface characterization of retrieved NiTi orthodontic archwires. *Euro J Orthod* 2000;22:317-326.
13. Lausmaa J, Kasemo B, Hansson S. Accelerated oxide grown on titanium implants during autoclaving caused by fluoride contamination. *Biomaterials* 1985;6:23-27.
14. Siirilä HS, Könönen M. The effect of oral topical fluorides on the surface of commercially pure titanium. *Int J Oral Maxillofac Impl* 1991;6:50-54.
15. Pröbster L, Lin W, Hüttemann H. Effect of fluoride prophylactic agents on titanium surfaces. *Int J Oral Maxillofac Impl* 1992;7:390-394.
16. Boere G. Influence of fluoride on titanium in an acidic environment measured by polarization resistance technique. *J Appl Biomater* 1995;6:283-288.
17. Toumelin-Chemla F, Rouelle F, Burdairon G. Corrosive properties of fluoride-containing odontologic gels against titanium. *J Dent* 1996;24:109-115.
18. Mimura H, Miyagawa Y. Electrochemical corrosion behavior of titanium castings. I. Effects of degree of surface polishing and kind of solution. *Jpn J Dent Mater Dev* 1996;15:283-295.
19. Oda Y, Kawada E, Yoshinari M, Hasegawa K, Okabe T. The influence of fluoride concentration on the corrosion of titanium and titanium alloys. *Jpn J Dent Mater Dev* 1996;15:317-322.
20. Reclaru L, Meyer J-M. Effects of fluorides on titanium and other dental alloys in dentistry. *Biomaterials* 1998;19:85-92.
21. Nakagawa M, Matsuya S, Shiraiishi T, Ohta M. Effect of fluoride concentration and pH on corrosion behavior of titanium for dental use. *J Dent Res* 1999;78:1568-1572.
22. Yokoyama K, Hamada K, Asaoka K. Fracture analysis of hydrogen-charged nickel-titanium superelastic alloy. *Mater Trans* 2001;42:141-144.
23. Yokoyama K, Hamada K, Moriyama K, Asaoka K. Degradation and fracture of Ni-Ti superelastic wire in an oral cavity. *Biomaterials* 2001;22:2257-2262.
24. Asaoka K, Yokoyama K, Nagumo M. Hydrogen embrittlement of nickel-titanium alloy in biological environment. *Metallurg Mater Trans A* 2002;33A:495-501.
25. Yokoyama K, Ichikawa T, Murakami H, Miyamoto Y, Asaoka K. Fracture mechanisms of retrieved titanium screw thread in dental implant. *Biomaterials* 2002;23:2459-2465.
26. Könönen MHO, Lavonius ET, Kivilahti JK. SEM observations on stress corrosion cracking of commercially pure titanium in a topical fluoride solution. *Dent Mater* 1995;11:269-272.
27. Choo WY, Lee JY. Thermal analysis of trapped hydrogen in pure iron. *Metallurg Trans A* 1982;13A:135-182.
28. Ono K, Meshii M. Hydrogen detrapping from grain boundaries and dislocations in high purity iron. *Acta Metallurg Mater* 1992;40:1357-1364.
29. Nagumo M, Nakamura M, Takai K. Hydrogen thermal desorption relevant to delayed-fracture susceptibility of high-strength steels. *Metallurg Mater Trans A* 2001;32A:339-347.
30. Wu SK, Wayman CM. Interstitial ordering of hydrogen and oxygen in TiNi alloys. *Acta Metallurg* 1988;36:1005-1013.
31. Nam TH, Shimizu K, Saburi T, Nenno S. Crystal structure of a hydride formed by electrochemical hydrogenation in a Ti-Ni-Al alloy. *Mater Trans JIM* 1989;30:539-548.
32. Nagumo M, Uyama H, Yoshizawa M. Accelerated failure in high strength steel by alternating hydrogen-charging potential. *Scripta Mater* 2001;44:947-952.

Susceptibility to delayed fracture of Ni–Ti superelastic alloy

Ken'ichi Yokoyama^{a,*}, Shiyozo Watabe^b, Kenichi Hamada^a, Jun'ichi Sakai^b,
Kenzo Asaoka^a, Michihiko Nagumo^b

^a Department of Dental Engineering, School of Dentistry, The University of Tokushima, 3-18-15 Kuramoto-cho, Tokushima 770-8504, Japan

^b Department of Materials Science and Engineering, Waseda University, 3-4-1 Okubo Shinjuku-ku, Tokyo 169-8555, Japan

Received 18 January 2002; received in revised form 7 March 2002

Abstract

The susceptibility of Ni–Ti superelastic alloys to hydrogen embrittlement has been examined by means of a delayed-fracture test and hydrogen thermal desorption analysis. It was found that the time to fracture was drastically reduced when the applied stress exceeded the critical stress for martensite transformation. In the applied stress range lower than the critical stress, the time to fracture lessened in the order of instability of the alloys to undergo reversible martensite transformation. Hydrogen thermal desorption of specimens subjected to delayed-fracture test is classified into two types according to the applied stress level. The amount of desorbed hydrogen was markedly increased when the applied stress was higher than the critical stress. It was concluded that Ni–Ti superelastic alloys transformed to martensite are sensitive to environmental conditions accompanying accelerated hydrogen embrittlement.

© 2002 Elsevier Science B.V. All rights reserved.

Keywords: Ni–Ti; Hydrogen embrittlement; Delayed fracture; Thermal desorption analysis

1. Introduction

Ni–Ti alloys are widely used in industrial and medical devices because of their unique shape memory and/or superelastic effect, excellent ductility, and good fatigue life. In addition, Ni–Ti alloys exhibit good corrosion resistance and biocompatibility [1–5]. The shape memory and/or superelastic effect of Ni–Ti alloys results from martensitic transformation that takes place from a B2 to a B19' structure [6–9]. On loading, superelasticity appears at a critical stress, being associated with reversible martensite transformation. The transformation pseudoelasticity and deformation behavior of the alloys have been investigated [10,11]. However, the environmental effects on deformation and fracture behavior of the alloys remain to be examined. Environmental degradation is a very important consideration when the alloys are used under severe environmental conditions. In the human body, discoloration or corro-

sion of medical devices is widely observed, and their fracture occurs even though Ti and its alloys show high corrosion resistance [12–15]. For example, Ni–Ti orthodontic arch wires often exhibit failure in the oral cavity a few months after setting [16,17]. Therefore, it is important to investigate the environmental factors and their effects on the fracture behavior of Ni–Ti superelastic alloys. Particularly in the biomedical field, Ni–Ti alloys are expected to become more widely applicable in the future if such problems are solved.

One of the environmental factors is hydrogen. The influence of hydrogen on the shape memory and superelastic properties of Ni–Ti alloys has been reported [18–21]. We have also presented several papers on the degradation of the mechanical properties of non-loaded Ni–Ti superelastic alloys charged with hydrogen for various periods [17,22,23]. However, understanding the degradation of orthodontic arch wires in the oral cavity requires an evaluation of the effects of loading stress during hydrogen charging, namely, delayed-fracture tests.

In general, the delayed-fracture test is important for characterizing the hydrogen susceptibility of high-

* Corresponding author. Tel.: +81-88-633-7334; fax: +81-88-633-9125.

E-mail address: yokken@dent.tokushima-u.ac.jp (K. Yokoyama).

strength steel products such as fasteners and prestressed concrete bars [24–26]. In these materials, the susceptibility to hydrogen embrittlement is enhanced with increasing strength. Ni–Ti superelastic alloys show strength levels higher than 1200 MPa. However, no study of the delayed-fracture test of the alloys has been published thus far. The time to delayed fracture is one of the important properties of Ni–Ti alloys to be used in biomedical applications.

The purpose of the present study is to examine the delayed fracture of Ni–Ti superelastic alloys and the associated behavior of hydrogen absorption by means of hydrogen thermal desorption analysis (TDA). Hydrogen TDA has been employed as a means of detecting defects that act as hydrogen traps [27–29]. In high-strength steels, the desorption-rate peak appears at around 100–200 °C. On the other hand, in Ni–Ti superelastic alloys, two peaks appear at around 200 and 300 °C [23]. The amount of absorbed hydrogen i.e. the integrated desorption-rate peak intensity, and the desorption curve profile, are required to understand the delayed-fracture characteristics.

2. Experimental procedure

A commercial Ni–Ti (Ni: 55 mass%, Ti: balance) superelastic alloy of 0.50 mm diameter was used. The as-received superelastic alloy (specimen A) was heated to 500 °C (specimen B) or 550 °C (specimen C) for 30 min in an evacuated quartz tube (10^{-1} Pa), and then quenched in ice water. Temperatures of 500 and 550 °C were chosen to vary the martensite transformation stress of the as-received alloy. The surface of the specimens was finished using a #600 SiC paper to eliminate accretions. The transformation temperatures in the non-loaded state were measured for each specimen by means of an electrical resistance method. Tensile tests were carried out at room temperature on an Instron-type machine (Autograph AG-100A, Shimadzu) at a strain rate of $8.33 \times 10^{-4} \text{ s}^{-1}$. The total length of the specimen was 50 mm and a gage length of 10 mm was used. Hardness tests were carried out from the periphery to the center of the alloy specimen at intervals of 0.05 mm using a Vickers microhardness tester under an applied load of 0.98 N for a period of 15 s. For specimen A, measurements were conducted both before and after delayed fracture under applied stresses of 450 and 600 MPa for 5 h. Fig. 1 shows the scheme of the apparatus used for the delayed-fracture test under a sustained load at room temperature. A direct-current generator was used for hydrogen charging. Platinum and the specimen were immersed in 0.9 mass% NaCl aqueous solution as the anode and the cathode, respectively. The immersed length in the solution was 50 mm for all specimens. The fracture surface of the

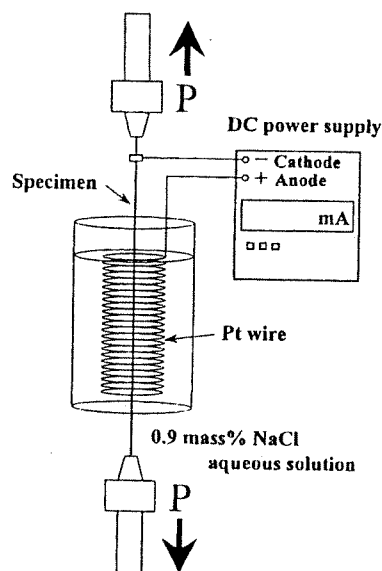


Fig. 1. Schematic diagram of delayed-fracture test apparatus.

specimens was examined using a scanning electron microscope (SEM).

The amount of desorbed hydrogen was measured for specimens A and C, which were subjected to delayed-fracture test for 5 h with a current density of 10 A m^{-2} . The starting time of TDA after the removal from the electrolyte solution was less than 10 min. Both sides of a specimen, immersed in the solution (50 mm in length) were cut into 30-mm-long pieces and subjected to ultrasonic cleaning with acetone for 2 min. The specimen was dried in ambient and used for measurement. A gas chromatograph was used for the detection of hydrogen with argon at a flow rate of 20 ml min^{-1} as the carrier gas. Sampling was conducted at 5-min intervals at a heating rate of 100 °C h^{-1} .

3. Experimental results

The three kinds of alloys prepared by heat treatment have different transformation temperatures, implying different defect structures. Fig. 2 shows the stress–strain curves of specimens A, B and C. The ultimate tensile strengths of specimens A and C were almost the same, while that of specimen B was slightly higher. The mechanical properties and transformation temperatures of the specimens are given in Table 1. Here, M_s and M_f indicate the start and finish temperatures for martensite transformation, respectively, during cooling. Similarly, A_s and A_f indicate the start and finish temperatures, respectively, for the reverse transformation. In specimen A, the critical stress for martensite transformation was 530 MPa at room temperature, while it was approximately 380 MPa in specimens B and C. The heat

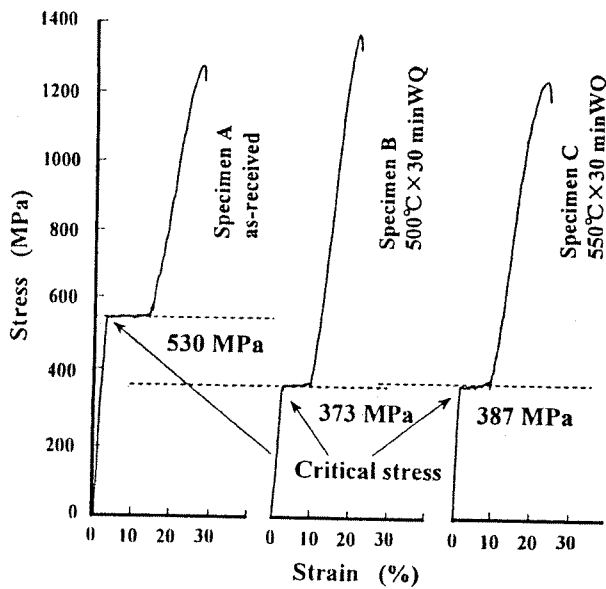


Fig. 2. Stress–strain curves of the Ni–Ti superelastic alloys: (a) specimen A, (b) specimen B, and (c) specimen C are as-received, 500 °C × 30 min WQ, and 550 °C × 30 min WQ, respectively. Strain is calculated from elongation (displacement of cross head) and the initial gauge length.

treatment of specimens B and C increased the transformation temperatures of the as-received specimen A. The decrease in the critical stress was associated with the increase in the transformation temperatures. Fig. 3 shows the Vickers microhardness of the alloys. In specimen A, the hardness number was approximately 360, while those of specimens B and C were approximately 330, being lower than that of specimen A. The hardness distribution was fairly uniform within a specimen.

The delayed-fracture test results are shown in Fig. 4 in terms of the time to fracture as a function of the applied stress. The current densities were 10 A m⁻² (Fig. 4(a)) and 100 A m⁻² (Fig. 4(b)). The time to fracture increased with decreasing applied stress, but it is noted that the slope of the linear dependence changed at the critical stress for martensite transformation in each specimen. Also, when Fig. 4(a) and (b) are compared, the increased current density reduced the time to fracture. The susceptibility to delayed fracture expressed

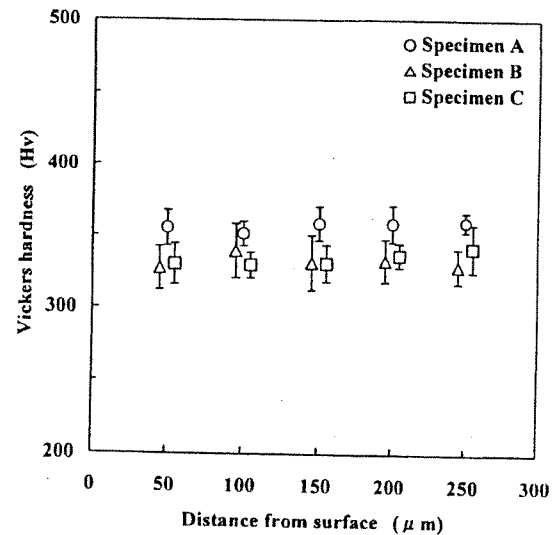


Fig. 3. Vickers microhardness values for specimens A, B, and C. The hardness was measured at intervals of 50 μm, and the standard deviation was calculated from eight indentations.

in terms of the time to fracture in the stress range lower than the critical stress was in the order of specimens A, C, and B.

Fig. 5 shows the fractographs of specimen A, which was hydrogen-charged with a current density of 10 A m⁻² under an applied stress of 450 or 600 MPa. The fractographic features corresponded to those shown in our previous paper [22]. The specimen exhibited negligible reduction in area. The outer part of the fracture surface was fairly flat, whereas the central part was composed of primary shallow dimples. It suggests that the failure was initiated at the outer part of the specimen. In Fig. 5(b) for the case of 600 MPa, crack propagation associated with river patterns was observed in the outer part, but the magnified view (Fig. 5(d)) showed flaky steps with quasi-cleavage patterns. The Vickers microhardness of specimen A subjected to delayed-fracture test is shown in Fig. 6. While the hardness of the non-charged specimen A was approximately 360, that of the charged specimens A was slightly higher, approximately 370–390. It was noted that the hardness in the outer part of specimen A charged with 10 A m⁻² for 5 h under an applied stress of 600 MPa had a high value of 420.

Table 1
Mechanical properties and transformation temperatures of the tested Ni–Ti superelastic alloys

Specimen	Critical stress (MPa)	Tensile strength (MPa)	Reduction of area (%)	Transformation temperature (°C)			
				A_r	A_s	M_s	M_f
A	530 ± 16.7	1250 ± 7.2	54.7	-4	-26	-3	-27
B	373 ± 2.7	1348 ± 17.8	54.0	26	19	24	18
C	387 ± 9.7	1215 ± 14.8	54.6	7	0	6	-1

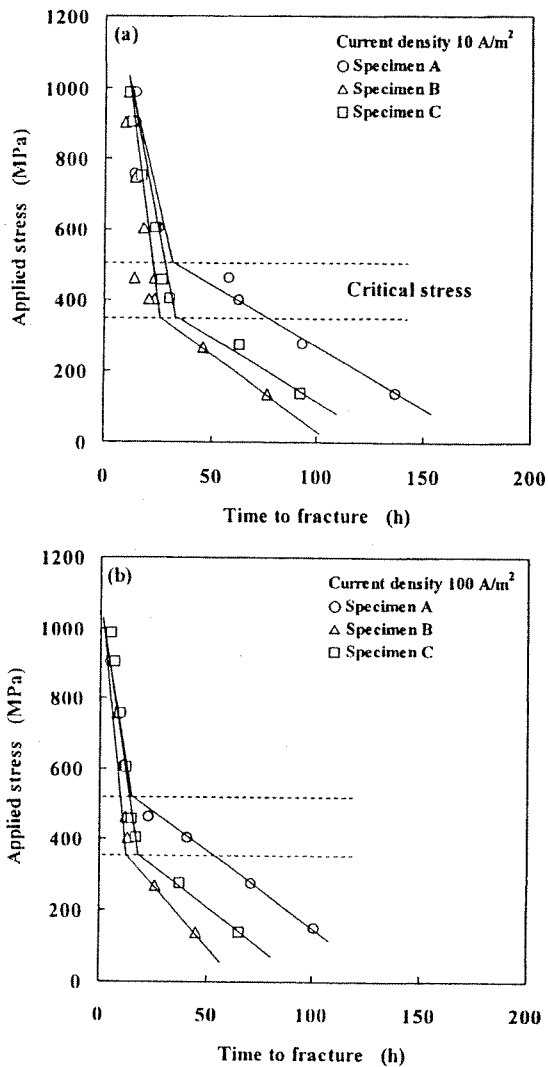


Fig. 4. Delayed-fracture diagrams of the Ni-Ti superelastic alloys charged with (a) 10 A m^{-2} and (b) 100 A m^{-2} .

Fig. 7 shows TDA curves of hydrogen charged to specimen A under various applied stresses with the current density of 10 A m^{-2} for 5 h. The desorption curves exhibited two peaks at around 200 and 300 °C. The total peak area was divided into two levels according to the applied stress, namely, whether it was higher or lower than the critical stress of 530 MPa. The total amount of desorbed hydrogen up to 400 °C is shown in Fig. 8 as a function of applied stress. When the applied stress is higher than the critical stress, hydrogen desorption i.e. hydrogen absorption, was considerably enhanced. The amount of the desorbed hydrogen increased from approximately 600 to 1000–1200 mass ppm when the applied stress exceeded the critical stress. Similar TDA curves of specimen C are shown in Fig. 9.

The charging time was 5 h with a current density of 10 A m^{-2} under the applied stress higher (450 MPa) or lower (300 MPa) than the critical stress (380 MPa). The amounts of desorbed hydrogen were 1490 and 650 mass ppm for the applied stresses of 450 and 300 MPa, respectively. It is noted that the TDA was for the specimens after unloading. The desorption was thus from the phases that remained after irreversible transformation took place.

4. Discussion

In our previous studies [22,23], we reported the tensile-test results for Ni-Ti superelastic alloy hydrogen-precharged for various periods. In that case, fracture took place before martensite transformation, and increasing charging time and current density accelerated the failure. The formation of brittle hydrides was thought to be the cause. In the present study, the delayed-fracture test under concurrent hydrogen charging and loading with various applied stresses indicated that the delayed-fracture susceptibility of Ni-Ti superelastic alloys, even if they had the same strength level, varied with the critical stress for martensite transformation. A noteworthy result shown in Fig. 4 is that the time to fracture is drastically reduced at applied stresses above the critical stress i.e. when irreversible martensite transformation took place on loading.

The associated hydrogen TDA results shown in Figs. 7–9 indicate a discontinuous increase in the amount of absorbed hydrogen at applied stresses above the critical stress. The double peaks in the TDA curves in Fig. 7 and Fig. 9 imply that at least two sources are present for the desorption, although they are difficult to distinguish. Two reasons can be considered for the increased absorption at high applied stress. One is due to the difference in the lattice constant between the parent and martensite phases. The crystal structure of the parent phase is the B2 type with a unit cell of $a_0 = 0.3015 \text{ nm}$, while that of the martensite phase is the B19' type with a unit cell of $a = 0.2898 \text{ nm}$, $b = 0.4108 \text{ nm}$, $c = 0.4646 \text{ nm}$, and $\beta = 97.78^\circ$ [9]. On the other hand, the transformation to B19' by applying stress above the critical stress is an irreversible process. It implies that the martensite involves a high density of defects. The increase in interatomic distance may increase the solubility of hydrogen, while a high density of defects may act as hydrogen traps.

The other reason is ascribed to hydride formation. A hydride formed by electrochemical charging has a body-centered tetragonal lattice with lattice parameters $a = 0.6221 \text{ nm}$ and $c = 1.2363 \text{ nm}$ [30,31]. The orientation relationship between the parent and the hydride lattice is $[100]_{\text{H}} // [100]_{\text{P}}$, $(001)_{\text{H}} // (001)_{\text{P}}$, with three orientation variants of the hydride. The crystal

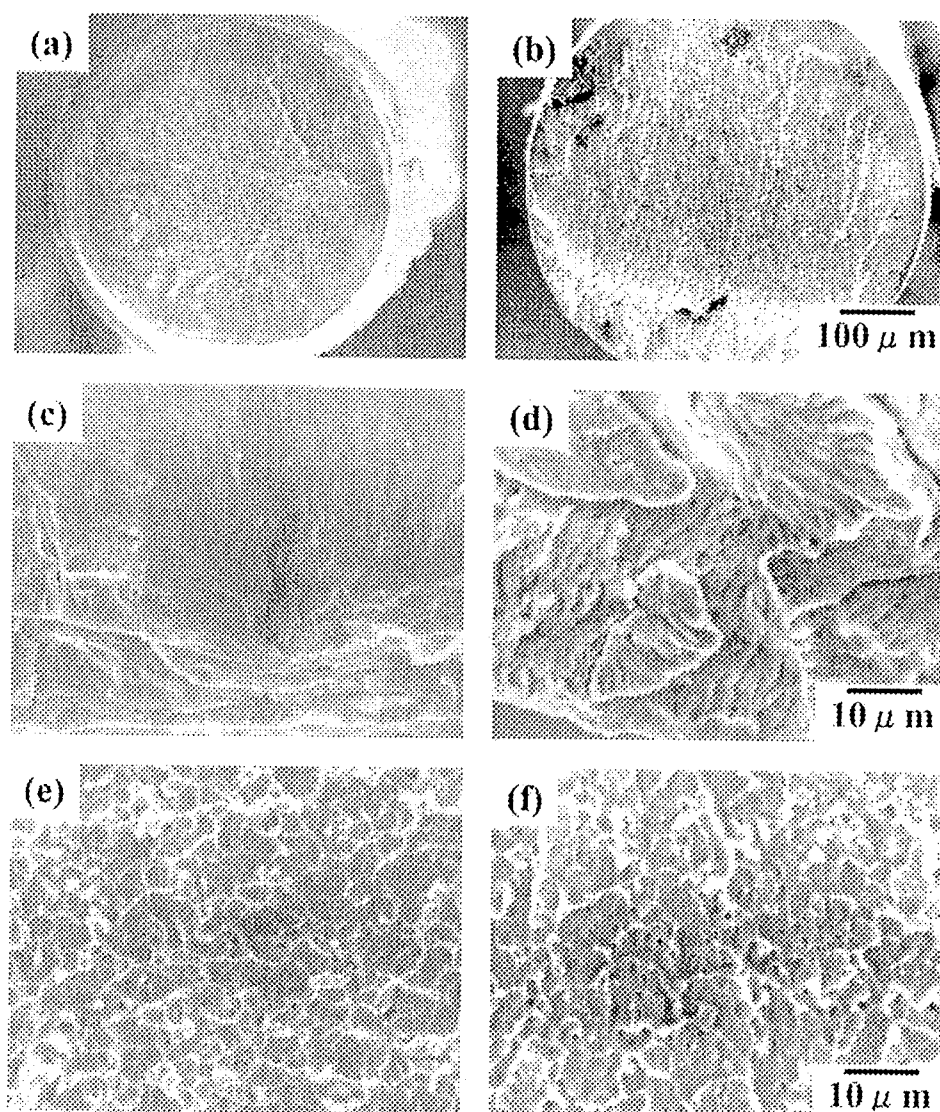


Fig. 5. SEM micrographs of the delayed-fracture surface in specimen A at applied stresses of (a) 450 and (b) 600 MPa. External (c) and internal (e) parts of the fracture surface at an applied stress of 450 MPa. External (d) and internal (f) parts of the fracture surface at an applied stress of 600 MPa.

structure and morphology are similar regardless of whether hydride formation takes place in the parent phase or the martensite phase. On the other hand, Adachi et al. reported [19] another type of hydride by charging at a current density of 1000 A m^{-2} . In the present case, the high hardness in the outer part of a specimen under the applied stress of 600 MPa, as shown in Fig. 6, might suggest the formation of such a type of hydride.

It is not certain which martensite structure for hydride formation is responsible for the increase in the amount of hydrogen absorption. The most essential issue is the mechanism of enhanced susceptibility when irreversible transformation takes place. It has been revealed [26,32]

with high-strength martensitic steels that hydrogen concentration is not the decisive factor for the delayed fracture. Instead, a model that the hydrogen-assisted increase in the deformation-induced vacancies plays a primary role in the failure has been proposed. In the present case, the formation of irreversible martensite produces a high density of defects, favoring the occurrence of the proposed mechanism. However, in Ni–Ti alloys, the amount of absorbed hydrogen is much higher than in the case of steels, and the possibility of hydride being the initiation site of brittle fracture cannot be eliminated. The fracture surface of the outer part of a specimen shown in Fig. 5(b) supports the brittle fracture model, but the magnified view in Fig. 5(d) suggests some

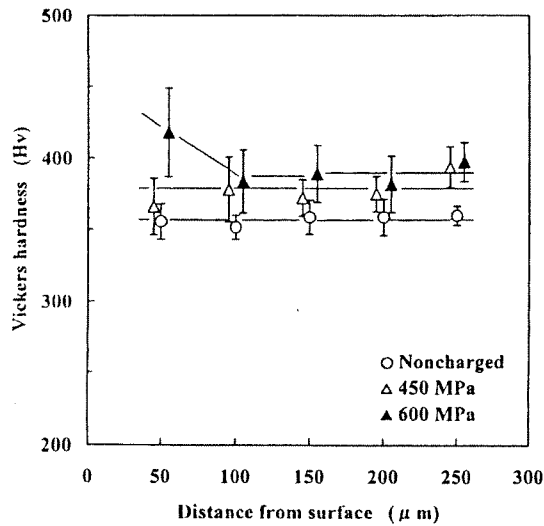


Fig. 6. Vickers microhardness values for specimen A, non-charged and with applied stresses of 450 and 600 MPa. The specimens were charged with 10 A m^{-2} for 5 h. The standard deviation was calculated from eight indentations.

contribution of plastic deformation to crack propagation. The results of further studies will be published elsewhere.

In Fig. 4(a) and (b), the time to fracture was reduced with increasing hydrogen-charging current density. This is in accord with the previous result [22,23] that showed the increase in hydrogen concentration with increasing current density. It should be noted that the stress levels at which the slope of the stress dependence of the time to fracture changes are immune to the current density. It implies that the critical stress for martensite transformation is not affected by hydrogen.

The effects of microstructure of the present Ni–Ti alloy on the susceptibility to delayed fracture appeared as the time to fracture varied with the three kinds of specimens in the applied stress range lower than the critical stress. In Fig. 4, the time to fracture at a given applied stress was in the order of specimens A, C and B, which also coincided with the order of the critical stress and the transformation temperature shown in Table 1. A higher transformation temperature is an indication of the lower stability of the B2 structure under stress, and a lower critical stress implies that the allowance of the applied stress to the critical stress is smaller. Therefore, even though the applied stress is lower than the critical stress, reversible transformation by sustained loading and/or by hydrogen entry may occur. At present, we lack direct evidence of the reversible transformation in the concerned stress range, and this aspect requires further examination for the proper use of this kind of alloy. The critical stress and delayed-fracture characteristics of the B and C specimens were similar as shown in Figs. 2 and 4. Effects of transformation temperatures in

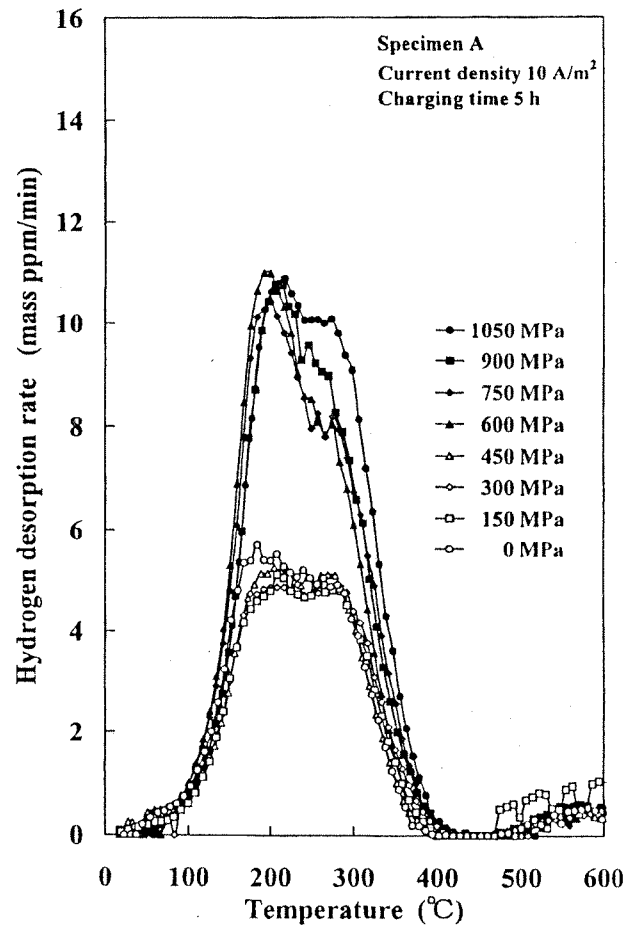


Fig. 7. Thermal desorption curves of hydrogen charged at various applied stresses for specimen A. The charging time was 5 h with the current density of 10 A m^{-2} .

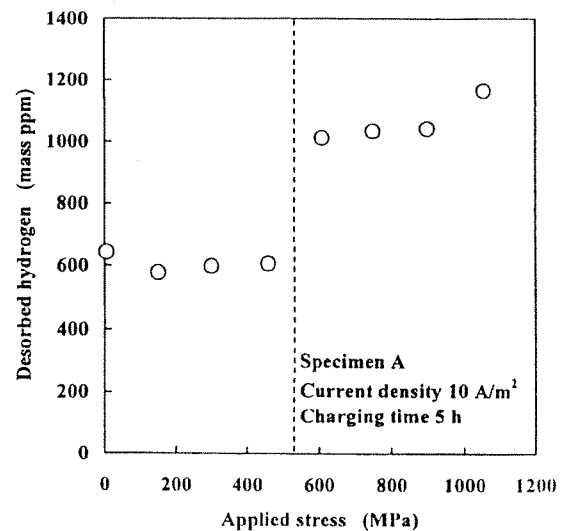


Fig. 8. Amount of desorbed hydrogen from TDA after hydrogen charging as a function of applied stress in specimen A. The charging time was 5 h with the current density of 10 A m^{-2} .

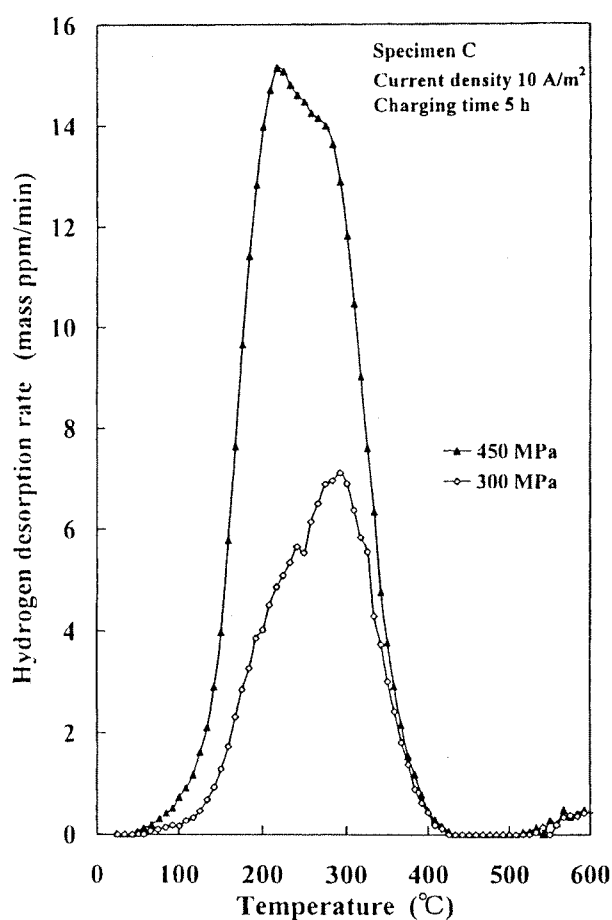


Fig. 9. Thermal desorption curves of hydrogen charged at applied stresses of 300 and 450 MPa in specimen C. The charging time was 5 h with the current density of 10 A m^{-2} .

Table 1 on hydrogen embrittlement is to be examined in future studies.

5. Conclusions

The susceptibility to hydrogen embrittlement of Ni–Ti superelastic alloys has been evaluated in terms of the time to fracture by a delayed-fracture test. The time to fracture was drastically reduced when the applied stress exceeded the critical stress for martensite transformation. In the applied stress range lower than the critical stress, the time to fracture lessened in the order of instability of the alloys to undergo reversible martensite transformation. The amount of hydrogen desorption i.e. hydrogen absorption, was markedly increased when the applied stress exceeded the critical stress. Irreversible

martensite transformation in Ni–Ti alloys increases the susceptibility of the alloys to hydrogen embrittlement, but the stability of the alloys to reversible transformation also affects the susceptibility even when the applied stress is lower than the critical stress.

References

- [1] K. Otsuka, K. Shimizu, *Int. Met. Rev.* 31 (1986) 93.
- [2] S.A. Shabalovskaya, *Bio-Med. Mater. Eng.* 6 (1996) 267.
- [3] K.N. Melton, O. Mercier, *Acta Metall.* 27 (1979) 137.
- [4] Y. Oshida, R. Sachdeva, S. Miyazaki, S. Fukuyo, *Mater. Sci. Forum* 56–58 (1990) 705.
- [5] T. Duerig, A. Pelton, D. Stöckel, *Mater. Sci. Eng. A* 273–275 (1999) 149.
- [6] K. Otsuka, T. Sawamura, K. Shimizu, *Phys. Stat. Sol.* 5(a) (1971) 457.
- [7] R.F. Henemann, G.D. Sandrock, *Scripta Metall.* 5 (1971) 801.
- [8] G.M. Michal, R. Sinclair, *Acta Cryst.* B37 (1981) 1803.
- [9] Y. Kudoh, M. Tokonami, S. Miyazaki, K. Otsuka, *Acta Metall.* 33 (1985) 2049.
- [10] S. Miyazaki, K. Otsuka, *Phil. Mag. A* 50 (1984) 393.
- [11] S. Miyazaki, K. Otsuka, Y. Suzuki, *Scripta Metall.* 15 (1981) 287.
- [12] A. Piattelli, A. Scarano, M. Piattelli, E. Vaia, S. Matarasso, *J. Periodontol.* 69 (1998) 185.
- [13] M.J. Morgan, D.F. James, R.M. Pilliar, *Int. J. Oral Maxillofac. Implants* 8 (1993) 409.
- [14] D.W. Klotch, J. Prein, *Am. J. Surg.* 154 (1987) 384.
- [15] K. Yokoyama, T. Ichikawa, H. Murakami, Y. Miyamoto, K. Asaoka, *Biomaterials* 23 (2002) 2459.
- [16] E.F. Harris, S.M. Newman, J.A. Nicholson, *Am. J. Orthod.* 93 (1988) 508.
- [17] K. Yokoyama, K. Hamada, K. Moriyama, K. Asaoka, *Biomaterials* 22 (2001) 2257.
- [18] M.Kh. Shorshorov, I.A. Stepanov, Yu.M. Flomenblit, V.V. Travkin, *Phys. Met. Metall.* 60 (1985) 109.
- [19] Y. Adachi, N. Wade, Y. Hosoi, *Jpn. Inst. Metals* 54 (1990) 525.
- [20] T. Hoshiya, S. Den, H. Katsuta, H. Ando, *Jpn. Inst. Metals* 56 (1992) 747.
- [21] T. Asaoka, H. Yamashita, H. Saito, Y. Ishida, *Jpn. Inst. Metals* 57 (1993) 1123.
- [22] K. Yokoyama, K. Hamada, K. Asaoka, *Mater. Trans.* 42 (2001) 141.
- [23] K. Asaoka, K. Yokoyama, M. Nagumo, *Metall. Mater. Trans. A* 33A (2002) 495.
- [24] J.P. Hirth, *Metall. Trans. A* 11A (1980) 861.
- [25] S. Matsuyama, *Tetsu-to-Hagané* 80 (1994) 679.
- [26] M. Nagumo, M. Nakamura, K. Takai, *Metall. Mater. Trans. A* 32A (2001) 339.
- [27] W.Y. Choo, J.Y. Lee, *Metall. Trans. A* 13A (1982) 135.
- [28] K. Kusakai, T. Kubo, T. Ooka, M. Matsubara, K. Watanabe, *Jpn. Inst. Met.* 51 (1987) 174.
- [29] K. Ono, M. Meshii, *Acta Metall. Mater.* 40 (1992) 1357.
- [30] S.K. Wu, C.M. Wayman, *Acta Metall.* 36 (1988) 1005.
- [31] T.H. Nam, K. Shimizu, T. Saburi, S. Nenno, *Mater. Trans. JIM* 30 (1989) 539.
- [32] M. Nagumo, H. Uyama, M. Yoshizawa, *Scripta Mater.* 44 (2001) 947.

研究成果の概要

研究は次の三つに大別できる。

1) 水素吸収特性と水素脆化挙動

- 1-1 フッ化ナトリウム水溶液中におけるベータチタン合金の水素吸収特性
- 1-2 塩酸を含むアルコール溶液中における Ni-Ti 超弾性合金の水素脆化特性
- 1-3 フッ化ナトリウム水溶液中で Ti 合金が吸収した水素の昇温放出分析による特徴付け
- 1-4 過酸化水素を含有した生理食塩水中における Ni-Ti 超弾性合金の破壊
- 1-5 酸性 NaF 溶液中における Ti-6Al-4V 合金の水素吸収と腐食挙動
- 1-6 次亜塩素酸ナトリウム水溶液中における Ni-Ti 超弾性合金の腐食挙動
- 1-7 フッ化ナトリウム水溶液中における Ni-Ti 超弾性合金の水素吸収抑制
-硝酸浸漬による表面処理-

2) 生体適合性を高めるための表面改質

3) 荷重付加状態を模擬した、フレットィング・腐食疲労特性

以下にそれぞれの研究成果概要を示す。

1) 水素吸収特性と水素脆化挙動

1-1 フッ化ナトリウム水溶液中におけるベータチタン合金の水素吸収特性

- ・対象材料：Ti-11Mo-7Zr-4Sn 合金 (β -Ti)
- ・検討項目：水素吸収量、水素放出挙動 (昇温分析)、材料脆化挙動、破面観察、表面生成皮膜解析、溶出挙動解析、腐食電位測定、分極測定、など

・概要：

口腔内でチタン及びチタン合金が破折する原因の一つとして、歯磨き粉や洗口液、歯面塗布剤などに含まれるフッ化物の影響による水素脆化がある。我々は先の研究において、酸性フッ化ナトリウム水溶液 (以下 APF: Acidulated Phosphate Fluoride) 中におけるベータチタン合金の遅れ破壊特性を明らかにした。しかしながら、遅れ破壊する際に水素吸収すること以外は、ほとんどわかっていない。そこで本研究では、APF 溶液中におけるベータチタン合金の水素吸収特性を、浸漬時間と負荷応力の影響について調べ、遅れ破壊特性との関連を議論した。試料は市販の直径 0.45 mm、引張強度 1100 MPa の歯科矯正用ベータチタンワイヤー (TMA; Ormco) を用いた。溶液は pH=5.0、容量 50 ml の 2.0% 及び 0.2% APF 溶液 (2.0% NaF + 1.7% H₃PO₄ 及び 0.2% NaF + 0.17% H₃PO₄) を用いた。浸漬試験は浸漬部の長さ 50 mm で室温にて行なった。水素吸収特性は昇温放出分析により調べた。2.0% APF 溶液中では、12 時間浸漬以降、急激に水素吸収し始め、24 時間で水素吸収量は 4000 ppm、48 時間で 7000 ppm 以上にも達した。この試料は 50-60 時間の 2.0% APF 溶液浸漬により、延性-脆性遷移を起こす。本実験からその時の水素吸収量はおよそ 10000 ppm であることがわかった。一方、0.2% APF 溶液中では浸漬 48 時間以降は水素吸収しにくくなり、100 時間を越えると、水素吸収量 3000 ppm 前後で飽和した。この結果は、0.2% APF 溶液中の低応力側で遅れ破壊しなくなることに一致する。また、浸漬初期 (6 時間) において負荷応力の影響は見られないが、24 時間では両溶液とも負荷応力によって水素吸収は促進された。特に 2.0% APF 溶液中の負荷応力 600 MPa 以上では、無負荷と比較すると 2 倍近い水素吸収が認められた。

1-2 塩酸を含むアルコール溶液中における Ni-Ti 超弾性合金の水素脆化特性

- ・対象材料：Ni-Ti（形状記憶合金、超弾性合金）
- ・検討項目：水素吸収量、水素放出挙動（昇温分析）、材料脆化挙動、破面観察、表面生成皮膜解析、溶出挙動解析、腐食電位測定、分極測定、など

・概要：

① 緒言： Ni-Ti 超弾性合金は優れた耐食性から、工業や医療分野など広く用いられているが、使用する環境においての水素吸収による材質劣化が問題となる。Ti 及び Ti 合金は、塩酸を含むメタノール溶液中で水素脆化することが知られている。著者らは、その塩酸を含むメタノール溶液中で Ni-Ti 超弾性合金が水素脆化することを報告した¹⁾。更に、純 Ti では水素脆化しないと考えられている塩酸を含むエタノール溶液中で、Ni-Ti 超弾性合金が水素脆化することを見出した²⁾。

Ni-Ti 超弾性合金の水素脆化特性は、カソードチャージによって水素を吸収させる方法で調べられてきた。しかしながら、自然浸漬で吸収した水素が機械的性質に及ぼす影響については明らかではない。そこで本研究では、Ni-Ti 超弾性合金が塩酸を含むメタノール及びエタノール溶液中で吸収する水素を、昇温水素放出分析によりキャラクターゼーションし、水素脆化特性の違いを検討した。

② 実験方法： 試料は市販の直径 0.50 mm、長さ 50 mm の Ni-Ti 超弾性合金を用いた。試料の機械的性質を Table 1 に示す (25 ± 2°C)。試料表面を 600 番の SiC 研磨紙で磨き、アセトン洗浄して乾燥させた後、0.1M 塩酸を含むメタノール及びエタノール溶液（溶液量：10 ml、比液量：12.7 ml/cm²、試験温度：37°C）に浸漬した。浸漬終了後は直ちに昇温水素放出分析（昇温速度：100°C/h）や重量減少測定及び引張試験などを行い、吸収した水素が機械的性質に及ぼす影響などを調べた。また、試料表面及び破面を SEM で観察した。

Table 1 Ni-Ti 超弾性合金の機械的性質

マルテンサイト変態応力 (MPa)	引張強度 (MPa)	断面減少率 (%)	ビッカース硬さ (Hv)
530 ± 16.7	1250 ± 7.2	54.7	355 ± 10
535 ± 1.4	1425 ± 12.6	54.6	362 ± 14

③ 実験結果及び考察：塩酸含有のメタノール及びエタノール溶液中で、Fig. 1 (a) - (c) に見られるように、表面 SEM 観察から局部腐食が確認された。メタノール浸漬では腐食ピットがいくつか見られた。一方、エタノール浸漬においては、24 h 浸漬ではほとんど変化が見られないものの、Fig. 1(c) に示すように 120 h 浸漬では、直径 150 μm 程度の浅い窪みが見られた。

メタノール溶液およびエタノール溶液浸漬した試料の重量減少と浸漬時間の関係を Fig. 2 (a)、(b) に示す。どちらの溶液中においても、浸漬時間と共に重量は減少していくが、エタノール溶液中ではほとんど重量減少しない試料も見られた。120 h 浸漬で、メタノール浸漬における重量減少量はエタノール浸漬のほぼ 10 倍の値となった。

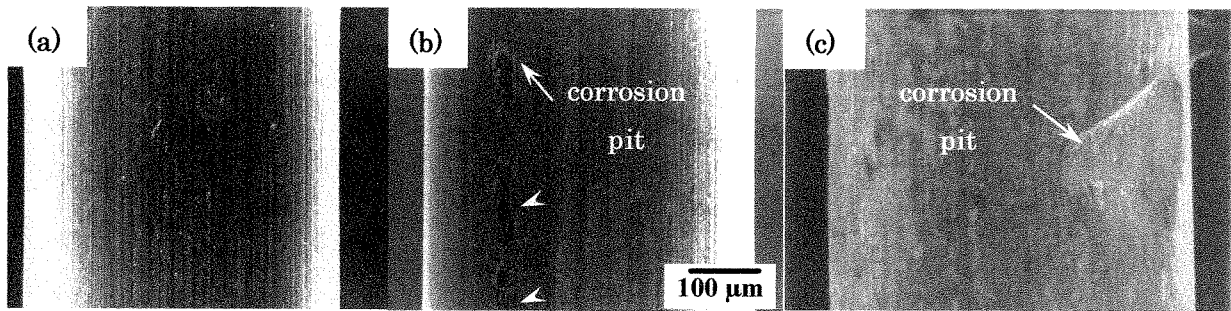


Fig. 1 表面 SEM 観察 (a) as-received, (b) メタノール 24 h 浸漬, (c) エタノール 120 h 浸漬

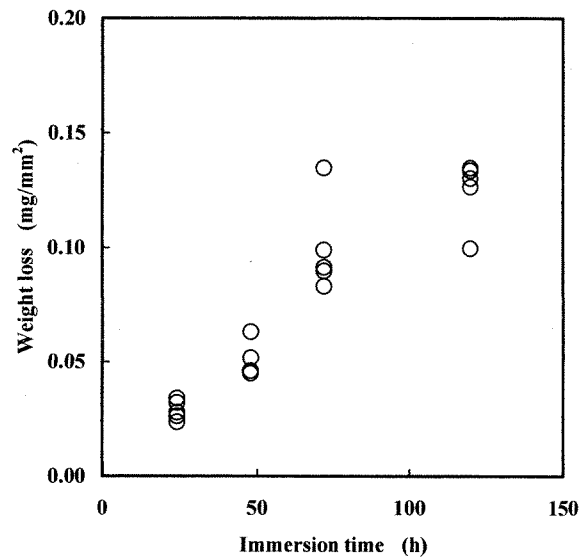
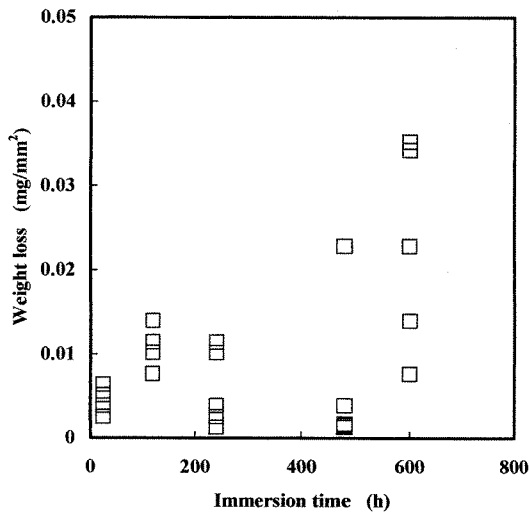


Fig. 2 (a) メタノール浸漬における重量減少

Fig. 2 (b) エタノール浸漬における重量減少

Fig. 3 (a) に示すように、メタノール溶液中では浸漬時間と共に水素吸収量も増加し、120 h 浸漬でおよそ 500 mass ppm の水素吸収量となった。それに対して、Fig. 3 (b) に示すエタノール溶液中で吸収した水素量は、バラつきが大きいものの、120、600 h の浸漬で、それぞれ最大 250、1200 mass ppm にも達した。このバラつきは、本実験で用いた溶液濃度が水素吸収の臨界条件にあるためであると考えられる。また、水素吸収量は重量減少量とともに増加し、重量減少が見られない試料では水素吸収がないことも確認した。Fig. 4 (a) はそれぞれの溶液に 72 h 浸漬、Fig. 4 (b) は 120 h 浸漬した昇温水素放出曲線である。メタノール溶液浸漬では 350°C 付近に放出ピークが現れ、エタノール溶液浸漬では 150 と 350°C 付近に放出ピークを有していた。この結果は、水素吸収する環境によって、試料中における水素の存在状態が異なることを示唆している。

Fig. 5 (a) と (b) にメタノール及びエタノール溶液浸漬における浸漬時間と強度低下の関係を示す。メタノール溶液中で水素吸収した試料は、浸漬時間が 12 h を越えると強度低下し始め、16 h でマルテンサイト変態応力付近まで強度低下した。しかしながら、さらに浸漬時間が長くなっても、強度はマルテンサイト変態応力以下にならなかった。これを水素吸収量で考え

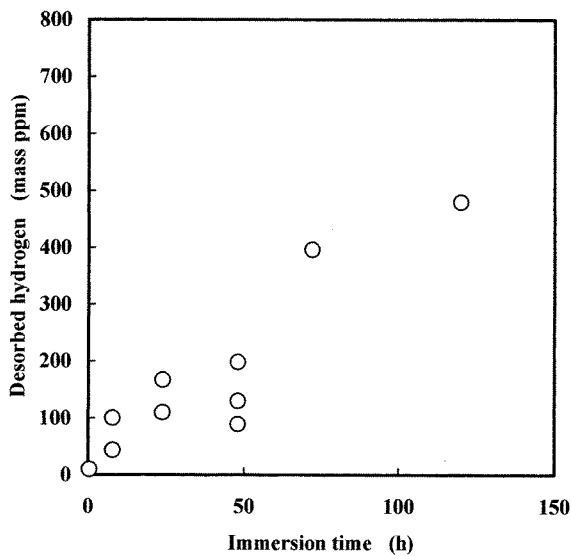


Fig. 3 (a) メタノール浸漬における水素吸収量

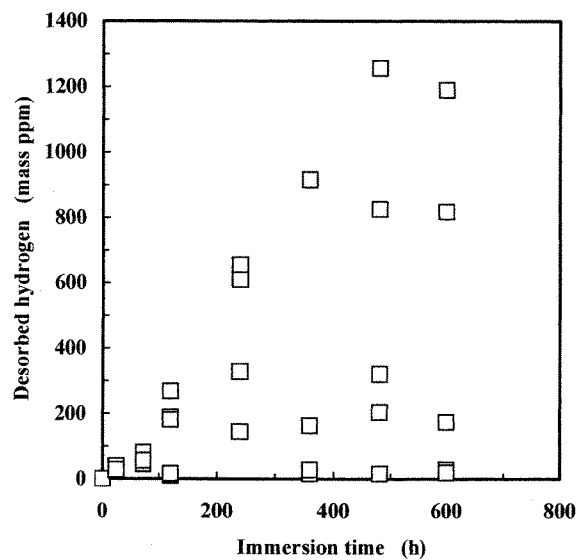


Fig. 3 (b) エタノール浸漬における水素吸収量

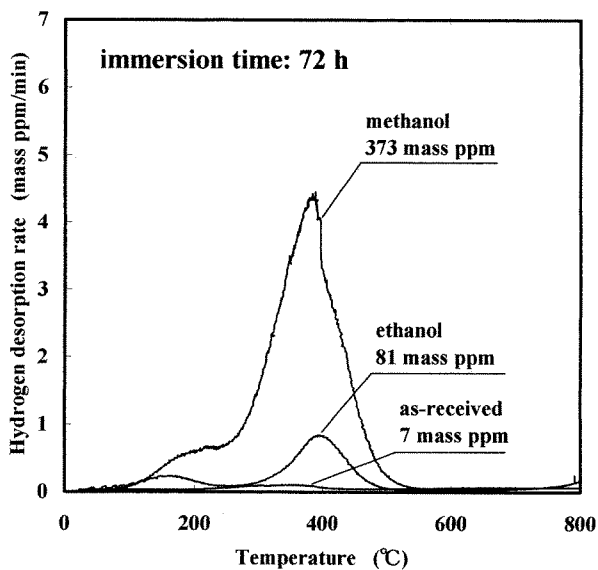


Fig. 4 (a) 72 h 浸漬における水素放出曲線

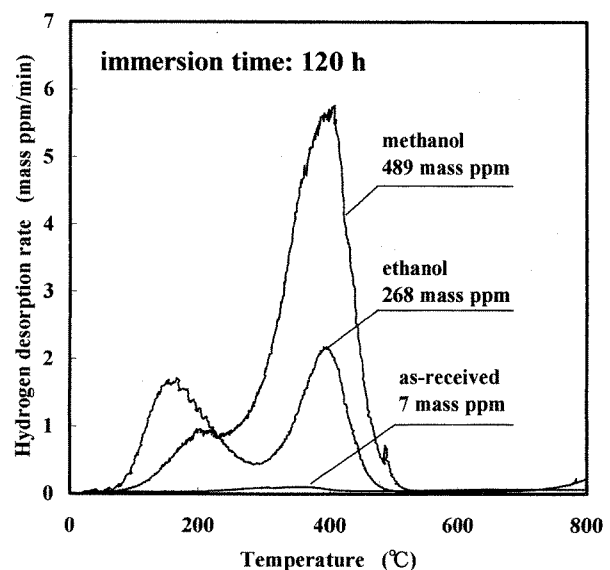


Fig. 4 (b) 120 h 浸漬における水素放出曲線

ると、Fig. 3 (a)から、50-200 mass ppm 程度の水素吸収量で強度低下すると考えられる。それに対して、エタノール溶液中では強度低下のバラつきが大きい。これは、エタノール溶液中では、水素吸収がバラつくことに起因すると考えられる。Fig. 3 (b) 及び 5 (b) から、エタノール溶液に浸漬した試料が強度低下し始める水素量は 300-400 mass ppm であり、メタノール溶液中で脆化する水素量より多かった。また注目すべきは、エタノール溶液に浸漬した試料の引張強度が、マルテンサイト変態応力以下になることである。

これは、昇温水素放出分析の結果より、両溶液中で吸収した水素の存在状態の違いが破壊に影響を与えているということが推察出来る。さらに、エタノール溶液中で吸収した水素のうち、150°Cで放出される水素は浸漬時間と共に増加するが、350°Cで放出される水素は 200 mass ppm

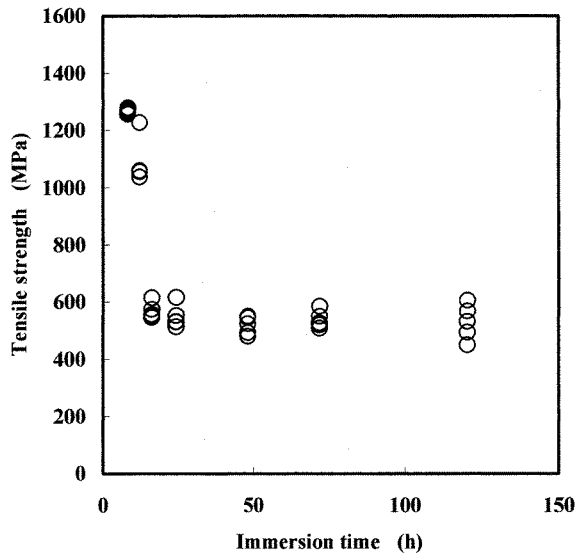


Fig. 5 (a) メタノール浸漬における強度低下

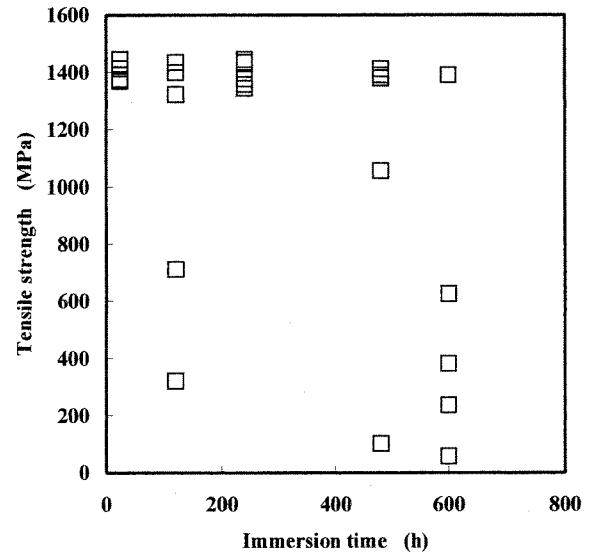


Fig. 5 (b) エタノール浸漬における強度低下

程度で飽和した。したがって、エタノール溶液中における水素脆化には、150°Cで放出される水素がより大きな影響を与えていると考えられる。

④ 結言

1. 水素吸収する環境の違いによって、試料中における水素の存在状態が異なることを示唆した。
2. メタノール溶液中では 50-200 mass ppm の水素吸収量で強度低下が見られたが、エタノール溶液中では、300-400 mass ppm まで水素吸収量が達しないと強度低下が見られなかった。
3. メタノール溶液中では 500 mass ppm 程度の水素吸収量でも、強度はマルテンサイト変態応力以下にはならなかったが、エタノール溶液中では、水素吸収量が 300-400 mass ppm を越えると、マルテンサイト変態応力以下で破断した。

⑤ 引用文献

- 1) Yokoyama K et al. Mater Sci Eng A 2003;360:153-159.
- 2) 小川登志男、横山賢一、浅岡憲三、酒井潤一；日本金属学会講演概要 2004年春期（第134回）大会

1-3 フッ化ナトリウム水溶液中でTi合金が吸収した水素の昇温放出分析による特徴付け

- ・対象材料：Ti (α -Ti)、Ti-11Mo-7Zr-4Sn合金 (β -Ti)
- ・検討項目：水素吸収量、水素放出挙動(昇温分析)、材料脆化挙動、破面観察、表面生成皮膜解析、溶出挙動解析、腐食電位測定、分極測定、など
- ・概要：我々は以前、う蝕予防に用いられるフッ化ナトリウム水溶液中でTi及びTi合金が水素脆化することを明らかにした。さらに、その水素吸収特性を昇温放出分析から調べる過程で、吸収した水素の放出挙動が、溶液濃度に影響されることを見出した^{1) 2)}。これは、浸漬溶液のフッ化ナトリウム濃度によって、合金中における水素の存在状態や水素濃度分布が異なることを示唆している。そこで本研究では、フッ化ナトリウム水溶液中でTi合金が吸収した水素の特徴を、昇温放出分析を用いて調べた。直径0.50 mmの工業用純Ti (α -Ti)及び直径0.45 mmのTi-11Mo-7Zr-4Sn合金 (β -Ti)を600番のSiC研磨紙で表面を仕上げ、50 mmに切り出したものを試料とした。溶液はpH 5.0、容量50 mlの2.0及び0.2% APF溶液(0.48M NaF + 0.18M H₃PO₄及び0.048M NaF + 0.018M H₃PO₄)を用いた。試料中の水素分布を調べるために、浸漬後の試料表面を180番のSiC研磨紙で25 μ mステップで研削し、昇温放出分析を行った。また、表面を研削した試料中の水素化物の有無を調べるために、XRD測定を行った。 α -Tiが溶液中で吸収した水素の大部分は試料表面から50 μ m以内に存在し、表面付近の水素濃度は2.0及び0.2% APF溶液中でそれぞれ少なくとも5000及び2000 mass ppmと見積もられた。一方、 β -Ti合金中の水素は試料中心部まで拡散しており、2.0% APF溶液中では表面付近の水素濃度が高いものの、0.2% APF溶液中においては試料全体に均一に拡散していると考えられた。浸漬試験後の α -Tiは500° Cにピークを有していたが、表面を徐々に研削するにつれて水素放出ピークも高温側にシフトし、径が0.45 mmになると600° Cにまでピークシフトした。また、XRD測定の結果、いずれの径の α -Tiからも水素化物が検出された。しかしながら、径が0.40 mmになると、水素化物が検出されなくなると共に、ピークも450° Cへと低温側にシフトした。このことから、450° Cのピークは試料中に固溶している水素、600° Cのピークは水素化物の分解に関連すると考えられる。また、浸漬後の試料を室温に600 h放置した時の水素量及び水素放出曲線は、室温放置前と比べても変化は見られなかった。一方、表面を研削後の β -Ti合金は、表面を研削する前と比べると低温側にピークシフトしたことから、表面の腐食生成物が水素放出の障壁となっているということが考えられる。

[参考文献]

- 1) Yokoyama K, Ogawa T, Asaoka K, Sakai J., Mater. Sci. Eng. A in press.
- 2) Ogawa T, Yokoyama K, Asaoka K, Sakai J., Biomaterials 2004;25:2419-2425.

1-4 過酸化水素を含有した生理食塩水中における Ni-Ti 超弾性合金の破壊

- ・対象材料：Ni-Ti（形状記憶合金、超弾性合金）
- ・検討項目：水素吸収量、水素放出挙動（昇温分析）、材料脆化挙動、破面観察、表面生成皮膜解析、溶出挙動解析、腐食電位測定、分極測定、など
- ・概要：生体内で発生する活性酸素の一種である過酸化水素が、チタンの溶出を促進させることがある。とは言え、短期的に見た場合、その溶出はチタン合金の機械的性質に大きな影響を与えるようなものではない。しかしながら、Ni-Ti 超弾性合金は負荷応力下で腐食環境の影響を受けやすく、過酸化水素の存在下で材質劣化する可能性がある。そこで本研究では、過酸化水素を含有した生理食塩水中における Ni-Ti 超弾性合金の破壊について調べた。試料は直径 0.50 mm の Ni-Ti 超弾性合金線（マルテンサイト変態開始応力：530 MPa、引張強度：1483 MPa）を 600 番の SiC 研磨紙で表面を磨き、アセトン洗浄したものをを用いた。0.15M NaCl + 0.3M H₂O₂ 水溶液（溶液量 50 ml、25° C）中で、一定の荷重を荷重し、破断するまでの時間を測定した。1000 時間以上経過しても破断しない場合は、試験を中止した。破断した試料の破面及び側面は SEM を用いて観察した。また、無負荷及び定荷重負荷下における腐食電位測定を行った。負荷応力がマルテンサイト変態開始応力以上になると、負荷応力の大きさによらず 100 時間以内に破断した。破面および側面観察から、局部腐食領域を起点として、き裂が放射状に伝播することによって破断したと考えられる。一方、マルテンサイト変態開始応力以下の負荷応力下では破断しにくくなり、300 MPa 以下の負荷応力下では、多数の腐食ピットが観察されるものの、1000 時間以内に破断しなかった。無負荷における腐食電位は 0.2-0.3 V (vs. SCE) 付近で安定するが、定荷重負荷下においては、局部腐食発生による電位の急激な降下が見られた。したがって、本研究から、生体内における過酸化水素の影響で Ni-Ti 超弾性合金が破折することが示唆される。

1-5 酸性 NaF 溶液中における Ti-6Al-4V 合金の水素吸収と腐食挙動

[緒言] Ti 合金は、う蝕予防に用いられるフッ化物の存在下で腐食し、水素脆化することがある。近年著者らは、酸性フッ化ナトリウム (APF: Acidulated Phosphate Fluoride) 水溶液中における Ti-6Al-4V 合金の遅れ破壊特性は、純 Ti のそれと異なり、溶液濃度に大きく影響されることを見出した⁽¹⁾。そこで本研究では、APF 水溶液濃度が Ti-6Al-4V 合金の水素吸収と腐食挙動に与える影響について調べた。

[実験方法] 市販の直径 0.50 mm の Ti-6Al-4V 合金を 600 番の SiC 研磨紙で表面を仕上げ供試材とした。腐食電位は、2.0 mass% APF (0.48M NaF + 0.18M H₃PO₄; pH 5.0) 水溶液を 2.0% から 0.1% まで希釈した溶液中 (25 ± 2° C) で調べた。浸漬後の試料表面は SEM, EPMA, XRD などで調べ、溶液中で吸収した水素量は昇温放出分析法によって測定した。

[結果および考察] 0.2%、0.3% APF 水溶液では、浸漬直後に腐食電位が -1.0 V (vs. SCE) に卑化するが、数時間後には -0.3 から -0.4 V へ徐々に貴化し安定した。一方、0.1% と 0.4% から 2.0% APF 水溶液では、溶液濃度によらず腐食電位は -1.0 V で安定した。(Fig. 1)

0.2%、0.3% APF 水溶液では、試料表面に析出物 (Na₃AlF₆) が付着するとともに、腐食電位が貴化した。(Fig. 2) 溶液濃度 0.4% 以上になると、Na₃AlF₆ の他に腐食生成物 (Na₃TiF₆) が確認され、溶液濃度が高くなるとこの腐食生成物の割合が増加した。注目すべきは、溶液濃度によって試料表面の腐食形態が大きく異なったことである。(Fig. 3)

水素吸収量は、溶液濃度 0.3% 以下では浸漬時間によらず数十 mass ppm 程度だったが、0.4% 以上では溶液濃度が高くなるにつれて水素吸収量が増加し、2.0% APF 水溶液では 24 時間で 200 mass ppm 吸収した。(Fig. 4) このことは溶液濃度 0.4% 以上では、腐食電位と水素吸収量に関連がなく、腐食形態の違いが水素吸収に影響を及ぼすことを示唆している。Fig. 5 において、24 h における電位と水素吸収量の関係を示す。

ここで 0.2、0.3% APF において、Na₃AlF₆ が水素吸収を抑制する可能性が示唆されたため、低時間における水素吸収量を測定した結果、水素吸収量が一定になった時間と Na₃AlF₆ が全面を覆う時間と一致した。(Fig. 6) そこで、前述の供試材と、前処理として、0.2% APF に 24 h 浸漬させ、全面に Na₃AlF₆ 析出させた試料をを 2.0% APF に 120 h 浸漬させて水素吸収量を測定した。前者は約 800 ppm 水素を吸収したのに対し、後者は約 180 ppm に抑制された。

[結言] APF 溶液中において、Ti-6Al-4V 合金における腐食電位と水素吸収量には関連がなく、腐食形態の違いが水素吸収に影響を及ぼす事が示唆された。

Na₃AlF₆ が全面に析出した場合、水素吸収を抑制する。

0.4% APF から水素吸収が増加し始め、溶液濃度が高くなるにつれ、時間が経過するにつれ、水素吸収量が増加した。

[参考文献]

1. 横山 賢一 徳島大・歯 日本金属学会春季大会講演概要(第 134 回・東京) P.126 (32) 1

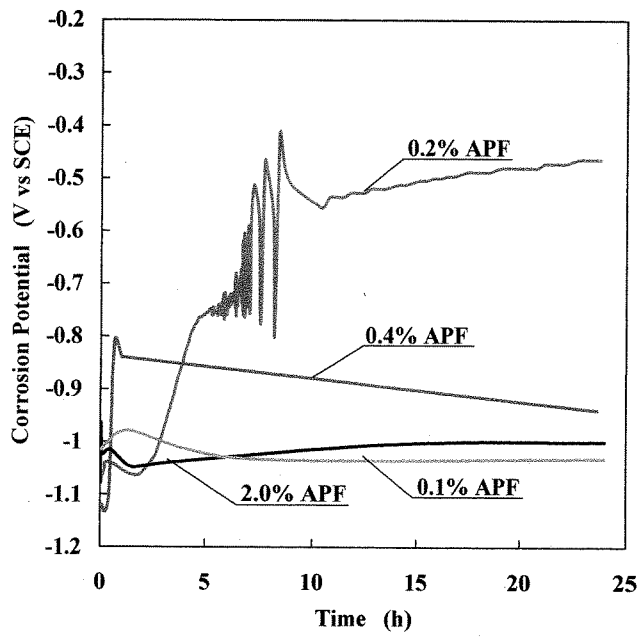
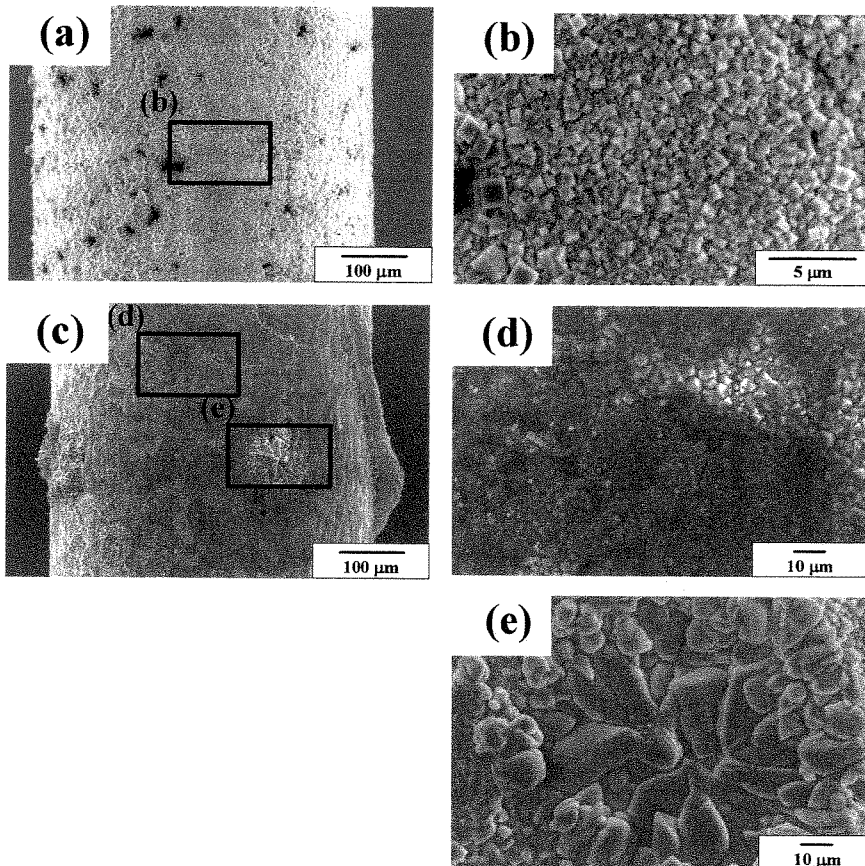
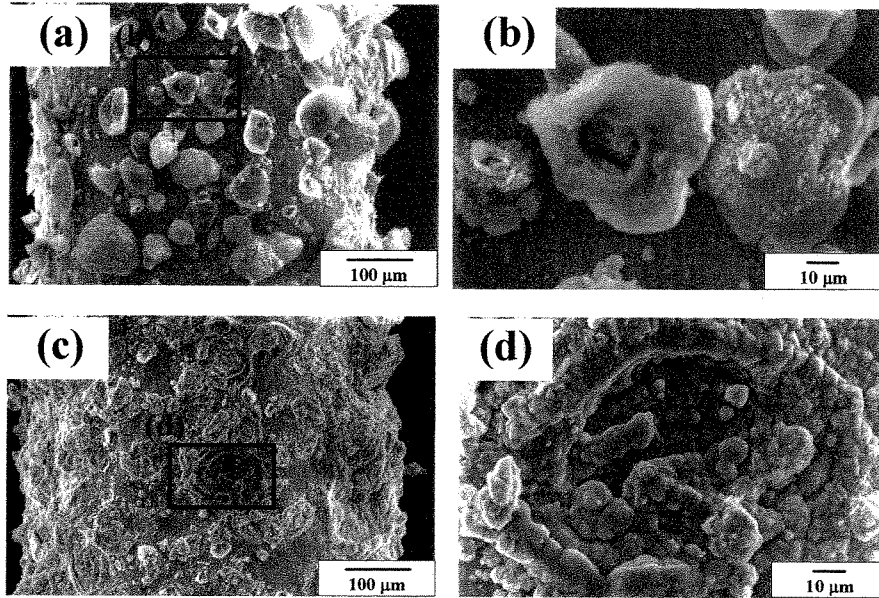


Fig.1 各 APF 溶液濃度における 24 h 浸漬の腐食電位



(a) , (b) 0.2% APF, (c), (d),(e) 0.4% APF

Fig.2 0.2、0.4% APF24 h 浸漬後の SEM 写真



(a), (b) 1.0% APF, (c), (d) 2.0% APF

Fig. 3 1.0、2.0% APF24 h 浸漬後の SEM 写真

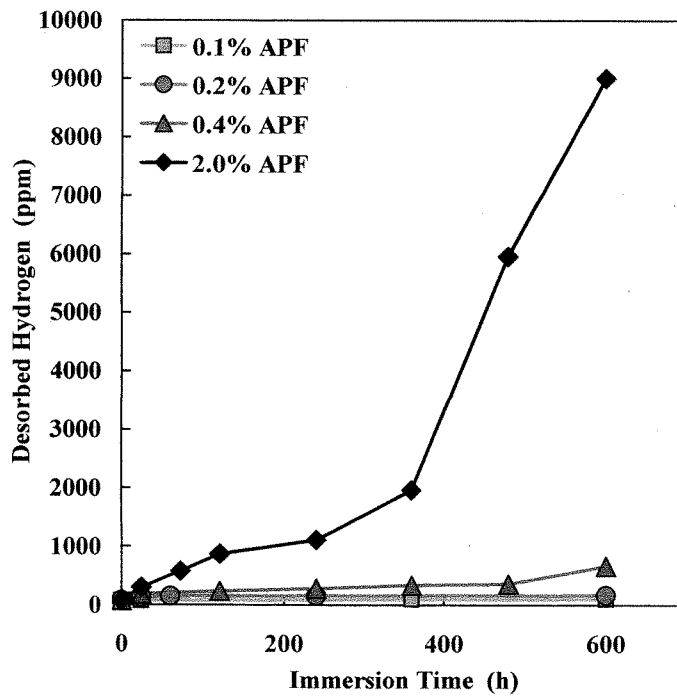


Fig. 4 各 APF 溶液濃度における水素吸収量の経時変化

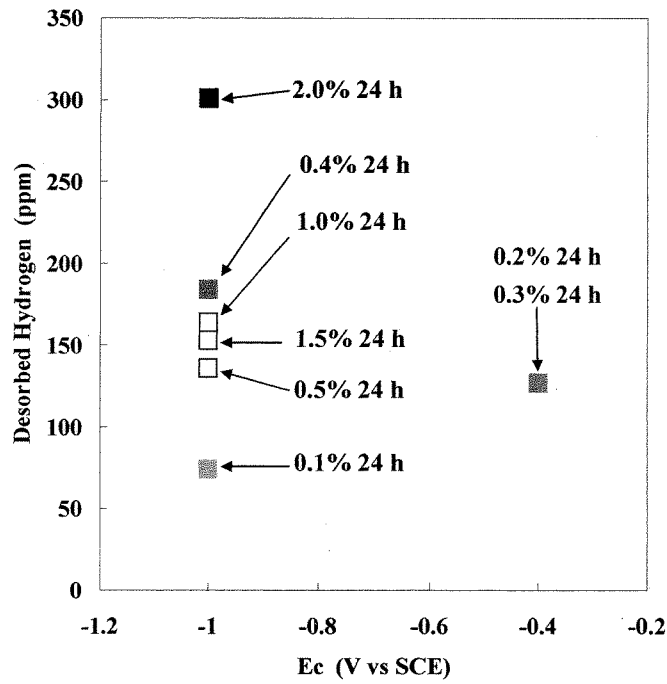


Fig. 5 各 APF 溶液濃度における 24 h 浸漬後の電位と水素吸収量の関係

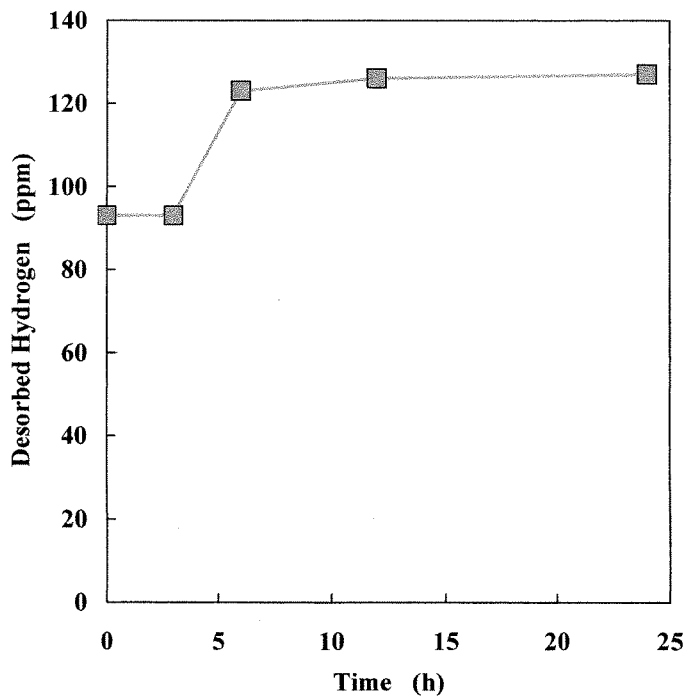


Fig. 6 0.2% APF 溶液濃度における水素吸収量の経時変化

1-6 次亜塩素酸ナトリウム水溶液中におけるNi-Ti 超弾性合金の腐食挙動

[緒言]Ni-Ti 超弾性合金は、機械的特性、耐食性などに優れることから、歯科医療において、矯正用ワイヤーや根管治療用ファイルとして利用されている。しかし、根管内の治療中にNi-Ti ファイルの破断や損傷がみられる。その原因の一つとして、根管の治療や器具の消毒の際に用いられる次亜塩素酸ナトリウム(NaOCl)水溶液による腐食の影響があると考えられる⁽²⁾。しかしNaOCl水溶液中でのNi-Ti 超弾性合金の詳細な腐食挙動については十分に解明されていない。そこで本研究では、NaOCl 水溶液環境におけるNi-Ti 超弾性合金の腐食挙動について明らかにすることを目的とした。

[実験方法] 試料は直径0.5 mmのNi-Ti超弾性合金 ((株)大同特殊鋼製, マルテンサイト変態誘起応力: 530 MPa, 引張強さ: 1350 MPa)を600番の湿式研磨紙で研磨し、アセトンで超音波洗浄したものを使用した。参照試料としてPt、純Ni、CP-Tiワイヤーを用いた。試験溶液は0.1、1.0、5.0% NaOCl水溶液を使用し、溶液温度を $37 \pm 1^\circ\text{C}$ に制御した。溶液のpHはそれぞれ10.9、11.9、12.4である。またCl⁻イオンの影響を調べるために、参照溶液として試験溶液と同じpHに調節したNa₂SO₄水溶液を用いた。電気化学測定にはポテンショスタット((株)北斗電工製、HZ-3000)を用い、セルを密閉した状態で実験を行なった。参照電極にはSCEを用いた。分極曲線測定は、20 mV/minの速度で、-1.5~1.5 Vの範囲で掃引した。表面観察にはSEM(日本電子(株)製、JSM-5310)、また腐食生成物の同定には、高出力XRD((株)理学電機製、RINT-TTR, target Cu, 50 kV, 200 mA)を使用した。

[結果と考察] NaOCl溶液中でのPtの腐食電位は、浸漬直後から貴化し、0.5V~0.6 V (vs. SCE)の間で安定した。この電位の値から、NaOCl水溶液中は高い酸化性環境であるといえる。Ni-Tiの腐食電位の経時変化をFig. 1(a)に示す。腐食電位は浸漬直後から貴化し、0.45~0.55 V付近に到達すると、急激に卑化した。その後0~0.5 Vの間でスパイク挙動を示した。また、5.0%においては、電位卑化後に再度0.5 V付近まで貴化、その後安定した挙動を示した。これはNaOCl水溶液の高い酸化性のために、不動態皮膜の破壊、再不動態化が繰り返されることにより、スパイク挙動を示したと考えられる。Ni、Tiについても同様の試験を行った。その結果をそれぞれFig. 1(b)、(c)に示す。Niは、Ni-Tiと同様に腐食電位のスパイク挙動を示した。また局部腐食が認められ、腐食生成物が確認された。これとは対照的に、Tiの腐食電位は、浸漬後緩やかに貴化し、5.0%においては24時間後に0.55 Vまで貴化し安定した。また重量減少も認められなかった。以上の結果から、Ni-Tiの腐食において、Niが大きく影響していることが確認された。またNa₂SO₄水溶液におけるNi-Tiの分極曲線を測定した。その結果、-0.5~0.5 Vの領域において数~10数 $\mu\text{A}/\text{cm}^2$ の不動態保持電流密度を示した。また浸漬試験後、重量減少は認められず、試料表面は金属色を保持していた。このことからCl⁻を含まない高アルカリ環境では、Ni-Tiは高い耐食性を示すことが確認された。Fig. 2(a)に浸漬前のNi-Ti表面を、Fig. 2(b)に5.0% NaOCl水溶液に3時間浸漬後のNi-Ti表面の腐食部分を示す。浸漬試験後、試料表面に局部腐食が認められ、その部分から黒色の腐食生成物が発生していた。その他の部分では研磨キズが残っており、腐食が認められなかった。またXRDで、腐食生成物として β -NiOOHとNi-Tiが同定された。

[結言] Ni-Ti超弾性合金は、NaOCl水溶液中で局部腐食を示し、また高い酸化性環境のため、腐

食電位のスパイク挙動が確認された。その原因としては、Ni含有による耐食性の低下によるものと考えられる。

[参考文献]

2. Busslinger A, Sener B, Barbakow F: *Int. Endo. J.* 31, 290-294 (1998)

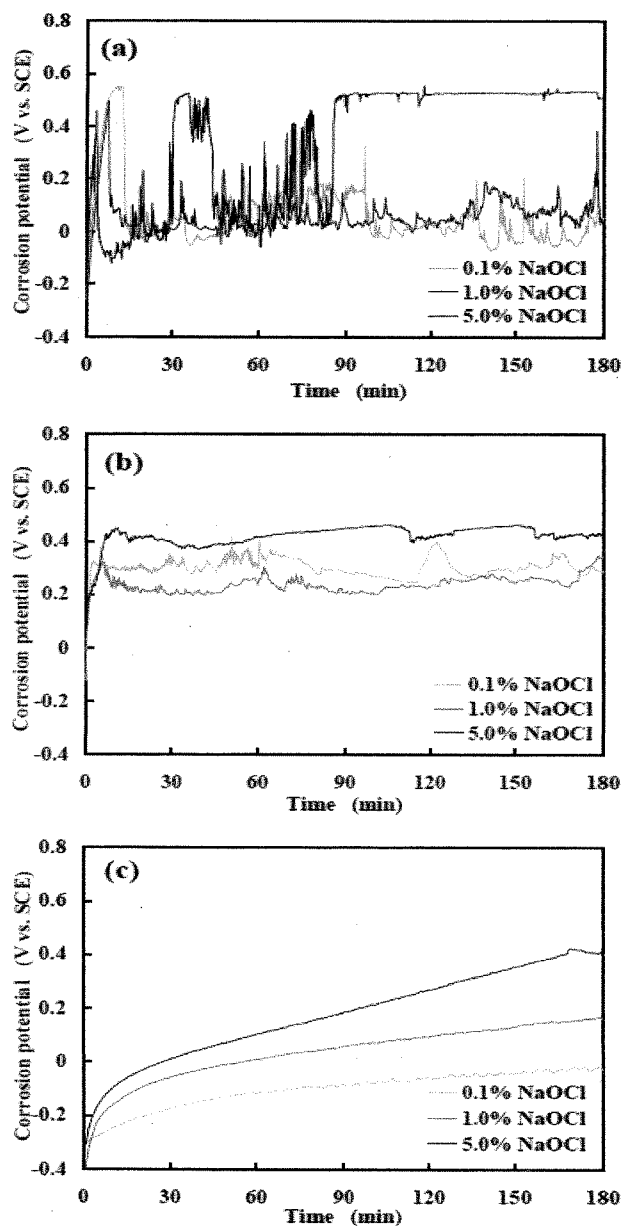


Fig.1 Shifts of corrosion potential in 0.1~5.0% NaOCl solutions of (a) Ni-Ti, (b)Ni, and (c) Ti

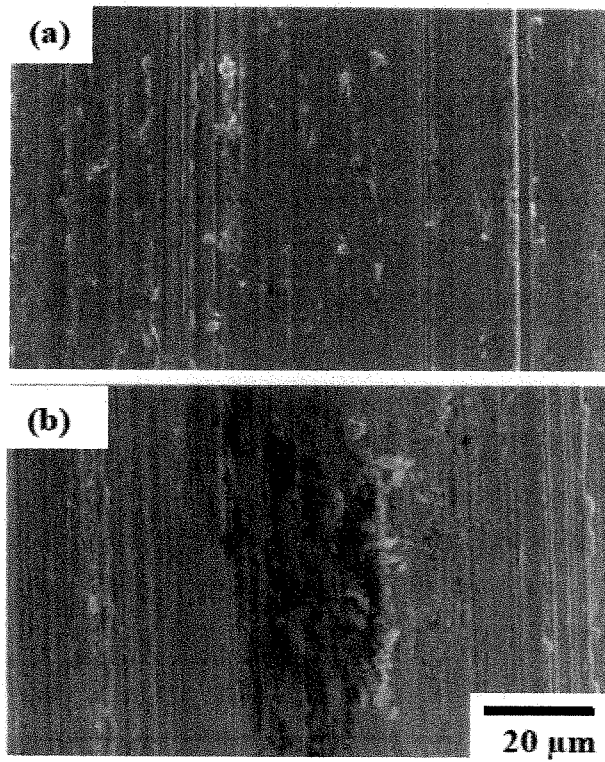
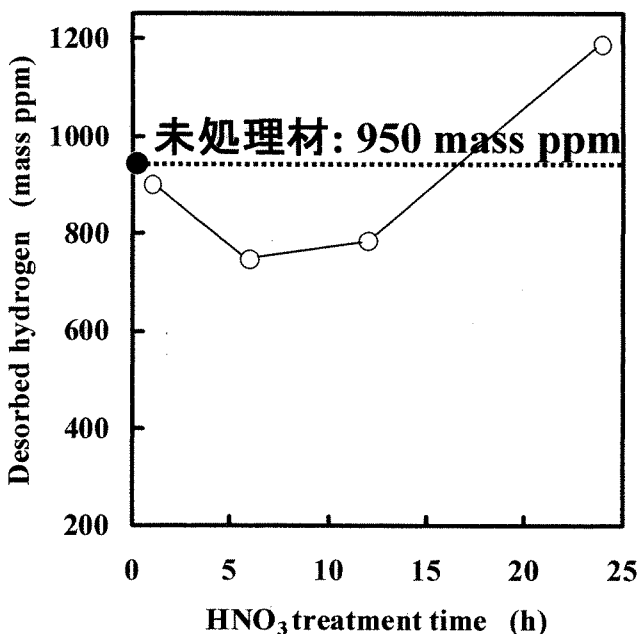


Fig.2. SEM micrographs of the surface of Ni-Ti superelastic alloy: (a) as polished and (b) immersed in 5.0% NaOCl solutions for 3 hours.

1-7 フッ化ナトリウム水溶液中におけるNi-Ti超弾性合金の水素吸収抑制

-硝酸浸漬による表面処理-

- ・対象材料：Ni-Ti（形状記憶合金、超弾性合金）
- ・検討項目：水素吸収量、水素放出挙動（昇温分析）、材料脆化挙動、破面観察、表面生成皮膜解析、溶出挙動解析、腐食電位測定など
- ・概要：我々は以前、う蝕予防の際に用いられるフッ化ナトリウム水溶液中において、歯科用材料として広く用いられているNi-Ti超弾性合金が水素吸収し材質劣化することを報告した¹⁾。本研究では、硝酸浸漬による表面皮膜処理によって、フッ化ナトリウム水溶液中におけるNi-Ti超弾性合金の水素吸収の抑制を試みた。市販の直径0.50 mm、長さ50 mmのNi-Ti超弾性合金線の表面を600番のSiC研磨紙で磨いたものを試料とし、35 mass%、60°C硝酸に各1、6、12、24 h浸漬させて表面皮膜処理を施した。表面皮膜処理による水素吸収抑制効果は、昇温放出水素分析を用いて、0.2%acidulated phosphate fluoride (APF) 溶液中に24 h浸漬させた際に吸収する水素量で評価した。また、SEM、XPSなどを用いて硝酸浸漬前後の表面解析を行った。



昇温放出分析による水素吸収量の測定結果を Fig. 1 に示す。研磨後、0.2%APF 溶液中に24 h浸漬させた試料の水素吸収量はおよそ950mass ppmとなった。この試料を未処理材と称す。未処理材と比較すると、6及び12 h処理材において水素吸収抑制効果が確認された。特に6 h処理材はおよそ750mass ppmという値を示し、20%以上の水素吸収抑制に成功した。また、表面皮膜処理によって、0.2%APF 溶液中での腐食による重量減少も抑制された。これらの抑制効果は、硝酸浸漬による表面酸化皮膜の変化に起因すると考えられる。以上の結果から、硝酸浸漬による表面皮膜処理によって、フッ化ナトリウム

水溶液中におけるNi-Ti超弾性合金の水素吸収を抑制出来ることが示された。

【参考文献】

- 1) Yokoyama K, Kaneko K, Moriyama K, Asaoka K, Sakai J, Nagumo M, J. Biomed. Mater. Res. 2003; 65A: 182-187.

2) 生体適合性を高めるための表面改質

- ・対象材料：CP-Ti(α)
- ・検討項目：表面生成皮膜解析(SEM、EPMA)、溶出挙動解析(ICP)
- ・主たる結果：Tiに150~200Vの高電圧での陽極酸化を施すことで、その表面には数 μm オーダーの孔径、粗さ、厚さを持った多孔質な表面が生成される。このような多孔質な陽極酸化皮膜は、骨と接合した際に強固に結合するため、インプラント材への適応が考えられ、実際に使用されている。また、皮膜の結晶構造も骨との結合の重要な因子と考えられている。TiO₂には主たる結晶構造として、アナターゼ型のもの、ルチル型のものがあるのだが、従来の研究では、このルチル型のTiO₂が存在することで、骨との接合性が向上することが示されている。以上のことより、表面の物理的な形状の制御及び結晶構造の制御をもって、表面改質とする。

本研究では以下の条件で陽極酸化実験を行った。

試料：CP-Ti(Gr.-1)電極 30mm×15mm×0.6mm

(うち約10mm×15mmを半浸漬、陽極酸化)

電解浴： β -グリセロリン酸ナトリウム 0.01mol/l
+ 酢酸カルシウム 0.15mol/l

最終電解電圧 250V, 300V, 350V

電流密度 約0.2A/cm²

※ 実験手順：定電流電解で上記の電圧まで昇圧した後、定電圧電解に移行し5分間保持

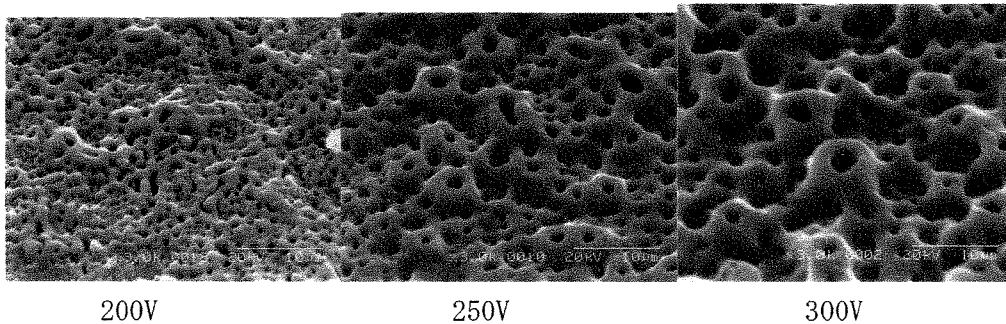
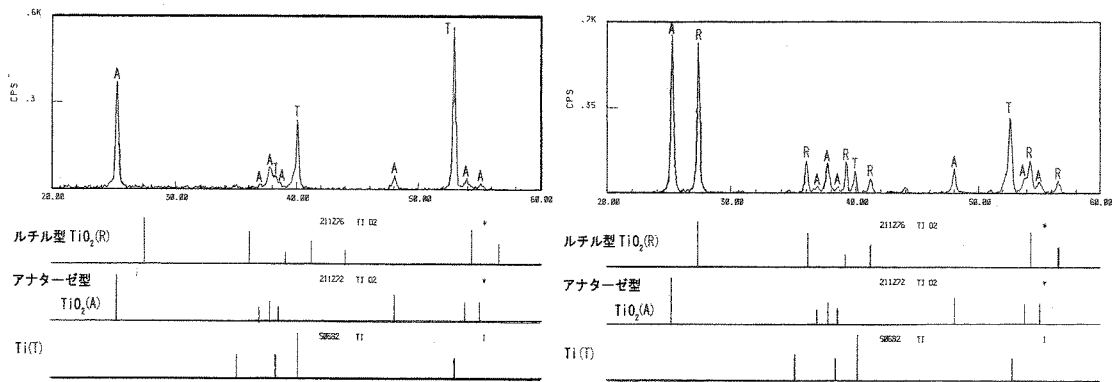


写真1 SEM観察例

結果の一例を上写真に示す。このように、電解電圧の値が高くなるにつれて孔のサイズは大きくなっていき、また、その結晶構造はルチル型とアナターゼ型のTiO₂が混在しているものへと移行していった。よって、電解初期段階ではアナターゼ型のみが生成していた表面皮膜の結晶構造は、電圧の上昇に従ってアナターゼ型がルチル型へと変化すると考えられる。

結晶構造に関しては熱処理による変化という方法も挙げることができる。文献によると、アナターゼ型TiO₂というものは高温においてルチル型TiO₂に変化するということがわかっている。また、この反応は不可逆的なもので、除冷したからといってルチル型がアナターゼ型に変化するということはない。以下に、陽極酸化皮膜(電解電圧250V)を生成した後、600℃大気熱処理を施す前後のTi材のX線回折結果を載せる。



600°C大気熱処理前のTiのX線回折結果 600°C大気熱処理後のTiのX線回折結果
 図1 表面構造のXRD解析結果

このように、大気中熱処理によって陽極酸化皮膜中のTiO₂について、結晶構造の大きな変化が発生したことがわかる。このことから、Ti材の生体適合性を高める手法として、適切な熱処理というものは十分期待できるといえる。

生体適合性を高める方法として、骨の成分に近い物質をTi材表面に析出させるというものがある。この、骨に近い物質として、ハイドロキシアパタイト(以下HA)という物質がある。これを不均一な表面上に析出させることで、一種の誘起的役割を持つ表面皮膜にしようということである。

HAを析出させる前段階として、二つの処理が挙げられる。一つは本実験の要である陽極酸化法であり、もう一つがアルカリ処理法である。

陽極酸化を施すと、これまで述べてきた通り、表面が多孔質で不均一な表面皮膜が出来上がる。また、今回の実験で用いられている電解浴のように、骨の主成分であるCaやPを含んだ溶液によって陽極酸化されたTi材というものは、HAをその表面上に形成する能力が向上する。

一方、アルカリ処理を施した場合、その表面はゲル状の組織が出来上がる。こちらも同様にHA析出能力が向上するといわれている。

これら前処理を施した後、擬似体液(Simulated body fluid)中にTi材を7日ほど浸漬することで、その表面上にはHAが析出する。以下に擬似体液イオン濃度を示す。

表 擬似体液及び人体血漿内のイオンとその濃度

Ion	Concentration (mmol/dm ³)	
	Simulated body fluid (SBF)	Human blood plasma
Na ⁺	142.0	142.0
K ⁺	5.0	5.0
Mg ²⁺	1.5	1.5
Ca ²⁺	2.5	2.5
Cl ⁻	147.8	103.0
HCO ₃ ⁻	4.2	27.0
HPO ₄ ²⁻	1.0	1.0
SO ₄ ²⁻	0.5	0.5

3) 荷重付加状態を模擬した、フレットィング、腐食疲労特性

- 対象材料：CP-Ti (α)
- 検討項目：S-N 曲線、腐食電位、破面観察、側面観察、ハイドロキシアパタイト、カソードチャージ、欠陥密度
- 主たる結果：我々は生体内を模擬した環境下での腐食疲労特性及びフレットィング腐食疲労特性についての研究を進めてきた。生体内環境を模擬した環境として従来、擬似体液の 1 つとして使われている SBF (Simulate Body Fluid) 溶液を使用し、その環境下での腐食疲労特性として S-N 曲線を Fig.1 に示す。

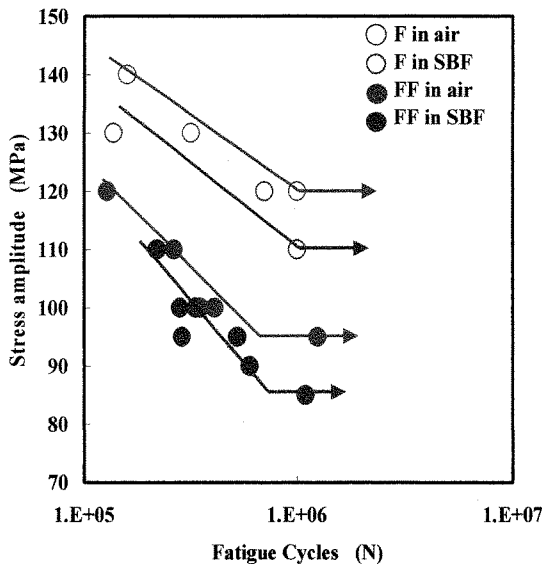


Fig.1:大気中及び擬似体液中における純 Ti の S-N 曲線

電位 (フレットィング疲労を開始する前の電位) にもどるまでに時間がかかっていることから、酸化皮膜の再形成に時間がかかっていることが示唆される。SBF 溶液中で低応力側におけるフレットィング腐食疲労の疲労寿命が減少するという事は、大気中のフレットィング疲労と比較して、破壊に至るまでのプロセスに違いあるということが考えられる。そこで応力振幅、

周波数そして面圧を全て一定とし、大気中及び擬似体液中におけるフレットィング腐食疲労の側面・破面観察をおこなった。破面観察の結果を Fig. 3、側面観察の結果を Fig. 4 に示す。

周波数そして面圧を全て一定とし、大気中及び擬似体液中におけるフレットィング腐食疲労試験における応力振幅の違う 2 条件での腐食電位を測定した。その結果を Fig. 2 に示す。 $\sigma_a=110\text{MPa}$ では破断前に徐々に電位が下がり破断するという挙動が確認された。

また、 $\sigma_a=95\text{MPa}$ では電位が下がってから元の

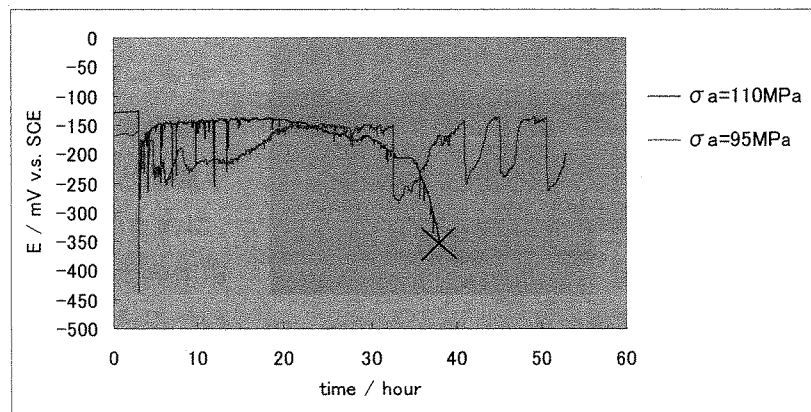


Fig.2:フレットィング腐食疲労環境下での腐食電位

破面観察からは、大気中及び擬似体液中の双方に顕著な差は見られず、き裂が破面外周部から放射線状に伝播し、その後破断するという一般的な疲労と同等の見解が伺えた。しかしながら、側面観察からは表面での微視き裂に違う挙動が確認された。この応力下 (100MPa) で

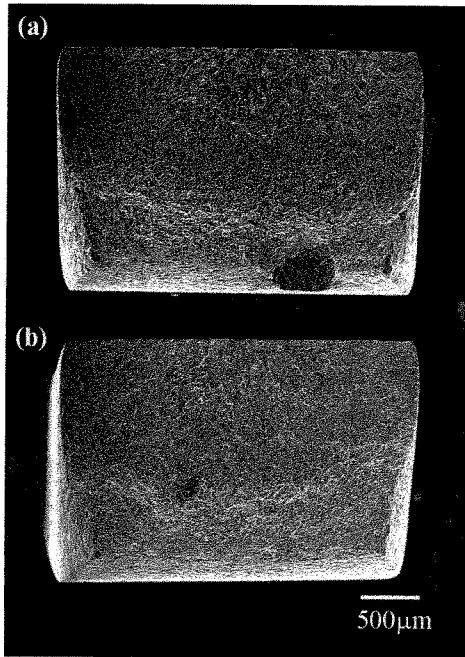


Fig.3:フレット疲労後の破面
(a)大気中(b)擬似体液中

は疲労寿命は大気中では約 35 万サイクルであり、擬似体液中では約 30 万サイクルである。しかしき裂発生は大気中では約 30 万サイクルと破断直前であるのに比べて、擬似体液中では約 10 万サイクルと疲労過程初期段階で確認された。大気中では 10 万サイクル及び 20 万サイクルではき裂は確認できなかった。疲労過程はき裂が発生し、その後進展し破断する。また、破面観察からもき裂進展領域 (ステージ 2) にそこまで変化がないところからも、擬似体液中におけるフレット疲労の方がき裂進展速度も遅いのではということ

が示唆され、従来の報告とは違う結果が得られた。単純な腐食疲労のき裂進展は、き裂の酸素不足、金属イオンの加水分解による pH 低下により、き裂内部がアノード、外部がカソードとなり、進展が促進される可能性がある一方で、腐食によるき裂の文化及び鈍化、腐食生成物のために遅くなる可能性もあり、環境などに強く依存する。純チタンは摩擦係数が高いために、摩耗が溶液の作用でき裂内に侵入し、その作用で遅くなったなど考えられるが、これらについては今後の課題となる。

また、フレット疲労のメカニズムの解明の 1 つの試みとして「欠陥密度」に着目した。

そこで欠陥と水素が結合することを利用し、陰極電解チャージにより水素を添加し、昇温放出水素分析により水素をトレーサーとした欠陥の検出をおこなった。従来、チタンに有用であることは知られていないが、Fig. 5 に示すように塑性変形により欠陥が増加した純チタン (大気中引張試験で破断した試料) に陰極電解チャージした時の水素量は、as-polished 材に陰極電解チャージ時のものに比べて増加している。このことから、純チタンにおいても欠陥

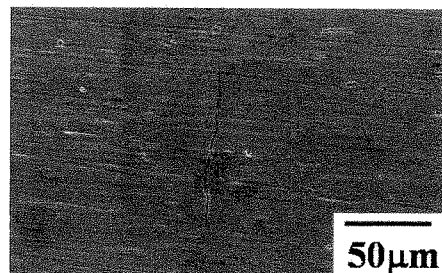
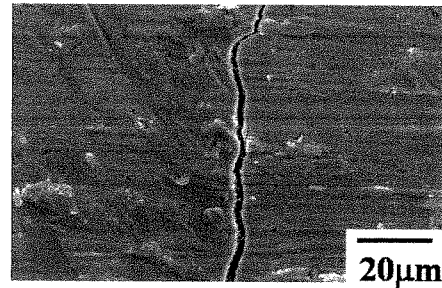


Fig.4:フレット疲労における側面観察 (a) 大気中 30 万サイクル
(b) 擬似体液中 10 万サイクル

の増加により水素量も増加することが示された。

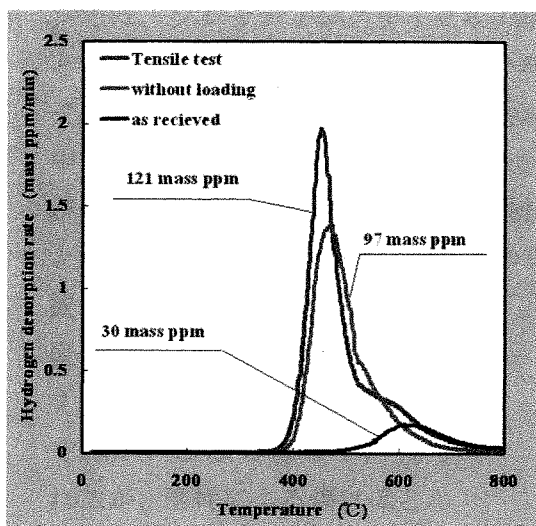


Fig.5:引張試験後、無付加に陰極電解チャージした試料と as-received 材の水素量と水素放出曲線

考えられる。また、水素量が多い（欠陥密度が高い）程水素放出の温度領域は高温側にシフトした (Fig. 6)。従来の報告より、純チタン中の歪（欠陥）に固溶もしくはトラップされた水素は、600-700°Cの温度領域で放出されることが知られている。水素化物は水素原子と比べて特異な体積のために、水素化物の形成には大きな歪み（欠陥）を伴う。高温側で水素が放出されるのは、水素化物分解後に水素原子が欠陥に強くトラップされたためである。つまり、純チタン中の欠陥が増加する程高温側（600°C以上）での水素放出が増加すると考えられ、これは本研究の結果と一致する。以上の結果から、水素をトレーサーとした場合、純チタン中の欠陥密度の違いは水素量だけでなく、水素放出挙動にも現れることが示された。この方法は今後もさまざまな観点からメカニズム解明の一手として着目される方法であると考えている。

またフレット疲労試験で破断した試料の水素量 (Fig. 6) は、FF in SBF (144 mass ppm) > FF in air (133 mass ppm) > Tensile test (121 mass ppm) であり、一方向引張り試験と比べて純チタンのフレット疲労試験には水素を伴う多くの欠陥を伴うことが推察される。さらに、SBF 溶液中では大気中疲労試験と比べて破断サイクル数が少ないにも関わらず、より多くの水素を吸収している。これは、先ほど示したとおり、SBF 溶液中フレット疲労では疲労初期段階 (N=100,000) でき裂が発生することから、き裂進展速度は大気中と比べて遅い、つまりより多くの欠陥を伴うためであると

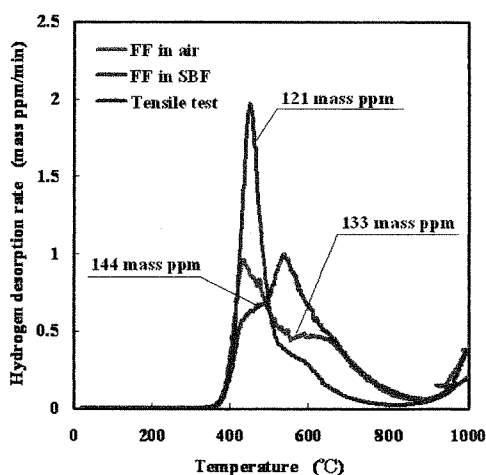


Fig.6:それぞれの試験で破断した試料からの水素量と水素放出曲線

従来、プラズマ溶射法によってハイドロキシアパタイト (HA) をコーティングしたチタンでは、フレットングサイクルの増加と共に HA が剥離し、耐摩耗性が大きく低下するという報告がある。また、生体内に埋入されたチタン表面に析出する HA がフレットング腐食疲労寿命を低下させる可能性が考えられる。そこで、NaOH 処理後に擬似体液 (SBF) 中で HA をあらかじめ表面に析出させたチタンのフレットング腐食疲労試験を行い、HA が寿命に及ぼす影響を調べた。HA 材のフレットング腐食疲労寿命は、未処理材のそれと比べ、高応力側ではほとんど変わらないが、低応力側では長くなる傾向を示した。SEM 観察からは、スティック部では表面の損傷はほとんど見られず、スリップ部では HA の剥離や細かい粒状の固まりが見られたが、磨耗による傷はほとんどみられず、比較的滑らかであった。また、レーザー顕微鏡観察により、未処理材の表面は HA 材の表面よりも凹凸が激しいことが確認された。さらに、腐食電位 (Fig. 7) からは、HA 材においては試験前及び試験中での電位の変動はほぼ見られず安定した挙動を示した。表面観察、電位測定の結果より、試料表面に HA が存在することによって、耐摩耗性が向上し、結果的に下地のアノード溶解反応が起こりにくくなったと考えられる。以上の結果より、NaOH 処理を用いて試料表面に析出させた HA は、フレットング疲労寿命の低下を招くことはなかった。よって、生体内環境で析出する HA がインプラント材料のフレットング疲労寿命を低下させないことが示唆された。

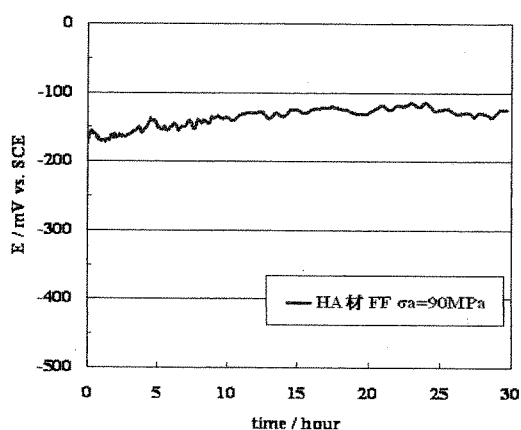


Fig.7:HA コーティングした純 Ti のフレットング腐食疲労試験中の腐食電位